Figure 8 : Zigzag truss cores with different gaps

3. Analytic Solutions

To estimate the mechanical properties of a sandwich panel with a zigzag truss core, the analytical solution based on elementary mechanics of material are derived as follows. The basic unit of a zigzag truss core is a wire formed into two triangles with the vertex angle of 90° (Fig. 9). Next to a zigzag unit truss, a pyramidal truss unit is shown. The length and diameter of each strut are L and d, respectively. The angle of a strut with the base plane is co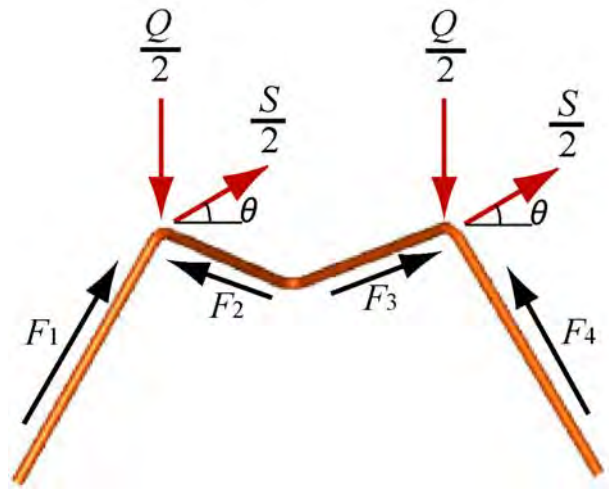nstant as $45°$. With the assumption that struts composing a zigzag truss are joined each other with ball-jointed ends so as to transmit axial forces only, the load capacity is estimated. In Fig. 9,

Figure 9 : Applied compression and shear load and reaction forces occurring in struts composing a zigzag truss

the compressive force, Q, and the force transmitted by a strut, F, are related by Eq.(1).

$$F_1 = F_2 = F_3 = F_4 = F$$
$$Q = 4F \sin 45°$$

(1)

The other assumption is that zigzag truss fails only by elastic or plastic buckling of the struts, but never by tensile yielding or brittle fracture. A slender member such as a strut buckles plastically under compression as soon as the strut starts to yield, if the material has a distinct yield point on its stress-strain curve. The critical forces causing plastic and elastic buckling of a strut, $F_{cr-plastic}$ and $F_{cr-elastic}$ are given by

$$F_{cr-plastic} = \sigma_0 \frac{\pi d^2}{4} \quad \text{and} \quad F_{cr-elastic} = \frac{\pi EI}{L^2} = \frac{\pi^3 E}{64} \frac{d^4}{L^2}$$

(2)

Here σ_0, E and I are the yield stress, Young's modulus of the material, and the moment of inertia of the strut cross-section, respectively. From Eq. (1), the maximum compressive load which causes elastic or plastic buckling of the struts is

$$Q_{max} = 2\sqrt{2} F_{cr}.$$

(3)

Under shear loads at the vertices acting parallel to the base plane, as shown in Fig. (9), the similar relations can be derived. The forces transmitted by struts are

$$F_1 = \frac{S}{2}\cos\theta + \frac{S}{2}\sin\theta,$$

$$F_2 = -\frac{S}{2}\cos\theta + \frac{S}{2}\sin\theta,$$

$$F_3 = \frac{S}{2}\cos\theta - \frac{S}{2}\sin\theta,$$

$$F_4 = -\frac{S}{2}\cos\theta - \frac{S}{2}\sin\theta. \tag{4}$$

According to Eq. (4), the maximum shear load, S_{max}, which causes elastic or plastic buckling of the struts depends on the direction scaled by an angle θ as follows:

$$S_{max}(\theta) = \text{positive minimum of} \left(\frac{-2F_{cr}}{\sin\theta + \cos\theta}, \frac{-2F_{cr}}{\sin\theta - \cos\theta}, \frac{-2F_{cr}}{-\sin\theta + \cos\theta}, \frac{2F_{cr}}{\sin\theta + \cos\theta} \right). \tag{5}$$

Fig.(10) shows variation of S_{max} with θ. For example, in the case of $\theta = 0°$, $90°$, where all four struts transmit the same absolute value of force, and $S_{max} = 2F_{cr}$. In the case of $\theta = 45°$, where only two struts withstand the shear load, and $S_{max} = \sqrt{2}F_{cr}$. All the above equations are valid as long as there is no relative displacement between the two vertices on the top (and the other two on the bottom). Therefore, those equations are valid for a pyramidal truss.
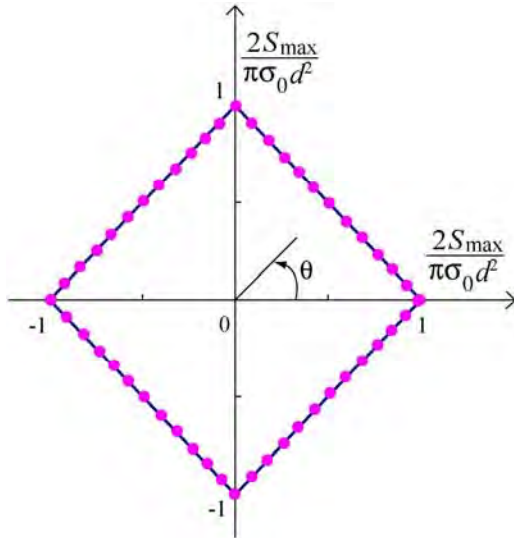

Figure 10 : Variation of maximum shear load as a function of the loading direction

Maximum stress of a zigzag truss is obtained by dividing the maximum load by the area of the base plane which is supported by the truss. For the unit truss shown in Fig.(7), the area is $A = 2eL^2$. Hence, from Eq. (3), the maximum compressive stresses of a zigzag truss are expressed by

$$\sigma_{max}|_{plastic} = 2\sqrt{2}\frac{\sigma_0 \pi d^2}{4}\frac{1}{2eL^2} = \frac{\pi\sigma_0}{2\sqrt{2}e}\left(\frac{d}{L}\right)^2 \tag{6a}$$

$$\sigma_{max}|_{elastic} = 2\sqrt{2}\frac{\pi^3 E d^4}{64L^2}\frac{1}{2eL^2} = \frac{\pi^3 E}{32\sqrt{2}e}\left(\frac{d}{L}\right)^4 \tag{6b}$$

Maximum shear stress can be derived similarly. For example, in the case of $\theta = 0°$ and $90°$,

$$\tau_{max}|_{plastic} = 2\sigma_0 \frac{\pi d^2}{4}\frac{1}{2eL^2} = \frac{\pi\sigma_0}{4e}\left(\frac{d}{L}\right)^2$$

$$(7a)$$

$$\tau_{max}\big|_{elastic} = 2\frac{\pi^3 E d^4}{64 L^2}\frac{1}{2eL^2} = \frac{\pi^3 E}{64e}\left(\frac{d}{L}\right)^4 \tag{7b}$$

Also, relative density of a zigzag truss depends on the gap between zigzag-formed wires, eL, as follows:

$$\rho_{rel} = \frac{4\pi d^2/4}{2L^3 \sin 45°} = \frac{\pi}{\sqrt{2}\, e}\left(\frac{d}{L}\right)^2 \tag{8}$$

Meanwhile, for a pyramidal truss, all the above equations about the maximum stress and the relative density are still valid with $e = 0.5$.

4. EXPERIMENTS AND THE RESULTS

4.1. Tensile Tests

Wires used in fabricating the zigzag truss core specimens are of low-carbon steel, JIS SS41. The diameter was d=1.2mm. Tensile tests were performed to obtain material properties of the wires at two states, namely, as-received and annealed during brazing with face sheets. Fig.11 shows the measured stress-strain curves. While Young's modulus was unchanged as about E=200 GPa before and after the brazing, the yield stress was decreased from σ_o= 340 MPa to 175 MPa. Because the proportional limits for these wires were distinct, they were taken as the yield stresses, which were believed to give the more accurate estimation of the maximum stresses due to plastic buckling than a typical 0.2% offset yield stress. Not only the tensile tests but also compression and shear tests were performed with an electro-hydraulic material test system INSTRON 880.

4.2. Specimen Preparation

First, wires were pressed by to form into a triangular wave shape, and turned 90° about their longitudinal direction so as to lie on a plane. And then, the wires were pressed again by another pair of V-grooved jigs which has a half of wave length. See Fig.12 for configurations of the two directional bending process
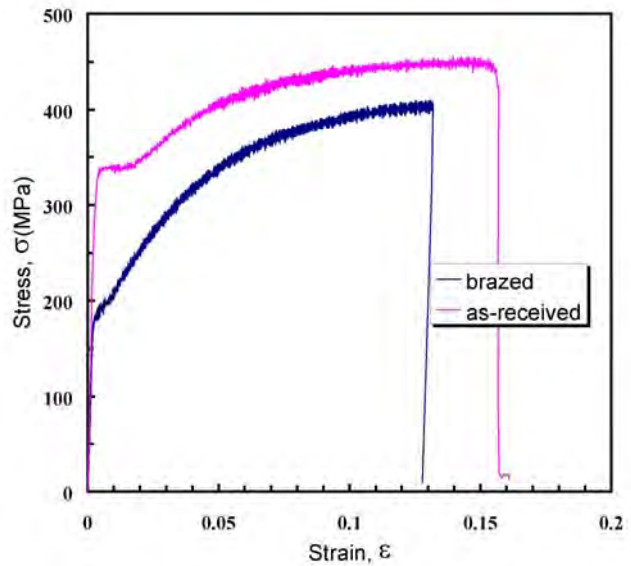
Figure 11 : Tensile stress-strain curves of the SS41 wires as-recieved and anneled during brazing
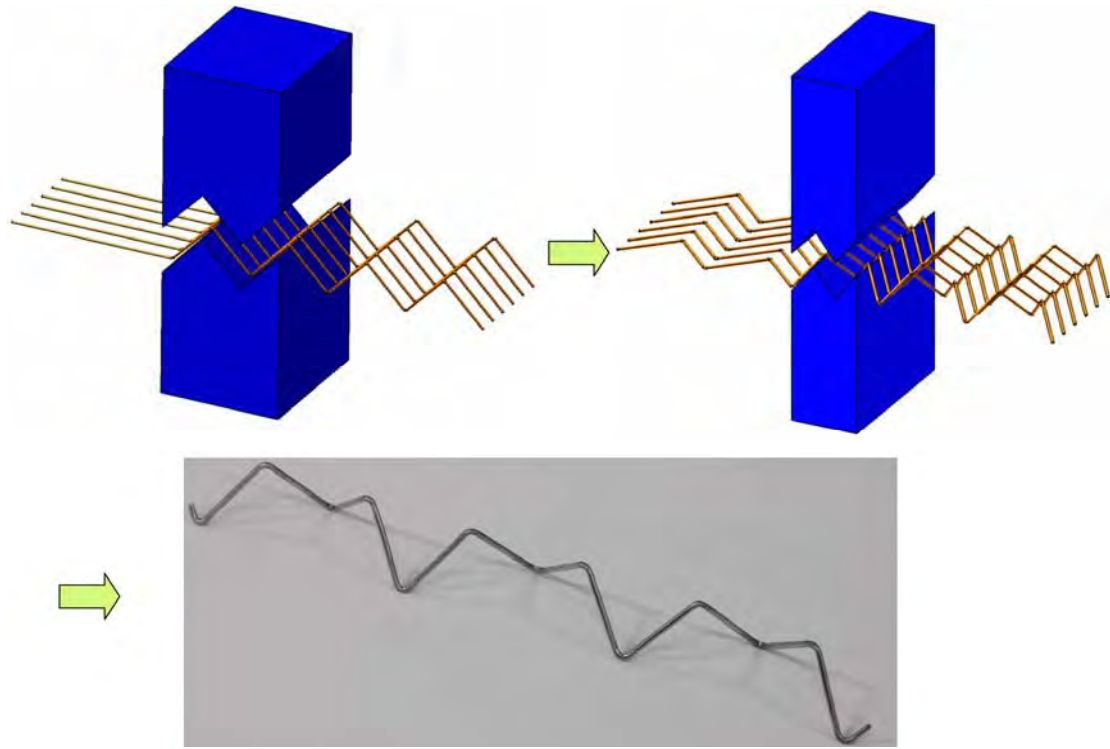
Figure 12 : Forming process of zigzag trusses and a final configuration

and a wire formed through the process.

Finally, the formed wires were parallel arranged with a specific gap between wires on a lower face sheet of the same low carbon steel, and assembled with an upper face sheet, and put into an electric furnace. Brazing was performed at 1120°C with pure cupper paste (CTK-C699, CHEM-TECH Korea Co.). A finished specimen has the configuration shown in Fig.7. The length of struts composing the zigzag trusses was L=20 mm. Specimens with cores of two different relative densities were fabricated by adjusting the gap to e=1 and 0.5, which result in their relative densities of $\rho_{relzigzag-1} = 0.008$, and $\rho_{relzigzag-2} = 0.016$, respectively.
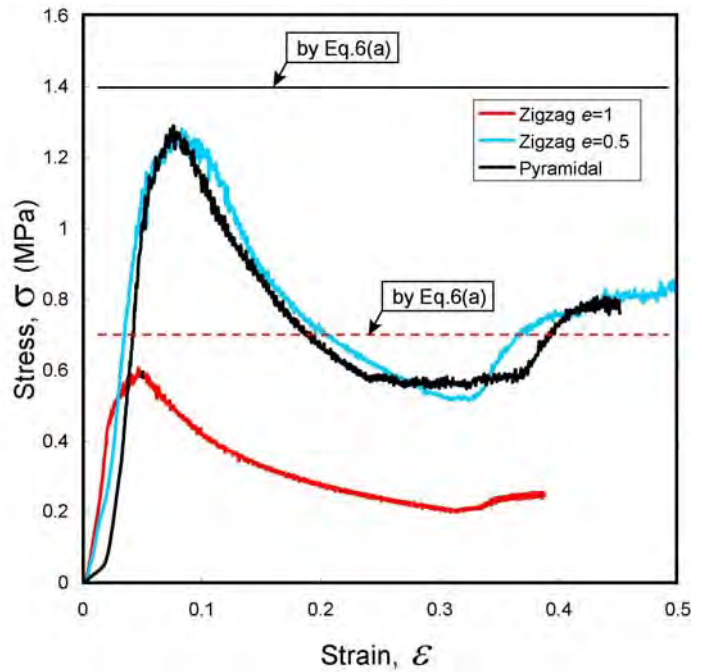

Figure 13 : Compression tests results compared with analytic estimations

The specimens were named 'Zigzag-1' and 'Zigzag-2', respectively. The specimens were named 'Zigzag-1' and 'Zigzag-2', respectively. For purpose of comparison, specimens with pyramidal truss cores which were composed of struts of the same length as that of zigzag truss cores were fabricated in a similar way. The specimens were named 'Pyramidal'. Table 1 lists external dimensions of the specimens used in the tests, and number of unit trusses contained in each specimen.

4.3. Compression Tests

Compressive tests were performed with the sandwich panel specimens with the zigzag truss and pyramidal truss cores. Each specimen's core had three rows with four unit trusses in a row. The load and displacement data measured via a digital data acquisition system were divided the area supported by the truss core and the core height, respectively, to give the stress and strain plots. The results are illustrated in Fig. 13. In the figure the maximum compressive stresses estimated by Eq. 6(a) are presented together. The specimen 'Zigzag-1' gave the lower maximum stress about σ_{max} =0.6 MPa than two others, while Eq. 6(a) gave somewhat over-estimation, σ_{max} =0.7 MPa. Eq. 6(b) corresponding to elastic buckling gave much higher estimations, which were discarded. The specimens 'Zigzag-2' and 'Pyramidal' gave the higher maximum stresses, σ_{max} =1.26 and 1.28 MPa, while Eq. 6(a) gave somewhat over-estimation, σ_{max} =1.4 MPa. If the fact that the specimens were manually but not precisely prepared is considered, the test results of the maximum stress are regarded to agree fairly well with those estimated based on ideal truss topologies. Virtually no difference in the compressive strength was observed between zigzag-truss-cored and pyramidal-truss-cored specimens.

4.4. Shear Tests

Shear tests were performed with the longer sandwich panel specimens. Each specimen's core had three rows with 11 unit trusses in a row. According to ASTM standard-C273 test method, each specimen was attached to a pair of two thick plates and the specimen was loaded in compression along the diagonal. Fig. 14 shows a picture of

Figure 14 : Shear test specimen installed on grips

the specimen and grip assembly.

The test results are illustrated in Fig. 15. In the figure the maximum shear stresses estimated by Eq. 7(a) are presented together. The specimen 'Zigzag-1' gave the lower maximum stress about σ_{max} =0.47 MPa than two others, while Eq. 7(a) gave a little over-estimation, σ_{max} =0.49 MPa. The specimens 'Zigzag-2' and 'Pyramidal' gave the higher maximum stresses, σ_{max} =1.11 and 1.08 MPa, while Eq. 7(a) gave a little under-estimation, σ_{max} =0.99 MPa. These test results of the maximum shear stress are regarded to agree fairly well with those estimated based on ideal truss topologies. Again, virtually no difference in the shear strength was observed between zigzag-truss-

Figure 14 : Shear tests results compared with analytic estimations

cored and pyramidal-truss-cored specimens. In Table 1, the measured and estimated maximum stresses for the three designs of specimens and the two loading are listed with the relative errors. Table 2 summerizes the maximum stresses measured by the tests and estimated by the analytic solutions with errors.
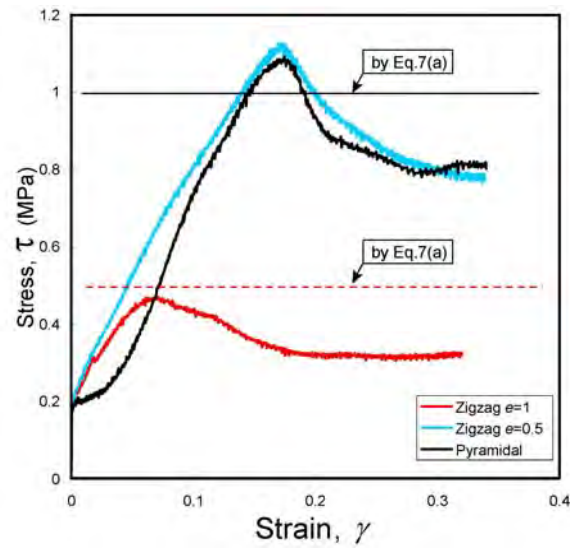
		Compression		Shear	
		Size (mm) $W \times L \times H$	No .of trusses	Size (mm) $W \times L \times H$	No .of trusses
Pyramidal		$80 \times 60 \times 16$	$4 \times 3 = 12$	$60 \times 220 \times 16$	$3 \times 11 = 33$
Zigzag	e=1	$80 \times 60 \times 16$	$2 \times 3 = 6$	$60 \times 200 \times 16$	$3 \times 5 = 15$
	e=0.5	$80 \times 60 \times 16$	$2 \times 6 = 12$	$60 \times 220 \times 16$	$6 \times 5.5 = 33$

Table 1. External dimensions of the specimens used in compression and shear tests, and number of unit trusses contained in each specimen.

		Relative density	Maximum compressive stress (MPa)			Maximum shear stress (MPa)		
			test	estimation	error(%)	test	estimation	error(%)
Pyramidal		0.016	1.28	1.4	-9.4	1.08	0.99	+8.3
Zigzag	e=1	0.008	0.6	0.7	-16.7	0.47	0.49	- 4.3
	e=0.5	0.016	1.26	1.4	-10.0	1.11	0.99	+12.1

Table 2 : Comparison of peak stresses from tests with estimated stresses

Heonsoo Kim, Byung-Chul Lee and Ki-Ju Kang.

5. CONCLUDING REMARKS

The biggest benefit of a single-layered truss core is that it is easily fabricated by simply bending an expanded or plain woven metal mesh. For heavy load applications, the height of core is needed to get increased. In a consequence, however, if the sandwich panel is subjected to a bending load, the face sheet is vulnerable to buckling because the higher core inevitably leads to the larger truss step between connection points with the face sheets regardless of strength of the core. See Figs. 16(a) and 16(b) for side views of sandwich panels with two different truss cores. Contrarily, Zigzag truss cores shown in Fig. 16(c) can prevent the face sheets from buckling, which means more flexibility in the strength design. For example, if a lighter core for a given height is needed without any increase in risk of face sheet buckling, the thinner wire formed zigzag truss core can be used with the gap between the trusses unchanged. If a face sheet is at risk of indentation due to sharp foreign objects, thick wires can be used as the raw material and the gap between the zigzag trusses can be tightened without any interference among wires. In the near future, the bending performance which determines whether a new technology of sandwich panel survives or not will be explored and optimal design will be studied to prove the flexibility in design and the usefulness.

In summary, the new topology for a truss PCM which is named 'zigzag truss' has been described and its mechanical performances under compression and shear loading have been explored by analytic solutions and experiments. As the results, the zigzag truss has been proved to have equivalent strength to a pyramidal truss core for a given relative density under both loadings.
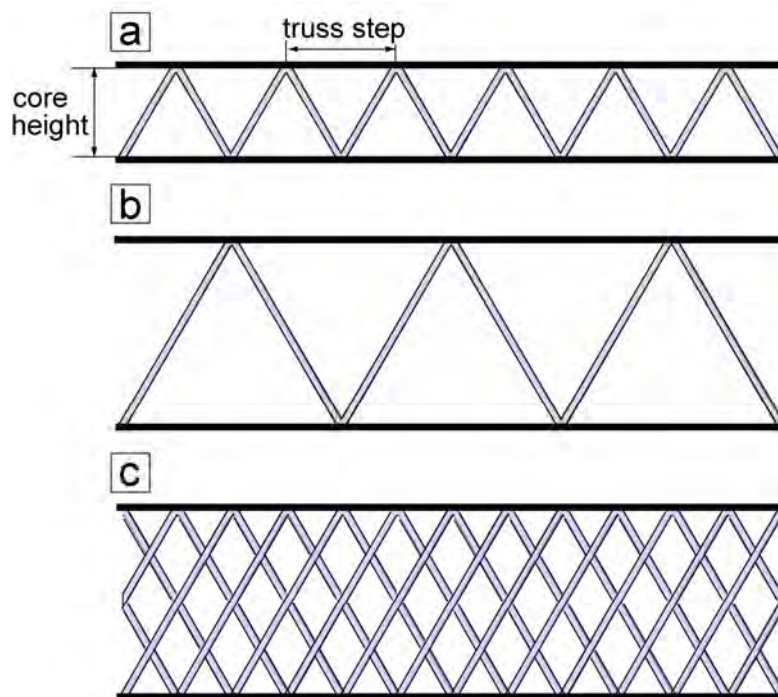

Fig. 15 : Zigzag truss cores with different gaps and different core heights

ACKNOWLEDGEMENTS

REFERENCES

[1] A. G. Evans, J. W. Hutchison, N. A. Fleck, M. F. Ashby and H. N. G. Wadley, "The Topological Design of Multifunctional Cellular Metals," *Progress in Materials Science*, 46, 309-327 (2001).

[2] J.C. Wallach and L.J. Gibson, US Patent 6,644,535B2 (2003).

[3] F. W. Zok, S. A. Waltner, Z. Wei, H. J. Rathbun, R. M. McMeeking, and A. G. Evans, "A Protocol for Characterizing the Structural Performance of Metallic Sandwich Panels: Application to Pyramidal Truss Cores," *Int. J. of Solids and Structures*, 41, 6249-6271 (2004).

[4] S. Chiras, D. R. Mumm, N. Wicks, A. G. Evans, J. W. Hutchinson, K. Dharamasena, H. N. G. Wadley and S. Fichter, "The Structural Performance of Near-optimized Truss Core Panels," *International Journal of Solids and Structures* , 39, 4093-4115 (2002).

[5] S. Hyun, A. M. Karlsson, S. Torquato and A. G. Evans, "Simulated Properties of Kagome and Tetragonal Truss Core Panel," *Int. J. Solids and Structures* , 40, 6989-6998 (2003).

[6] D. J. Sypeck and H. N. G. Wadley, "Cellular Metal Truss Core Sandwich Structures," *Proceedings of the 2nd International Conference on Cellular Metals and Metal Foaming Technology (MetFoam 2001)* edited by J. Banhart, M. F. Ashby, N. A. Fleck, 381-386 (2001).

[7] H. N. G. Wadley, N. A. Fleck and A. G. Evans, "Fabrication and Structural Performance of Periodic Cellular Metal Sandwich Structures," *Composite Science and Technology*, 63, 2331-2343 (2003).

[8] C. H Lim, I. S. Jeon, and K. J. Kang, "A New Type of Sandwich Panel with Periodic Cellular Metal Cores and Its Mechanical Performances," submitted to *International J. of Solids & Structures* (2007).

[9] J. H. Lim and K. J. Kang, "Mechanical Behavior of Sandwich Panels with Tetrahedral and Kagome Truss Cores Fabricated from Wires," *International J. of Solids & Structures* 43, 5228-5246 (2006).

[10] J. H. Lim and K. J. Kang, " Wire formed cellular metals," *Materials Transactions* 47, 2154-2160 (2006).

[11] K. J. Kang, C. J. Lee, D. S. Lee, and B. C. Lee, "A Light Weight Sandwich Panel with a Core Constructed of Wires and the Manufacturing Method of the Same", PCT/KR2007/006413/10 DEC (2007).

THE POLYPROPYLENE HONEYCOMB CORE FOR STRUCTURAL SANDWICH PANELS

R. Filippi[*] - Marketing & Development Manager–

[*]nidaplast® rue R.V. Couturier F-59224 Thiant

Keywords: Structural sandwich panels, polypropylene honeycombs, bending calculation, working up

Summary: nidaplast®, inventor and specialist of extruded polypropylene honeycombs for 20 years, continue to innovate in opening the structural sandwich panel technology to industries other than the traditional ones: aeronautic and yachting.

With some various examples in the building area, transport industry, yachting and industrials goods,

the lecture presents all the expectancies of the customer and all the various solutions brought. nidaplast® do not only sell a product but brings a global solution, from:

* the simple argument which presents the multifunctionality of sandwich panels with polypropylene honeycombs. It widely opens the application fields.

* to exact advice on possibilities but also limitations for the use of such products still new to these industries.

*to the development of modern working up techniques such as infusion for thermoset resins and thermowelding in the case of thermoplastics.

* including some help for predimensioning, a prerequisite to the utilisation of a structural sandwich panel .

Economical and very light, these structural honeycombs with hexagonal cells have a thickness from 5 to 150 mm. They have very good mechanical and physical properties. They are thermal and acoustic insulators. Recyclable, they are chemically inert and environamentally friendly.

Their use implies a low consumption in energy, whether during processing or when being used. The lightness of the achieved sandwich panels restricts the gas consumption. They come within the scope of the sustainable growth approach followed by nidaplast® for a few years and materialized by the ISO 14001 certification

1 GENERALITIES ON SANDWICH PANELS

When nidaplast® invented the polypropylene honeycombs to be used as a core for structural sandwich panels, only aeronautics and yachting, were using this technique for the lightness / resistance couple it brings

Due to the high level of price of existing cores and the need for structured engineering

offices, this technique remained only in hi-tech industries where weight saving was a necessity

Using an economical and industrial method, extrusion, combined with a common thermoplastic resin, polypropylene. nidaplast®widens the use of structural sandwich panels to a lot of industries. Polypropylene honeycombs provide sandwich panel with complementary functions along with a cost effective solution.

The principle of sandwich panel has been known and used for many years. To give rigidity to an element the easiest way is to increase its thickness, which is why the sandwich panel is made from a light and shear resistant core separating two heavy and resistant skins. This technique allows to optimize the components of the panels, skins give surface aspect and resistance, core brings shear resistance, lightness …
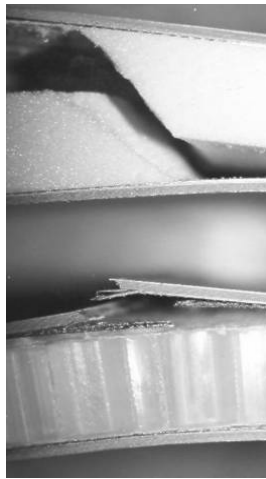
Picture 1: kind of break of a sandwich panel

The above picture (1) shows the same sandwich panels with 2 kinds of core:

a) the shear breaking of a polyurethane foam (not structural), without break of the rigid facings.

b) the breaking of the rigid facings, without break of the nidaplast® core. The load applied in this case is twice as high as with the polyurethane foam.

This picture is very useful to understand the concept of structural sandwich panel. The structural core has to transmit the shear stress between the 2 rigid facings.

2 POLYPROPYLENE HONEYCOMBS CORE, NIDAPLAST

2.1 Presentation

nidaplast®core is composed of:
1) a polypropylene honeycombs core, dimensions 8 and 20 mm
2) on both sides 2 polyester non woven plies intended for a good adhesion with the
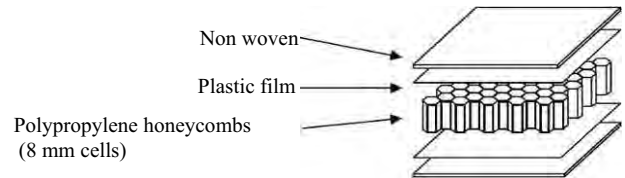
facings of the sandwich panel
3) a polypropylene film to allow the adhesion by thermowelding and to avoid resin penetrating the cells in the case of lamination:

Picture 2: nidaplast®8 panel

Picture 3: nidaplast®8 description

Dimensions
Length   : 2500 mm
Width :   1200 mm
Thickness from 5 to 90 mm

2.2 Mechanical characteristics

Apparent volumic mass :   40 to 110 kg/m3
compression strength: 0,3 to 2,5 MPa
shear strength   0,3 to 0,6 MPa
perpendicular strength   0,2 to 0,7 MPa

2.3 Other characteristics

Thermal resistance
20 mm thick   : $R = 0,3$ m².°C/W (i.e $\lambda = 0,067$ W/(m.°C))
90 mm thick $R = 0,6$ m².°C/W (i.e $\lambda = 0,14$ W/(m.°C))
Fire properties: flammable product. M1/F0 Possibility for the complete sandwich sandwich panel, depending on the panel facings.
Chemical properties: Excellent resistance to most acid and base. Humidity take off (< 0,2 %)

3 THE STRUCTURAL SANDWICH PANEL ISSUE

The basic solution of an element usually is a monolithic skin which gives esthetical aspect, and surface resistance, reinforced underneath by a load bearing structure which resists to the loads transmitted to the element.
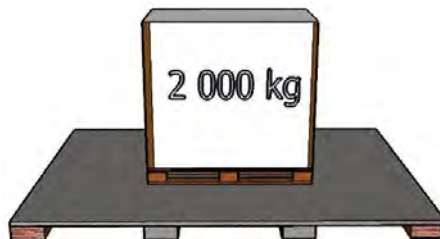
The first approach of our customers is to change the monolithic skin by a sandwich panel without changing the load bearing structure which is already calculated and optimized. They only want to change the monolithic skin by an equivalent sandwich panel
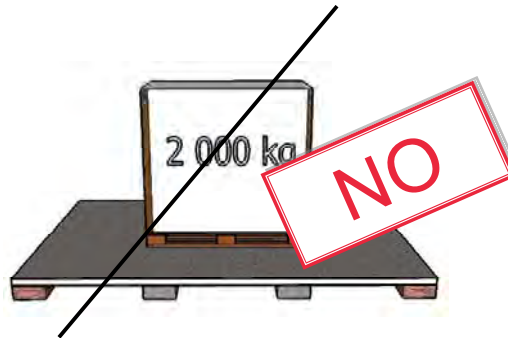
bad solution

This solution which seems simple is not efficient and not cost effective because not optimized. It is the object of the following draft

3.1 Principle of a sandwich panel principle

The objective of a structural sandwich panel is to give rigidity at the same time as lightness
Exposed to a bending load, the stresses in a sandwich panel are distributed as shown in the following diagram:
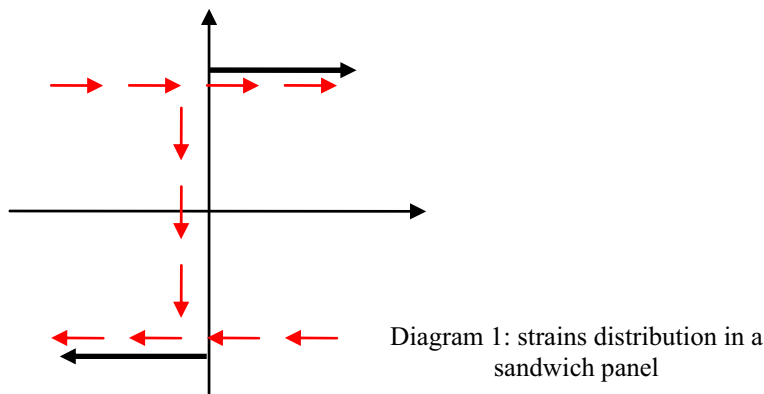
Diagram 1: strains distribution in a sandwich panel

Compression in the upper facing/Traction in the lower facing/Shear in the core

3.2 Rigidity of the sandwich panel

Rigidity is characterized by the possibility of being distorted by a load. It is different from the resistance which measures breakability.
For a monolithic panel, the deflection is calculated through the following formula:

$$\textbf{(1) Y= K*P*L}^{3}\textbf{/D} \qquad \text{with} \qquad \text{Kg = constant}$$

$$P = \text{load}, \; L = \text{span}$$

(2) D = EI,   rigidity   with   E Young modulus; I Inertia

Applied to a structural sandwich panel this formula becomes

(3) Y = Y$_1$ + Y$_2$ **Y** = total deflection

with   **(3a) Y$_1$ = Kg*P*L^3/DY$_1$ deflection due to the skins**

and   **(3b) Y$_2$ = Ks*P*L/b(c+f)Gc Y$_2$ deflection due to the shear of core**

with b = width of panel ; c = thickness of core ; f = thickness of facings

and   (5) **D = « E » I** with   (5a) **« E » = E$_f$*(1-c^3/h^3)**   **E$_f$** = facings E modulus

The total deflection of the sandwich panel appears in 2 distortion types: Y$_1$ due to skins deflection, Y$_2$ bound to the shear of the core. As these 2 types do not evolve on the same way according to span length it is impossible to define a rigidity independent of the span length. It is therefore difficult to estimate a sandwich panel

3.3 Influence of the span length

As the rigidity depends on the span length it is necessary to make different calculations to optimize the bearing structure according to the deflection of the sandwich panel.

For a 1/200 deflection, for 2 different thicknesses of **nidaplast**®8 core 20 and 40 mm, and same 2 mm GRP E = 10 000 Mpa skins, the diagram below shows 2 curves:

- in comparison to monolithic panel it is possible to define an **apparent (or real) rigidity** Da= Kg*P*L^3/(Y1+Y2). It grows with the span length because the shear deflection decreases. In this diagram this **apparent rigidity** tends to an asymptote.
- this asymptote can be called the **intrinsic rigidity,** when the span tends towards infinity and the shear deflection zero.
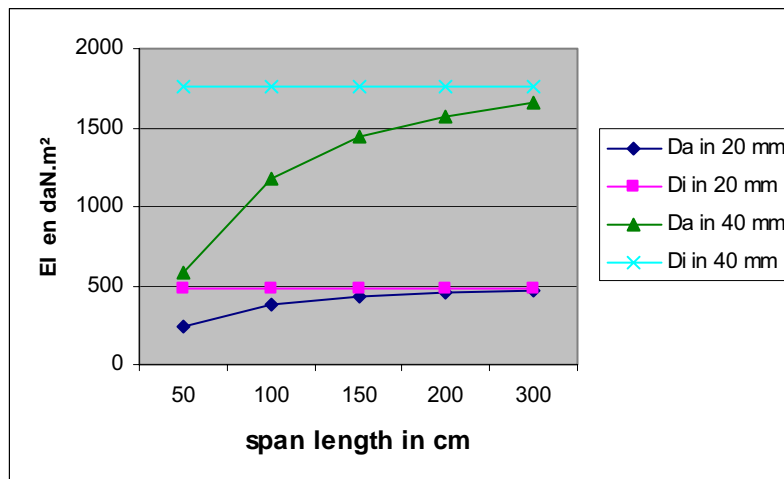

Diagram 2: apparent and intrinsic rigidity / span length

Because of this it is important to note that bending tests carried out in a laboratory with small samples cannot be directly used to determine the apparent rigidity, it needs to be interpreted through a calculation.

The diagram above shows that it is only for a span length above 50 times the core thickness that the shear deflection becomes low enough. For a short span length, the core is proportionally too strained in shear but perhaps also in compression.

3.4 Lightness

After rigidity, weight is the second parameter to use a structural sandwich panel. The table underneath shows the intrinsic rigidity compared to the weight for a sandwich panel made with a nidaplast$^{\circledR}$ 8 core and 2 GRP skins E = 10 000 Mpa.

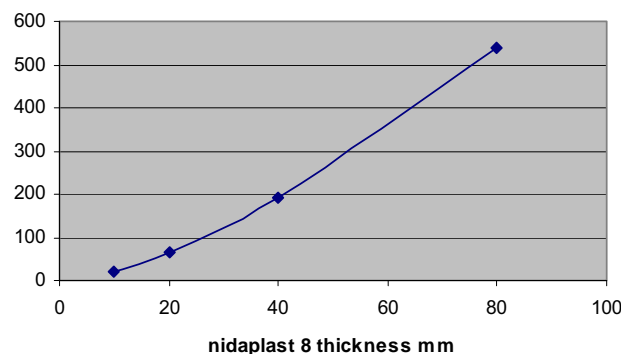| nidaplast$^{\circledR}$ mm	Intrinsic rigidity daN.m²	Weight daN	Ratio Rigidity/weight
10	145	6.8	21
20	485	7.6	64
40	1765	9.2	192
80	6705	12	540

Table 1 lightness /rigidity

Diagram 3 ratio rigidity / thickness

The rigidity / weight ratio increases drastically from 20 to 540 when the core thickness increases from 10 to 80 mm.

3.5 Strains in a sandwich panel

nidaplast (mm)	Shear strain (MPa)	Strains skins (MPa)	Deflection (mm)
5	0,07	17,9	46
10	0,04	10,4	17
20	0,02	5,7	6
40	0,01	3	1,9

Table 2 nidaplast with 2 GRP skins E = 10 000 Mpa span 1 m central load 100 daN

Increasing the thickness decreases all the strains in the core but also in the skins

3.6 First conclusion

Rigidity, weight and level of strains in a structural sandwich panel plead for thick sandwich panel. The substitution of a monolithic solution has to be optimized and done globally.
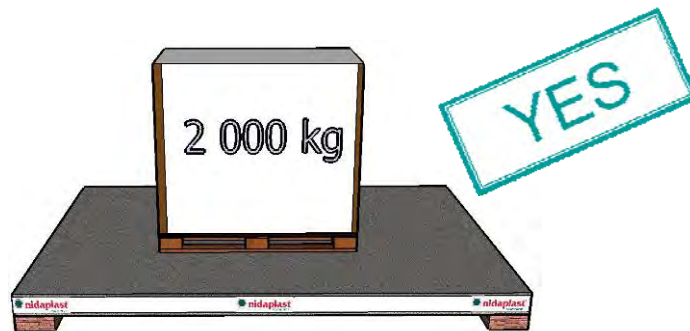
Good solution

The sandwich panel and the load bearing structure are calculated together. The load bearing structure is moved apart and the thickness of the sandwich panel increase.

Other properties, more specific to the use of the panel depends more or less on the skins or the core ore the couple. We can quote:

> Compression where the core is predominant
> Puncturing, abrasion or hardness where the skins have a great influence
> Shock where skin and core play the same role

The above properties only deal with the mechanical aspect of the element. Other characteristics are important for the realisation of a piece: thermal or acoustic insulation water resistance or recyclability. These characteristics are often separately dealt with. Thermal or acoustic insulation are brought later with specific products

Another advantage of the structural sandwich panel is that it is intrinsically multifunctional, without adding complementary products.

4 MULTIFUNCTIONALITY OF THE STRUCTURAL SANDWICH PANEL MADE WITH NIDAPLAST 8 CORE

4.1 Thermal insulation

A light core between 2 skins gives thermal insulation like quiet air. The table underneath gives the values of 4 panels, 2 monolithic ones and 2 sandwiches, one only for insulation such as EPS and a structural one like **nidaplast**[®] 8:

Thermal resistance R in m²°C/ W for 20 mm thick panel			
EPS	nidaplast[®]	Wood	GRP
0.5	0.3	0.1	0.01

Table 3: thermal resistance

Contrarily to a monolithic panel, a structural panel with nidaplast[®] provides thermal insulation and avoids risks of condensation.

4.2 Noise insulation

A viscoelastic core like nidaplast[®] will absorb many more vibrations compared to a rigid and monolithic panel.
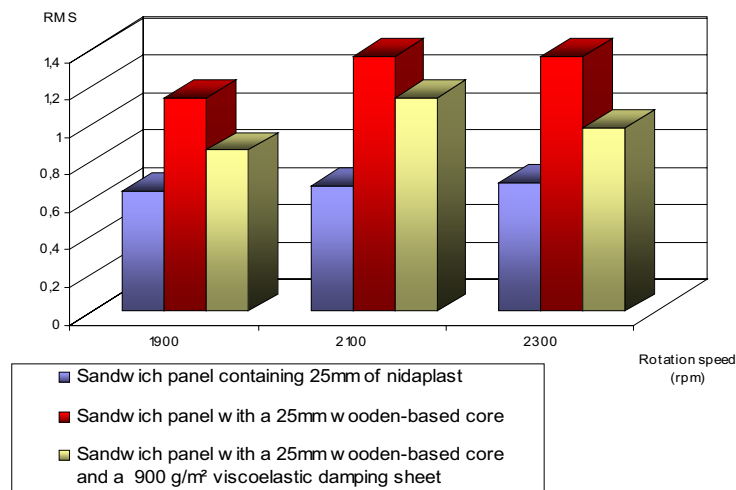

Diagram 4: vibrations level on the bulkheads for a motor boat in relation to the engine speed rotation

The diagram above shows the vibration level measured between a **nidaplast**[®] 8 panel and a wooden based panel. Even with the viscoelastic damping sheet glued on the wooden based

panel, the values with **nidaplast**[®] are better.

4.3 Miscellaneous

Thanks to its composition polypropylene and PET, the nidaplast core is very stable to water and most chemical agents as acid and base. It is also easily recyclable

5 WORKING UP

Moving from a traditional and monolithic solution to a sandwich panel goes through working up. In spite of being very innovative ,the nidaplast solution allows traditional working up.

► thermoset glass reinforced lamination is directly done on nidaplast core :
• by hand lay up or Spay lay up;

Picture 3: Spray lay up

Picture 4: Hand lay up

• by RTM ; or infusion with nidaplast[®] 8R and 8RI
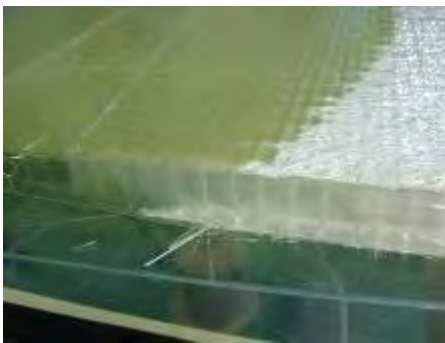
Picture 5: Infusion of a nidaplast 8RI
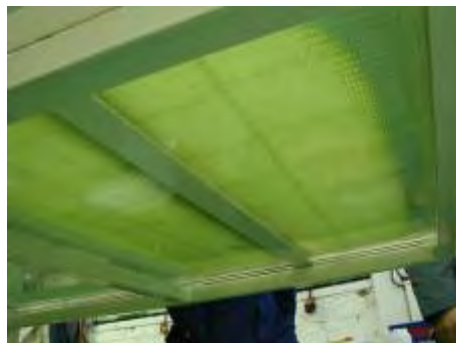
Picture 6: Homogenous impregnation of the fibres on the mould side

Picture 7: Drainage on the vacuum bag side

These new techniques allow manufacturing big and cost effective panels (both skins are made simultaneously). Industrial working up improves quality.

► gluing of prefabricated skins as wood, steel, aluminium, is traditionally carried out with every kind of glues (PUR, épozy, vinylique…). More innovative bonding as Thermogluing is

also possible.
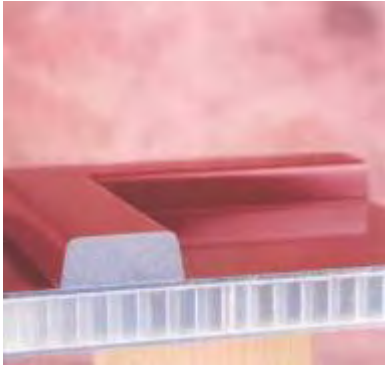
| Picture 8: Aluminium skin glued on a nidaplast core | Picture 9: Steel skin glued on a nidaplast core | Picture 10: Wood skin glued on a nidaplast core |

►direct thermowelding of glass reinforced polypropylene skins is achieved in the automotive industry

6 CONCLUSIONS

This presentation shows the importance of the various parameters to be taken into account when studying a structural sandwich panel. It also shows the difficult optimization of such panels.

Yet it soon appears that the structural sandwich with a **nidaplast**® polypropylene honeycombs core integrates several complementary functions in one single operation, which quickly improves the economical competitivity of this type of panels.

The association of a thermoplastic honeycombs core with thermoset, wood, metal or mineral facings appears to be most interesting. Each of the constituents of the sandwich panel is used under the best conditions to optimize the manufactured product:

- The core brings lightness, chemical inertia, resistance to shocks, thermal and acoustical insulation.
- The rigid facings offer resistance, surface protection and the esthetic aspect.
- Both combined result in big and easy to handle panels.

7 APPLICATIONS

This new and cost effective solution then perfectly suits large volume industries such as:

7.1 Building industry

nidaplast® is well adapted to both interior panels and outside facings. It can be used for large flat or curved panels. These panels will then be stiff, light and easy to handle. The polypropylene is also rot-proof and totally water-proof.

The polyester non woven applied on each side of the honeycomb allows the gluing of a

Picture 11: Doors

Picture 12: Claddings

large range of facings such as metal, wood or stone, but also the lamination of polyester skins. Thus, the **nidaplast**® PP honeycombs are present in marble or steel claddings, in wood or polyester doors, in decorative panels made with high pressure laminate (HPL), in marble or technical floors, in prefabricated bathrooms, in furniture, roofs, or swimming pools…

7.2 Transport

nidaplast is used in trucks (lateral panels, doors), ambulances (floors, furniture), commercial vehicles (body…), firemen trucks, caravans, trailers, cars…

Such sandwich panels are easy to handle and can be glued or laminated directly without any particular processing. For floor applications with high stress, the **nidaplast**® **8HP** with a higher density has got improved mechanical properties, especially regarding compression. The polypropylene honeycombs, mainly used for replacing plywood or foam panels, have the advantage of being light, water-proof and structural. This cost effective solution allows to get a lighter vehicle. So the user has a vehicle with larger capacity load and moderate gas consumption.

Picture 13: special vehicle

Picture 14: ambulance

Finally, for the automotive industry, the new requirements to reduce CO_2 releases have compelled all the manufacturers to lighten vehicles. So we developed the **nidacar**® and the **tubucar**®, especially adapted. These are used with glass reinforced thermoplastic skins within a thermoforming process. It allows very short manufacturing cycles for a complete composite piece (bottom of car boots for example). Thus the sandwich panels combine a light weight and a high stiffness for a low cost.

7.3 Boat industry

Like other sandwich cores, our products are used for structural applications for sailing boats or motor boats. Sandwich panels using **nidaplast**® are placed in decks, cabin floors, roofs, bulkheads and furniture. It is an economical alternative to replace most of traditional cores of this sector. The polyester non-woven on the surface of **nidaplast**® can

Picture 15: sealing boat

Picture 16: inner equipment

be directly laminated. It is thermo-bonded to the honeycomb structure and it enables to bond strongly the skins and the core.

Our products have very good acoustical properties in addition to all the advantages above: the polypropylene is viscoelastic and absorbs most of the vibrations. Thus the background sound level generated by the engine and the displacement is reduced.

7.4 Equipment goods

For equipment goods **nidaplast** is used in a very wide range of applications requiring a cost effective and easy to use product. However one field is in a fast developing period: the wind energy industry is now the most promising sector because of the big investments from many countries in the next few years. Used today in the windmill cabins, our honeycombs are attractive for their acoustical properties and their light weight. Furthermore this industry is very concerned with the protection of environment and so does our company by providing a fully recyclable product.

Picture 17:
decorative structure

Picture 18:
wind turbine

Picture 19:
Random structure

Picture 20:
Art sculpture

Eventually all solutions which decreases the use of raw materials are sustainable solutions for manufacturing, transport and utilization.

POLYPROPYLENE HONEYCOMBS FOR STORMWATER MANAGEMENT

Richard FILIPPI –

Marketing & Development Manager–
nidaplast® rue Paul Vaillant Couturier 59224 Thiant, France
e-mail : rfilippi@nidaplast.com, web page : http://www.nidaplast.com

Key words: stormwater management, polypropylene honeycombs, SAUL, SUDS, soil, flood

Summary: *Beyond the composites industry, nidaplast® has developed a very innovative application for polypropylene honeycombs for stormwater management : storage, infiltration and treatment of rain water.*

Urban growth and its direct consequence, soil impermeabilization, raise the problem of evacuation of high quantities of rainwater during storms. One solution is to create stormwater storage basins to store the high volumes of rainwater during storms. Restitution of water to the natural environment is then spread on a long period with a regulated flow.

To meet these new ecological requirements and European laws, nidaplast® range of products offers different solutions to answer the various issues of rainwater draining in towns. It is composed of blocks or panels with different mechanical properties and specially adapted sizes to meet all the different challenges of stormwater management.

For big volume storage basins: nidaplast® et nidagreen® EP, blocks are used to make grabbed basins to store heavy storms and avoid floods by overflow of sewage pipes. To create porous and circulating surfaces: nidagravel® stabilizes gravel surfaces and avoids soil impermeabilization

To store rainwater on roofs: nidaroof® allows planted roofs and the storage of water on flat roofs

For storage and re-use in private gardens : nidagarden®, in low thickness panels, is very well adapted to the garden environment.

Manufactured with recycled products, a low consumption of energy during production, nidaplast® products are used for maintaining a good hydraulic state of urban areas. They come within the scope of the sustainable growth approach followed by nidaplast® HONEYCOMBS for a few years and materialized by the ISO 14001 certification.

1) GENERALITIES ON STORMWATER MANAGEMENT:

Construction of buildings, roads, footpaths and parking areas on previously undeveloped areas avoid rainwater to infiltrate slowly in the soil. Normally the runoff rainwater must be collected, generally in the city network sewer, but with increasing urbanization and changing weather patterns this collection becomes more and more problematic. During heavy rainfalls the sewers network cannot absorb the entire runoff because of urbanization, so they overflow. It is one of the reasons why floods get more and more frequent in big cities.
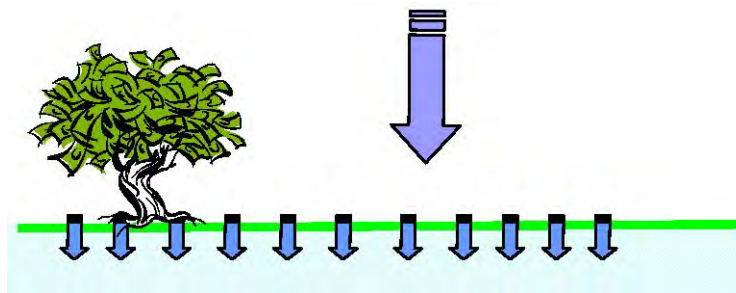
Fig. 1: natural area leads to infiltration
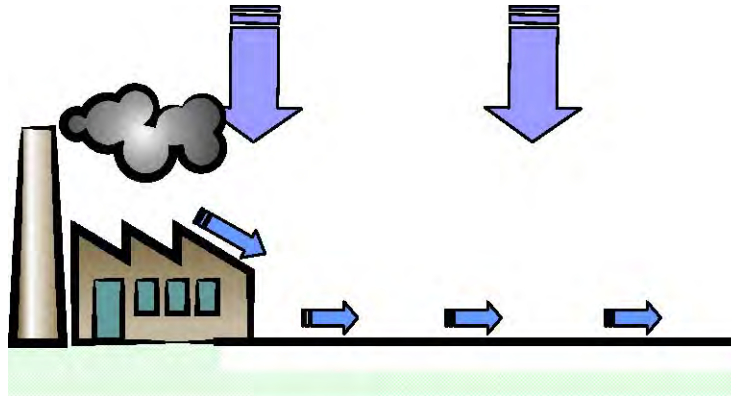
Fig. 2: Urbanised area leads to stormwater runoff

In the late eighties **nidaplast** patented the first modular drainage tank system with polypropylene blocks to store the rainwater and its runoff during storms, allowing a slow discharge after event. With **nidaplast**®**EP** blocks which present a high compression strength and a void ratio of 95%, it is possible to get a buried structure, considered as SUDS (sustainable drainage system) where the exceeding rainwater from storms is stored, and then infiltrates or gets into the sewer pipes with a controlled flow .

Other products have been developed for global stormwater management:

-nidagravel® to make porous gravel alleys   -nidaroof® to store water on flat roofs

Fig. 3: nidagravel®

Fig. 4: nidaroof®

History:

- 1987 : patenting of the first drainage tank system for stormwater management.

- 1991: a first **European Directive** appears on stormwater.

- 2000: The **European Water Framework Directive**, gives a new approach of rainwater and a good quality of surface water as an objective for 2015.

- Step by step this **European Water Framework Directive** is transposed into different national directives. The rainwater management becomes a priority. For example publication in France of a technical guide «la ville et son assainissement » published in 2003.

Fig.5 : French guide « la ville et son assainissement »

2) NIDAPLAST EP BLOCKS

2.1) Presentation

Polypropylene honeycombs cells, dimensions 20 and 50 mm
2 permeable polyester non woven plies on both sides

Dimensions:

Length:	Width :	Thickness:
2400 mm	1200 mm	120 and 520 mm

Table 1 : Dimensions of products

2.2) Mechanical characteristics

Apparent volumic mass   30 to 45 kg/m3
Compressive strength: 30 to 60 T/m²

2.3) Other characteristics

Void ratio: 95%
Thermal resistance: 90 mm thick $R = 0,6$ m².°C/W (i.e $\lambda = 0,14$ W/(m.°C))
Chemical properties: Excellent resistance to most acid and base. Humidity take off < 0,2 %

2.4) "nidaplast EP system" storage basin

During heavy rainfalls, the stormwater storage basin stores rainwater streaming from waterproofed surfaces. Then it returns them with a regulated flow to the receiving medium. The enclosed scheme presents a lengthwise and a transverse section of a **nidaplast**®**EP** storage basin.
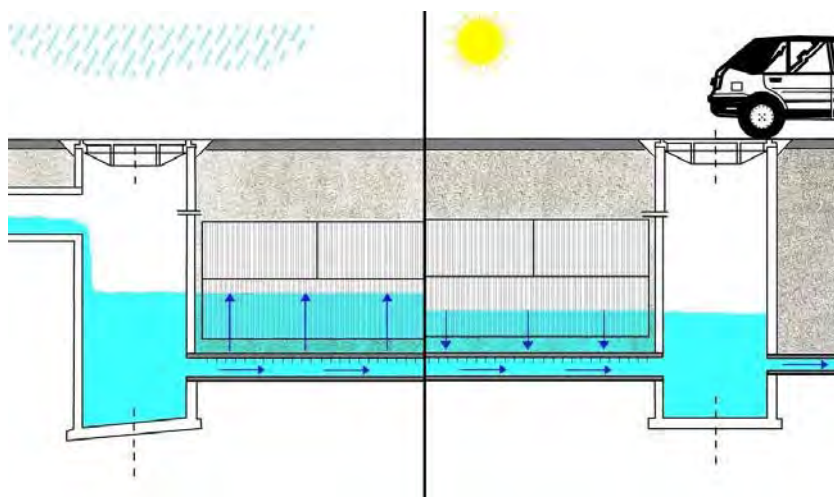
Fig.6 scheme of operating principle from a nidaplast basin

Stormwater reaches the **nidaplast®EP** storage or infiltration basin by one or more collecting pipes. The stormwater is scattered in the **nidaplast®EP** basin thanks to an included drain network uniformly spread out in the bottom of the basin in a diffusion layer (gravel 20/40 for example). It is realized thanks to a drain network with a large harnessing surface (role of injection).
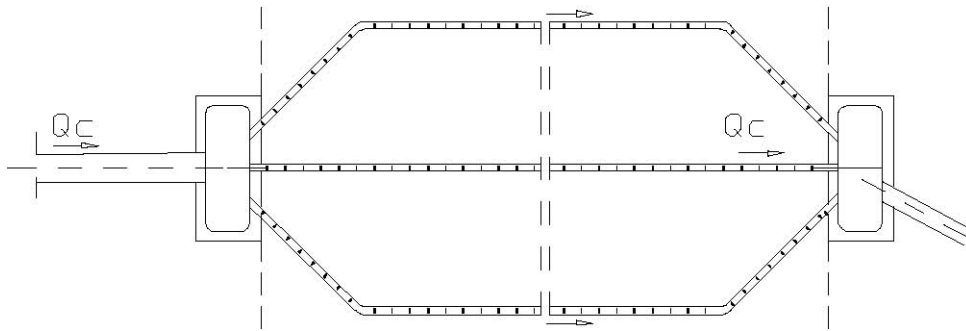
Fig.7 Plan view from the distribution network

It is to be noted that small stormwater flows do not get into the **nidaplast ®EP** blocks. While emptying the basin, the water drains out either directly through the soil, or thanks to the drains network, which works in the opposite way, and by the collector located downstream the basin.
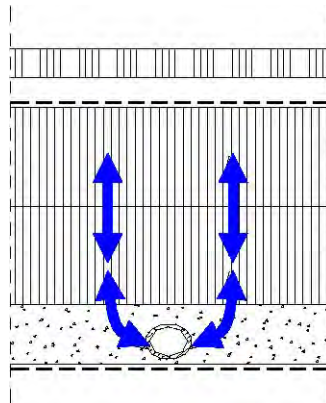
Fig. 8 side view of the principle of diffusion/emptying

The highest level of the **nidaplast®EP** basin determines water level in the supply network. Depending on the type of basin, a geotextile or a watertight membrane is installed on all surfaces located between the soil and the **nidaplast®EP** basin. The geotextile will have to suit the nature of the soil to ensure an anticontaminating function and a protection against punching.

Laying out the ballast on an underground storage basin depends on the nature and the use of the surface of the basin. To install a road on the basin, the most important factor is the road traffic, and more precisely the lorries traffic. Laying out the size of the ballast cannot be limited to the punctual resistance to an axle when a lorry drives. In the case of moving loads, two cases must be distinguished:

Low traffic : minimum 25 cm of non treated aggregate then road in accordance with the French "*Manuel des chaussées à faible trafic*", a technical guide that specifies the road structure depending on the nature of traffic.

**Medium and high traffic, minimum 55 cm of D2 aggregate** then road in accordance with the French "*Mémento des chaussées françaises sur plateforme de type PF2*", a technical guide that specifies the road structure depending on the nature of traffic.

The peripheral and above embankment is realized in accordance with the guide, to optimize the use of the surface of the basin.

The patented system permits both the drainage of the first polluted rainwater and the functioning of the basin by filling from the bottom. A self-cleaning is ensured thanks to the emptying that flushes the particles that may be fixed under the diffusion layer. As a complement, the incoming collector has a settling pit, a depressed sewer and a leaf basket. A regular maintenance of the system contributes to avoid any clogging.

Ecological constraints and the nature of rainwater may require more sophisticated treatment installations. They must then be installed in accordance with the regulations and their batch operating conditions with the **nidaplast®EP** basin.

Fig.9: working up of a nidaplast EP storage basin

3) UNIVERSITY RESEARCH ON THIS SYSTEM:

It was carried out in 2003 at the University of Sheffield (GB), Department of Civil and Structural Engineering. The purpose was to study the behaviour of different kinds of pollutants, in modular block stormwater storage systems.

Modular block stormwater storage systems allow both flood prevention in case of storm and regulation of the treated flow downstream the system while offering an area available for traffic. This kind of installation often generates cause for concern for decision makers: if silt deposits form within them, it may be difficult, if not impossible to gain access to remove them. Such deposits could have the effect of reducing storage volumes, and could potentially obstruct flow passages.

The study establishes the difference of behaviour between modular block stormwater storage systems **"with an under-pipe" and "without an under-pipe"**, as both following configurations show:

A)Configuration without an underpipe   B):**nidaplast** E**P** system with underpipe
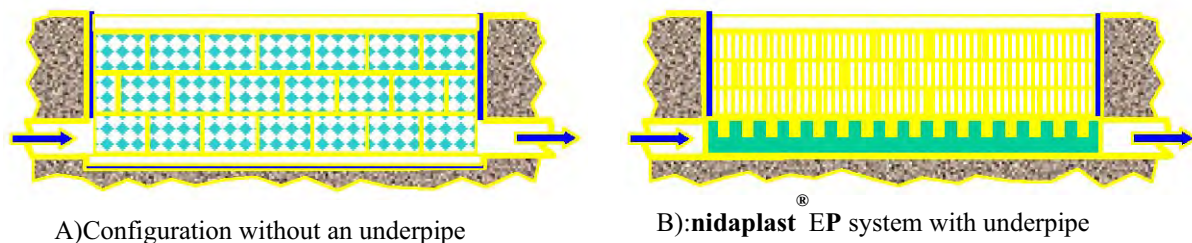
Fig.10: scheme of test apparatus

3.1.) Protocol:

A 3.6m long x 1.8m wide x 1.2m deep chamber, the flow of water at around 7 l/s for a 1m upstream head.

A) « Modular blocks » : milk crates

Dimensions : L 450 x l 360 x h 240 mm. 4 layers of 8 by 5 storage blocks (160 in total). The faces of the crates immediately adjacent to the chamber entry and exit points were removed, to allow free flow passage.

B) **nidaplast EP** system

A 225 mm diameter plastic pipe, slotted in its upper half, was connected between the chamber inlet and outlet. 25-40 mm stone was then added, leaving a flat surface above the pipe ridge. Above, **nidaplast® EP** blocks, L=2400 x 1200 x 520 mm, on 2 layers.

Three different tracers were studied in established mode of 7 l/s

- Tracer studies :   * measurement of the inlet and outlet concentration of a fluorescent solute**,** Rhodamine WT,
    * ground olive stone (granulometry < 75 µm at 75 %).

- Big waste tracking (supermarket plastic bags)

-

Fig.11 : test apparatus

3.2.) Results:

The retention time of stormwater in both systems can be compared thanks to the evolution of the Rhodamine and ground olive stone concentration

Configuration	Tracer material	Retention time (s)	Flow rate (l/s)	Velocity (m/s)
without under pipe	Rhodamine	530	7.14	0.0083
without under pipe	Ground olive stone	488	7.14	0.0090
nidaplast®EP with under pipe	Rhodamine	24	7.20	0.1860
nidaplast®EP with under pipe	Ground olive stone	19	7.72	0.2275

Table 2: retention time, velocity in the system

During the test the concentration of ground olive stone has been noted in the 2 apparatus :

- **75% of the ground olive stones remain in the structure without an under pipe,** resulting, by accumulation in time, in a high clogging risk.
-
- **100% of the ground olive stones are drained off with the nidaplast®EP system, with an under pipe.**

Plastic bags were also added in the water flow

	Nb of plastic bags added	Nb of plastic bags in outlet	Transfer rate
Without underpipe	20	0	0 %
nidaplast®EP with underpipe	20	20	100 %

Table 3: number of plastic bags catched in the apparatus

Computational Fluid Dynamics (CFD) Studies were also carried out using the « Fluent CFD » software (Version 6.1). Simulations were produced of the different chamber configurations described previously with the following results:

Configuration without underpipe   **nidaplast®EP** system, with underpipe
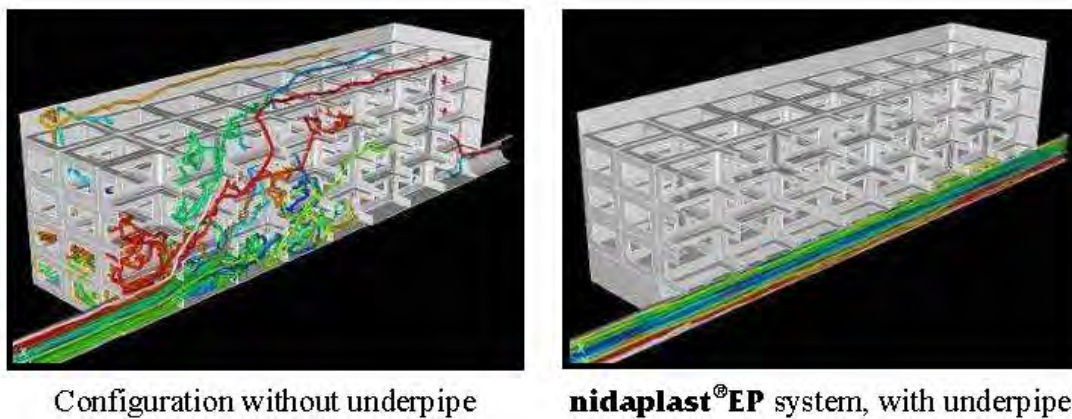
Fig. 12: computer modelization

Thus it can be noted that:

- In the configuration without underpipe, **the particles tend to disperse in the whole blocks volume,**

- In the **nidaplast®EP** system, with underpipe, **particles go directly to the outlet** and are drained off without passing through the blocks. **All risks of clogging by these fine particles are thus avoided**.

With this research the following elements can be pointed out :

-**Retention time** : in a system « without underpipe », stormwater stays 25 times longer than in the **nidaplast®EP** system, with underpipe : this high retention time favours **sediments accumulation inside the modular blocks installed without underpipe**.

-**Sediments**: Sediments, frequently present inside stormwater, are totally drained off with the **nidaplast®EP** system with underpipe, there is no risk of accumulation or clogging. On the contrary, in the system **without underpipe**, **75% of the incoming sediments stay inside the system, resulting in a high clogging risk.**

-**Supermarket plastic bags** : Plastic bags entering a system without underpipe stay inside the blocks, while they all are drained off with a **nidaplast®EP** system.

The specific configuration of **nidaplast**®**EP** storage systems, with an underpipe, allows to avoid sediments and debris to pass through the blocks. Thus, there is no risk of clogging for the storage system, which ensures the durability of the **nidaplast**®**EP** installations.

4) A RECOGNIZED AND PROVED SOLUTION:

This solution has been recognized and described in 1998 in an official French guide called:
« Les structures alvéolaires ultra légères (SAUL) en assainissement pluvial ».
It was written by :
 -LCPC (Laboratoire central des ponts et chaussées)
-CERTU (Centre d'Etudes sur les Réseaux de Transport et l'Urbanisme)
-Water Agencies
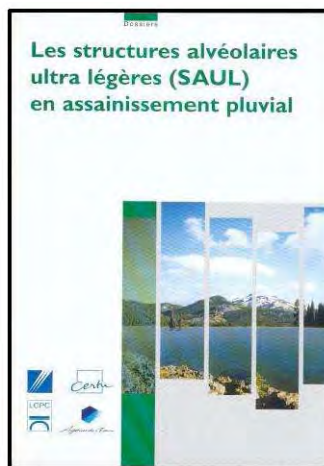
Fig. 13: French guide SAUL

5) OTHER PRODUCTS FOR STORMWATER MANAGEMENT

   Beside the blocks for rainwater storage, nidaplast developed other products to complete the range of plastic honeycombs suitable for water management

5.1.) nidagravel

Presentation:
2400*1200*40 mm plates with polyester non woven on the underface
37 mm honeycombs cells

Principle:
   To avoid impermeabilization of alleys when placed on a porous soil, the plates filled with gravel create a porous circulating surface.

Fig. 14: Children's playground

5.2.) nidaroof

Presentation:
2400*1200 plates with a thickness from 40 mm to 100 mm
1 or 2 permeable non woven polyester plies on sides

Principle:
One layer of nidaplast is installed on the waterproofing membrane to store water like a stormwater basin then surmounted by an other layer filled with gravel to make the roof accessible

Fig 15 first layer for storage   Fig. 16 2 layers, storage & gravel stabilization   Fig. 16: Final result

6 CONCLUSION

The extruded polypropylene honeycombs structure invented 20 years ago by nidaplast shows its multifunctionality in the 2 markets which have been created :

* composites where it is used as a structural sandwich core
* but also in a totally new field :for honeycombs the stormwater management.

In this last field polypropylene honeycombs structures provide the following properties:

1) lightness
2) compression strength
3) high void ratio
4) Chemical and water resistance

For these two markets nidaplast is proud to be an actor in developing sustainable growth. Polypropylene honeycombs is made of:
A fully recyclable raw material
Very light, it uses a small quantity of raw material
Products made with nidaplast core are also lighter, which saves raw material and also energy for working up and utilization
Rainwater is a more and more rare resource and needs to be protected.

The company is ISO 1401 certified since 2001

[1]Source : *« Assesment of modular block stormwater storage systems », Dr Michael G. Faram, Dr Ian Guymer and Prof Adrian Saul* – Novatech 2004.

DAMPING & ACOUSTICS

A VISCOELASTIC FINITE ELEMENT MODEL FOR THE ANALYSIS OF PASSIVE DAMPING IN ANISOTROPIC LAMINATED SANDWICH STRUCTURES

Aurélio L. Araújo⋆, Cristóvão M. Mota Soares†, and Carlos A. Mota Soares†

⋆ESTIG – Polytechnic Institute of Bragança
Campus de Sta. Apolónia, Apartado 1134, 5300-440 Bragança, Portugal
e-mail: aaraujo@ipb.pt, web page: http://www.ipb.pt

†IDMEC/IST – Technical University of Lisbon
Av. Rovisco Pais, 1049-001 Lisbon, Portugal
e-mail: (cristovao.mota.soares@ist.utl.pt, carlosmotasoares@dem.ist.utl.pt), web page:
http://www.ist.utl.pt

Key words: Sandwich structures, Finite Element Modelling, Layerwise models, Passive damping.

Summary. *We present a new finite element model for the analysis of passive sandwich laminated plates with a viscoelastic core and laminated anisotropic face layers. The model is formulated using a mixed* layerwise *approach, by considering a higher order shear deformation theory (HSDT) to represent the displacement field of the viscoelastic core and a first order shear deformation theory (FSDT) for the displacement field of the adjacent laminated anisotropic face layers. The complex modulus approach is used for describing the viscoelastic material behaviour of the core, and the problem is solved in the frequency domain using frequency dependent material data for the core. The model is validated and compared with reference solutions from the literature.*

1 Introduction

Passive damping treatments are widely used in engineering applications in order to reduce vibration and noise radiation [1, 2]. Passive layer damping is the most common form of damping treatments and it is usually implemented in two ways: unconstrained layer damping (extensional deformations) and constrained layer damping (shear deformations). The unconstrained layer damping consists in a simple layer of damping material bonded to the surfaces of the structure where flexural vibration occurs. Consequently, the damping material dissipates energy in extensional deformation mode, which is not the most efficient mechanism, as damping materials are known to work better in shear mode. Hence, applying a layer with flexural modulus comparable to that of the base structure on top of the damping layer, forces the damping layer to deform in shear mode, thus dissipating energy in a more efficient way. Increasing the thickness and length of the viscoelastic layers increases the energy dissipation and hence the

damping. Of course, limitations exist when using passive damping treatments as viscoelastic materials have frequency and temperature dependent properties, which can compromise the effective frequency and temperature ranges of treatment. To overcome this limitation and provide adequate damping over a broad frequency band, different viscoelastic materials may be used.

The theoretical work on constrained layer damping can be traced to DiTaranto [3] and Mead and Markus [4] for the axial and bending vibration of sandwich beams. Since then, different formulations and techniques have been reported for modelling and predicting the energy dissipation of the viscoelastic core layer in a vibrating passive constrained layer damping structure [5, 6, 7]. Other proposed formulations include thickness deformation of the core layer dealing with the cases where only a portion of the base structure receives treatment [8].

Sandwich plates with viscoelastic core are very effective in reducing and controlling vibration response of lightweight and flexible structures, where the soft core is strongly deformed in shear, due to the adjacent stiff layers. Hence, due to this high shear developed inside the core, equivalent single layer plate theories, even those based on higher order deformations, are not adequate to describe the behaviour of these sandwiches, mainly due to the high deformation discontinuities that arise at the interfaces between the viscoelastic core material and the surrounding elastic constraining layers. The usual approach to analyse the dynamic response of sandwich plates uses a layered scheme of plate and brick elements with nodal linkage. This approach leads to a time consuming spatial modelling task. To overcome these difficulties, the *layerwise* theory has been considered for constrained viscoelastic treatments, and most recently, Moreira et al. [9, 10], among others, presented generalized *layerwise* formulations in this scope.

In this paper a *layerwise* sandwich plate finite element model is proposed, where the viscoelastic core layer is modelled according to a higher order shear deformation theory and adjacent elastic layers are modelled using the first order shear deformation theory, and all materials are considered to be orthotropic, with elastic face layers being formulated as laminated composite plies. Passive damping is dealt with using the complex modulus approach, allowing for frequency dependent viscoelastic materials and the dynamic response of the finite element model is validated using reference solutions from the literature.

2   Sandwich plate model

The development of a *layerwise* finite element model is presented here, to analyse sandwich laminated plates with a viscoelastic (v) core and laminated anisotropic face layers (e_1, e_2), as shown in Figure 1.

The basic assumptions in the development of the sandwich plate model are:

1. All points on a normal to the plate have the same transverse displacement $w(x, y, t)$, where t denotes time, and the origin of the z axis is the medium plane of the core layer;

2. No slip occurs at the interfaces between layers;

3. The displacement is C^0 along the interfaces;

Aurélio L. Araújo, Cristóvão M. Mota Soares and Carlos A. Mota Soares
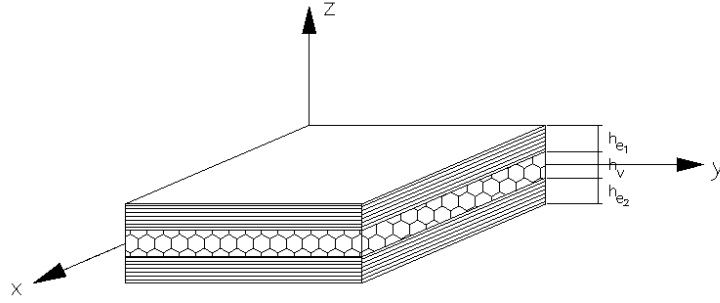
Figure 1: Sandwich plate

4. Elastic layers are modelled with first order shear deformation theory (FSDT) and viscoelastic core with a higher order shear deformation theory (HSDT);

5. All materials are linear, homogeneous and orthotropic and the elastic layers (e_1) and (e_2) are made of laminated composite materials;

6. For the viscoelastic core, material properties are complex and frequency dependent.

The FSDT displacement field of the face layers may be written in the general form:

$$
\begin{aligned}
u^i(x,y,z,t) &= u_0^i(x,y,t) + (z - z_i)\theta_x^i \\
v^i(x,y,z,t) &= v_0^i(x,y,t) + (z - z_i)\theta_y^i \\
w^i(x,y,z,t) &= w_0(x,y,t)
\end{aligned}
\tag{1}
$$

where u_0^i and v_0^i are the in-plane displacements of the mid-plane of the layer, θ_x^i and θ_y^i are rotations of normals to the mid-plane about the y axis (anticlockwise) and x axis (clockwise), respectively, w_0 is the transverse displacement of the layer (same for all layers in the sandwich), z_i is the z coordinate of the mid-plane of each layer, with reference to the core layer mid-plane ($z = 0$), and $i = e_1, e_2$ is the layer index.

For the viscoelastic core layer, the HSDT displacement field is written as a second order Taylor series expansion of the in-plane displacements in the thickness coordinate, with constant transverse displacement:

$$
\begin{aligned}
u^v(x,y,z,t) &= u_0^v(x,y,t) + z\theta_x^v + z^2 u_0^{*v} + z^3 \theta_x^{*v} \\
v^v(x,y,z,t) &= v_0^v(x,y,t) + z\theta_y^v + z^2 v_0^{*v} + z^3 \theta_y^{*v} \\
w^v(x,y,z,t) &= w_0(x,y,t)
\end{aligned}
\tag{2}
$$

where u_0^v and v_0^v are the in-plane displacements of the mid-plane of the core, θ_x^v and θ_y^v are rotations of normals to the mid-plane of the core about the y axis (anticlockwise) and x axis

(clockwise), respectively, w_0 is the transverse displacement of the core (same for all layers in the sandwich). The functions u_0^{*v}, v_0^{*v}, θ_x^{*v} and θ_y^{*v} are higher order terms in the series expansion, defined also in the mid-plane of the core layer.

The displacement continuity at the layer interfaces can be written as:

$$
\begin{aligned}
u^{e_1}\left(x, y, z_{e_1} - \frac{h_{e_1}}{2}, t\right) &= u^v\left(x, y, \frac{h_v}{2}, t\right) \\
v^{e_1}\left(x, y, z_{e_1} - \frac{h_{e_1}}{2}, t\right) &= v^v\left(x, y, \frac{h_v}{2}, t\right) \\
u^{e_2}\left(x, y, z_{e_2} + \frac{h_{e_2}}{2}, t\right) &= u^v\left(x, y, -\frac{h_v}{2}, t\right) \\
v^{e_2}\left(x, y, z_{e_2} + \frac{h_{e_2}}{2}, t\right) &= v^v\left(x, y, -\frac{h_v}{2}, t\right)
\end{aligned}
\tag{3}
$$

where the coordinates of layer mid-planes are:

$$
\begin{aligned}
z_{e_1} &= \frac{h_v}{2} + \frac{h_{e_1}}{2} \\
z_v &= 0 \\
z_{e_2} &= -\frac{h_v}{2} - \frac{h_{e_2}}{2}
\end{aligned}
\tag{4}
$$

Applying displacement continuity conditions at the layer interfaces, one obtains:

$$
\begin{aligned}
u_0^{e_1} &= \frac{h_{e_1}}{2}\theta_x^{e_1} + u_0^v + \frac{h_v}{2}\theta_x^v + \frac{h_v^2}{4}u_0^{*v} + \frac{h_v^3}{8}\theta_x^{*v} \\
v_0^{e_1} &= \frac{h_{e_1}}{2}\theta_y^{e_1} + v_0^v + \frac{h_v}{2}\theta_y^v + \frac{h_v^2}{4}v_0^{*v} + \frac{h_v^3}{8}\theta_y^{*v} \\
u_0^{e_2} &= -\frac{h_{e_2}}{2}\theta_x^{e_2} + u_0^v - \frac{h_v}{2}\theta_x^v + \frac{h_v^2}{4}u_0^{*v} - \frac{h_v^3}{8}\theta_x^{*v} \\
v_0^{e_2} &= -\frac{h_{e_2}}{2}\theta_y^{e_2} + v_0^v - \frac{h_v}{2}\theta_y^v + \frac{h_v^2}{4}v_0^{*v} - \frac{h_v^3}{8}\theta_y^{*v}
\end{aligned}
\tag{5}
$$

These relations allows us to retain the rotational degrees of freedom of the face layers, while eliminating the corresponding in-plane displacement ones. Hence, the generalized displacement field has 13 mechanical unknowns.

2.1 Linear strains

2.1.1 Viscoelastic core

The non-zero linear strains associated with the assumed displacement field for the viscoelastic core layer are:

$$
\varepsilon_x^v = \frac{\partial u_0^v}{\partial x} + z\frac{\partial \theta_x^v}{\partial x} + z^2\frac{\partial u_0^{*v}}{\partial x} + z^3\frac{\partial \theta_x^{*v}}{\partial x}
$$

$$
\varepsilon_y^v = \frac{\partial v_0^v}{\partial y} + z\frac{\partial \theta_y^v}{\partial y} + z^2\frac{\partial v_0^{*v}}{\partial y} + z^3\frac{\partial \theta_y^{*v}}{\partial y}
$$

$$
\gamma_{yz}^v = \theta_y^v + 2zv_0^{*v} + 3z^2\theta_y^{*v} + \frac{\partial w_0}{\partial y}
$$

$$
\gamma_{xz}^v = \theta_x^v + 2zu_0^{*v} + 3z^2\theta_x^{*v} + \frac{\partial w_0}{\partial x} \tag{6}
$$

$$
\gamma_{xy}^v = \left(\frac{\partial u_0^v}{\partial y} + \frac{\partial v_0^v}{\partial x}\right) + z\left(\frac{\partial \theta_x^v}{\partial y} + \frac{\partial \theta_y^v}{\partial x}\right)
$$

$$
+ z^2\left(\frac{\partial u_0^{*v}}{\partial y} + \frac{\partial v_0^{*v}}{\partial x}\right) + z^3\left(\frac{\partial \theta_x^{*v}}{\partial y} + \frac{\partial \theta_y^{*v}}{\partial x}\right)
$$

which can be written in the form:

$$
\varepsilon_x^v = \varepsilon_{x0}^v + z\kappa_x^v + z^2\varepsilon_{x0}^{*\ v} + z^3\kappa_x^{*v}
$$

$$
\varepsilon_y^v = \varepsilon_{y0}^v + z\kappa_y^v + z^2\varepsilon_{y0}^{*\ v} + z^3\kappa_y^{*v}
$$

$$
\gamma_{yz}^v = \gamma_{yz0}^v + z\kappa_{yz}^v + z^2\gamma_{yz0}^{*\ v} \tag{7}
$$

$$
\gamma_{xz}^v = \gamma_{xz0}^v + z\kappa_{xz}^v + z^2\gamma_{xz0}^{*\ v}
$$

$$
\gamma_{xy}^v = \gamma_{xy0}^v + z\kappa_{xy}^v + z^2\gamma_{xy0}^{*\ v} + z^3\kappa_{xy}^{*\ v}
$$

where ε_{x0}^v, ε_{y0}^v, γ_{xy0}^v, γ_{yz0}^v and γ_{xz0}^v are the core mid-surface strains, κ_x^v, κ_y^v, κ_{xy}^v, κ_{yz}^v and κ_{xz}^v represent the curvatures associated with the first order terms in the series expansion, $\varepsilon_{x0}^{*\ v}$, $\varepsilon_{y0}^{*\ v}$, $\gamma_{xy0}^{*\ v}$, $\gamma_{yz0}^{*\ v}$ and $\gamma_{xz0}^{*\ v}$ describe the strains associated with the second order terms and κ_x^{*v}, κ_y^{*v} and $\kappa_{xy}^{*\ v}$ correspond to curvatures associated with the third order terms.

2.1.2 Elastic laminated face layers

The non-zero linear strains associated with the assumed first order displacement field for these layers are:

$$\varepsilon_x^i = \frac{\partial u_0^i}{\partial x} + (z - z_i)\frac{\partial \theta_x^i}{\partial x}$$

$$\varepsilon_y^i = \frac{\partial v_0^i}{\partial y} + (z - z_i)\frac{\partial \theta_y^i}{\partial y}$$

$$\gamma_{yz}^i = \theta_y^i + \frac{\partial w_0}{\partial y} \tag{8}$$

$$\gamma_{xz}^i = \theta_x^i + \frac{\partial w_0}{\partial x}$$

$$\gamma_{xy}^i = \left(\frac{\partial u_0^i}{\partial y} + \frac{\partial v_0^i}{\partial x}\right) + (z - z_i)\left(\frac{\partial \theta_x^i}{\partial y} + \frac{\partial \theta_y^i}{\partial x}\right)$$

where $i = e_1, e_2$.

These linear strains for the elastic layers can also be written in the form:

$$\varepsilon_x^i = \varepsilon_{x0}^i + z\kappa_x^i$$

$$\varepsilon_y^i = \varepsilon_{y0}^i + z\kappa_y^i$$

$$\gamma_{yz}^i = \gamma_{yz0}^i \tag{9}$$

$$\gamma_{xz}^i = \gamma_{xz0}^i$$

$$\gamma_{xy}^i = \gamma_{xy0}^i + z\kappa_{xy}^i$$

where: ε_{x0}^i, ε_{y0}^i, γ_{xy0}^i, γ_{yz0}^i and γ_{xz0}^i are the layer mid-surface strains, and κ_x^i, κ_y^i and κ_{xy}^i describe the curvatures for layer $i = e_1, e_2$.

2.2 Constitutive relations

As for the constitutive relations, we consider that fibre-reinforced laminae in elastic multi-layers (e_1) and (e_2), and viscoelastic core (v) are characterized as orthotropic. Constitutive equations for each lamina in the sandwich may then be expressed in the principal material directions $(x_1, x_2, x_3 = z)$, and for the zero transverse normal stress situation, as [11]:

$$\left\{\begin{array}{c} \sigma_{11} \\ \sigma_{22} \\ \sigma_{23} \\ \sigma_{13} \\ \sigma_{12} \end{array}\right\} = \left[\begin{array}{ccccc} Q_{11} & Q_{12} & 0 & 0 & 0 \\ Q_{12} & Q_{22} & 0 & 0 & 0 \\ 0 & 0 & Q_{44} & 0 & 0 \\ 0 & 0 & 0 & Q_{55} & 0 \\ 0 & 0 & 0 & 0 & Q_{66} \end{array}\right] \left\{\begin{array}{c} \varepsilon_{11} \\ \varepsilon_{22} \\ \gamma_{23} \\ \gamma_{13} \\ \gamma_{12} \end{array}\right\} \tag{10}$$

where σ_{ij} are stress components, ε_{ij} and γ_{ij} are strain components, and Q_{ij} are reduced stiffness coefficients. Expressions for the reduced quantities mentioned above can be found in [11]. For

the viscoelastic core layer, the reduced stiffness coefficients Q_{ij} are complex quantities, since the complex modulus approach was used in this work, using the elastic-viscoelastic principle. In this case, the usual engineering moduli may be represented by complex quantities:

$$
\begin{aligned}
E_1(i\omega) &= E_1'(\omega)(1 + i\eta_{E_1}(\omega)) \\
E_2(i\omega) &= E_2'(\omega)(1 + i\eta_{E_2}(\omega)) \\
G_{12}(i\omega) &= G_{12}'(\omega)(1 + i\eta_{G_{12}}(\omega)) \\
G_{23}(i\omega) &= G_{23}'(\omega)(1 + i\eta_{G_{23}}(\omega)) \\
G_{13}(i\omega) &= G_{13}'(\omega)(1 + i\eta_{G_{13}}(\omega)) \\
\nu_{12}(i\omega) &= \nu_{12}'(\omega)(1 + i\eta_{\nu_{12}}(\omega))
\end{aligned}
\tag{11}
$$

where the prime quantities denote storage moduli, associated material loss factors are represented by the letter η, ω represents frequency of vibration and $i = \sqrt{-1}$ is the imaginary unit. Furthermore, in Equation (11), E, G and ν denote Young's moduli, shear moduli and Poisson's ratio, respectively.

The definition of constitutive relations of a laminate is usually made in terms of stress resultants. These forces and moments are defined separately for the viscoelastic core (v) and the elastic multilayered laminates (e_1) and (e_2) [12].

3 Finite Element Formulation

The equations of motion for the plate are obtained by applying Hamilton's principle, using an eight node serendipity plate element with 13 mechanical degrees of freedom per node:

$$
[M]\{\ddot{a}\} + [K]\{a\} = \{F\}
\tag{12}
$$

where $\{a\}$ and $\{\ddot{a}\}$ are mechanical degrees of freedom and corresponding accelerations, respectively, $[M]$ and $[K]$ are the mass and complex stiffness matrices, respectively, and $\{F\}$ is the externally applied mechanical load vector. One should note that the viscoelastic behaviour of the core translates into a complex stiffness matrix $[K]$.

Assuming harmonic vibrations, the final equilibrium equations are given by:

$$
\left[[K(\omega)] - \omega^2[M]\right]\{a\} = \{F\}
\tag{13}
$$

The forced vibration problem is solved in the frequency domain, which implies the solution of the following linear system of equations for each frequency point:

$$
\left[[K(\omega)] - \omega^2[M]\right]\{a(\omega)\} = \{F(\omega)\}
\tag{14}
$$

where $\{F(\omega)\} = \mathcal{F}(\{F(t)\})$ is the Fourier transform of the time domain force history $\{F(t)\}$.

For the free vibration problem, Equation (14) reduces to the following non-linear eigenvalue problem:

$$[[K(\omega)] - \lambda_n^* [M]] \{a\}_n = \{0\} \tag{15}$$

where, the complex eigenvalue λ_n^* is written as:

$$\lambda_n^* = \lambda_n (1 + i\eta_n) \tag{16}$$

and λ_n is the real part of the complex eigenvalue and η_n is the corresponding modal loss factor.

The non-linear eigenvalue problem is solved iteratively using ARPACK [13] with a shift-invert transformation. The iterative process is considered to have converged when:

$$\frac{\|\omega_i - \omega_{i-1}\|}{\omega_{i-1}} \leq \epsilon \tag{17}$$

where ω_i and ω_{i-1} are current and previous iteration values for the real part of the particular eigenfrequency of interest, respectively, and ϵ is the convergence tolerance.

Eigenvalues and modal loss factors are also determined in this work from the frequency domain response [1, 2].

4 Model validation

The validation of the sandwich plate finite element model for passive damping is conducted comparing eigenfrequencies and modal loss factors for a beam and a plate with a central viscoelastic core layer and two equal thickness face layers made of an isotropic material [14, 15].

4.1 Cantilever sandwich beam

The viscoelastic material is assumed to have constant properties with frequency, and simulations are conducted using two different values for the material loss factor η. The beam is 177.8 mm long by 12.7 mm wide and the thickness of the viscoelastic layer is $h_v = 0.127$ mm, while the isotropic elastic face layers have a thickness of $h_{e_1} = h_{e_2} = 1.524$ mm. Material properties for the isotropic elastic layers are $E = 69$ GPa, $\nu = 0.3$ and $\rho = 2766$ kg m^{-3}, and for the isotropic viscoelastic core $E = 1.794(1 + i\eta)$ MPa, $G = \frac{E}{2(1+\nu)}$, $\nu = 0.3$ and $\rho = 968$ kg m^{-3}.

The beam was discretised using 30 elements in the length dimension and one in the width dimension, and excited with an impulsive 1 N force at the free end. The natural frequencies and corresponding modal loss factors are shown in Table 1 for the first three bending modes, and compared with the ones reported in [14], using 2D eight node quadrilateral plane strain elements to model the beam in the thickness-length plane.

The present results were obtained using the frequency domain technique described in the previous section, as the eigenvalue technique presented convergence issues for this case. The obtained frequency domain curves are presented in Figures 2 through 4, and one can conclude that the present model produces results which are fairly close to the ones reported in [14]. Except for the fundamental modal loss factor in the case where $\eta = 0.1$, all results have a deviation that is less than 4%.

Aurélio L. Araújo, Cristóvão M. Mota Soares and Carlos A. Mota Soares

	Present		[14]	
η	f_n [Hz]	η_n [%]	f_n [Hz]	η_n [%]
	64.2	3.48	64.2	2.81
0.1	296.8	2.39	296.9	2.42
	745.0	1.56	745.5	1.53
	65.3	14.99	65.6	14.76
0.6	298.8	13.39	299.5	13.92
	746.8	8.77	747.3	9.12

Table 1: Cantilever sandwich beam: natural frequencies (f_n) and corresponding modal loss factors (η_n) for different material loss factors (η) of the viscoelastic core
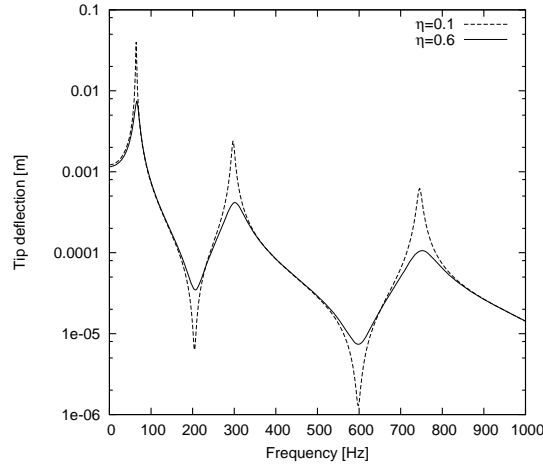
Figure 2: Magnitude of frequency response plot for cantilever sandwich beam

4.2 Clamped sandwich plate

The viscoelastic material is assumed to have constant properties with frequency, and the material loss factor $\eta = 0.5$. The plate in-plane dimensions are 348 mm × 304.8 mm and the thickness of the viscoelastic core layer is $h_v = 0.254$ mm, while the isotropic elastic face layers have a thickness of $h_{e_1} = h_{e_2} = 0.762$ mm. Material properties for the isotropic elastic layers are $E = 69.9$ GPa, $\nu = 0.3$ and $\rho = 2740 \, \text{kg m}^{-3}$, and for the isotropic viscoelastic core $E = 2.67008(1 + i\eta)$ MPa, $G = \frac{E}{2(1+\nu)}$, $\nu = 0.49$ and $\rho = 999 \, \text{kg m}^{-3}$.

The plate was discretised using a 12 × 12 mesh, and natural frequencies and modal loss factors are extracted by solving the associated eigenvalue problem. The obtained results are presented in Table 2 and compared with the ones reported by [15], using shell elements for the face layers and volume elements for the core.

From the results one can conclude that the present model produces results which are fairly close to the ones reported in [15], specially considering that the present model has only 3465 degrees of freedom (DOF), against the reported 10248 DOF.
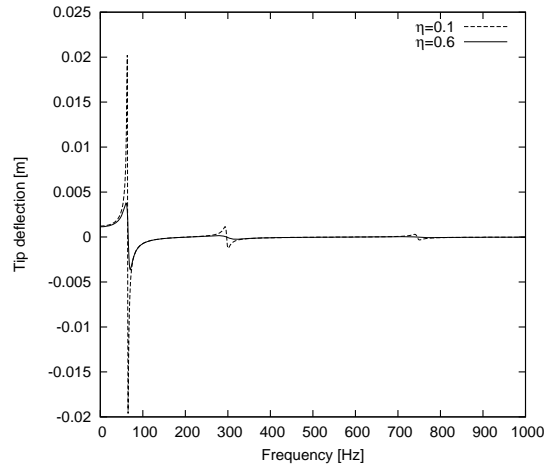
Figure 3: Real part of frequency response plot for cantilever sandwich beam
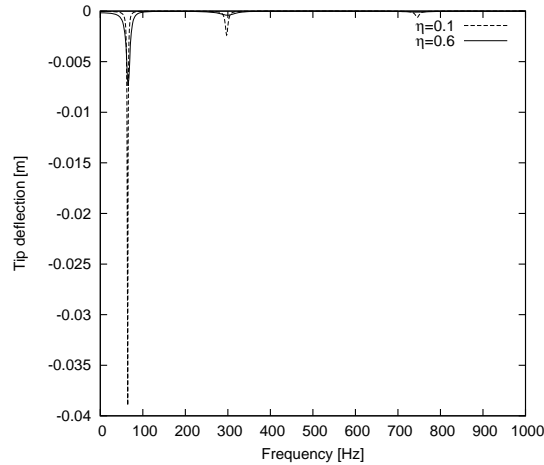
Figure 4: Imaginary part of frequency response plot for cantilever sandwich beam

5 Conclusions

A new sandwich plate finite element model has been developed for the analysis of the dynamic response of plate structures with passive damping. The model is capable of handling a high variety of layer configurations and the complex modulus approach was used, along with frequency domain response analysis, allowing for frequency dependent material data. The developed eight node finite element model presents a good behavior with passive damping, when compared to reference solutions.

Acknowledgements

Present		[15]	
f_n [Hz]	η_n [%]	f_n [Hz]	η_n [%]
87.66	18.86	87.4	18.95
150.10	16.30	148.9	16.45
170.99	15.27	169.9	15.40
229.07	13.42	223.9	19.90
243.79	13.23	241.0	13.45
292.21	11.79	289.8	11.95

Table 2: Clamped sandwich plate: natural frequencies (f_n) and corresponding modal loss factors (η_n) for a viscoelastic core with material loss factor $\eta = 0.5$

REFERENCES

[1] A.D. Nashif, D.I.G. Jones, and J.P. Henderson, *Vibration Damping*, John Wiley & Sons, (1985).

[2] C.T. Sun and Y.P. Lu, *Vibration Damping of Structural Elements*, Prentice Hall PTR, Englewood Cliffs, New Jersey, (1995).

[3] R.A. DiTaranto, "Theory of vibratory bending for elastic and viscoelastic layered finite-length beams", *ASME Journal of Applied Mechanics*, 32, 881–886 (1965).

[4] D.J. Mead and S. Markus, "The forced vibration of a three-layer, damped sandwich beam with arbitrary boundary conditions", *AIAA Journal*, 10, 163–175 (1969).

[5] D.K. Rao, "Frequency and loss factors of sandwich beams under various boundary conditions", *International Journal of Mechanical Engineering Science*, 20, 271–278 (1978).

[6] M.J. Yan and E.H. Dowell, "Governing equations of vibrating constrained-layer damping sandwich plates and beams", *ASME Journal of Applied Mechanics*, 39, 1041–1046 (1972).

[7] M.D. Rao and S. He, "Dynamic analysis and design of laminated composite beams with multiple damping layers", *AIAA Journal*, 31, 736–745 (1993).

[8] B.E. Douglas and J.C.S. Yang, "Transverse compressional damping in the vibratory response of elastic-viscoelastic beams", *AIAA Journal*, 16, 925–930 (1978).

[9] R.A.S. Moreira, J.D. Rodrigues, and A.J.M. Ferreira, "A generalized layerwise finite element for multi-layer damping treatments", *Computational Mechanics*, 37, 426–444 (2006).

[10] R.A.S. Moreira and J.D. Rodrigues, "A layerwise model for thin soft core sandwich plates", *Computers and Structures*, 84, 1256–1263 (2006).

[11] A.L. Araujo, H.M.R. Lopes, M.A.P. Vaz, C.M. Mota Soares, J. Herskovits, and P. Pedersen, "Parameter estimation in active plate structures", *Computers and Structures*, 84, 1471–1479 (2006).

[12] A.L. Araujo, C.M. Mota Soares, J. Herskovits, and P. Pedersen, "Development of a finite element model for the identification of mechanical and piezoelectric properties through gradient optimisation and experimental vibration data", *Composite Structures*, 58, 307–318 (2002).

[13] D.C. Sorensen, "Implicitly restarted Arnoldi/Lanczos methods for large scale eigenvalue calculations", *Technical Report TR95-13*, Department of Computational and Applied Mathematics, Rice University, Houston, Texas, (1995).

[14] E.M. Daya and M. Potier-Ferry, "A numerical method for nonlinear eigenvalue problems application to vibrations of viscoelastic structures", *Computers and Structures*, 79, 533–541 (2001).

[15] L. Duigou, E.M. Daya, and M. Potier-Ferry, "Iterative algorithms for non-linear eigenvalue problems. Application to vibrations of viscoelastic shells", *Computational Methods in Applied Mechanics and Engineering*, 192, 1323–1335 (2003).

APPLICATION OF CORK COMPOUNDS IN SANDWICH STRUCTURES FOR VIBRATION DAMPING

J. Santos Silva[*], R.A.S. Moreira[†], and J. Dias Rodrigues[*]

[*]Faculdade de Engenharia da Universidade do Porto (FEUP)
Universidade do Porto
Rua Dr. Roberto Frias, 4200-465 Porto, Portugal
e-mail: jdr@fe.up.pt, santos.silva.joao@fe.up.pt, web page: http://www.fe.up.pt

[†]Departamento de Engenharia Mecânica da Universidade de Aveiro (UA)
Universidade de Aveiro
Campus de Santiago, 4200-465 Aveiro, Portugal
e-mail: rmoreira@ua.pt, web page: http://www.ua.pt

Key words: Sandwich plate, Cork compound, Damping, Complex modulus, Layerwise.

Summary. *The remarkable damping over a broad temperature range and thermal insulation properties of cork make it an excellent material to be applied on integrated and surface damping treatments in sandwich structures improving its dynamic behavior. Experimental analysis and numerical modeling of sandwich structures with cork compound layers is therefore essential for a better understanding of the cork compound influence on the dynamic properties of a layered structure. In this paper an evaluation study on the dynamic properties of a set of sandwich plates with cork compound cores inside two aluminium faces is performed. For this purpose, three test samples were assembled following the described configuration, using cork compounds with different properties (density, granulometry and thickness). To numerically simulate these layered plates, a partial layerwise plate finite element, with a multilayer configuration, was developed and integrated in a* MATLAB *finite element code. The dynamic properties of the cork compounds are included in the* FE *model by using the material complex modulus in a direct frequency analysis procedure. For the different cork compounds hereby considered, the extensional complex modulus was previously identified by using a specific experimental methodology which simulates a semidefinite two degree of freedom system, where the cork compound test sample represents the complex stiffness. From the complex modulus data, both extensional storage modulus and loss factor of the cork compound were obtained. The experimental evaluation of the dynamic properties of the sandwich plates was performed carrying out an experimental modal analysis on each test specimen, being measured a set of mobility* FRF *functions. Additionally, the developed layerwise plate element was validated through the comparison between the measured driving point* FRFs *and the* FEM *predicted ones.*

1 Introduction

Natural cork is a material with a remarkable combination of properties that has been used for long time in various applications like fishing boats, shoe soles and wine bottle sealers [1]. It

is obtained from the bark of a species of oak, the Quercus Suber. The cellular structure of cork provides an effective dissipation energy mechanism. The application of cork in anti-vibratory supports is one of the few examples of this capability. The applicability of cork compounds in sandwich plates to improve damping performance and its dynamic behavior characterization motivated the present study.

In order to perform an accurate analysis of a sandwich plate with a cork compound core and have a representative numerical model, it is necessary to characterize the cork compound dynamic properties and their frequency dependence. Despite the wide range of applications of cork compound, the material dynamic properties, namely its storage modulus and loss factor, are scarcely described and unavailable.

To understand and study the behavior of a structure with cork compound based passive damping treatments, a representative and accurate numerical model is also required. The layerwise theory, based on a piecewise description of the displacement field [2], has evidenced a good accuracy in the simulation of the damping layer effects in surface and integrated passive damping treatments, as published in [3, 4] and is adopted in this study.

2 Sandwich plates with cork compound core: Experimental results

The experimental study hereby presented consists of a modal analysis to characterize the dynamic behavior of sandwich plates with two aluminum faces and a cork compound core. The main purpose is to determine the cork compound influence on the dynamic response, namely its influence on its modal damping ratios, as well as to obtain its natural frequencies. To verify the influence of cork compound formulation parameters, three sandwich plates with different cork compound cores have been tested and its results were compared. To perform the experimental modal analysis of the test samples a set of frequency response functions were measured from which the modal parameters were identified by using the modal analysis functionality of the MATLAB toolbox SDT® [5]. The measurement of frequency response functions (FRFs) on the test samples will also, further on, allow to validate the formulated plate element by comparison between the experimental FRFs and the FE predicted ones.

2.1 Description of the test samples

The test samples analyzed are sandwich plates with a cork compound core and two aluminum faces as schematically depicted in figure 1. Three test samples were manufactured, each one with a different grain size and density cork compound core, as illustrated in figure 2. In table 1 a short description of the test samples cork compound cores is presented.

2.2 Experimental setup

The experimental setup was built up in order to achieve free boundary conditions to the sandwich plates. Each test sample was suspended from a frame by two very thin nylon cables, while the electromechanical exciter was also suspended from another independent frame, as depicted in figure 3.
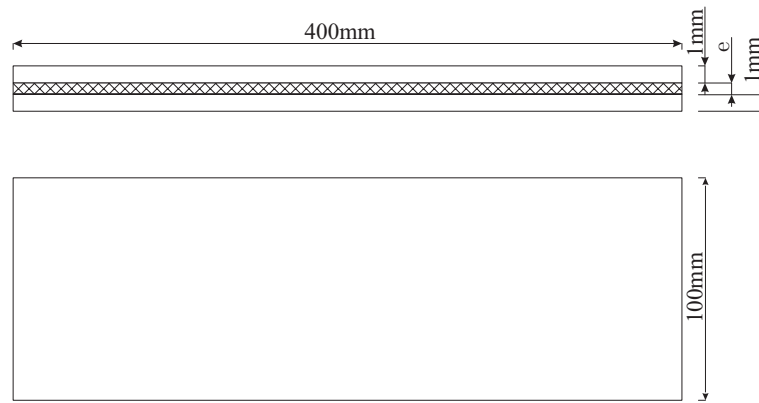
Figure 1: Schematic drawing of the test samples

(a) 8003　　　　　　(b) 8123　　　　　　(c) 8303

Figure 2: Cork compound samples

Table 1: Test samples characteristics

Sample reference	Cork compound reference	Core description	Thickness e [mm]
PLT8003	8003	• small grain • low density	1.2
PLT8123	8123	• small grain • high density	1.2
PLT8303	8303	• coarse grain • high density	1.2
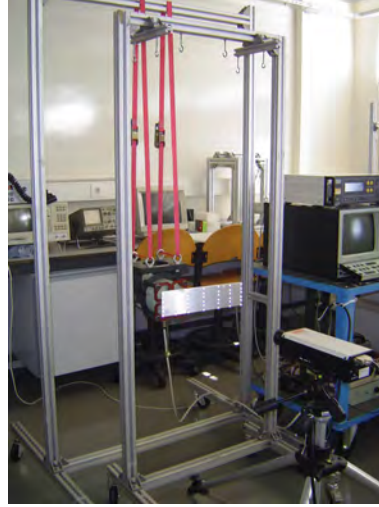
Figure 3: Assembled experimental setup

The measurement mesh, with 42 measurement points, is depicted by figure 4. The test samples were excited with an electromagnetic shaker (LDS-401) at point number 17, figure 4, being at that same point measured the exciting force with a piezoelectric force transducer (B&K-8203). The exciter was connected to the structure by a thin steel rod, allowing an high axial stiffness but a low bending stiffness connection, assuring a good directional control of the excitation force.
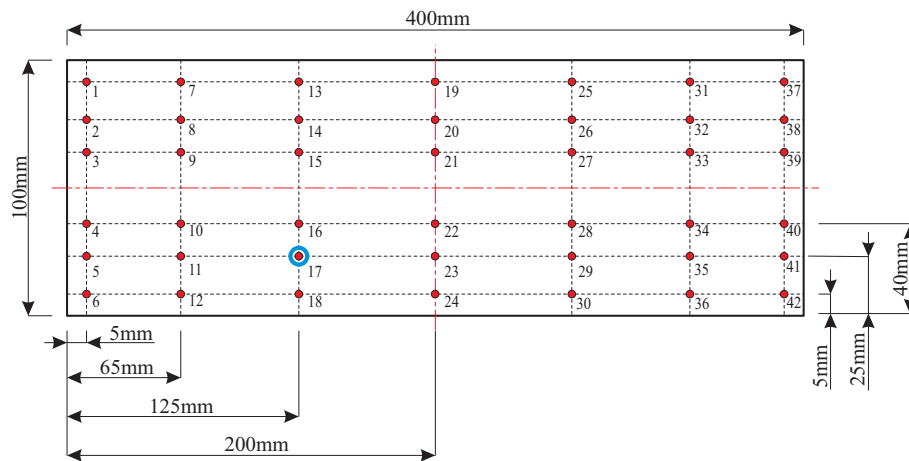
Figure 4: Measuring mesh

The response was measured in velocity at each point of the measuring mesh by a laser vibrometer (Polytec-OFV303) using the vibrometer controller (Polytec-OFV3001).
To acquire the response and the excitation force signals and estimate the frequency response

functions (FRFs), an FFT analyzer (B&K-2035) was used. The measurements were made in the frequency range $[0;\ 400]$ Hz.

2.3 Measured FRFs

For each test sample, a set of 42 mobility FRFs were measured corresponding to each measuring point. The driving point FRFs, obtained at the excitation point 17, are depicted from figure 5 to figure 7 for the three test samples in the measured frequency range $[0;\ 400]$ Hz.
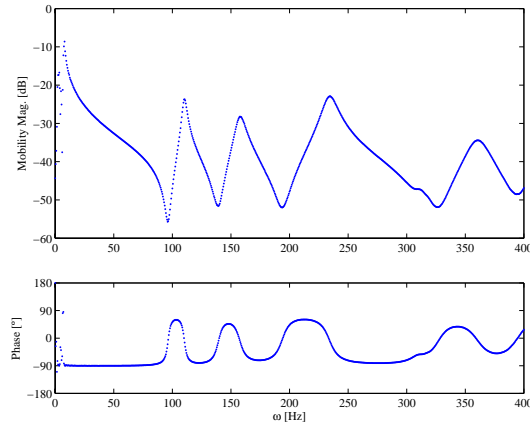
Figure 5: Driving point mobility of sample PLT8003
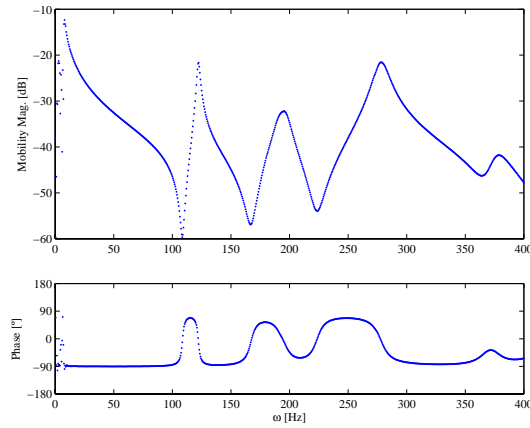
Figure 6: Driving point mobility of sample PLT8123
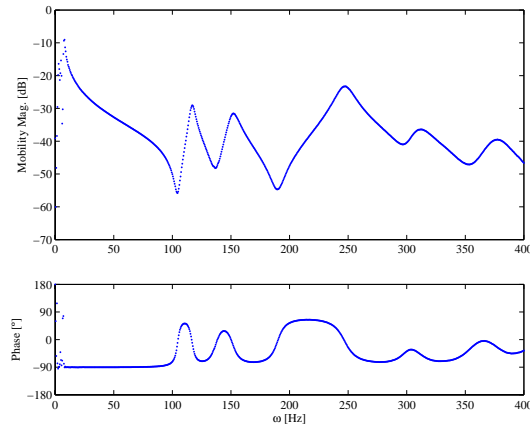
Figure 7: Driving point mobility of sample PLT8303

2.4 Modal identification

From the measured FRFs, in a first stage, a multi degree of freedom (MDOF) technique, which uses the "Least Squares Complex Exponential" time domain algorithm, was applied in order to identify the natural frequencies and damping values for each mode. In a second stage, the residues were identified with a "Least Squares Frequency Domain" technique.

The natural frequencies and damping ratios identified in the frequency range $[0; 400]$ Hz are summarized in tables 2 and 3 and are also represented in figures 8 and 9 for the three test samples.

Table 2: Natural frequencies of the sandwich test samples

Sample reference	Natural frequencies [Hz]				
	1st mode	2nd mode	3rd mode	4th mode	5th mode
PLT8003	110.27	157.70	233.96	311.36	360.22
PLT8123	122.19	194.95	278.32	375.98	-
PLT8303	116.91	151.66	246.84	307.40	374.41

Table 3: Damping ratios of the sandwich test samples

Sample reference	Damping ratio [%]				
	1st mode	2nd mode	3rd mode	4th mode	5th mode
PLT8003	1.73	2.75	2.62	1.88	2.76
PLT8123	1.12	3.89	2.28	2.49	-
PLT8303	2.10	3.18	3.19	3.45	3.57
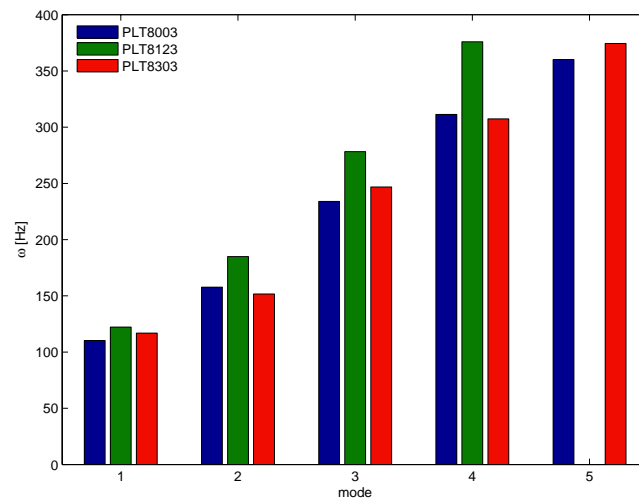
Figure 8: Natural frequencies of the three sandwich test samples
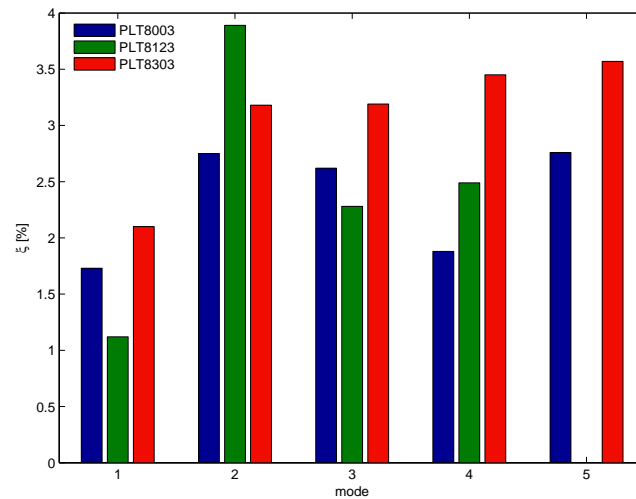
Figure 9: Damping ratios of the three sandwich test samples

2.5 Discussion of the modal identification results

From the results identified in the previous section it can be said that:

- comparing the natural frequencies of sample PLT8003 and sample PLT8123, it can be seen that the second ones are higher than the first ones; this fact is due to the higher density of the cork used in PLT8123 which makes the plate structure stiffer than if it was used the same cork compound as used in sample PLT8003 (figure 8);

- the grain size also influences directly the sample stiffness, as it can be seen in figure 8; the natural frequencies of sample PLT8303, which has a coarse grain size cork compound, are lower than the ones presented for sample PLT8003 and PLT8123 evidencing that a coarse grain size mandatory reduces the structure stiffness;

- in all the test samples it is evident that the introduction of a cork compound layer in the sandwich plates improves its damping capability (figure 9);

- when comparing the damping ratios of sample PLT8003 (small grain, low density) with sample PLT8123 (small grain, high density), as it can be seen in figure 9, it is evident that sample PLT8123 presents a lower damping ratio than the ones obtained for sample PLT8003 for modes 1 and 3 which represent the predominantly flexural plate modes . The opposite happens for modes 2 and 4, which are predominantly torsional plate modes, being the damping ratios of PLT8123 higher than the ones of PLT8003, suggesting that high density cork compounds should provide a better damping capability when submitted to shear strains, at predominantly torsional modes, while low density ones should provide a better structural damping for predominantly flexural modes;

- it is also suggested from figure 9 that a coarse grain size introduces a bigger structural damping than small grain size which can be seen when comparing damping ratios from sample PLT8303 with the ones from samples PLT8003 and PLT8123; again, the only observed exception occurs at the second mode.

3 Cork compound dynamic properties

In order to establish a representative numerical model of the sandwich test samples it is necessary to identify the properties of the cork compounds. Since cork compound has viscoelastic properties [6], it is necessary to obtain its frequency dependent dynamic properties, such as its storage modulus and loss factor [7, 8]. The experimental characterization methodology adopted to identify the cork compound properties is based on the evaluation of the dynamic response of a semi-definite two degrees of freedom system with two masses m and M and which stiffness and damping is represented by an element of cork compound, as schematized in figure 10 and illustrated in figure 11. The dynamic excitation $f(t)$ is applied on mass m.

Modeling the stiffness and damping properties of the cork compound through a complex stiffness $\bar{K}$, the material complex modulus is directly identified [9] from both the frequency
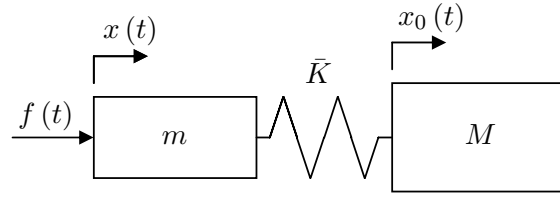
Figure 10: Two degree of freedom analytical model

Figure 11: Experimental setup

response function accelerance $A(\text{j}\omega)$ and transmissibility function $T(\text{j}\omega)$ measured on the experimental setup as follows [10],

$$\bar{E}(\text{j}\omega) = \frac{\omega^2 M T(\text{j}\omega)}{1 - T(\text{j}\omega)} \frac{h}{A_E} \tag{1}$$

$$\bar{E}(\text{j}\omega) = \frac{\omega^2 M \left(m A(\text{j}\omega) - 1\right)}{(M + m) A(\text{j}\omega) - 1} \frac{h}{A_E} \tag{2}$$

where h and A_E represent, respectively, the thickness and cross-section area of the cork compound element. Once the complex modulus $\bar{E}(\text{j}\omega) = E(\omega)\left(1 + \text{j}\eta(\omega)\right)$ is identified, afterwards the cork compound extensional storage modulus $E(\omega)$ and loss factor $\eta(\omega)$ can be easily obtained.

The identified extensional storage modulus and loss factor from both the accelerance and transmissibility frequency functions are represented in figures 12-14 for the three different cork compounds used.

4 Plate layerwise formulation

Assuming that the sandwich plate can be divided into several homogeneous and isotropic layers, each layer can be individually treated as a thick plate following the Reissner-Mindlin assumptions and ensuring the interface continuity directly at the respective displacement field description. Each layer is modeled according to the following assumptions:

- extensional and shear deformations of all the layers are accounted;

(a) Extensional storage modulus $E(\omega)$
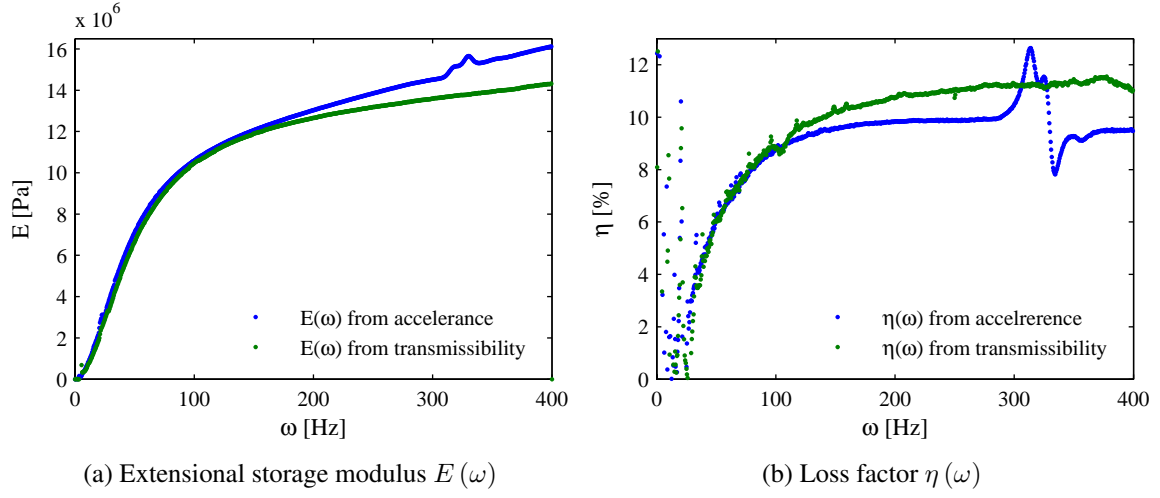
(b) Loss factor $\eta(\omega)$

Figure 12: Storage modulus and loss factor for cork compound 8003

(a) Extensional storage modulus $E(\omega)$
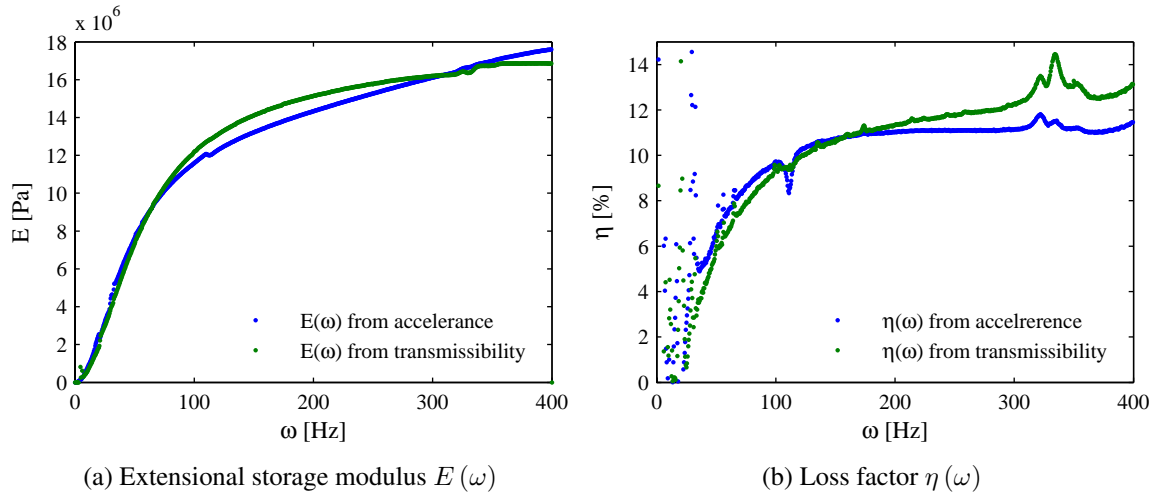
(b) Loss factor $\eta(\omega)$

Figure 13: Storage modulus and loss factor for cork compound 8123

- deformation through the thickness is neglected;

- translational and rotary inertias of all the layers are accounted;

- linear theories of elasticity and viscoelasticity are used;

- materials are isotropic and homogeneous in each layer.

(a) Extensional storage modulus $E\left(\omega\right)$ (b) Loss factor $\eta\left(\omega\right)$
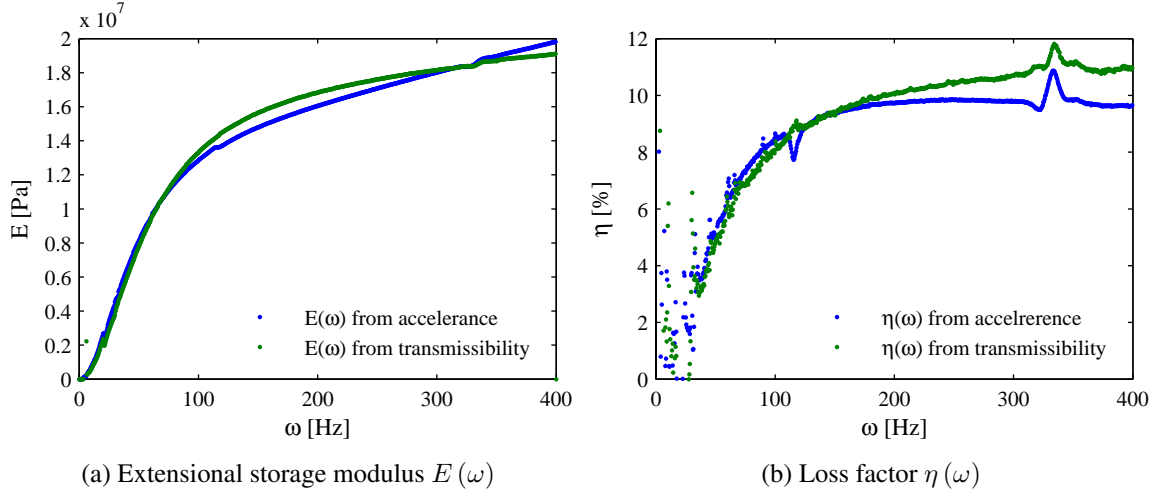
Figure 14: Storage modulus and loss factor for cork compound 8303

4.1 Displacement field

Considering a generic layer k with thickness h_k of a laminate plate, figure 15, the displacement field $\{\mathbf{u}_k\}$ can be described by

$$\{\mathbf{u}\}_k = \left\{ \begin{array}{c} u_k \\ v_k \\ w_k \end{array} \right\} = \left\{ \begin{array}{c} \frac{u_t+u_b}{2} + z\frac{u_t-u_b}{h} \\ \frac{v_t+v_b}{2} + z\frac{v_t-v_b}{h} \\ w \end{array} \right\} \tag{3}$$

where u_b, u_t and v_b, v_t represent, respectively, inplane x-displacements and y-displacements at bottom and top interfaces while w represents the normal displacement.

From equation (3) it can be noticed that the continuity condition between layers is established directly from the displacement field definition.

The displacement field (3) can be expressed through a set of generalized variables as,

$$\{\mathbf{u}\}_k = [\mathcal{N}]_k \{d\} \tag{4}$$

where $[\mathcal{N}]_k$ is an allocation matrix and vector $\{d\}$ represents the generalized displacement field and is defined as,

$$\{d\} = \left\{ \begin{array}{cccccccc} w & \dots & u_b^k & v_b^k & u_t^k & v_t^k & \dots \end{array} \right\}^{\mathrm{T}} \tag{5}$$

4.2 Strain and stress fields

The strain field $\{\varepsilon\}_k$ for a generic layer is obtained from the displacement through the application of a linear differential operator matrix $[\mathcal{L}]$ and it is expressed as,
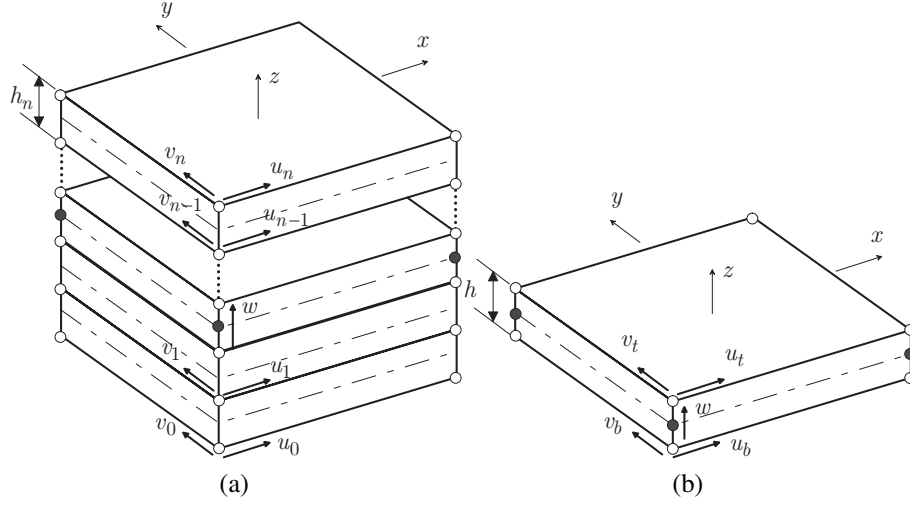
Figure 15: Layer displacement field

$${\varepsilon}_k = [\mathcal{L}] {\mathbf{u}}_k . \tag{6}$$

According to (4), the strain field can be directly related to the generalized displacement field through the deformation matrix $[\mathcal{B}]_k$,

$${\varepsilon}_k = [\mathcal{B}]_k {d} \tag{7}$$

where

$$[\mathcal{B}]_k = [\mathcal{L}] [\mathcal{N}]_k . \tag{8}$$

The stress field in the generic layer is determined from its strain field and the material constitutive relation represented by the constitutive matrix $[\mathcal{D}]_k$,

$${\sigma}_k = [\mathcal{D}]_k {\varepsilon}_k \tag{9}$$

If the layer material is frequency dependent, like cork compound layers in sandwich structures, and a complex modulus approach is adopted, the constitutive matrices become complex frequency dependent and require a special solution method, like the direct frequency analysis [11] to determine a frequency domain solution. Regardless the constitutive model approach and solution method adopted, the finite element spatial model formulation is completely independent of the viscoelastic constitutive relation.

4.3 Velocity field

The velocity field for a generic layer can be obtained by deriving the displacement field from (3) in order to time. Using matrix $[\mathcal{N}]_k$, which relates the displacement field with the generalized displacements vector ${d}$, the velocity field can be expressed as,

$$\{\dot{\mathbf{u}}\}_k = [\mathcal{N}]_k \left\{\dot{d}\right\} \tag{10}$$

where $\left\{\dot{d}\right\} = \left\{ \begin{array}{ccccccc} \dot{w} & \dots & \dot{u}_b & \dot{v}_b & \dot{u}_t & \dot{v}_t & \dots \end{array} \right\}^{\mathrm{T}}$ represents the time derivative of the generalized displacements vector.

4.4 Strain energy

The laminate strain energy is given by summing up the contribution of each individual layer,

$$\Pi^P = \sum_{k=1}^{n} \left(\frac{1}{2} \int_{\Omega_k} \{\varepsilon\}_k^{\mathrm{T}} \{\sigma\}_k \, \mathrm{d}\Omega_k \right) = \sum_{k=1}^{n} \left(\frac{1}{2} \int_A \int_{z_k} \{\varepsilon\}_k^{\mathrm{T}} [\mathcal{D}]_k \{\varepsilon\}_k \, \mathrm{d}z_k \, \mathrm{d}A \right) \tag{11}$$

where A is the layer area, $z_k \in \left[-\frac{h_k}{2}, \frac{h_k}{2} \right]$ and n denotes the number of layers.

Introducing the relation (7), the strain energy (11) can be rewritten as,

$$\Pi^P = \sum_{k=1}^{n} \frac{1}{2} \int_A \int_{z_k} \{d\}^{\mathrm{T}} [\mathcal{B}]_k^{\mathrm{T}} [\mathcal{D}]_k [\mathcal{B}]_k \{d\} \, \mathrm{d}z \, \mathrm{d}A. \tag{12}$$

4.5 Kinetic energy

Like the strain energy, the laminate kinetic energy is given by the sum of each layer kinetic energy,

$$\Pi^K = \sum_{k=1}^{n} \left(\frac{1}{2} \int_{\Omega_k} \{\dot{\mathbf{u}}\}_k^{\mathrm{T}} [\mathcal{J}]_k \{\dot{\mathbf{u}}\}_k \, \mathrm{d}\Omega_k \right) \tag{13}$$

where $[\mathcal{J}]_k$ represents the inertia layer matrix that is a diagonal matrix which terms are the generic layer mass density ρ_k.

Inserting the generalized velocities on expression (13), the kinetic energy can be rewritten as

$$\Pi^K = \sum_{k=1}^{n} \left(\frac{1}{2} \int_A \int_{z_k} \left\{\dot{d}\right\}^{\mathrm{T}} [\mathcal{N}]^{\mathrm{T}} [\mathcal{J}] [\mathcal{N}] \left\{\dot{d}\right\} \, \mathrm{d}z_k \, \mathrm{d}A \right) = \sum_{k=1}^{n} \left(\frac{1}{2} \int_A \int_{z_k} \left\{\dot{d}\right\}^{\mathrm{T}} [J]_k \left\{\dot{d}\right\} \, \mathrm{d}z \, \mathrm{d}A \right) \tag{14}$$

where matrix $[J]$ is defined as

$$[J]_k = [\mathcal{N}]_k^{\mathrm{T}} [\mathcal{J}]_k [\mathcal{N}]_k. \tag{15}$$

4.6 Virtual work of the surface loads

If the face layers of the layered plate are loaded by a normal distributed load $\{q\}$ then the virtual work δW done by this external load will be given by

$$\delta W = \int_S \{\delta d\}^T \{q\} \, \mathrm{d}S \tag{16}$$

where S is the surface area of the distributed load and $\{\delta d\}$ is the virtual displacement.

4.7 Variational formulation

In the derivation of the variational statement equivalent to the governing differential equations of motion, as well as the natural boundary conditions, the Hamilton's principle is adopted. Taking the kinetic and strain energies expressions as well as the virtual work, performing the variation and an integration by parts, the Hamilton's principle yields the variational statement or the weak form of the governing differential equations, expressed as,

$$\sum_{k=1}^{n} \int_A \int_{z_k} \{\delta d\}^{\mathrm{T}} [J]_k \left\{ \ddot{d} \right\} \mathrm{d}z_k \, \mathrm{d}A + \sum_{k=1}^{n} \int_A \int_{z_k} \{\delta d\}^{\mathrm{T}} [\mathcal{B}]^{\mathrm{T}} [\mathcal{D}] [\mathcal{B}] \{d\} \, \mathrm{d}z_k \, \mathrm{d}A - \int_S \{\delta d\}^{\mathrm{T}} \{q\} \, \mathrm{d}S = 0 \tag{17}$$

5 Multilayer finite element formulation

The proposed multilayer finite element is based on the 4-node isoparametric quadrilateral element. The multilayer element is three-dimensional and described in the global cartesian axes (X, Y, Z), its stiffness and mass matrices being computed in the local cartesian axes (x, y, z), where the plane $x - y$ is coplanar with the element face. The local geometry of the finite element is mapped into a natural coordinate system (ξ, η, ζ), where the ζ direction is coincident with the z direction, in which the standard set of bilinear interpolation functions are used to interpolate the geometry and the generalized displacement field within the finite element domain.

The elemental generalized displacements $\{d^e\}$ are approximated through the set of interpolation functions and the elemental vector of nodal displacements $\{d_i^e\}$ as follows,

$$\{d^e\} = [N] \{d_i^e\} \tag{18}$$

where matrix $[N]$ is the so-called shape functions matrix.

5.1 Weak form finite element discretization

The global weak form stated in (17) can be expressed as a sum of the elemental integral forms, allowing the definition of the matrices and vectors at the element domain. Therefore, summing up the contributions of the n_E finite elements, the discretized global weak form is given by

$$\sum_{e=1}^{n_E} \left(\{\delta d_i^e\}^{\mathrm{T}} \sum_{k=1}^{n} \int_{A^e} \int_{z_k^e} [N]^{\mathrm{T}} [J]_k [N] \, \mathrm{d}z_k^e \, \mathrm{d}A^e \left\{\ddot{d}_i^e\right\} \right.$$

$$+ \{\delta d_i^e\}^{\mathrm{T}} \sum_{k=1}^{n} \int_{A^e} \int_{z_k^e} [N]^{\mathrm{T}} [\mathcal{B}]_k^{\mathrm{T}} [\mathcal{D}]_k [\mathcal{B}]_k [N] \, \mathrm{d}z_k^e \, \mathrm{d}A^e \{d_i^e\} \tag{19}$$

$$\left. - \{\delta d_i^e\}^{\mathrm{T}} \int_{A^e} [N]^{\mathrm{T}} \{q\} \, \mathrm{d}A^e \right) = 0.$$

From the weak form finite elements discretization (19), the element mass $[M^e]$ and stiffness $[K^e]$ matrices, as well as the elemental load vector $\{f_i^e\}$, are defined as,

$$[M^e] = \sum_{k=1}^{n} [M_k^e] = \sum_{k=1}^{n} \int_{A^e} \int_{z_k^e} [N]^{\mathrm{T}} [J]_k [N] \, \mathrm{d}z_k^e \, \mathrm{d}A^e \tag{20}$$

$$[K^e] = \sum_{k=1}^{n} [K^e] = \sum_{k=1}^{n} \int_{A^e} \int_{z_k^e} [B]_k^{\mathrm{T}} [\mathcal{D}]_k [B]_k \, \mathrm{d}z_k^e \, \mathrm{d}A^e \tag{21}$$

$$\{f_i^e\} = \int_{A^e} [N]^{T} \{q\} \, \mathrm{d}A^e \tag{22}$$

where $[B]_k = [\mathcal{B}]_k [N]$ is the deformation matrix for a generic layer k of the multilayer finite element.

In this finite element formulation, the shear locking is alleviated through the application of a generalization of the MITC [12] approach to the layerwise model. Details on this strategy and its implementation into the layerwise formulation can be found in [3, 4].

5.2 Equations of motion

The global semi-discrete equations of motion for the laminate or sandwich plate are obtained by assembling the elemental matrices through the connectivity matrices that relate the global degrees of freedom vector $\{d_i\}$ with the elemental ones $\{d_i^e\}$.

Since the intended main application of this multilayer finite element is the modeling of sandwich or layered composite plates with cork compound layers which properties are frequency dependent, the global stiffness matrix will be frequency dependent and complex when a complex modulus approach (CMA) is used. Therefore, the global equations of motion can be written as [13],

$$[M] \{\ddot{d}_i\} + \left([K] + \left[\bar{K}(\mathrm{j}\omega)\right]\right) \{d_i\} = \{f_i\} \tag{23}$$

where $[M]$ is the mass matrix, $[K]$ is the stiffness matrix of the laminate elastic layers and $\left[\bar{K}\left(\mathrm{j}\omega\right)\right]$ is the frequency dependent stiffness matrix of the viscoelastic layers. The vectors $\{d_i\}$ and $\{f_i\}$ represent respectively the time dependent displacements and excitation forces at the FE degrees of freedom.

6   Finite element analysis of the experimental samples

To verify the physical representativeness of the developed multilayer finite element as well as the accuracy of the measured cork properties, a FEM analysis of the sandwich test samples analyzed in section 2 was performed. A finite element spatial model was generated with 600 three layer elements (30 by 20 element mesh), allowing a mesh node to be coincident to the location of point 17 depicted in figure 4 and where excitation was applied.

Using a complex modulus approach (CMA) and a direct frequency analysis (DFA) procedure to include the frequency dependent properties of cork compounds, which are represented by the identified complex modulus at section 3, the driving point mobility frequency response function was generated in the bandwidth $[0;\ 400]$ Hz for the three test samples.

In figures 16-18, a comparison between the FEM predicted and the experimental driving point mobility function $(Y_{17,17}(\omega))$ is shown for the sandwich test samples PLT8003, PLT8123 and PLT8303.
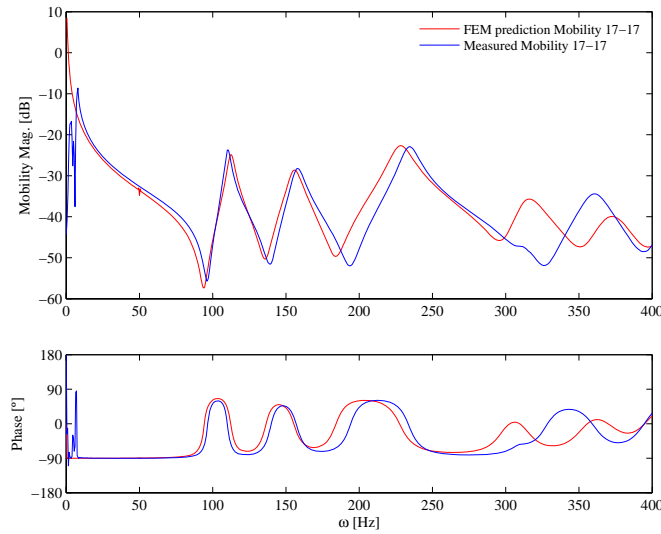
Figure 16: Comparison between FEM predicted and experimental driving point mobility of PLT8003

6.1   Discussion of results

As it can be seen in figure 16, the five modes identified experimentally, for sample PLT8003, are also visible in the FEM predicted mobility. For the first three modes, the predicted mo-
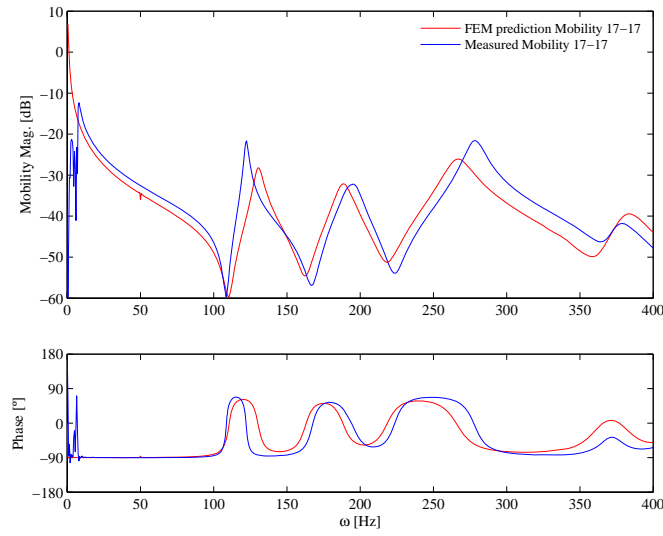
Figure 17: Comparison between FEM predicted and experimental driving point mobility of PLT8123
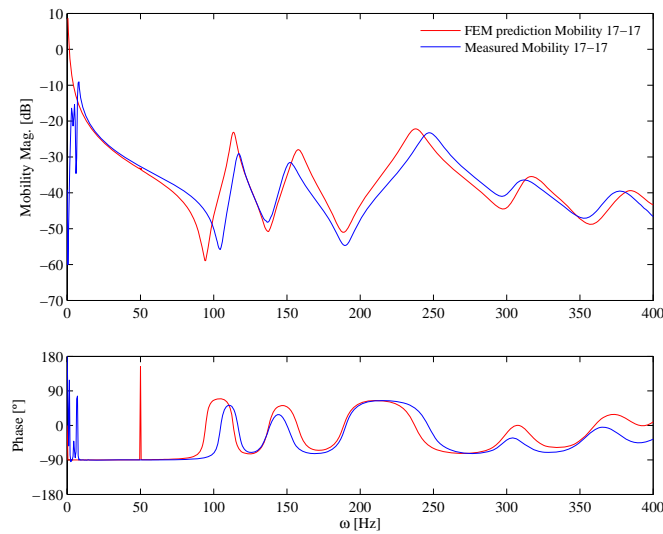
Figure 18: Comparison between FEM predicted and experimental driving point mobility of PLT8303

bility is quite close to the measured one suggesting that for this frequency range, [0; 250] Hz, the cork properties determined and the multilayer FE correctly describe the sandwich plate. Above 250 Hz, apparently the predicted mobility does not follows the experimental one but the natural frequencies predicted for the fourth and fifth mode are not very far from the identified experimentally, despite the fact of the FRF magnitude difference.

In figure 17, the four modes of sample PLT8123 identified experimentally can also be found in the FEM predicted mobility. In this case, the predicted mobility reproduces quite well the experimental one but, the increasing of difference while the mode frequencies increases suggests that the material properties at high frequencies might not be as accurate as at the low frequency range.

For sample PLT8303, figure 18, the predicted mobility presents all five modes identified experimentally and the predicted FRF reproduced quite well the measured one, suggesting that the accuracy of the cork compound properties determined for sample 8303 is very good and the spatial FEM model is representative of the sandwich plate.

7 Conclusion

According to the obtained results, cork compounds can be used as an effective passive damping treatment in sandwich or multilayer structures, increasing the host structure damping capability due to its viscoelastic properties. Moreover, the experimental characterization methodology of the frequency dependent cork compound properties allows an accurate identification of the extensional storage modulus and loss factor functions which can be included in the finite element model for a direct frequency analysis evaluation of the frequency response functions. Finally, the multilayer plate finite element hereby presented, which comprises an arbitrary number of layers, was experimentally validated through the comparison between FE predicted and measured frequency response functions showing a good representativeness and adequacy to model laminates and sandwich plates with cork compound cores.

Acknowledgments

REFERENCES

[1] Fortes, M.A., Rosa, M.E. and Pereira, H., *A Cortiça*, IST Press, Lisboa, 2004.

[2] Reddy, J.N., *Mechanics of Laminated Composite Plates Theory and Analysis*, CRC Press, 1997.

[3] Moreira, R.A.S., Dias Rodrigues, J., Ferreira, A.J.M., A generalized layerwise finite element for multi-layer damping treatments, *Computational Mechanics*, **37** (5): 426 444, 2005

[4] Moreira, R.A.S., Dias Rodrigues, J., A layerwise model for thin soft core sandwich plates. *Computers and Structures*, **84** (19-20): 1256-1263, 2006.

[5] Balmès, E., Structural Dynamics Toolbox, V5.0, SDTools, France, 2001.

[6] Mano, J.F., The viscoelastic properties of cork, *Journal Material Sciences*, **37**:257-263, 2002.

[7] ASTM, D4092-908 standard terminology relating to dynamic mechanical measurements on plastics, *In Annual Book of ASTM Standards*, **vol. V**:345-347, 1990.

[8] Jones, D.I.G., *Handbook of viscoelastic vibration damping*, John Wiley, 2001.

[9] Allen, B.R., A direct complex stiffness test system for viscoelastic material properties, *In Proceedings of 3th Smart Structures and Materials (SPIE)*, San Diego, CA, USA, 1996.

[10] Moreira, R.A.S. and Dias Rodrigues, J., An efficient experimental methodology for viscoelastic complex modulus identification, *In II ECCOMAS Thematic Conference on Smart Structures and Materials*, Lisbon, Portugal, 2005.

[11] Moreira, R. and Rodrigues, J.D., Constrained damping layer treatments: the finite element modelling, *Journal of Vibration Control*, **10**(4): 575-595, 2004.

[12] Dvorkin EN, and Bathe K-J A continuum mechanics based four-node shell element for general non-linear analysis, *Engineering Computations*, **1**: 77-88, 1984.

[13] Vasques, C.M.A., Moreira, R.A.S. and Dias Rodrigues, J., Viscoelastic damping: mathematical modeling and finite element implementation, *In Proceedings of the International Conference on Engineering Dynamics*, Carvoeiro, Portugal, 16-18 April 2007.

STRUCTURAL – ACOUSTIC DESIGN OF A MULTI-FUNCTIONAL SANDWICH BODY PANEL FOR AUTOMOTIVE APPLICATIONS

Christopher J. Cameron⋆, Per Wennhage⋆, Peter Göransson⋆ and Sven Rahmqvist†

⋆Centre for ECO^2 Vehicle Design
KTH Aeronautical and Vehicle Engineering,
Kungliga Tekniska Högskolan (KTH)
SE-100 44 STOCKHOLM, SWEDEN
e-mail: cjca@kth.se, web page: http://www.eco2vehicledesign.kth.se

†Technical Integration Engineer - Body Structure and Closures
Noise & Vibration Center
Saab Automobile AB
A2-1 TRV-05
SE-461 80,TROLLHÄTTAN,SWEDEN

Key words: Sandwich structures, Acoustic Modelling, Design Optimization.

Summary. *This paper deals with the design and optimization of a multi-functional vehicle body panel. An existing vehicle design has provided functional design requirements regarding acoustic, static, and dynamic behaviour with the aim to investigate the possibilities of replacing a traditional design by a novel, multi-functional design and to analyze and optimize this structure.*

1 INTRODUCTION

Common to all vehicles which transport either people or goods, is the need for certain functionality, such as e.g. protection and comfort, usually provided by a vehicle compartment, with different requirements depending on the vehicle application. For a passenger carrying vehicle, the compartment in general consists of the following components: body structure, acoustic treatments, and interior trim. Traditionally, these components have been designed, produced and assembled separately, each fulfilling different aspects of the protective functions, sometimes with considerable weight penalty but almost without exception with poor manufacturing efficiency and ergonomics during assembly.

To alleviate this, an approach based on simultaneous consideration of several such functions is investigated. The main objective is to investigate the potential benefits that may be realized in a multi-functional, integrated multi-layered sandwich design. In this study, the performance in terms of NVH (Noise Vibration and Harshness) and structural requirements of a proposed multi-functional component is investigated in an automotive context.

The vehicle of study in this case is a Saab 9-3 SportCombi. In selecting a panel for the study several areas of the vehicle were considered. The roof panel was chosen because it is relatively simple geometrically and relatively platform independent. Other panels such as the

hood, doors and floor panel were considered, but deemed too constrained by governmental regulations [1, 2] and too geometrically complex for an initial study. The roof structure is also subject to governmental requirements however to a lesser extent[3].

The roof construction is also an acoustically relevant panel. External noise can be carried into the vehicle compartment via airborne paths such as leaky seals or via structural vibrations. From an NVH standpoint, noise can be defined as audible sound within the frequency range of 30-4000Hz and vibration as tactile vibration within the frequency range of 30-200Hz [4]. The air cavity within the passenger compartment of a typical European waggon type car will have a first acoustic mode in the region of 65-75Hz [4] wich can be excited by vibrations of adjacent panels causing discomfort for the occupants. Transmission of airborne noise into the vehicle is prevented using materials with high sound absorption capability in strategic places. Vibrations are suppressed by optimizing the structure and applying damping materials, of which the necessary amount and location is difficult to calculate. The materials and construction of the roof structure can directly effect the excitation of cavity modes and absorption of airborne sound.

The current roof assembly of the vehicle consists of outer sheet metal, stamped steel cross-members, dampening material, adhesive, sound absorbant, and a multi-layer inner roof liner.

In the current paper, two possible design concepts are discussed wherein the roof panel sheet metal, cross beams located near the B and C pillars of the vehicle, as well as all damping layers and the inner roof liner are replaced by a single sandwich construction. Two sandwich configurations are proposed and described in detail in section 4. Both concepts are optimized according to current design requirements and evaluated acoustically. Results of the optimization and acoustic analysis are given as well as a discussion of their interpretation.

2 METHOD

To establish the current state of the art, acoustic testing was first performed on the roof construction in-situ followed by a laboratory test of the isolated roof. These results are compared in order to asses the baseline performance of the component.

NXNastran finite element analysis software was used to perform a wide variety of static and dynamic analysis of the existing roof structure. Based on the data gained in testing and analysis together with information provided in Saab's own engineering documentation, a novel design is suggested and the new panel is weight optimized against a set of static and dynamic constraints.

Advanced acoustic analysis of optimized panels was performed using a new software tool for analyzing porous materials in Nastran.

3 DETERMINATION OF BASELINE SYSTEM CHARACTERISTICS

3.1 Acoustic Characteristics

The sound reduction index (SRI) is used to quantify the difference in sound power between incident and transmitted sound waves through a medium. For these tests, a diffuse field is assumed wherein sound waves are considered equally likely from all angles.

Christopher J. Cameron, Per Wennhage, Peter Göransson and Sven Rahmqvist

The sound reduction index, expressed in $\frac{1}{3}$ octave bands, obtained from [7] is calculated according as

$$R_I = L_{p1} - L_{In} - 6 - 10log(\frac{S_m}{S})\,dB \tag{1}$$

where:
S_m = area of the measurement surface
S = area of the test specimen ($S_m = S$ for these measurments)
L_{p1} = average sound pressure in the source room
L_{In} = average sound intensity level over the scanned panel surface

3.1.1 Full Vehicle Testing

A sound source was fed with a signal in the frequency range 250Hz -10kHz in the form of white noise. The average sound pressure was calculated by using microphones placed at 24 random locations during the course of testing. Sound transmission loss for the roof system was measured by scanning the roof with a sound intensity probe according to international standards[6]. Size constraints prohibited scanning of the entire roof at once, and so it was broken up into 9 subsections. Subsections 1–7 were drawn out based on the location of cross-beams and additional structure under the outer sheet metal. Subsections 8 & 9 are the centre and edges of the roof panel. The roof was redundantly scanned in an attempt to see the effect of sound leakage through door and window seals. Scanning was performed for two vehicle configurations, one with the inner roof liner and one without the inner roof liner. Figure 1 shows the subsection layout for scanning.

Sound intensity for each subsection was measured and SRI for each section was calculated. SRI for the entire roof is calculated using the area weighted average of the subsection values. Figure 2 shows the calculated SRI for all 9 sections measured as well as the mean values for sections 1–7 and 8–9. It should be noted that while values of SRI for each subsection are included, due to the relatively small area and short measuring time these individual values should only be considered for reference purposes.

In general, the trend for the individual sections agree with each other with the exception of a few measuring points. The largest deviation from the mean values occurs for subsection 8 in the region of 630hz, and subsection 7 from 1250Hz and upwards. A peak in absorption for sections 1,2, and 3 at the 800Hz measurement point can also be seen.

3.1.2 Component Testing

After full vehicle testing, the roof section was removed from the car and attached to a steel frame. All glass openings were replaced with chip-board panels and thick sound insulation material. This was done in an effort to eliminate any potential flanking transmission and allow

Christopher J. Cameron, Per Wennhage, Peter Göransson and Sven Rahmqvist
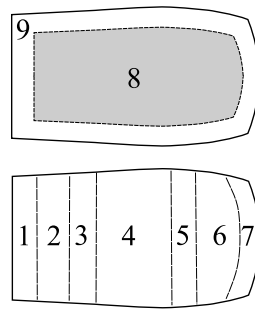
Figure 1: Full Vehicle Testing setup at SAAB
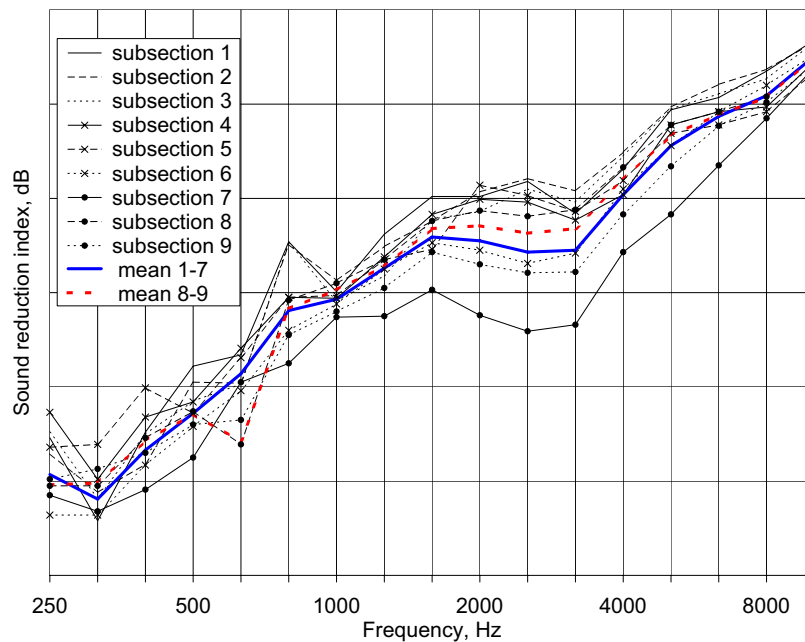
Figure 2: Sound Reduction Index measured at SAAB

a more isolated analysis of the roof construction. The structure was mounted between the reverberant and anechoic rooms at the Marcus Wallenberg Laboratory for Sound and Vibration Research (MWL) at KTH with the exterior section of the roof facing the reverberant room. Figure 3 shows the roof as mounted in MWL for testing. A sound source in the reverberant room was fed using a signal between 100Hz-5khz in the form of white noise. Average sound pressure levels in the reverberant room were measured using the rotating microphone. Measurements were performed in according to international standards[7].

In the laboratory it was possible to measure the entire inner roof at once in addition to the individual subsections. This enables SRI to be measured directly rather calculated as a sum of weighted averages. Figure 4 shows a comparison of SRI for the roof as tested in MWL, and the

Christopher J. Cameron, Per Wennhage, Peter Göransson and Sven Rahmqvist

Figure 3: Roof mounted in MWL for testing

results of full vehicle testing at SAAB, both with and without the interior roof panel.
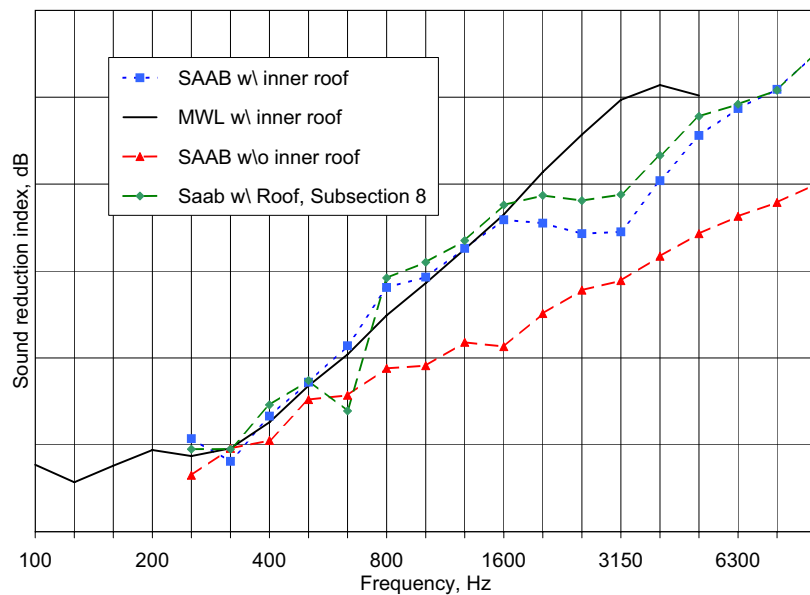
Figure 4: MWL Lab and SAAB full vehicle comparison

From the curves in figure 4 it can be seen that up to 1.6kHz, there is very good agreement between the full vehicle testing performed at SAAB and the laboratory testing performed at MWL. Above 1600Hz there is significant deviation between the laboratory measurements and the mean value calculated from the full vehicle testing. Initially, it was thought that leakage through window and door seals was the cause of this discrepancy. While there may still be some leakage through these seals, some brief calculations show that the glass in the windshield and side windows may be a larger contributor. Glass has a reduced sound reduction index compared to the full roof structure in the frequency range in question. Whatever the source, an indicator that sound leackage takes place can be seen in subsection 8. This section is measured further away from the glass surfaces and any potential leakage sources and shows a higher sound reduction index through the frequency range in question. For the laboratory case where

the glass was removed and replaced with chip board and sound insulation, the curve does not deviate as in full vehicle testing. For reference purposes,the curve for sound reduction index without the inner roof panel as obtained at Saab is also included.

3.2 FE Static/Dynamic requirements

In order to establish a complete set of design requirements for the replacement roof system, it was necessary to evaluate the existing construction. For this purpose, a complete Nastran finite element model was provided by SAAB Automobile as well as comprehensive design documentation. From this documentation, two specific design criteria were chosen to be examined in this study.

External bodywork is required to fulfil a "palm loading test" wich simulates the load applied by a customer washing the vehicle. Under a defined load, the deformation of the panel must not exceed predefined magnitude and no residual deformation may be present after the load is removed. Dynamically, a local panel mode criteria is also defined stating the minimum allowable natural frequency for a body panel.

These structural characteristics were studied by way of finite element calculations using the model provided by Saab. Stiffnesses and deformation behaviour of additional components targeted for replacement but not defined by the chosen requirements were also studied. Additional simulations under differing loading and boundary conditions than those specified in design documentation were also performed to obtain a general understanding of the total structures behaviour. All of this information was used to create a basic starting point for creating a new roof system.

4 New Roof Structure

Both of the proposed concepts consist of four layers; two external skin panels with typical aluminium properties, one layer of structural foam with properties of Divinycell H100, and one layer of acoustic foam, see Figure 5. One concept is symmetric with respect to face sheet properties, and one nonsymmetric. The nonsymmetric configuration is perforated on the side facing the passenger compartment, and solid at outer finish surface. Geometry of the perforations is also shown in Figure 5

4.1 Structural Modelling

For the initial calculations the acoustic foam is given a fixed thickness of 15mm. The acoustic foam modelled is considerably softer than the structural foam, having a Youngs modulus in the range of 0.1 MPa. This leads to a resulting sandwich panel that is distinctly non-typical of most structural sandwich panels. Perforations are advantageous from an acoustic perspective because a proportion of incident sound waves pass into the structure and are absorbed rather than reflected. The higher degree of perforation, the higher the acoustic absorption (see figure6), however the structural capability is obviously reduced.
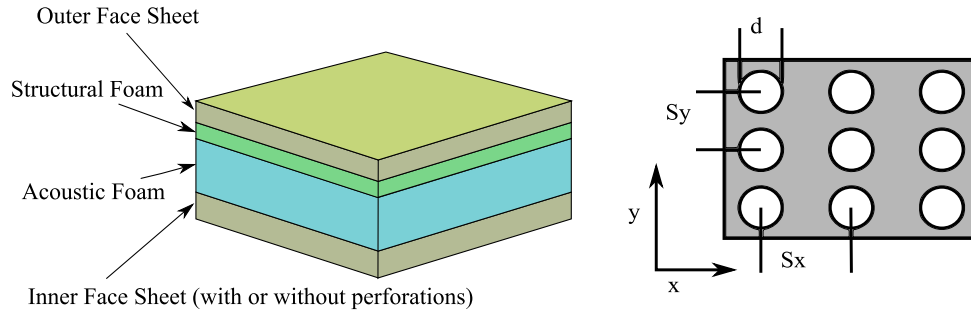
Figure 5: The Four Layer Sandwich Structure and Perforation Geometry
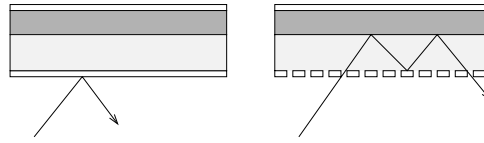
Figure 6: Incident sound wave behaviour for non-perforated and perforated face sheets

For a panel perforated with circular holes in a rectangular pattern as in Figure 5, the relative density can be calculated as follows [9]:

$$\frac{\rho^*}{\rho} = 1 - \left[\frac{\pi}{8}\left(1 - \frac{S_x - 2d}{S_x}\right)\left(1 - \frac{S_y - 2d}{S_y}\right)\right] \tag{2}$$

Additionally, from [9] we can extrapolate an equation for the relative youngs modulus of the material:

$$E^* = \frac{E}{1 - \pi d^2/\left(\sqrt{3}Sx^2\right)}\left(1 - \frac{\pi}{2\sqrt{3}}\left(1 - \frac{S_x - d}{S_x}\right)^2\right)^{(2S_x - d)/(0.8S_x)} \tag{3}$$

To obtain a value for the effective poissons ration, data from [8] was used to extract a value for the given ratio of $\frac{Sx-2d}{Sx}/\frac{Sy-2d}{Sy}$. In this case, a value of $\frac{\rho^*}{\rho} = 0.45$ was used. These equivalent properties were used to model the perforations in the second panel configuration.

An FE model of a sandwich panel was constructed by extruding the mesh for the outer sheet metal in the existing roof. Each panel was modelled using approx. 235000 3D CHEXA elements [12]. Translational DOF 1,2,3 were restricted for all nodes along the sides and rear of the panel and along the bottom-most row of nodes across the front of the panel. This boundary condition was meant to approximately simulate of a panels in-service condition. A comparison of modal behaviour with the existing structure showed good agreement.

5   Structural Optimization

Both panel configurations were weight optimized using the method of moving asymptotes[10]. The optimization and mesh morphing software package Ropt created by Alfgam Optimering

Christopher J. Cameron, Per Wennhage, Peter Göransson and Sven Rahmqvist

AB[1] was used. Constraints were placed on the static displacement under load as well as the frequency of the first mode of the panel. Thickness of the internal face sheet,external face sheet, and structural foam were chosen as design variables. Changes in thickness were evenly distributed through each of the element layers in a given material. A lower limit for each layers thickness was defined so that the aspect ratio of CHEXA elements would not exceed 50.

An essentially static optimal solution was attained within 10 iterations for both configurations. Figure 7 shows the mass of the panel during optimization.
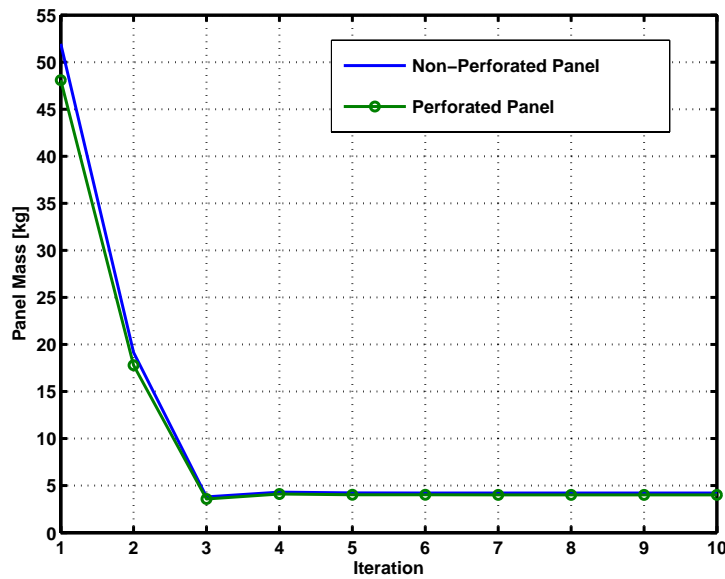
Figure 7: Mass of panel during optimization

Thickness [mm]		
Layer	Perforated	Non-Perforated
Inner Face	0.2000	0.2000
Structural Foam	4.7231	4.6004
Outer Face	0.2000	0.2000
Mass[kg]	4.0188	4.2150

Table 1: Optimized Panels Dimensions and Mass

---

[1] www.alfgam.se

Table 1 shows the final thickness of the optimized panel. Inner and outer face sheets for both panels were reduced to the minimum allowable thickness. Thickness of the structural foam varied approximately 2.60% between the perforated and non perforated panel. Acoustic foam thickness was held constant at 15mm. Final mass of the panels varied by approximately 4.65%. Results show that static displacement rather than natural frequency was the limiting factor for the optimization of the panels. Both panels fulfilled displacement constraints and exceeded frequency constraints by approximately 15%.

6 ACOUSTIC ANALYSIS

Acoustic analysis of the two optimized panels was performed using NXNastran in addition to the software CDH\EXEL by CDH AG. An air cavity model of the vehicle's passenger compartment was created wich followed the internal geometry of the BIW and roof panel. The cavity was mesh incompatible (i.e. no coincident nodes or elements) with the roof and consisted of approximately 1.7 million CTETRA elements.

Standard Nastran treats fluid elements and structural elements separately linking the translational degrees of freedom in a solid element to the first translational degree of freedom in a fluid element wich is interpreted as pressure [11]. Coupling of the fluid elements to the structure may be performed using automatic coupling algorithms within Nastran [13] or with external plug-ins. However, including also the volumetric coupling and the pressure fluctuations within a porous material, is not readily accessible in standard Nastran.

Here a recent module integrated with Nastran was used, CDH\EXEL , which augments the standard functionality of Nastran in coupled fluid – structure analysis by adding a fourth DOF to solid elements matrices representing open cell porous materials. Frequency dependant material properties can also be defined in a way not previously possible with Nastran. The augmented structural elements matrices are used to calculate the effects of fluid pressure within a porous media. Special algorithms to obtain coupling elements between the solid elements of a fluid cavity and the porous media are used. For a given node in the porous solid, the resulting DOF matrix will appear as in equation (4)

$$
\begin{bmatrix}
{}^{Nastran}_{solid}\mathbf{D}_{ij}(\omega) + {}^{Exel}_{solid}\mathbf{D}_{ij}(\omega) & symm \\
\hline
{}^{Exel}_{coupling}\mathbf{D}_{4j}(\omega) & {}^{Exel}_{fluid}\mathbf{D}_{44}(\omega)
\end{bmatrix}_{\substack{inode \\ jnode}}
\tag{4}
$$

The acoustic foam in both panels is modelled using the porous, elastic solid model. The perforated inner panel is also modelled as an elastic porous material. Properties such as frequency dependancy and flow resistivity come from laboratory testing performed at KTH.

The analysis performed is approximately equivalent to the full vehicle laboratory tests. A source is placed on a node within the air cavity in the region of the driver head, and excited at a certain frequency. Figure 8 shows the comparison of sound levels within the cavity for both panels. The perforated inner surface reduces the interior sound pressure levels by an order of magnitude, compared to the solid surface.
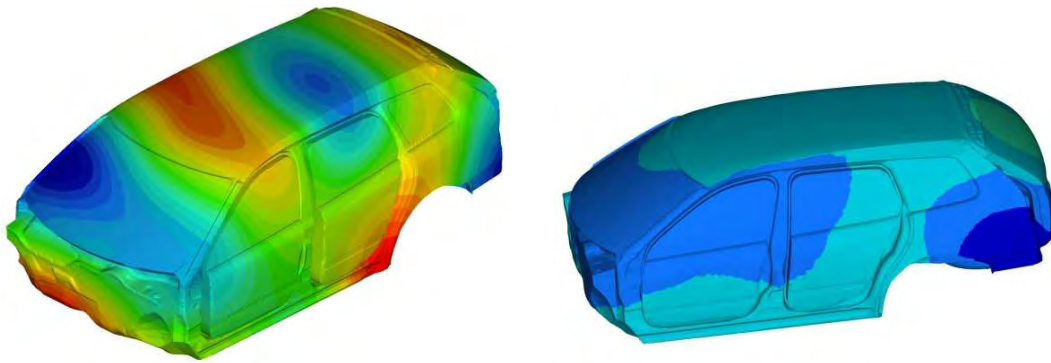
Figure 8: Acoustic pressure responses of the interior cavity for the two roof panel configurations studied at a frequency of 250 Hz.

Figure 9 shows the vibration displacement response of the two roof panel configurations studied here. Note the large difference in vibration amplitude, which is several orders of magnitude between the two cases, with the perforated panel vibrations being considerably lower. The changed stiffness of the complete, unsymmetric sandwich with perforated inner face, also changes the dynamic response of the whole roof.
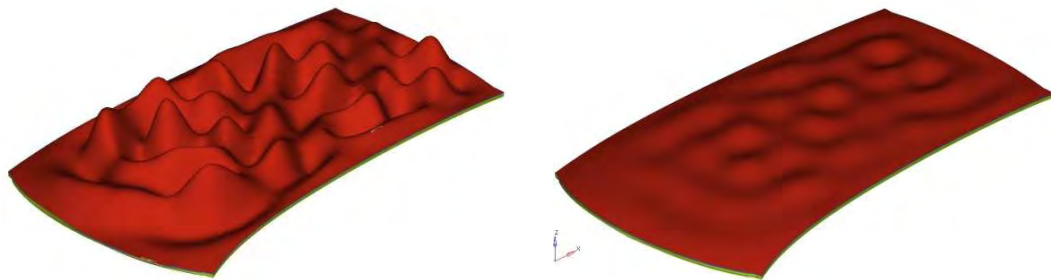
Figure 9: Vibration response of the two roof panel configurations for a frequency of 250 Hz.

As mentioned above, the perforation serves to introduce absorption to the interior acoustic field. However, it also reduces the structural-acoustic coupling between the inner panel surface and the passenger compartment cavity. This effect can be readily observed in Figure 9, and is the main reason for the substantial reductions observed. Obviously, the stiffness of is diminished and this is one of several conflicting mechanisms in the current problem.

7 DISCUSSION OF RESULTS

The structural optimization performed in this study yields a panel capable of fulfilling two critical design criteria at a vastly reduced mass compared to the current design. These criteria are however, not sufficient to completely define the requirements of the component. Additionally, while the loading conditions used in simulation are correct according to Saabs specifications, the simplified boundary conditions are not necessarily representative of the panels in-

service conditions. From a practical perspective the face sheets dimensions are not reasonable. The presented panels would be extremely sensitive to local impacts, and have poor durability.

One conclusion that could be drawn out of this optimization is that the material used is overly stiff and a weaker, lighter, cheaper material might be of interest. Alternatively, as the structural foam in this case no doubt caries a large amount of load, a weaker and lighter version of sandwich foam may be of interest.

Acoustic analysis shows that, despite a tremendous reduction in weight, and thus inertial damping, the optimized panels are capable of performing on nearly the same level as the current construction. However, the high degree of perforation used, rendering the panel almost totally acoustically transparent, could most probably be reduced.

8 FUTURE WORK

In future work, it is planned to increase the number of design variables within the optimization as well as to include the acoustic evaluation as part of the design cycle. Studies are planned to explore the effects of the acoustic foam layer thickness, perforation size and geometry on the panels structural and acoustic performance. The panel should also be modelled within the framework of the existing full vehicle model and its structural performance evaluated. This should take into account both static and dynamic structural performance. In the present study, the inner sheet is only loaded in tension which is beneficial for the analyses and other load cases should be considered. Additional engineering materials such as fibre reinforced composites will be examined for applicability to the face sheets.

9 ACKNOWLEDGEMENTS

REFERENCES

[1] National Highway Traffic Safety Administration *Federal Motor Vehicle Safety Standard No. 208; Occupant crash protection*, U.S.Department of Transportation, http://www.nhtsa.dot.gov/cars/rules/import/FMVSS/

[2] National Highway Traffic Safety Administration *Federal Motor Vehicle Safety Standard No. 214; Side impact protection*, U.S.Department of Transportation, http://www.nhtsa.dot.gov/cars/rules/import/FMVSS/

[3] National Highway Traffic Safety Administration *Federal Motor Vehicle Safety Standard No. 216; Roof crush resistance*, U.S.Department of Transportation, http://www.nhtsa.dot.gov/cars/rules/import/FMVSS/

[4] M. Harrison *Vehicle Refinement, Controlling Noise and Vibration in Road Vehicles* Elsevier Butterworth-Heinemann,2004

[5] Handbook of noise and vibration control,4th edition,*ISBN 85461 0731* ⓒ1979 Trade and Technical Press Limited, Crown House,Morden, Surrey.

[6] International Standard 9614-2:1996 *Acoustics-Determination of sound power levels of noise sources using sound intensity- Part 2:Measurement by scanning*, International Organization for Standardization(ISO)

[7] Swedish Standard SS-EN ISO 15186-1 *Acoustics-Measurement of sound insulation in buildings and of building elements using sound intensity-Part 1:Laboratory Measurements(ISO 15186-1:2000)*, Swedish Standards Institute

[8] M.Forskitt, J.R.Moon, and P.A.Brook. Elastic properties of plates perforated by elliptical holes *Appl. Math.Modelling*, **15**, 182–190, April 1991.

[9] K.A.Burgemeister and C.H.Hansen. Calculating resonance frequencies of perforated panels *Journal of Sound and Vibration*, **196**(4), 387–399, 1996.

[10] Krister Svanberg. The method of moving asymptotes-a new method for structural optimization *International Journal for Numerical Methods in Engineering*, **24**, 359–373, 1987.

[11] UGS Corp.*NX Nastran User Guide* UGS Corporation.

[12] UGS Corp.*NX Nastran Quick Reference Guide* UGS Corporation.

[13] UGS Corp.*NX Nastran Advanded Dynamic Analysis Users Guide* UGS Corporation.

[14] CDH AG *Poroelastic material modeling and anliysis with CDH\EXEL*

THE VIBRATION PROPERTIES OF SANDWICH PANELS; EIGENFREQUENCIES AND DAMPING

Robert Adams[*], Reza Maheri[*], and Julien Hugon[†]

[*]Department of Mechanical Engineering, University of Bristol, UK

[†]Alcatel Space, Etablissement de Cannes, France

Key words Vibration, eigenfrequencies, damping, theory, experiment

Summary *In this work, the inherent vibration damping mechanism in sandwich panels, including those with both aluminium and carbon fibre-reinforced plastic (CFRP) skins, is considered. It is first shown how the theoretical modal properties of the sandwich panel can be predicted from the stiffness and damping properties of its constituent components using the basic laminate theory, a first order shear deformation theory and a simple discretization method. Next, a finite element transcription of this approach is presented. It is shown to what extent this method can be implemented using a finite element software package to predict the overall damping value of a sandwich honeycomb panel for each specific mode.*

1 INTRODUCTION

In aerospace applications, there are many environmental inputs which can either limit performance or make it uncertain. An important consideration is the response to vibration excitation due to wind loading, gusts, or engine sources due to gas turbine or launch rocket excitation.. These excitations contain frequencies over a wide range, thus making it impossible to avoid coincidence with natural frequencies of the structure. These coincidences lead to resonance with the consequent build up of harmful levels of vibration. The only control against high levels of resonant vibration is damping; if the damping is too low, fatigue damage or malfunction of electronic components can occur. Damping arises from the material itself, acoustic radiation, friction at joints, or added damping treatments. In space or at high altitudes, acoustic radiation is small to zero. Frictional losses imply slipping which is to be avoided as it leads to fretting fatigue. Damping treatments add unwanted mass.

Fortunately, even advanced composites such as CFRP have significant damping properties compared with aerospace metals. This is due to the polymeric matrix. However, there is a complication. Just as strength and stiffness characteristics are anisotropic, so are the damping properties. Also, when multidirectional laminates are used, the laminate damping is a complex function of lamina orientation and position. Prediction of laminate damping is possible provided the damping and moduli of the individual laminae are known. However, when used as a sandwich panel with two skins and a lightweight [usually honeycomb] core, the predictive technology has to be considerably revised to allow for the dynamic properties of the core and the fact that it is dimensionally so much thicker than the skins. The objective

of this work is to show composite/honeycomb/composite plates. Eigen frequencies and damping values predicted by a Rayleigh-Ritz method and a NASTRAN finite element program will be compared with experimental results.how to predict the damping of sandwich panels together with the natural frequencies [which is a rather easier task]. Examples will be given for several composite/honeycomb/composite plates. Eigen frequencies and damping values predicted by a Rayleigh-Ritz method and a NASTRAN finite element program will be compared with experimental results. Excellent agreement will be demonstrated.

By using these proven predictive techniques, the designer can now safely calculate the contribution to the overall structural damping of the CFRP and core. He can therefore decide whether it is necessary to add further damping, such as using constrained layer treatment, and how much of it, thus minimising the added mass and improving the performance of the composite structure.

2 THEORY

Definitions and assumptions

The measure of damping used here is the specific damping capacity, SDC, defined as the ratio of the energy dissipated per cycle in the material to the maximum strain energy reached in one cycle of vibration. Thus,

$$\Psi = \frac{\Delta U}{U} \tag{1}$$

Ψ is related to other commonly used damping parameters such that

$$\frac{\Psi}{2\pi} = \eta = \frac{\Delta f}{f_n} = \frac{\delta}{\pi} = \frac{2c}{c_c} = 2\zeta \tag{2}$$

where η is the loss factor, δ is the logarithmic decrement, c is the viscous damping coefficient, ζ is the proportion of critical damping c_c, f_n is the natural frequency and Δf is the bandwidth of the amplitude *versus* frequency response curve at $1/\sqrt{2}$ of the resonance amplitude.

A strain-rate independent damping mechanism can be assumed for carbon fibre composites and honeycomb [2],[3]. Thus, both of the terms in equation (1) can be computed solely from the nature of the modal deformation (mode shape), and the modulus and damping values in the fibre direction and transverse to this direction (axes *1*, *2* and *3* in Fig. 1).

It is assumed that there exists mid-plane symmetry through the thickness of the sandwich in terms of material and geometry, and also in terms of the orientation of any orthotropic constituent parts. It is also assumed that the sandwich consists of two uniform skins of high normal stiffness and a uniform core which is of sufficient rigidity to render the sandwich mid-plane as the neutral bending axis of the whole sandwich cross-section.

A Mindlin-type, first order shear deformation predominates in the sandwich plate, in which case the total rotation of the plate cross-sections will consist of not only the rotation due to the bending slope but also the rotation due to the interlaminar shearing in the plate. In this

situation, and for small lateral deformations, a straight line normal to the mid-plane before deformation will remain straight but no longer normal after deformation. We take a simplified approach in estimating the strain energy of a sandwich with thin, layered FRP skins, in that we treat the sandwich as a whole as consisting of 'layers' of transversely isotropic materials, albeit of different mechanical properties and geometry. In so doing, however, we apportion the strain energy generated due to the in-plane deformations solely to the skins, and the strain energy generated due to the out-of-plane deformations solely to the core. In effect, the in-plane stresses of the sandwich core, and the transverse shear stresses in the sandwich skin are all assumed to be negligible. The first simplification is only justifiable for a shear-soft sandwich, which is normally the case with practical sandwich materials. The second assumption is only justified when there exists a sufficiently high ratio of the skin/core thickness. It should be emphasised that due to the particularly low interlaminar shear modulus of the FRP materials, the interlaminar shearing of relatively thick, laminated sandwich skins or, by extension, of thick laminated plates cannot in general be ignored without incurring serious loss of accuracy in the results.

Finally, and in correspondence with an assumed Mindlin-type first-order shear deformation in the two-dimensional plate, we follow the approach taken by Dawe and Roufaeil [4] and by Craig and Dawe [5] in using the equivalent one-dimensional displacement functions, namely the Timoshenko beam equations, in the Rayleigh-Ritz expansions.

On subjecting the plate described above to bending only, one may write

$$u = z\psi_x(x, y) \tag{3.a}$$

$$v = z\psi_y(x, y) \tag{3.b}$$

$$w = w(x, y) \tag{3.c}$$

where u and v are displacements at a distance z through the thickness along the x and y directions respectively, w is the mid-plane displacement in the z direction, and ψ_x and ψ_y are the total rotations along the x and y directions respectively (Fig. 1).

Fig. 1. Plate coordinates and lamina orientation: 1, 2 and 3 relate to the fibre direction in a lamina; x, y, and z relate to the major axes of the plate

Development of the energy expressions

Strain energy

Denoting the co-ordinate system of any orthotropic material in the sandwich by *1, 2,* and *3* (Fig. 1), and assuming that the through-thickness strain is negligible, then the strain energy of the plate is given by

$$U = \frac{1}{2}\int_{v} \{\sigma_i\}^T \{\varepsilon_i\}\, dv \quad (i = 1, 2, 4, 5, 6) \tag{4}$$

in which

$$\{\sigma_i\} = [Q_{ij}]\{\varepsilon_j\} \quad (i, j = 1, 2, 4, 5, 6) \tag{5}$$

and

$$\{\varepsilon_i\} = \begin{Bmatrix} \chi_1 z \\ \chi_2 z \\ \chi_4 \\ \chi_5 \\ \chi_6 z \end{Bmatrix} \tag{6}$$

and the matrix $[Q_{ij}]$ is a symmetric matrix whose components consist of the on-axis, reduced plane stress stiffness matrix (*i, j=1, 2, 6*), as well as the transverse shear stiffness terms (*i, j=4, 5*).

Damping energy

Assuming that the damping energy is the sum of separable energy dissipations due to the individual strain components [6], then the total dissipated energy for the five stress components considered in the present analysis is given by

$$\Delta U = \frac{1}{2}\int_{v}\{\sigma_{i}\}^{T}[\psi]\{\varepsilon_{i}\}dv \quad (i = 1, 2, 4, 5, 6) \tag{7}$$

where the damping matrix $[\psi]$ is the diagonal matrix

$$[\psi] = \begin{bmatrix} \psi_{1} & & & & \\ & \psi_{2} & & 0 & \\ & & \psi_{4} & & \\ & 0 & & \psi_{5} & \\ & & & & \psi_{6} \end{bmatrix} \tag{8}$$

whose components quantify the proportion of the energy loss in each cycle of vibration due to each stress component.

The development of the expression for damping energy in equation (7) is similar to that for the strain energy, and it will not be reproduced here for brevity reasons.

The Rayleigh-Ritz energy minimization method

The Rayleigh-Ritz method is covered extensively in the literature. A detailed account for isotropic plates has been given by Young [7] and for anisotropic plates by Ashton and Waddoups [8] and by Ashton and Whitney [9]. The method involves expressing the lateral deflection of a rectangular plate in terms of suitable beam functions in the x and y directions. On subsequent minimisation of the total energy of the plate, the plate modal properties including modal frequency and deformations (mode shapes) are obtained.

The Rayleigh-Ritz trial functions in the present case are given by Craig and Dawe [5] as

$$w(x,y) = \sum_{m=1}^{M}\sum_{n=1}^{N}a_{mn}w_{m}(x)\,w_{n}(y) \tag{9.a}$$

$$\psi_{x}(x,y) = \sum_{m=1}^{M}\sum_{n=1}^{N}b_{mn}\,\psi_{m}(x)\,w_{n}(y) \tag{9.b}$$

$$\psi_{y}(x,y) = \sum_{m=1}^{M}\sum_{n=1}^{N}c_{mn}\,w_{m}(x)\,\psi_{n}(y) \tag{9.c}$$

in which a_{mn}, b_{mn} and c_{mn} are unknown coefficients to be determined through the minimisation of energy, and w and ψ are the Timoshenko beam functions satisfying the free-free boundary conditions (these are the boundary conditions applicable to the present work)

Finally, the kinetic energy is given by

$$T = \frac{1}{2} \int_\Omega (\rho h w^2 + \rho \frac{h^3}{12} (\psi_x^2 + \psi_y^2)) \, d\Omega . \omega^2 \tag{10}$$

In a similar manner, following the substitution of the trial functions (9) in equation (10) and rearranging so that the functions of x and y are separated into their respective integration domains, the following expression can be obtained for the kinetic energy

$$T = \frac{1}{2} \sum_{i=1}^{M} \sum_{j=1}^{N} \{ \rho h [a_{ij} \int_a w_i w_m \, dx \int_b w_j w_n \, dy] a_{mn} + \rho \frac{h^3}{12} \{ [b_{ij} \int_a \psi_i \psi_m \, dx \int_b w_j w_n \, dy] b_{mn}$$

$$+ [c_{ij} \int_a w_i w_m \, dx \int_b \psi_j \psi_n \, dy] c_{mn} \} \} . \omega^2$$

TheFinite Element Approach

A finite element approach allowing the determination of the specific damping capacity of a damped layered composite panel has been proposed by Maheri and Adams [10]. This method can be applied to a honeycomb sandwich panel with composite or aluminium skins.

The strain energy U is then calculated using the following expression

$$U = \frac{1}{2} \{\delta\}^T [K] \{\delta\} \tag{11}$$

where {the elemental division integrated over the total volume of the structure.δ} are nodal displacements and $[K]$ the structural stiffness matrix.

We use here the fact that a mean elasticity matrix $[D^m]$ can be used to assemble the $[K]$ matrix with the conventional formulation

$$[K] = \int_V \{[B]^T [D^m][B]\}_e \, dV \tag{12}$$

where $[B]$ is the strain-displacement matrix and the suffix e refers to

To calculate the dissipated energy ΔU using a finite element software package, the damped structural stiffness matrix $[K_d]$ must be first assembled. This could be done easily if the $[\bar{R}]$ matrix can be made symmetric.

The relatively negligible $[D^m_{d16}], [D^m_{d26}], [D^m_{d61}]$ and $[D^m_{d62}]$ terms can be ignored and the quite small $[D^m_{d12}]$ and $[D^m_{d_{21}}]$ terms can be averaged such that

$$[D^m_{d12}] = [D^m_{d21}] = \frac{[D^m_{d12}] + [Dd^m_{21}]}{2} \tag{13}$$

With such modifications, the damped mean elasticity matrix is indeed symmetric.

Using this justified approximation, we now define the equivalent damped elastic properties of the skins as

$$E_x^* = [D_{d11}^m] - \left(\frac{[D_{d12}^m]}{[D_{d22}^m]}\right)^2 [D_{d22}^m] \ , \ E_y^* = \frac{[D_{22}^m]}{D_{11}^m} E_x^* \ , \ v_{xy}^* = \frac{[D_{d12}^m]}{[D_{d22}^m]} \tag{14}$$

and of the core as

$$G_{xz}^* = [D_{d44}^m] \ , \ G_{xy}^* = [D_{d55}^m] \tag{15}$$

This method allows, with the same finite element model and with two different sets of material, data to solve on one hand the eigenvalue problem giving frequency, nodal displacements and strain energy for each mode using the software functionality, and on the other hand a damped structural stiffness matrix $[K_d]$ taking into account modified equivalent damped materials. A last matrix calculation using the nodal displacements gives ΔU and so Ψ for each mode.

3 EXPERIMENTAL

Tests were carried out on two systems of mid-plane symmetric rectangular sandwich plates, namely sandwich plates with CFRP skins, and sandwich plates with aluminium skins, both systems having the same low density, aluminium honeycomb (HC) material as their core. Each composite skin consisted of only 3-plies of CFRP material, with a skin/core thickness ratio of 80 (in the case of the aluminium skins, this ratio was 60). Also, in both systems, the core orthotropic axes were aligned along the plate axes.

The experimental work essentially consisted of two parts. First, dynamic tests were carried out on the constituent parts of the sandwich panels in order to determine their moduli of elasticity and SDC. These data were then used to predict the modal characteristics, as described above. Free-free modal tests were then carried out on sandwich panels as a whole, and the experimental results were compared to the theoretical predictions.

The constituent elastic and damping data were determined in correspondence to the prevalent mode of deformation in the constituent parts when the sandwich is loaded laterally. That is, the skin material was tested for its in-plane properties, whereas the core material was tested for its transverse shear properties.

Sandwich plate modal properties

The sandwich plates were subjected to free-free modal tests. The free-free plate modal tests are primary used for qualitative purposes and are aimed at establishing the damping properties of the typical plate under various modal deformations.

Unless otherwise stated, the tests were carried out using the test method described by Maheri and Adams [1,10]. Both bandwidth and free-decay methods were used for the damping measurements, the choice of the method being dependent on the suitability of each method for each particular test. Furthermore, in all the plate tests, the linearity of the variation of SDC with displacement amplitude was verified by using a simple and quick method in

which the output voltage from the vibration pickup device was observed to vary linearly with the input current to the vibration drive device.

The experimentally obtained modal characteristics were subsequently compared with theoretically predicted results and NASTRAN finite element model results. The mode shapes shown in the following results are all theoretical mode shapes although, as will be explained later, in most cases these could be verified experimentally.

Sandwich with CFRP composite skins

In testing composite skin sandwich panels, substantial damping was observed which was not predicted by theory. As the results in Table 1 show, there is a large discrepancy between the experimental and the predicted damping results, especially in the second mode. The amount of damping in the subsequent modes was so large that it effectively hindered obtaining the resonance frequencies and mode shapes with any degree of certainty. However, as the table shows, the frequency values of those modes that could be established experimentally, namely the first and the second mode, are reasonably close to the theoretical values.
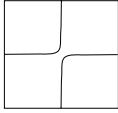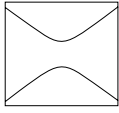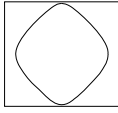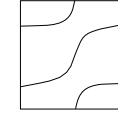
	Mode shape				
Freq. (Hz)	Experiment	518	779	⊂	⊂
	Rayleigh-Ritz Method	531	816	989	1259
SDC (%)	Experiment	3.79	15.1	⊂	⊂
	Rayleigh-Ritz Method	1.38	0.83	0.84	0.94

Table 1. Modal results of the SP1-1 plate, tested in air

The large amount of damping was attributed to air-damping (see below). To verify this, a test was conducted in a vacuum chamber whereby the pressure was reduced to 1 millitorr in several steps; at each step the SDC of the second mode of vibration of the plate was measured. Because of the size limitation of the vacuum chamber, the size of the plate was reduced from a 500(mm) to a 400(mm) square plate, the latter referred to here as the SP1-2 plate. The test results are plotted in Fig. 2.

As the test results in Fig. 2 show, in this particular case, air-damping has caused an almost 3-fold increase in the SDC, while the frequency has fallen by about 2%.

Generally, if a stiff, heavy plate vibrates in air, there is little or no effect of the air on the natural frequencies and damping. Even in water, the effect can be very small. However, when a 'light' plate vibrates, the mass and stiffness of the adjacent air can be significant, and

acoustic radiation (air-damping) can account for a large proportion of the vibrational energy. The effect is pronounced when the dimensions of the plate (and hence also the nodal patterns) are in approximate coincidence with the wavelength of sound waves in air. At 1000 (Hz), the wavelength of these sound waves is approximately 330 (mm), which is close to the plate dimensions. At reduced pressure, the acoustic radiation is reduced.

Following the above test, all the modal tests on the plate were conducted in vacuum. The *in-vacuo* results are given in Table 2.
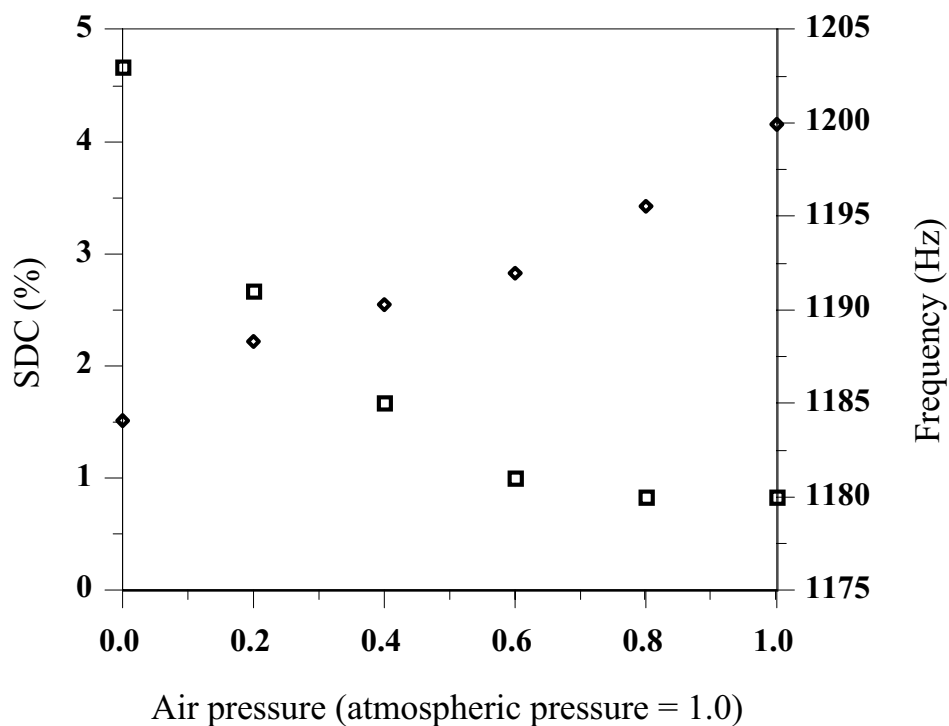

Fig. 2 Variation of damping and frequency with air pressure for the second mode of the SP1-2 plate with CFRP skins (+60, 0, ⊂60) and aluminium honeycomb core. ◇ SDC ; □ frequency
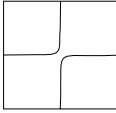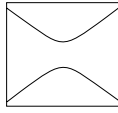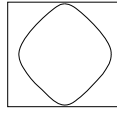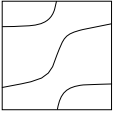
	Mode shape				
Freq. (Hz)	Experiment	757	1202	1471	1755
	Rayleigh-Ritz method	796	1221	1469	1817
	NASTRAN model	750	1140	1381	1655
SDC (%)	Experiment	1.11	1.51	1.06	1.21
	Rayleigh-Ritz method	1.39	0.84	0.84	0.94
	NASTRAN model	1.03	1.00	0.76	0.97

Table 2. Modal results of the SP1-2 plate, tested *in-vacuo*

4 CONCLUSIONS

It was shown that it is possible to predict modal characteristics, including damping, of practical sandwich panels using basic laminae theory and a simplified plate deformation analysis. A first order shear deformation theory was used, although the transverse shearing in a relatively thin sandwich skin was considered to be negligible. Test results tend to suggest that this was a justified assumption, at least in so far as modal characteristics of thin-skinned, free-free sandwich panels are concerned.

The Rayleigh-Ritz expressions used for the present case are a fairly straightforward extension of the classical method, namely the addition of the two transverse shear rotations to the lateral displacement as the trial functions. Although the derivations and subsequent computer codification are inevitably more voluminous, and notwithstanding the fact that the application of the method is limited to rectangular plates, this numerical method is known to be fast and accurate where it can be applied.

A finite element approach using NASTRAN software package capabilities has also been used and gives results which are close to the Rayleigh-Ritz and experimental values.

In modal testing of the sandwich panels, it was shown that these experienced enormous damping when tested in air, owing to acoustic radiation. It was concluded, therefore, that in order to obtain data for modal damping due to the inherent damping of the material in sandwich panels, which data that should be of particular interest in space applications, tests will have to be carried out *in-vacuo*.

Both the analytical Rayleigh-Ritz method and the NASTRAN finite element approach have given quite satisfactory results for both frequencies and specific damping capacities for specific free-free *in-vacuo* tests using two kinds of ALCATEL SPACE sandwich aluminium panels (aluminium skins and CFRP skins).

REFERENCES

[1] MAHERI M.R. and ADAMS R.D., Modal Vibration Damping of Anisotropic FRP Laminates Using the Rayleigh-Ritz Energy Minimization Scheme, *Journal of Sound and Vibration*, vol259(1),17-29, 2003.
[2] ADAMS R.D. and MAHERI M.R., The Dynamic Shear Properties of Structural Honeycomb Materials, *Composites Science and Technology*, vol47(1), 15-23, 1993.
[3] ADAMS R.D. and MAHERI M.R., Dynamic Flexural Properties of Anisotropic Fibrous Composite Beams, *Composites Science and Technology*, vol50(4), 497-514, 1994.
[4] DAWE D.J. and ROUFAEIL O.L., Rayleigh-Ritz Vibration Analysis of Mindlin Plates, *Journal of Sound and Vibration*, vol 69(3), 345-359, 1980.
[5] CRAIGE T.J. and DAWE D.J., Flexural Vibration of Symmetrically Laminated Composite Rectangular Plates Including Transverse Shear Effects, *International Journal of Solids and Structures* vol22(2), 155-169, 1986.
[6] ADAMS R.D. and BACON D.G.C., Effect of Fibre Orientation and Laminate Geometry on the Dynamic Properties of CFRP, *Journal of Composite Materials* vol7, 402-428, 1973.
[7] YOUNG D., Vibration of Rectangular Plates by the Ritz Method, *Journal of Applied Mechanics*, vol17, 448-453. 1950.
[8] ASHTON J.E. and WADDOUPS M.E., Analysis of Anisotropic Plates, *Journal of Composite Materials*, vol3, 148-165, 1969.
[9] ASHTON J.E. and WHITNEY J.M., Theory of laminated plates, *Conn., USA: Technomic Publishing Company*, 1970.
[10] MAHERI M.R. and ADAMS R.D., Finite Element Prediction of Modal Response of Damped Layered Composite Panels, *Composites Science and Technology*, vol55(1), 13-23, 1995.

JOINING

EVALUATION OF CLINCHING AND CENTER-PUNCHING AS MECHANICAL JOINING PROCESSES FOR SANDWICH ELEMENTS

J. Feldhusen[*], C. Warkotsch[*], M. Benders[*]

[*] Chair and Institute for Engineering Design (IKT)
RWTH Aachen University
Steinbachstr. 54 B, 52074 Aachen, Germany
e-mail: feldhusen@ikt.rwth-aachen.de, web page: http://www.ikt.rwth-aachen.de

Key words: Sandwich structures, mechanical joining technology, clinching, center-punching.

Summary: *This document examines the question if the two manufacturing processes of joining by clinching and by center-punching can be used for joining sandwich elements. The characteristics of the two joining processes are analyzed. Principle solutions are developed following the design methodology of Pahl et al. [1, 2]. Proof of feasibility is given by the implementation of the results in a prototype.*

1 INTRODUCTION

Kempf has developed a mechanical joining technology for sandwich elements [3]. It aims for avoiding the disadvantages of existing technologies. Welding or brazing can lead to changes in the material structure due to the application of heat. The use of adhesives requires a precise fixation of the joined parts during setting. Bolts work with an elastic elongation; a certain clamping length as well as a high force to achieve this elongation is needed, making it an impracticable joining process for sandwiches.

1.1 Preliminary work

The development and evaluation process in [3] is characterized by a systematic approach based on the design methodology of *Pahl et al.* [1, 2]. The results are 18 possible principle solutions for a mechanical joining technology for sandwich elements. These principle solutions were classified in six groups according to characteristics of the underlying joining processes. For five groups mathematical descriptions of the behavior under loadings were defined and finally prototypes were built [3]. The sixth group – the so-called "low-cost connectors" – was evaluated separately [4]. The results of this evaluation of using clinching and center-punching as joining methods for sandwich elements are presented in this paper. The denotation "low-cost" has been chosen because the focus here lies on methods which allow a quick connecting of sandwiches without extensive and time-consuming preparation steps such as cleaning. Also, costly fastening elements such as special bolts are not required.

1.2 Terminology and constraints

Figure 1 explains the terminology of the joint. The core material is removed in the area of

the joint and the sandwich faces are inserted between the tongues of the connecting element. The term of fastening element denotes the location of the clinching respectively the punching. Thus, the following considerations focus on sandwiches with metal faces. The approach that has led to this design of the joint is described in [3, 6]. Furthermore, for economical reasons the preferred manufacturing process for the connecting element is extrusion.
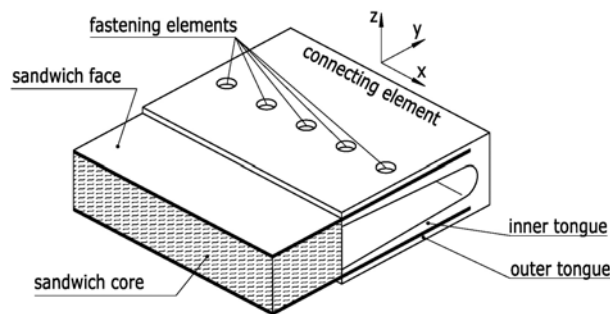
Figure 1: Terminology of the joint

3 CLINCHING

Clinching is defined as a manufacturing process for joining sheet metal parts, pipes or profiles by forming them [5]. In practice, there are several clinching methods that differ in various aspects. Usually two sheetlike parts of metal are joined by being pressed into the cavity of a die by a punch. The knowledge about the differences and the particular character-istics of the different methods is necessary for an evaluation of clinching for the given task.

3.1 Classification of clinching methods

The clinching process can be characterized by the kind of the die (with or without moving parts), the shape and the kind (with or without cutting of the joining partners) of the fastening element and the kinematics of the process (single-stage or multi-stage) [4].

Dies with or without moving parts differ in the way that in the first case, the actual die is surrounded by several die plates which will move sideward when the punch draws the join partners into the cavity. During this process, the material at the clinching location can be cut, partly cut and formed or only formed depending on the geometry of the die. Tools without moving parts however only consist of a solid die with a fixed cavity. Here, the connection is usually established by forming and not cutting the material.

The kinematics of the clinching process can vary in the number of stages. For single-stage methods usually the punch drives into and out of the cavity in a single, continuous motion. In contrast multi-stage processes involve punch and die and consist of at least two separate motions.

Another differentiation factor is the fastening element. Depending on the clinching tech-nology the join partners may both be cut (cp. fig. 2, right) or only be formed during the clinching process (cp. fig. 2, left). There are also technologies where only the die-sided partner is cut while the punch-sided partner is formed. Considering the shape, the fastening

elements can be round, oval, cross-, star- or bar-shaped.

In addition, a clinching method has been developed which makes it possible to join a well-formable part with a join partner that is difficult to form. This allows clinching parts that are too thick or materials that are too brittle for common clinching methods. For this method holes are drilled into the non-ductile partner first. Then the clinching process is carried out, this time however only forming the ductile material into the holes of the pre-drilled partner.

3.2 Characteristics of the fastening element

Single-stage clinching methods and those that have a die without moving parts use a set of tools that is customized to the thickness of the joining partners. A change in thickness or material of the joining partners necessitates a change of the clinching tools. Multi-staged processes and those that have a die with moving parts are more tolerant in this respect.

The fastening element of all clinching methods is characterized by an undercut (see fig. 2). This mechanical interlock between the joining partners originates from a plastic deformation of the material during the clinching process. Due to the shape of the die and the pressure of the punch some material of the upper joining partner is formed in a way that it flows underneath the lower joining partner. The result is a connection which is tension-proof even in axial direction.
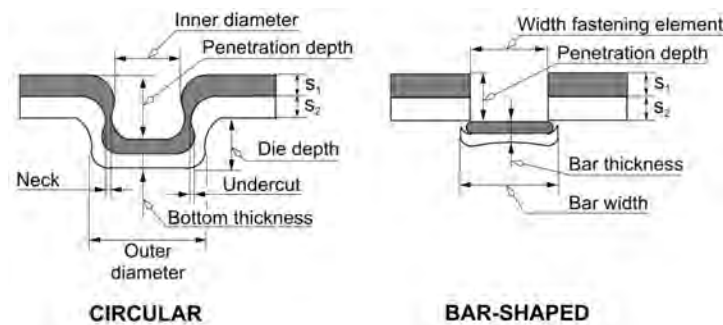
Figure 2: Relevant parameters of clinching elements [4]

The tensile strength of a clinched connection depends on the size of the undercut. In principle, the bearable axial load increases with the size of the undercut. The same tendency holds true for the resistance of the connection to static loads. For the resistance to shear loads and dynamic loads however the thickness of the neck is crucial. For dimensioning circular clinching elements eq. 1 can serve as compromise between those two contrary requirements [4].

$$undercut = neck\ thickness = 0.5 \cdot s_1 \tag{1}$$

Besides, the bottom thickness can be used to measure the quality of a clinching element non-destructively. It should fulfill one of the following equations depending on the shape [4]:

$$bottom\ thickness = \frac{1}{3}(s_1 + s_2) \qquad \text{for round clinching elements} \tag{2}$$

$$bottom\ thickness = \frac{1}{2}(s_1 + s_2) \qquad \text{for angled clinching elements} \tag{3}$$

3.3 Characteristics of clinching as manufacturing process

Clinched parts are permanently connected. The connection combines the advantage of form fit – the transmission of high loads – and the advantage of a frictional connection – freedom of play. The joining partners – ferrous and non-ferrous metals – can differ in thickness within a range from about 0.6 mm to 8 mm for steel and up to 11 mm for aluminum [4]. Using the clinching method with pre-holes (see above) it is even possible to join a sheet-metal with plastic materials, brittle parts or also very thick parts like sandwiches. The surface of the joined parts is not impaired by clinching and can be of any treatment, e. g. coated, anodized or even oiled. Clinching necessitates no preparation of the surface prior to clinching. Another asset is that intermediate layers can be put between the actual parts. Those layers can for example serve as insulation. Refinishing or reworking of the connected parts is not necessary, too. In case of clinching methods that do not cut the connected parts the connection is gas- and liquid-tight. The greatest disadvantage of clinching is the necessary high joining force. In single applications, it can be as much as 120 kN. For common usage it still ranges between 40 and 50 kN [4].

Due to the multitude of different clinching technologies with different parameters, an exact calculation of the strength of the connection is difficult. Furthermore most knowledge about seems to be owned exclusively by the companies offering clinching technologies. Different influences on the strength of clinched connections have been discussed in [4].

3.4 Conceptual design and evaluation

The present problem of the structural design of a connecting element is characterized by the fact that the joint is accessible only from one side. However, all known clinching technologies analysed above use a two-piece tool-kit consisting of a punch and a die. This necessitates access to the joint from both sides. Thus for a possible solution, the die must be integrated into the fixed inner tongue of the connecting element. This consideration allows to exclude the multi-stage clinching methods with movable die. Processes which produce a fastening element of the kind that the joining partners are cut can be excluded as well. Specially manufactured cutting edges of high hardness would have to be integrated into the inner tongue resulting in a multi-part assembly of the connecting element. This would be contradictory to the requirements of a low-cost solution. For the same reason solutions are not feasible that use moving parts for the die.

At this point some considerations for the material of the connecting element shall be made. As seen before, the forces required for clinching and thus the pressure on the die are very high. The die and in this case the inner tongue respectively must withstand those forces at any rate to ensure the forming of a correct fastening element. Of all technically relevant materials only metals and ceramics show the required hardness. The latter are excluded from further considerations due to their brittleness and usually high manufacturing costs. Plastics would need an extra insert of high hardness at the location of the fastening element leading again to a multi-part assembly of the connecting element. This leaves metals as possible material for the

connecting element. The use of ferrous metals very likely contradicts the main benefit of sandwiches, i.e. the light weight. Besides extrusion has already been determined as the preferred manufacturing process for the connecting element. So further considerations focus on aluminum as material for the connecting element. Aluminum alloys suitable for extrusion show a Brinell hardness of up to 100 HB. High-strength alloys with a lower resistance to corrosion can even reach 140 HB [4]. It has yet to be examined whether this is hard enough for a die integrated in the inner tongue.

It has now been determined that the connecting element has the function of a die without moving parts and cutting edges. The clinching process is single-staged. This leaves two possible shapes for the die:

- Linear, i.e. a groove along the inner tongue of the connecting element.
- Punctual, i.e. discrete cavities in the inner tongue.

The first possibility requires a bar-shaped or oval fastening element in order to have a sufficient contact area between connecting element and sandwich face. For the second possibility a point-shaped fastening element is preferable to other shapes like a cross or a star. A round cavity is easy to manufacture and above all, experiences can be taken from well proven clinching technologies that use a point-shaped fixed die with a single-staged kinematics.

The next step considers the outer tongues of the connecting element. As for the inner tongues there are two possible solutions:

- The outer tongue can be designed like a sheet-metal. The fastening element would then be a mechanical interlock of the outer tongue and the sandwich face in the cavity of the inner tongue.
- The outer tongue has holes at the locations of the later fastening elements, i.e. it does not become part of actual connection between connecting element and sandwich. This is comparable to the clinching technology that uses a hole on the die side material (see above). There as well only one join partner is used to establish a connection.

Combining the preceding options for the design of the inner and outer tongues there are four possible principle solutions for the connecting element left (see table 1):

1. Point-shaped cavity in the inner tongue as die, sheet-metal like outer tongue (no pre-holes at the locations of the fastening elements)
2. Linear cavity in the inner tongue as die, sheet-metal like outer tongue (no pre-holes at the locations of the fastening elements)
3. Point-shaped cavity in the inner tongue as die, outer tongue with holes at the location of the fastening elements
4. Linear cavity in the inner tongue as die, outer tongue with holes at the location of the fastening elements

The last question that must be discussed for a complete principle solution for the connecting element concerns the actual shape of the cavities. The answer is easily given for the two solutions no. 1 and no. 3 with point-shaped cavity. Here it should be taken advantage of the pool of experience arising from existing clinching methods. They have proven their functional capability in practice. However, the answer is not at hand for solutions no. 2 and no. 4. Despite an extensive literature research there seem to be no practically used clinching meth-

ods that are based on a linear cavity. Obviously, a linear cavity can provide resistance to the material flow during the forming process of the clinching element only in transverse direction. So the necessary undercut will develop only in this direction, too. This must be reached by the correct combination of strain hardening and yielding. Thus, it seems reasonable to layout the linear cavity with the same cross-section as the punctual cavity which is based on a known clinching technology. Furthermore it can be expected that the thickness of the joining partners will not decrease significantly in longitudinal direction. Of what is know from the different clinching methods this rather leads to a higher resistance to shear forces in transverse direction. It must however be experimentally verified whether these assumptions are true.

1: Point-shaped cavity, outer tongues without pre-holes	2: Linear cavity, outer tongues without pre-holes
3: Point-shaped cavity, outer tongues with pre-holes	4: Linear cavity, outer tongues with pre-holes

Table 1: The four principle solutions; principle sketches on the left,
suggested cross-section of the cavity on the right

In the discussion at the beginning of this chapter a multi-part assembly of the die in the inner tongue was defined as exclusion criterion for a principle solution. Solution no. 1 however with point-shaped cavities and sheet-metal like outer tongues necessitates a connecting element that consists of at least three parts: two outer tongues and a center bar with the inner tongues. Otherwise it is not possible to manufacture the cavity. Yet, this assembly is less complex than a die with movable parts and so solution no. 1 shall not be excluded from further considerations. The advantages and disadvantages of the four principle solutions are discussed in tables 2 to 5.

The final step of the discussion of clinching is an evaluation which considers the above said. An objectives tree is set up and the four principle solutions are rated. The three upper level objectives are:

- Good fulfillment of function; weighted with a percentage of 50%
- Cost; weighted with a percentage of 25%
- Easy Handling; weighted with a percentage of 25%

Points are given on a scale from 0 to 10, 10 indicating a perfect fulfillment of an objective. As result of the evaluation, principle solution no. 2 is rated best (score: 6.05) followed by no. 4 (score: 4.86), no. 1 (score: 4.56) and finally no.3 (score: 4.47). So the two highest rated

principle solutions are realized in a prototype which will be discussed at the end of this paper

Advantages	Disadvantages
• Corresponds to a known clinching technology, experience available • Connecting element assembled from more than one part, thus exact adjustment of the outer tongue to the requirements of the connection with regards to material and shape • Presumably best behavior under load • Point-shaped clinching element transmits forces in longitudinal direction of the connecting element, no extra locking necessary • Optically unobtrusive clinching element	• Multi-part assembly of connecting element is compulsory, thus highest manufacturing effort • Highest joining forces of all principle solutions • Exact positioning of punch in x- and y-direction required • Good appearance of clinching elements might be weakened by the multi-part assembly (e.g. visible bolts or splices) • Possible bending upwards of outer tongue during clinching must be prevented

Table 2: Advantages and disadvantages of principle solution 1

Advantages	Disadvantages
• Connecting element as single part possible • High strength of connection comparable to solution no. 1 • Connecting element easy to manufacture, e.g. by extruding • Second-best appearance • Exact positioning of punch only in y-direction necessary	• High joining forces • Unknown joining technology with regards to the die • Possibly extra locking in x-direction necessary due to the linear die • Possible bending upwards of outer tongue during clinching must be prevented

Table 3: Advantages and disadvantages of principle solution 2

Advantages	Disadvantages
• Corresponds to a known clinching technology, experience available • Connecting element as single part possible • Joining forces not as high as for the solutions without pre-holes in the outer tongues • Point-shaped clinching element transmits forces in longitudinal direction of the connecting element, no extra locking necessary	• Manufacturing of complex shape of die is problematic • Presumably lower strength of connection since only the sandwich faces are clinched • Exact positioning of punch in x- and y-direction required • Optical appearance affected by pre-holes • Depending on the materials of connecting element and sandwich face high loads on the die up to failure

Table 4: Advantages and disadvantages of principle solution 3

Advantages	Disadvantages
- Connecting element as single part possible - Connecting element easy to manufacture, e.g. by extruding, additionally the pre-holes have to be manufactured - Presumably lowes joining forces, thus saving of material and low weight because the inner tongues do not have to be as rigid as for the other solutions - Exact positioning of punch only in y-direction necessary	- Unknown joining technology with regards to the die - Presumably lowest strength of connection of all solutions - Possibly extra locking in x-direction necessary due to the linear die - Worst appearance of all solutions due to pre-holes and asymmetric clinching elements - Depending on the materials of connecting element and sandwich face high loads on the die up to failure

Table 5: Advantages and disadvantages of principle solution 4

4   CENTER-PUNCHING

Center-punching was taken into consideration as a cost-effective and fast joining process which necessitates a minimum of tools and preparation steps of the materials to be connected. With regard to this, the demands for the strength of the connection were lower. Since punching is not a widely used joining process, there is not much information about it in literature.

4.1 Characteristics of the joining process

A known application in practice is punching nuts or bolts to prevent them from loosening. Also center-punching is sometimes used to lock parts into position which will later be joined through material closure (welding, brazing). This reduces the effort of fitting and adjusting the parts. This shows that center-punching is in principle seen as a joining process for secondary applications. So there is little knowledge about the characteristics of this method. The joining force occurs impulse-like on a rather small area. The surface is highly impaired sometimes leading to cracks or promoting corrosion. Another fact to be considered is that center-punching might negatively affect the position of the joining partners. They should be correctly positioned and fixed prior to the joining process.

Both center-punching and clinching apply a force to the joining partners at a right angle to the surface. This force of course is much lower for center-punching. Under the effect of this force, the material is deformed plastically forming a mechanical interlock between the joining partners. An important difference between center-punching and clinching is that the fastening element produced by center-punching shows no undercut. This means there is only form fit in the sandwich plane but not perpendicular to it as it is for clinching. Of course, it is to expect that the retention forces of the fastening element produced by punching are much lower than those of clinching. The tools needed for center-punching – a hammer and a punch – are usually available at any construction site. This fits well to the concept of a low-cost connection and is certainly an asset over clinching.

4.2 Conceptual design

Basically, the same considerations employed in the analysis of clinching are also valid for center-punching. The outer tongue can be designed with or without pre-holes at the locations of the fastening elements. In the first case the punch directly touches the sandwich face. For the inner tongue there are three possible designs: with point-shaped or linear cavity as known from clinching but also completely without cavity. In contrary to clinching, the shape of the cavity is not crucial. It might only help reduce the joining force as the punch only has to intrude into sandwich face and/or outer tongue.

So there are six possible combinations of the designs of inner and outer tongue, two of which however do not make sense. Firstly, this is the combination of an inner tongue with point-shaped cavities with an outer tongue without pre-holes. This design would necessitate a connecting element which is assembled of more than one part. Otherwise it is not possible to manufacture the point-shaped cavities due to the lack of accessibility of the inner tongue. A multi-part connecting element is however not desired as already mentioned before. The second combination not being considered further is an inner tongue with linear cavity together with an outer tongue with pre-holes. It is not apparent why this combination should differ significantly in its properties from the combination of outer tongues with pre-holes and inner tongues with punctual cavities. The latter one even offers the advantage of manufacturing pre-holes and cavities in one single step using for example a drill. This leaves four reasonable designs for the connecting element which are listed below:

1. Outer tongues without pre-holes, inner tongues without cavity
2. Outer tongues with pre-holes, inner tongues without cavity
3. Outer tongues without pre-holes, inner tongues with a linear cavities
4. Outer tongues with pre-holes, inner tongues with point-shaped cavities

Since no data or experience exist for the joining process of center-punching it is not possible to do an objective evaluation as it was done for clinching. Thus, the influence of the parameters of the different principle solutions is examined by experimental testing.

4.3 Experimental analysis

The test set up consists of different aluminum profiles that simulate the inner and outer tongues (fig. 3) and sheet-metals of different materials and thickness as sandwich faces. In figure 3 (left) the two shapes of cavities – circular and linear – are clearly visible. The top part simulates the inner tongue without cavity as needed for principle solutions no. 1 and 2. The U-shaped test profiles for the outer tongues (fig. 3, right) are used to gain information whether it is crucial to prevent the outer tongues from bending upwards when being hit by the punch. The parts simulating the tongues are bolted to a heavy iron plate with the sandwich faces in between them. The sandwich faces are simulated by sheet-metals from aluminum with thicknesses of 0.8 mm and 1.0 mm and by sheet-metals from steel which are 0.5 mm and 0.8 mm thick.

Figure 3: Test parts for inner (left) and outer (right) tongues

Five different punches are used for testing. They differ in weight and the shape of their tip (see fig. 4). Commercially available tools were chosen deliberately.

Figure 4: Punches used for experiments

The results of the experiments show that only the principle solutions with a cavity in the inner tongue have acceptable functional properties. Without a cavity the punch does not penetrate far enough even under heavy hits to create a connection between the sandwich faces and the connecting element. The sheet-metals serving as sandwich faces can easily be pulled out of the test stand by hand. Here it makes no difference whether the outer tongue is very rigid as simulated by the U-profile. The version of the outer tongue without pre-holes leads to the highest strength of the connection. The version with pre-holes however is recommendable if a low weight and an uncomplicated construction of the connecting element are demanded. The best fastening elements are achieved with a heavy punch with a rounded tip. The sharp-edged punch tears the sandwich faces instead.

The optimal shape of the linear cavity of solution no. 3 depends basically on the material and the thickness of both the sandwich face and the outer tongue. Like the geometry of the punch it has to be determined individually for each application. However, some guidelines for dimensioning the point-shaped cavity of solution no. 4 can be derived from the experiments. The use of a punch with round tip is required. Measurements in the cross-section of the fastening elements show that the thickness of the sandwich faces does not change significantly. Thus, the following simple equations for the diameter d_M and the depth t_M of the cavity can be derived:

$$d_M = 2 \cdot (r_k + k_d \cdot s) \qquad 0.8 < k_d < 1.0 \tag{4}$$

$$t_M = k_t \cdot r_k + s \qquad 0.8 < k_t < 1.2 \tag{5}$$

s denotes the thickness of the sandwich faces, r_k is the radius of the tip of the punch. The

values for the two factors k_d and k_t are estimated and must be determined for each application.

4   PROTOTYPE

As part of the work of [3], the two best rated solution of both clinching and center-punching have been realized in a prototype (fig. 5). The clinching was processed by means of a path-controlled hydraulic press. The penetration depth was about 2 mm for both solutions. However, due to the restrictions in manufacturing processes of the institute's workshop, it was not possible to manufacture a cavity that fulfills the requirements stated above. As a result the clinching points showed no undercut. Thus, the outer tongue of the connecting element and the sandwich faces could be separated from each other in axial direction of the fastening element. Yet, in radial direction the connection showed a satisfying strength. No play at all occurred.

The center-punched connection could be established quick and easy. It also showed satisfying strength and was as well free from play. One cavity however was designed to deep as the sandwich faces were partly ripped.
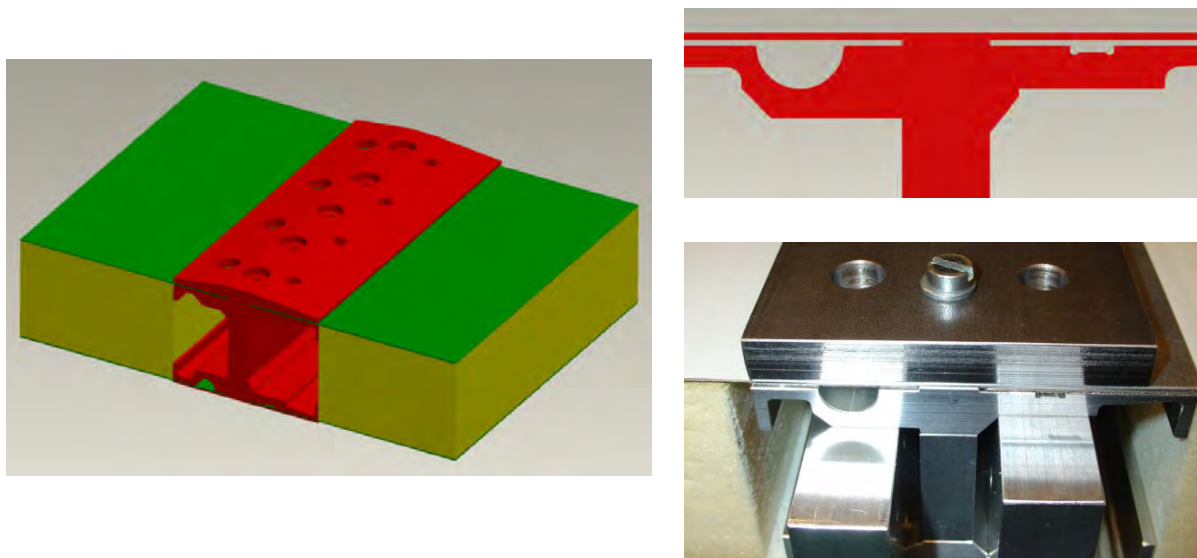
Figure 5: CAD-model of prototype (left: assembly; upper right: cross-section with cavity for punching on the left and cavity for clinching on the right; lower right: same view but actual prototype)

5   CONCLUSION

The prototype showed a satisfying strength for both clinched and punched joints. Both joining processes seem to be feasible to connect sandwiches in the described manner. Most problems of the prototype can be resolved by further research and improved manufacturing processes. For the considered application case, the problem of high joining forces for clinching remains unsolved though. For the given requirements, center-punching can be consi-

dered a very promising joining process. However, further research must be carried out to find out more about the geometric parameters of both fastening elements. It is also necessary to gain data about the actual strength of both joining technologies. This will be done in near future on a servo-hydraulic testing machine.

REFERENCES

[1] G. Pahl, W. Beitz, J. Feldhusen and K. H. Grote, *Engineering Design: a systematic approach*, London: Springer, 3. Edition 2007, ISBN 978-1-84628-318-5.

[2] G. Pahl, W. Beitz, J. Feldhusen and K. H. Grote, *Projeto na engenharia: fundamentos do desenvolvimento eficaz de produtos, métodos e aplicações*, São Paul: Editora Edgard Blücher ltda., 1ª edição 2005, ISBN 85-212-0363-2.

[3] A. Kempf, *Entwicklung einer mechanischen Verbindungstechnik für Sandwichwerkstoffe*, Aachen, RWTH University, Inst. for Eng. Design (IKT), Diss., 2004.
http://darwin.bth.rwth-aachen.de/opus3/volltexte/2005/1003/

[4] C. Warkotsch, *Verbindung von Sandwichelementen mittels Durchsetzfügen, Körnen und fließlochformenden Schrauben*, Aachen, RWTH University, Inst. for Eng. Design (IKT), Project Work, 2004.

[5] DIN Deutsches Institut für Normung e. V., *DIN 8593: Fertigungsverfahren Fügen,* Berlin: Beuth, 2003.

[6] J. Feldhusen, C. Warkotsch and A. Kempf, *Development of a mechanical technology for joining sandwich elements*, Conference Paper, 8th International Conference on Sandwich Structures, Portugal, 2008.

DEVELOPMENT OF A MECHANICAL TECHNOLOGY FOR JOINING SANDWICH ELEMENTS

J. Feldhusen[*]**, C. Warkotsch**[*] **and A. Kempf**[†]

[*] Chair and Institute for Engineering Design (IKT)
RWTH Aachen University
Steinbachstraße 54 B, 52074 Aachen, Germany
E-mail: feldhusen@ikt.rwth-aachen.de, web page: http://www.ikt.rwth-aachen.de

[†] MAN Nutzfahrzeuge AG
Dachauer Straße 667, 80995 Munich, Germany
E-mail: alexander.kempf@de.man-mn.com, web page: http://www.man-mn.com

Key words: Sandwich structures, mechanical joining technology, design methodology.

Summary: *When developing a new technology for joining sandwich elements, the improved technique should overcome the disadvantages of existing methods. Wide spread use of sandwich structures is still inhibited by the lack of a consistent joining technology one which is easy to work with, quantifiable and not dependent on special knowledge about manufacturing processes. A mechanical technology for joining sandwiches as developed in this paper shall achieve these goals. The developing process followed the design methodology according to Pahl et al. [1, 2]. The resulting systematic approach to the problem facilitated the generation of a complete solution field. This approach led to 18 promising concepts of 783 possible original solutions. Prototypes of those concepts showed that a reliable mechanical technology for joining sandwich elements is feasible.*

1 INTRODUCTION

Sandwich construction is known as a very efficient method of structural design as it combines material-specific properties in a composite of different materials to the best advantage. However, its widespread, high-volume practical use in the realm of mechanical engineering is still inhibited by the lack of a consistent joining technology, one which is easy to work with, quantifiable and not dependent on special knowledge about manufacturing processes. Heat-applying methods like welding can lead to changes in material structure. Like the use of adhesives, they also require complex preparation, positioning and fixation of the parts to be joined. Other methods, such as bolts or inlays weaken the sandwiches or require specialized manufacturing, making it impossible to use prefabricated sandwiches. A mechanical technology for joining sandwiches as developed in [3] shall overcome those disadvantages.

2 SYSTEMATIC DEVELOPMENT OF PRINCIPLE SOLUTIONS

The developing process in [3] follows the design methodology according to *Pahl et al.* [1, 2]. At first, the requirements that have to be fulfilled by the joint are determined. The function carriers, i. e. all components which could possibly be part of the connection, are

identified and their geometric parameters are systematically configured in all possible combinations. Principle solutions for a fastener for sandwich elements are then developed by combining the variations mentioned above with all known mechanical joining technologies. Evaluation steps and inspection for geometric incompatibilities help sort out invalid or impractical concepts. A final evaluation leads to 18 promising concepts.

2.1 Requirements list

The requirements are identified and collected the requirements list. Requirements are subdivided into absolute requirements and preferences. The difference here is that the first ones must be fulfilled by a possible solution. The latter ones may be considered under justifiable effort and they will later serve as basis for the determination of the evaluation criteria. The requirements have partly been found by interviewing two companies which work and design with sandwich elements, partly they have arisen from the author's own practical experiences. The requirements list is presented below. R and P indicate absolute requirements (R) and preferences (P).

- The connection must be able to transmit all occuring forces and moments (R).
- The dimensions of the joint shall be as small as possible yet as large as necessary (R).
- Elastic deformations that will occur under load must not become so large as to harm the joint (R).
- The principle of uniform strength shall be applied to sandwich elements and joint. The fatigue life of all involved parts shall be the same (R).
- The joint shall be as lightweight as possible (R).
- The intersection area between sandwich and joint shall be designed in a way that sharp deflections of the force flowlines or strong changes in their "density" are avoided (R).
- The material of the joint must be compatible to the material of the sandwiches, e.g. contact corrosion must be avoided (R).
- The utilization of the joint shall be independent of the material combination of the sandwich (P). If this is not possible, adaptions have to be made for the different materials (R).
- Forces and moments shall be transmitted from the joint directly into the sandwich faces. The distance between as well as the position relative to each other of the sandwich faces shall remain constant even under load (R).
- With regard to manufacturing, the design of the joint shall be as simple as possible. The use of large scale production methods shall be considered (P).
- The preparation of the joint beforehand shall require as few steps as possible. If preparation is necessary it shall be kept as simple as possible, e.g. if the joining technology necessitates holes they should be in the shape of a circle instead of a square (P).
- The sandwich elements shall be unambiguously positioned to each other by means of the joint. This facilitates the joining process (P).
- The assembly procedure shall be as easy and clear as possible (P).
- The joint shall be visually unobtrusive (P).

2.2 Development of principle solutions

As mentioned before, the first step is to identify the function carriers. The basic parts of the joint are the sandwich core, the sandwich faces, a connecting element, fastening elements and if necessary inserts (fig. 1). The function of the connecting element is that of an auxiliary part that connects the sandwiches by means of the fastening elements (as opposed to connecting the sandwiches directly, e. g. through the faces). Potentially necessary inlets will later be counted to be part of the connecting element. The fastening elements are the parts that are needed to finally establish the connection between the sandwiches and the connecting element or the sandwiches themselves respectively. Examples are bolts or rivets.
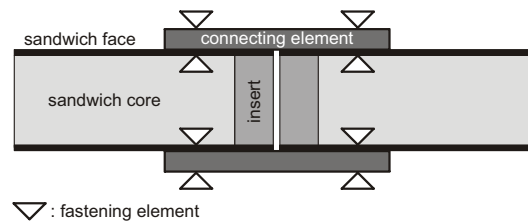

Figure 1: Basic parts of a joint for sandwich elements

The basic elements of the connection have now been determined. They are used to define all possible basic configurations of how a connection between two sandwiches can be established. For this work, the considerations are restricted to two sandwiches lying in-plane to each other. The derivation of rectangular or any other kind of joints of sandwiches will be part of later examinations. The four resulting possibilities are shown in table 1.

Connecting element – sandwich face	Connecting element – sandwich core	Sandwich face – sandwich face	Sandwich core – sandwich core

Table 1: Basic possibilities of connecting two sandwiches using the elements of fig. 1

Those possibilities can again be varied with respect to the four parameters shape, position, size and number leading to the 15 basic configurations shown in table 2. Those configurations are deliberately called "basic" as they are directly derived by altering the parameters mentioned before. There are apparently more configurations which will now be identified by systematically combining the 15 basic configurations. This combination procedure is carried out in compliance with the following rules:

- Beginning with the first, each configuration is combined with all following ones leading to all possible combinations.
- If two connecting elements touch or penetrate each other, then the resulting geometric body is seen as a new, complex connecting element.

- The considerations are of qualitative nature. The exact embodiment design or quantitative parameters are not defined at this point.
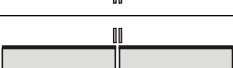
With connecting element(s)					Without connecting element	
1		5		8		
2		6		9		
3		7a		10		
4a		7b		11		
4b		7c				
4c						

Table 2: The 15 basic configurations for connecting two sandwiches

This approach naturally leads to a large number of possible configurations some of which will not be useful or make sense. In order to sort out those invalid configurations, a rough evaluation is conducted along with the combination procedure. The following criteria mark a configuration as invalid:

- Geometric incompatibility: The sandwich faces or one sandwich face and the connecting element penetrate each other; or a sandwich face has to be formed into two different directions at the same time.
- One connecting element completely encloses another.
- A connecting element from the group of 15 basic configurations (see above) is rebuilt.
- A newly added element serves no function.

The result of this combination procedure is 454 possible configurations of which 376 can be considered invalid for the reasons above. Table 3 shows the remaining 78 configurations. An evaluation step shall reduce this number to the 10 most promising configurations. The evaluation criteria are derived from the requirements list and weighted according to their importance for the joint. This results in an objectives tree whose three upper level objectives are:

- Good fulfillment of function; weighted with a percentage of 55%
- Cost; weighted with a percentage of 20%
- Easy Handling; weighted with a percentage of 25%

The lower levels are not presented here. The 78 configurations are then scored on a scale from 0 to 10. The 10 highest rated concepts for a connecting element are in the order of their

ranking starting with the best (cp. table 3): G2, D10, D1, A1, C11, F7, B3, C1, E7, G10

Table 3: Overview of the 78 feasible configurations for connecting two sandwiches

So far, only the connecting elements have been considered. However, the definition of the basic parts of a joint for sandwich elements also included the fastening elements. The rather abstract term "fastening element" denotes the element or part that is necessary to join two or more parts, e. g. bolts, rivets or clamps. As for the connecting element it is demanded to identify all possible fastening elements. Here, the German standard DIN 8593 [4] is useful because it lists all known manufacturing processes for joining. Of those, the mechanical joining processes, a total of 32, are systematically combined with the 10 most promising connecting elements from above. Again, a rough evaluation, conducted simultaneously to the combination procedure, helps sorting out invalid principle solutions. Three criteria are defined for this rough evaluation:

- Ability of transmitting high forces and moments.

- Simple and quick joining procedure.
- Little changes and preparations of the sandwich necessary.

This approach results in originally 783 principal solutions of which 83 remain after the rough evaluation. A final evaluation using a similar objectives tree as mentioned above produces the 18 best principle solutions for a mechanical technology for joining sandwich elements. They are shown in table 4.
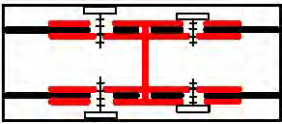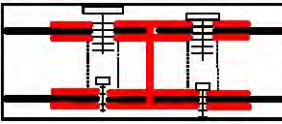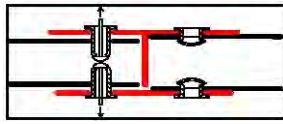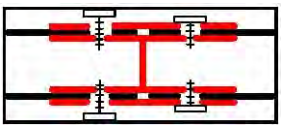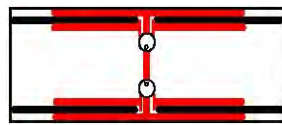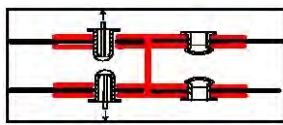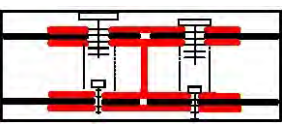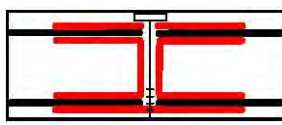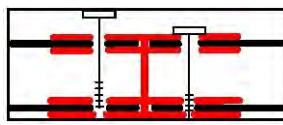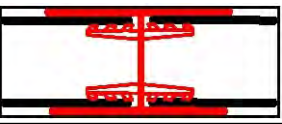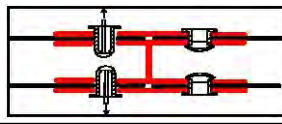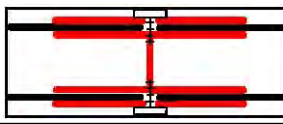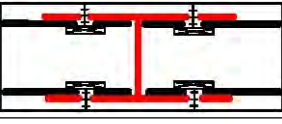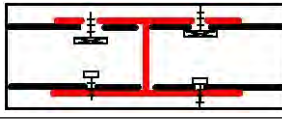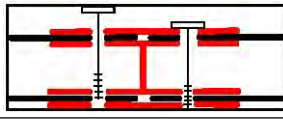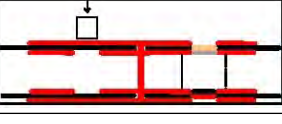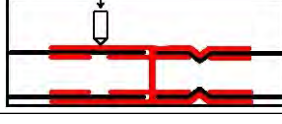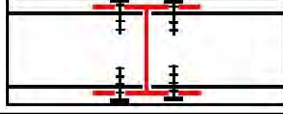
1: Bolts, screwed into inner tongue, single-pieced connecting element	2: Bolts of diff. diameter	3: Rivets, connecting element with only outer tongues
4: Like 1, but separate outer tongues of connecting element	5: Quick-connect mechanism built into connecting element	6: Rivets, connecting element with inner and outer tongues
7: Like 2, but separate outer tongues of connecting element	8: Long bolts through center bar of connecting element	9: Long bolts, off-centered, single-pieced connecting element
10: Quick-connect mechanism with pawls on inner tongues	11: Like 6, but separate outer tongues of connecting element	12: Short centered bolts
13a: Interlocking bolts	13b: Like 13a, but normal bolts on one side	15: Like 9, but separate outer tongues of connecting element
Low-cost 1: Clinching	Low-cost 2: Center-punching	Low-cost 3: Self-tapping screws

Table 4: Basic possibilities of connecting two sandwiches using the elements of fig. 1

3   GENERAL STRUCTURAL ANALYSIS

The preceding considerations delivered 18 principle solutions for joining sandwiches mechanically. The second part of the developing process now consists of stating general mathematical calculations for a structural analysis. For that purpose the 18 principle solutions are divided into six different groups. The solutions within each group have in common that they are very similar to each other with respect to their underlying working principle (table 5). Thus their mathematical description is also similar. This facilitates further considerations as it makes it possible to formulate structural analyses for each group only, instead of doing this for each principle solution.

Group I combines all principle solutions that use bolts as joining elements. They differ slightly with respect to the length of the bolts. Solutions 1, 2, 4 and 7 use short bolts which clamp the sandwich faces between outer and inner tongue of the connecting element, whereas solutions 9 and 15 have long bolts working between the outer tongues. Group II again makes use of bolts. They are however located at the center of the connecting element clamping either both sides with long bolts (no. 8) or each side separately with short bolts (no. 12). The three solutions of Group III all use rivets. They only differ slightly in the assembly of the connecting element. The solutions 5 and 10 of group IV are referred to as quick fasteners. This group is an exception to the others in that the structural analyses of the two solutions differ much. The grouping is however justified by the common property of allowing a quick connection between sandwiches without much preparation. Group V contains the so-called self-locking bolts. Solution 13a differs from 13b only in the way that 13a uses the self-locking bolts on both sides of the connecting element whereas 13b has normal bolts on one side. Group VI combines three solutions which were not rated high in the evaluation before. Yet they remain for further considerations as solutions which will presumably cause little cost.

Group	Denotation	Belonging principle solutions
I	Bolts, off-center	1, 2, 4, 7 (using short bolts); 9, 15 (using long bolts)
II	Bolts, centered	8, 12
III	Rivets	3, 6, 11
IV	Quick fasteners	5, 10
V	Self-locking bolts	13a, 13b
VI	Low-cost fasteners	lc-1, lc-2, lc-3

Table 5: Classification of principle solutions in 6 groups of similar working principles

The result of the structural analysis shall be a set of generally applicable mathematical formulas, i. e. for any combination of external loads these formulas can be used to calculate the critical load for the sandwich connection. Thus, the first step is to define a general load case applicable to all solutions. This load case is based on a Cartesian coordinate system and consists of three forces and three moments according to figure 2. Besides, the calculations underlie the following constraints and assumptions:

- Forces are alway applied symmetrically to the sandwich faces.
- The sandwich is treated as a solid body.
- Loads applied to the sandwiches are transferred directly to the connecting element without being changed.
- The center bar is assumed to be fixed in place. External loads can be transmitted to the surrounding structure through this bar.
- The location of the highest combined loads is the reference for dimensioning. All loads occuring at this location are added according to their amount.
- At this early stage of development, assumptions are often made to the safe side. This might lead to over-dimensioned connecting elements.
- The structural analysis of the sandwiches themselves is not part of this work but will be subject of further research. This work relies on manufacturer's information.
- Group VI of principle solutions, the low-cost fasteners, is discussed separately in [5].
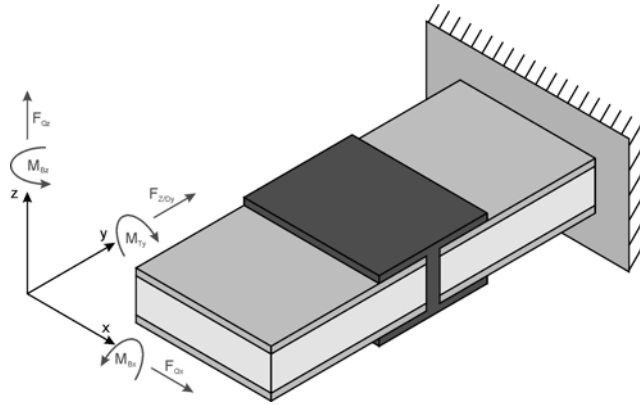
Figure 2: General load case

The structural analyses for the first five groups of principle solutions consist of six steps:
1. Determination of all relevant geometric parameters of the connection. This includes qualitative but not quantitative design of the connecting elements.
2. Each load of the general load case is translated into the corresponding load at the crucial location of the connection (usually the location of the fastening elements).
3. Addition of similar loads to a resulting total load of the same kind.
4. Dimensioning of the fastening elements. This includes the determination of the loads on the fastening elements and their subsequent structural analyses.
5. Determination of the critical stresses in the connecting element, if necessary by calculating an equivalent stress. Calculation of all necessary structural analyses for the connecting element.
6. Structurally analysing the sandwiches at the location of the fastening elements.

The presentation of the structural analyses of all five groups of principle solutions would exceed the limits of the paper. Thus, only the calculations for group I shall be presented here exemplarily. The geometric parameters of this group are shown in fig. 3. Table 6 sums up the result of step two – the translation of the external loads to loads at the locations of the bolts.
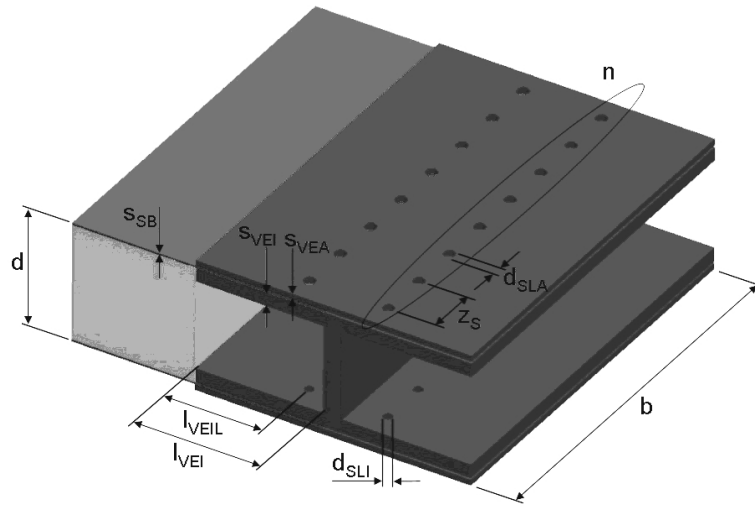
Figure 3: Geometric parameters of the connection of group I (off-centered bolts)

Ext. load	Load on bolts F_S	Direction of F_S	Accuracy	Loaded tongues of connecting element
$F_{Z/Dy}$	$F_{S1} = \dfrac{F_{Z/Dy}}{2 \cdot n}$	y-direction	Exact	All
M_{Bx}	$F_{S2} = \dfrac{M_{Bx}}{d \cdot n}$	y-direction	Very good	All
M_{Bz}	$F_{S3} = \dfrac{3 \cdot M_{Bz} \cdot (n-1)}{z_S \cdot (n^3 - n)}$	y-direction	Good	All
M_{Ty}	$F_{S4/ax,max} = \dfrac{\frac{1}{2} \cdot M_{Ty} \cdot (n-1) \cdot z_s}{d^2 + (n-1)^2 \cdot z_S^2}$ $F_{S4/rad,max} = \dfrac{\frac{1}{2} \cdot M_{Ty} \cdot d}{d^2 + (n-1)^2 \cdot z_S^2}$	z-direction (axial), x-direction (radial)	Sufficient	All
F_{Qz}	$F_{S5} = \dfrac{F_{Qz}}{2 \cdot n}$	z-direction	Sufficient	Inner
F_{Qx}	$F_{S6} = \dfrac{F_{Qx}}{2 \cdot n}$	x-direction	Exact	All

Table 6: Loads at the location of the fastening elements for the fasteners of group I: off-centered bolts

It is assumed that each connecting element has a number of 2n bolts. Eq. 1 and 2 are the results of the third step, i.e. the addition of similar loads to a resulting load. Eq. 1 denotes the maximum force on the bolts in radial direction, equation 2 in axial direction respectively.

$$F_{S,radial,max} = \sqrt{(|F_{S1}| + |F_{S2}| + |F_{S3}|)^2 + (|F_{S4,rad}| + |F_{S6}|)^2} \tag{1}$$

$$F_{S,axial,max} = |F_{S4,ax}| + |F_{S5}| \tag{2}$$

As mentioned above, the fastening elements are dimensioned in the fourth step. For bolts this is done in compliance with the guideline VDI 2230 [6] which gives detailed instructions about how to calculate bolted joints. The mathematical formulation is however too extensive to be presented here.

The next to last step in the structural analysis of group I is the examination of the connecting element with regards to critical stresses. Failure in the connecting element occurs if either the outer or the inner tongues fail. The structural analysis is in both cases the same because inner and outer tongues are frictionally connected through the sandwich face and hence are exposed to the same loads. The weakest and thus crucial location of the tongues which is considered for this step is the intersection through the holes of the bolts. At this location, an equivalent stress $\sigma_{V,GEH}$ is calculated:

$$\sigma_{V,GEH} = \sqrt{(|\sigma_1| + |\sigma_2| + |\sigma_3|)^2 + 3 \cdot \left(\tau_6^2 + (|\tau_4| + |\tau_5|)^2\right)} \tag{3}$$

Stability is proven if:

$$\sigma_{V,GEH} \leq \frac{R_{p,0.2,VE}}{s_F} \tag{4}$$

with $R_{p,0.2,VE}$ being the yield point of the connecting element and s_F being a safety factor.

The sixth step of the structural analysis considers the sandwich elements. Failure can only occur if the maximum surface pressure of the material of the sandwich faces is exceeded by the bolted connection. This calculation however is part of the calculations of the fastening elements in step four. Thus, it shall not be presented here separately.

4 DIMENSIONING AND LAYOUT OF PROTOTYPES

The last part of this work comprises the manufacturing of prototypes of each of the six groups from the preceding chapter. For this purpose, qualitative rules for the embodiment design of the fasteners are stated. They mainly concern the transition between the sandwich faces and the connecting element. They are summarized in table 7. Finally, the prototypes are built following these rules. They differ in the external loads which are assumed for the quantitative design. This allows testing more load cases in later experiments. At this point it must be mentioned that due to the restrictions of the institute's own workshop all prototypes are assemblies consisting of more than one part.

Similar to the preceding chapter only the prototype of group I (bolts, off-center) shall be presented here in detail. The external loads are assumed with $F_{Z/Dy} = 10000$ N and $F_{Qz} = 500$ N. The width is set to b = 200 mm. The material of the connecting element is aluminum with a Young's modulus of E = 70000 N/mm², a yield point of $R_{p,0.2} \approx 150$ N/mm² and a tensile strength of $R_m \approx 290$ N/mm². Figure 4 displays the computer-model and the final prototype.

Figure 5 shows all prototypes together.
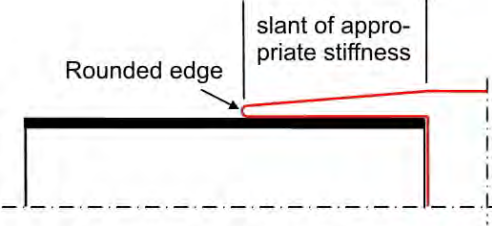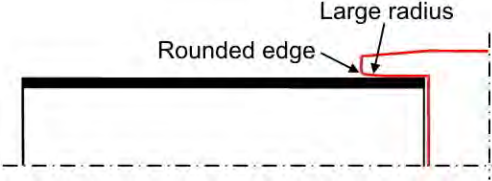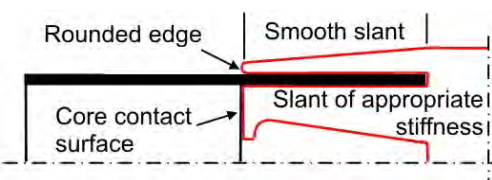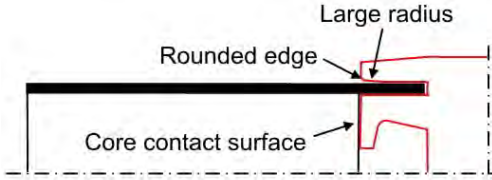
Single tongue connecting element, adequate workspace	Single tongue connecting element, inadequate workspace
Double tongue connecting element, adequate workspace	Double tongue connecting element, inadequate workspace

Table 7: Qualitative design rules for the connecting element
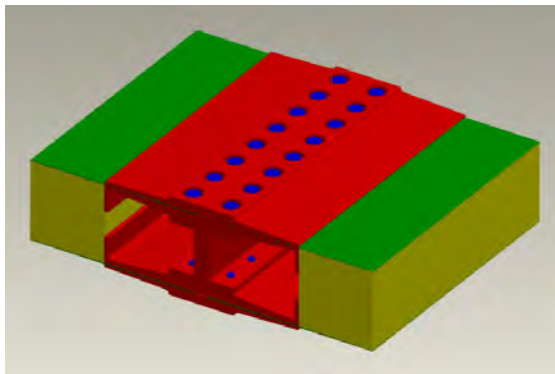
Figure 4: Prototype of group I (off-centered bolts)

5   CONCLUSION

It was shown that a reliable mechanical technology for joining sandwich elements is feasible. The systematic approach to the problem ensured that all possible concepts for joining sandwich elements mechanically were evaluated. The prototypes demonstrated a good fulfillment of the critical requirements. Most requirements defined at the beginning of the develop-

ment are absolutely fulfilled by the prototypes. In manual tests they showed a good ability of transmitting all occurring loads and no deformations of the joint under load. Experimental testing on a servo-hydraulic testing machine will be carried in the future. The requirement that demands the principle of uniform strength could not be fulfilled as the only one. This is however due to the restricted production facilities of the institute. Improved manufacturing processes will also result in smaller dimensions, a lower weight and a more unobtrusive design.
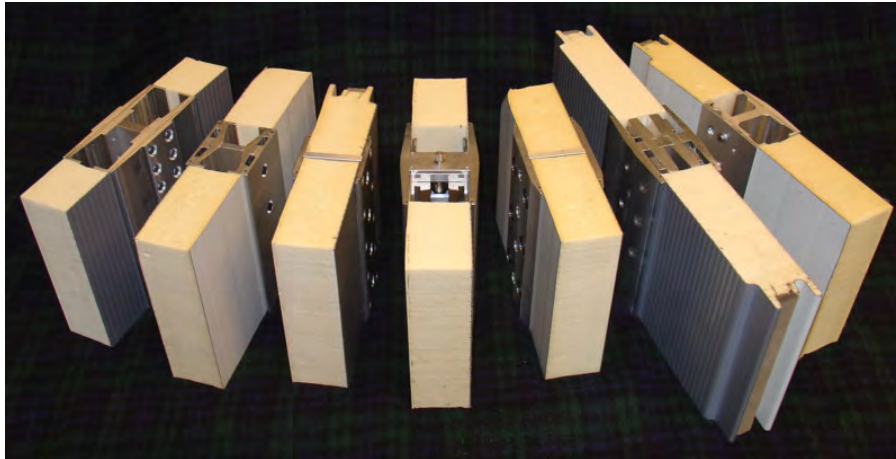
Figure 5: All prototypes

REFERENCES

[1] G. Pahl, W. Beitz, J. Feldhusen and K. H. Grote, *Engineering Design: a systematic approach*, London: Springer, 3. Edition 2007, ISBN 978-1-84628-318-5.

[2] G. Pahl, W. Beitz, J. Feldhusen and K. H. Grote, *Projeto na engenharia: fundamentos do desenvolvimento eficaz de produtos, métodos e aplicações*, São Paul: Editora Edgard Blücher ltda., 1ª edição 2005, ISBN 85-212-0363-2.

[3] A. Kempf, *Entwicklung einer mechanischen Verbindungstechnik für Sandwichwerkstoffe*, Aachen, RWTH University, Inst. for Eng. Design (IKT), Diss., 2004.
http://darwin.bth.rwth-aachen.de/opus3/volltexte/2005/1003/

[4] DIN Deutsches Institut für Normung e. V., *DIN 8593: Fertigungsverfahren Fügen,* Berlin: Beuth, 2003.

[5] J. Feldhusen, C. Warkotsch and M. Benders, *Evaluation of clinching and center-punching as mechanical joining processes for sandwich elements*, Conference Paper, 8th International Conference on Sandwich Structures, Portugal, 2008.

[6] Verein Deutscher Ingenieure: *VDI 2230: Systematische Berechnung hochbeanspruchter Schraubenverbindungen: Zylindrische Einschraubenverbindungen.* Berlin: Beuth, 2003.

MODELLING

VIBRATION AND BUCKLING OF SANDWICH LAMINATES HAVING INTERFACIAL IMPERFECTIONS

Anupam Chakrabarti [*]

[*] Department of Civil Engineering, Indian Institute of Technology Roorkee,
Roorkee: 247667, Uttarakhand, India
e-mail: anupam1965@yahoo.co.uk, achakfce@iitr.ernet.in

Key words: Sandwich laminates, Imperfection, Refined theory, Finite element method.

Summary. *Vibration and Buckling of sandwich laminates are studied for different degrees of imperfections at the layer interfaces using a refined plate theory. With this plate theory, the through thickness variation of transverse shear stresses is represented by piece-wise parabolic functions where the continuity of these stresses is satisfied at the layer interfaces by taking jumps in the transverse shear strains at the interfaces. The transverse shear stresses free condition at the plate top and bottom surfaces is also satisfied. The inter-laminar imperfections are represented by in-plane displacement jumps at the layer interfaces and characterized by a linear spring layer model. It is quite interesting to note that this plate model having all these refined features requires unknowns only at the reference plane. To have generality in the analysis, finite element technique is adopted and it is carried out with a new triangular element developed for this purpose, as any arbitrary existing element cannot model this plate model. As there is no published result on imperfect sandwich plates, the problems of perfect sandwich plates and imperfect ordinary laminates are used for validation.*

1   INTRODUCTION

In a sándwich plate structure, the core and face sheets deform in different manners due to wide variation of their material properties showing kink in in-plane displacements at the interface between the core and stiff face layers. The problem becomes more complicated due to interfacial imperfection for weak bonding or other reasons. This has inspired researchers to develop a number of refined plate theories [1-6] for suitable modeling of laminated plates, which are useful for the analysis of sandwich plates. In this group, the Refined Higher order Shear Deformation Theory (RHSDT) of Cho and Parmerter [6] seems to be most attractive and it is adopted in the present study.

In RHSDT a perfect interface between the layers is generally assumed. But in case of imperfect interfaces, there should be jumps in the displacement components at the interfaces whereas inter-laminar stresses would remain continuous from equilibrium point of view. The simplest way to represent this phenomenon is to use a linear spring layer model where the displacement jumps in a particular interface are proportional to the interlaminar stresses at that interface. Such an attempt has been made by Cheng et al. [7], Di Scuiva [8] and few

others where the linear spring layer model has been implemented in a plate model based on RHSDT. In all these studies application has been made to ordinary composite laminates where the problem has been solved analytically.

So far the authors have not found any study on vibration and buckling of sandwich plates with inter-laminar imperfections. However, there are some few investigations where the sandwich plate has no imperfection or the imperfection has been taken but the structure is an ordinary composite laminate. In this context the investigations carried out by few researchers [9-12] are some representative studies.

In this paper attempt has been made to study the vibration and buckling characteristics of laminated sandwich plates with inter-laminar imperfection of arbitrary variation at the different levels using RHSDT of Cho and Parmerter [6] in combination with the linear spring layer model of Cheng et al. [7]. The problem is solved by finite element technique in order to have generality in the analysis. In this context it should be noted that all these refined plate theories (RFSDT/RHSDT) including that of Cho and Parmerter [6] possess one difficulty and it is encountered at the time of their finite element implementation. Actually, it involves second order derivatives of transverse displacement (w) in the strain components, which requires C_1 continuity of w at the element interfaces (a well-known problem of plate finite element). In this situation, a simple option is to upgrade a conforming thin plate element according to the requirement of any refined plate theory [13-14] but the availability of such thin plate element is very few. Moreover, these elements possess certain drawbacks in general. In order to avoid these problems, Cho and Parmerter [15] have made an attempt where a nonconforming thin plate element has been upgraded according to RHSDT [6]. It is quite interesting that the element has successfully modeled RHSDT [6] though the basic element does not satisfy the inter-element continuity requirement. This may give an impression that any successful nonconforming thin plate element can be upgraded but the success is not assured, which has already been experienced.

In this situation there is a genuine requirement of an efficient and trouble free element for the solution of the present problem, which has inspired the authors to develop a new triangular element [16]. The element contains three corner nodes and three mid side nodes where each node possesses u, v (in-plane displacement components), w (transverse displacement), θ_x, θ_y (rotations), γ_x ($\theta_x - \partial w/\partial x$) and γ_y ($\theta_y - \partial w/\partial y$) as DOF at the reference plane. The new element has shown excellent performance when it has been applied to the static response of perfect composite plates [16]. The element is used in this Finite element model to validate problems of perfect sandwich plates and ordinary composite laminates with imperfect interfaces, as there is no study of laminated sandwich plates with inter-laminar imperfections so far. Finally the Finite element model is applied to solve the present problem to study the behavior of the sandwich laminates under different situations.

2 FORMULATION

The six noded triangular element having equal degrees of freedom (seven) in each node may be of any arbitrary triangular shape and orientation [18] and mapped in a different plane (ζ-η) from (x-y) to have a regular shape.

The displacement functions for the field variables at the reference plane may be expressed as:

$$u = [N_1]\{\alpha_u\} \qquad (1)$$
$$v = [N_1]\{\alpha_v\} \qquad (2)$$
$$w = [N_2]\{\alpha_w\} \qquad (3)$$
$$\gamma_x = [N_1]\{\alpha_{yx}\} \qquad (4)$$
$$\text{and } \gamma_y = [N_1]\{\alpha_{yy}\} \qquad (5)$$

where $\{\alpha_u\} = [\alpha_1 \quad \alpha_2 \quad \alpha_3 \quad \alpha_4 \quad \alpha_5 \quad \alpha_6]^T$, $\{\alpha_v\} = [\alpha_7 \quad \alpha_8 \quad \alpha_9 \quad \alpha_{10} \quad \alpha_{11} \quad \alpha_{12}]^T$,

$\{\alpha_w\} = [\alpha_{13} \quad \alpha_{14} \quad \alpha_{15} \quad \alpha_{16} \quad ...... \quad \alpha_{30}]^T$, $\{\alpha_{yx}\} = [\alpha_{31} \quad \alpha_{32} \quad \alpha_{33} \quad \alpha_{34} \quad \alpha_{35} \quad \alpha_{36}]^T$

$\{\alpha_{yy}\} = [\alpha_{37} \quad \alpha_{38} \quad \alpha_{39} \quad \alpha_{40} \quad \alpha_{41} \quad \alpha_{42}]^T$, $[N_1] = [1 \quad \varsigma \quad \eta \quad \varsigma^2 \quad \varsigma\eta \quad \eta^2]$

and $[N_2] = [1 \quad \varsigma \quad \eta \quad \varsigma^2 \quad \varsigma\eta \quad \eta^2 \quad \varsigma^3 \quad \varsigma^2\eta \quad \varsigma\eta^2 \quad \eta^3 \quad \varsigma^4 \quad \varsigma^3\eta$

$\varsigma^2\eta^2 \quad \varsigma\eta^3 \quad \eta^4 \quad (\varsigma^5 - 5\varsigma^3\eta^2) \quad (\varsigma^2\eta^3 - \varsigma^3\eta^2) \quad (\eta^5 - 5\varsigma^3\eta^2)]$.
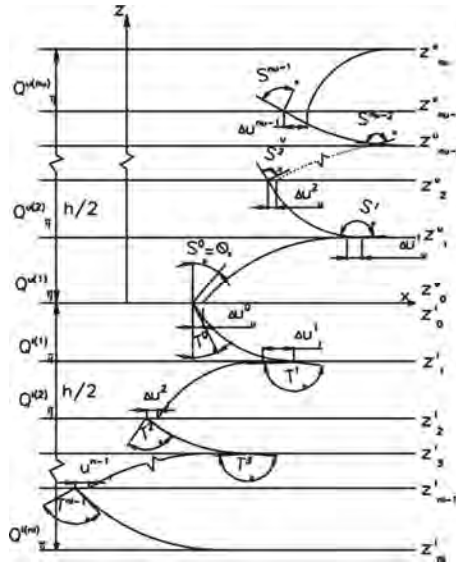
Figure 1 General lamination layup and displacement configuration

Using Eqs. (3-5), the rotations at the reference plane ($\theta_x = -S_1^0$ and $\theta_y = -S_2^0$) as shown in Fig. 1 may be expressed as:

$$\theta_x = \frac{\partial w}{\partial x} + \gamma_x = \frac{\partial w}{\partial \varsigma}\frac{\partial \varsigma}{\partial x} + \frac{\partial w}{\partial \eta}\frac{\partial \eta}{\partial x} + \gamma_x$$

$$= \left(\frac{\partial}{\partial \varsigma}[N_2]\frac{b_1}{2\Delta} + \frac{\partial}{\partial \eta}[N_2]\frac{c_1}{2\Delta}\right)\{\alpha_w\} + [N_1]\{\alpha_{yx}\} = [N_3]\{\alpha_w\} + [N_1]\{\alpha_{yx}\} \qquad (6)$$

$$\text{and} \quad \theta_y = \frac{\partial w}{\partial y} + \gamma_y = \frac{\partial w}{\partial \varsigma}\frac{\partial \varsigma}{\partial y} + \frac{\partial w}{\partial \eta}\frac{\partial \eta}{\partial y} + \gamma_y$$

$$= \left(\frac{\partial}{\partial \varsigma}[N_2]\frac{b_2}{2\Delta} + \frac{\partial}{\partial \eta}[N_2]\frac{c_2}{2\Delta} \right)\{\alpha_w\} + [N_1]\{\alpha_{yy}\} = [N_4]\{\alpha_w\} + [N_1]\{\alpha_{yy}\} \tag{7}$$

Substituting Eqs. (1-7) at the six nodes, the coefficients (α_i) in the Eqs. (1-5) can be expressed in terms of nodal unknowns as:

$$\{\Delta\} = [A]\{\alpha\} \text{ or } \{\alpha\} = [A]^{-1}\{\Delta\} \tag{8}$$

where, $\{\Delta\}^T = \begin{bmatrix} u_1 & v_1 & w_1 & \theta_{x1} & \theta_{y1} & \gamma_{x1} & \gamma_{y1} & u_2 & v_2 & w_2 & \cdots\cdots & \gamma_{y6} \end{bmatrix}$,

$\{\alpha\}^T = \begin{bmatrix} \alpha_1 & \alpha_2 & \alpha_3 & \alpha_4 & \cdots\cdots & \alpha_{42} \end{bmatrix}$ and the matrix $[A]$ having an order 42x42 can be formed with the coordinates of the six nodes.

According to the plate theory for general lamination configuration and the concept of linear spring layer model as discussed earlier, the variation of in-plane displacement components $\bar{u}$ (Fig. 1) and $\bar{v}$ across the thickness may be expressed as:

$$\bar{u} = u + \sum_{k=0}^{n_u-1}\left\{ S_1^k(z-z_k) + \Delta u_k \right\}H(z-z_k) + \sum_{k=0}^{n_l-1}\left\{ T_1^k(z-\xi_k) - \Delta u_k \right\}H(-z+\xi_k) + \beta_x z^2$$

$$+\phi_x z^3 \tag{9}$$

and

$$\bar{v} = v + \sum_{k=0}^{n_u-1}\left\{ S_2^k(z-z_k) + \Delta v_k \right\}H(z-z_k) + \sum_{k=0}^{n_l-1}\left\{ T_2^k(z-\xi_k) - \Delta v_k \right\}H(-z+\xi_k) + \beta_y z^2$$

$$+\phi_y z^3 \tag{10}$$

where $H(z-z_k)$ and $H(-z+\xi_k)$ are the unit step functions.

The transverse displacement is assumed to be constant over the plate thickness i.e.,

$$\bar{w} = w. \tag{11}$$

Now the stress-strain relationship of a lamina may be expressed in structural axes system (x-y) as:

$$\begin{Bmatrix} \sigma_x \\ \sigma_y \\ \tau_{xy} \\ \tau_{xz} \\ \tau_{yz} \end{Bmatrix} = \begin{bmatrix} \bar{Q}_{11} & \bar{Q}_{12} & \bar{Q}_{16} & 0 & 0 \\ \bar{Q}_{12} & \bar{Q}_{22} & \bar{Q}_{26} & 0 & 0 \\ \bar{Q}_{16} & \bar{Q}_{26} & \bar{Q}_{66} & 0 & 0 \\ 0 & 0 & 0 & \bar{Q}_{55} & \bar{Q}_{45} \\ 0 & 0 & 0 & \bar{Q}_{45} & \bar{Q}_{44} \end{bmatrix} \begin{Bmatrix} \varepsilon_x \\ \varepsilon_y \\ \gamma_{xy} \\ \gamma_{xz} \\ \gamma_{yz} \end{Bmatrix} \text{ or } \{\bar{\sigma}\} = \begin{bmatrix} \bar{Q}^k \end{bmatrix}\{\bar{\varepsilon}\} \tag{12}$$

where the rigidity matrix $\begin{bmatrix} \bar{Q}^k \end{bmatrix}$ can be formed with the material properties and fiber orientation of the k-th lamina following the usual techniques of laminated composites.

The imperfection at the k-th interface is characterized by the displacement jumps Δu_k (Fig. 1) and Δv_k, which may be expressed in terms of interlaminar shear stresses at that interface following the concept of linear spring-layer model of Cheng et al. [14] as:

$$\Delta u_k = R_{11}^k \tau_{xz}^k + R_{12}^k \tau_{yz}^k \tag{13}$$

$$\text{and } \Delta v_k = R_{21}^k \tau_{xz}^k + R_{22}^k \tau_{yz}^k \tag{14}$$

where R_{11}^k, R_{12}^k, R_{21}^k and R_{22}^k are the compliance coefficients [14] of the idealized linear spring layer at the k-th interface while τ_{xz}^k and τ_{yz}^k are the transverse shear stresses on that interface. Taking an adjacent layer of k-th interface, τ_{xz}^k and τ_{yz}^k may be expressed in terms of γ_{xz} and γ_{yz} (transverse shear strains) at that layer with the help of Eq. (12). Now Eqs. (9-11) may be used to express γ_{xz} ($= \partial \overline{w} / \partial x + \partial \overline{u} / \partial z$) and γ_{yz} ($= \partial \overline{w} / \partial y + \partial \overline{v} / \partial z$) where Δu_k and Δv_k will not appear and this will help to express Δu_k and Δv_k in terms of other terms of Eqs. (9-11) easily. Finally, S_1^k, S_2^k, T_1^k, T_2^k β_x, β_y, ϕ_x and ϕ_y may be expressed in terms of γ_x, γ_y, $\partial w/\partial x$ and $\partial w/\partial y$ utilizing transverse shear stress free condition at the plate top and bottom surfaces and the continuity condition of these stresses at the layer interfaces.

Now the strain $\{\overline{\varepsilon}\}$ at any point may be expressed as:

$$\{\overline{\varepsilon}\} = \left[\frac{\partial \overline{u}}{\partial x} \quad \frac{\partial \overline{v}}{\partial y} \quad \frac{\partial \overline{u}}{\partial y} + \frac{\partial \overline{v}}{\partial x} \quad \frac{\partial \overline{u}}{\partial z} + \frac{\partial \overline{w}}{\partial x} \quad \frac{\partial \overline{v}}{\partial z} + \frac{\partial \overline{w}}{\partial y} \right]^T = [H]\{\varepsilon\} \tag{15}$$

where

$$\{\varepsilon\} = \left[\frac{\partial u}{\partial x} \quad \frac{\partial v}{\partial y} \quad \frac{\partial u}{\partial y} + \frac{\partial v}{\partial x} \quad \frac{\partial^2 w}{\partial x^2} \quad \frac{\partial^2 w}{\partial y^2} \quad \frac{\partial^2 w}{\partial x \partial y} \quad \frac{\partial \gamma_x}{\partial x} \quad \frac{\partial \gamma_y}{\partial y} \right.$$

$$\left. \frac{\partial \gamma_y}{\partial x} \quad \frac{\partial \gamma_x}{\partial y} \quad \gamma_x \quad \gamma_y \quad \frac{\partial w}{\partial x} \quad \frac{\partial w}{\partial y} \right] \tag{16}$$

and the matrix $[H]$ having an order of (5 x 14) contains z and some constant quantities dependent on material properties and thickness of the different layers.

Now the field variables as expressed in Eqs. (1-5) may be substituted in the above equation and it may be expressed as:

$$\{\varepsilon\} = [\overline{B}]\{\alpha\} \tag{17}$$

It can be expressed in terms of nodal displacement vector $\{\Delta\}$ using Eq. (8) as:

$$\{\varepsilon\} = [\overline{B}][A]^{-1}\{\Delta\} \text{ or } \{\varepsilon\} = [B]\{\Delta\}. \tag{18}$$

With the help of above equations the element stiffness matrix $[k]$ can be easily derived and it may be expressed as:

$$[k] = \sum_{k=1}^{n_u+n_l} \int [B]^T [H]^T [\overline{Q}^k][H][B]\,dxdydz = \int [B]^T [D][B]\,dxdy \qquad (19)$$

$$\text{where } [D] = \sum_{k=1}^{n_u+n_l} \int [H]^T [\overline{Q}^k] \ [H] \ dz \qquad (20)$$

Now the consistent mass matrix and the geometric stiffness matrix of an element can be derived in a similar manner. With the help of Eqs. (1-14), the displacement components at any point may be expressed as:

$$\{\overline{f}\} = \begin{Bmatrix} \overline{u} \\ \overline{v} \\ \overline{w} \end{Bmatrix} = [F]\begin{Bmatrix} u & v & w & \dfrac{\partial w}{\partial x} & \dfrac{\partial w}{\partial y} & \gamma_x & \gamma_y \end{Bmatrix}^T = [F][X]\{\alpha\} = [F][X][A]^{-1}\{\Delta\} = [C]\{\Delta\} \qquad (21)$$

where $[F]$ is a matrix of order 3x7, which contains z and some constant quantities as in $[H]$. The matrix $[X]$ having an order of 7x42 contains $[N_1]$ and derivatives of $[N_2]$.

Using the above equation, the consistent mass matrix of an element can be derived and it may be expressed as:

$$[m] = \sum_{k=1}^{nu+nl} \iiint \rho_k [C]^T [C]\,dxdydz \qquad (22)$$

where ρ_k is the mass density of the k-th layer.

In a similar manner the geometric strain vector may be expressed as:

$$\{\boldsymbol{\varepsilon}_G\} = \begin{bmatrix} \dfrac{1}{2}\left(\dfrac{\partial \overline{w}}{\partial x}\right)^2 + \dfrac{1}{2}\left(\dfrac{\partial \overline{u}}{\partial x}\right)^2 + \dfrac{1}{2}\left(\dfrac{\partial \overline{v}}{\partial x}\right)^2 \\[4mm] \dfrac{1}{2}\left(\dfrac{\partial \overline{w}}{\partial y}\right)^2 + \dfrac{1}{2}\left(\dfrac{\partial \overline{u}}{\partial y}\right)^2 + \dfrac{1}{2}\left(\dfrac{\partial \overline{v}}{\partial y}\right)^2 \\[4mm] \left(\dfrac{\partial \overline{w}}{\partial x}\right)\left(\dfrac{\partial \overline{w}}{\partial y}\right) + \left(\dfrac{\partial \overline{u}}{\partial x}\right)\left(\dfrac{\partial \overline{u}}{\partial y}\right) + \left(\dfrac{\partial \overline{v}}{\partial x}\right)\left(\dfrac{\partial \overline{v}}{\partial y}\right) \end{bmatrix} = \dfrac{1}{2}\begin{bmatrix} \dfrac{\partial \overline{w}}{\partial x} & 0 & \dfrac{\partial \overline{u}}{\partial x} & 0 & \dfrac{\partial \overline{v}}{\partial x} & 0 \\[3mm] 0 & \dfrac{\partial \overline{w}}{\partial y} & 0 & \dfrac{\partial \overline{u}}{\partial y} & 0 & \dfrac{\partial \overline{v}}{\partial y} \\[3mm] \dfrac{\partial \overline{w}}{\partial y} & \dfrac{\partial \overline{w}}{\partial x} & \dfrac{\partial \overline{u}}{\partial y} & \dfrac{\partial \overline{u}}{\partial x} & \dfrac{\partial \overline{v}}{\partial y} & \dfrac{\partial \overline{v}}{\partial x} \end{bmatrix} \begin{Bmatrix} \dfrac{\partial \overline{w}}{\partial x} \\[2mm] \dfrac{\partial \overline{w}}{\partial y} \\[2mm] \dfrac{\partial \overline{u}}{\partial x} \\[2mm] \dfrac{\partial \overline{u}}{\partial y} \\[2mm] \dfrac{\partial \overline{v}}{\partial x} \\[2mm] \dfrac{\partial \overline{v}}{\partial y} \end{Bmatrix}$$

$$= \dfrac{1}{2}[A_G][\boldsymbol{\theta}] = \dfrac{1}{2}[A_G][N_G][\boldsymbol{\alpha}] = \dfrac{1}{2}[A_G][N_G][A]^{-1}[\boldsymbol{\Delta}] = \dfrac{1}{2}[A_G][G][\boldsymbol{\Delta}] \qquad (23)$$

With the matrix $[G]$ in the above equation, the geometric stiffness matrix $[k_g]$ of an element can be derived and it may be expressed as:

$$\left[k_g\right] = \sum_{k=1}^{n_u+n_l} \iiint [G]^T \left[S^k\right][G]\,dxdydz \tag{24}$$

where $[S^k]$ may be expressed in terms of in-plane stress components of the k-th layer as:

$$\left[S^k\right] = \begin{bmatrix} \sigma_x & \tau_{xy} & 0 & 0 & 0 & 0 \\ \tau_{xy} & \sigma_y & 0 & 0 & 0 & 0 \\ 0 & 0 & \sigma_x & \tau_{xy} & 0 & 0 \\ 0 & 0 & \tau_{xy} & \sigma_y & 0 & 0 \\ 0 & 0 & 0 & 0 & \sigma_x & \tau_{xy} \\ 0 & 0 & 0 & 0 & \tau_{xy} & \sigma_y \end{bmatrix}$$

Integrations found in the Eqs. (19-20), (22) and (24) are carried out numerically. The element stiffness matrix, geometric stiffness matrix and mass matrix are evaluated for all the elements and assembled together to form the overall stiffness matrix $[K]$, geometric stiffness matrix $[K_G]$ and mass matrix $[M]$ and these matrices are stored in single array following the skyline storage technique. With these matrices, the governing equation may be expressed as follows:

Vibration: $[K]\{\psi\} = \omega^2[M]\{\psi\}$, (25)

Buckling: $[K]\{\psi\} = \lambda[K_G]\{\psi\}$, (26)

where ω is the frequency of vibration and λ is the critical load of buckling.

3 RESULTS AND DISCUSSION

In this section a number of numerical examples covering different features are solved by the proposed finite element model to study different problems of vibration and buckling of laminated sandwich plates with / without imperfect interfaces. For the present problem of imperfection in a sándwich plate there is no published result as mentioned earlier. Thus the proposed model is validated with available results of laminated sandwich plates with perfect interface and laminated composites with imperfect interface. Finally, the proposed finite model is applied to the actual problem and a large number of results are generated to have some understanding on the present problem.

3.1 Simply supported cross-ply (0/90/0) square laminate having variable layer thickness

The vibration and buckling of this plate (thickness ratio, $h/a = 0.1$) is studied for different degrees of imperfections at the layer interfaces. The imperfections taken at both the interfaces are characterized by: $R_{11}^k = R_{22}^k = Rh/E_{11}$, where the non-dimensional parameter R is varied from 0.0 to 0.9. The values R_{12}^k and R_{21}^k are taken as zero and it is followed in all the subsequent examples. In this laminate the central layer has thickness of $0.8h$ while that is $0.1h$ for both the outer layers.

References	R				
	0.00	0.20	0.40	0.60	0.90
$K_t = 1$					
Present Analysis (20x20)	4.7422	4.7357	4.7290	4.7223	4.7121
Di Sciuva [15]	4.7698	-	-	-	-
Cheng et al. [10]	4.7405	4.7340	4.7275	4.7209	-
Srinivas and Rao [19]	4.7419	-	-	-	-
$K_t = 5$					
Present Analysis (20x20)	7.7161	7.6352	7.5523	7.4675	7.3380
Di Sciuva [15]	7.7296	-	-	-	-
Cheng et al. [10]	7.7135	7.6334	7.5511	7.4671	-
Srinivas and Rao [19]	7.7148	-	-	-	-
$K_t = 10$					
Present Analysis (20x20)	9.8135	9.6166	9.4179	9.2187	8.9221
Di Sciuva [15]	9.8222	-	-	-	-
Cheng et al. [10]	9.8091	9.6136	9.4161	9.2182	-
Srinivas and Rao [19]	9.8104	-	-	-	-
$K_t = 15$					
Present Analysis (20x20)	11.2092	10.9004	10.5940	10.2925	9.8536
Di Sciuva [15]	11.2137	-	-	-	-
Cheng et al. [10]	11.2021	10.8953	10.5907	10.2909	-
Srinivas and Rao [19]	11.2034	-	-	-	-

Table 1 Fundamental frequency parameters (Ω) of a simply Supported square composite plate having variable layer thickness

The elastic moduli taken for the thick core layer are $E_{22}/E_{11} = 0.543$, $G_{12}/E_{11} = 0.2629$, $G_{13}/E_{11} = 0.1599$, $G_{23}/E_{11} = 0.2668$ whereas these elastic moduli for the thin laminate composite outer layers are varied and these are taken as a factor (K_t) of those of the central layer. The value of ν_{12} is taken as 0.3 for all the layers.

The plate is analyzed with the proposed Finite element model using mesh size 20x20 (full plate). This is the mesh size corresponding to which the convergence is found to occur. The fundamental frequency parameters $\Omega = 100\omega\sqrt{(\rho h^2/E_{11})}$ and critical buckling load parameters ($\chi = 12N_x b^2/\pi^2 E_{11} h^2$) obtained in the present analysis are presented in Table 1 and Table 2 respectively. The three dimensional elasticity solution of Srinivas and Rao [19] and series solution of Di Sciuva [15] based on RFSDT for perfect interfaces are also shown in the same Tables to have some comparitive study. The results obtained by Cheng et al. [10] and Cheng et al. [14] are also included in Table 1 and Table 2 respectively to compare the present results for imperfect interfaces.

For the buckling analysis, the plate is subjected to N_x where it has different distribution at the different layers to have identical in-plane strain in all the layers. The tables show that the present results have very good agreement with those of the published results.

References	R				
	0.00	0.20	0.40	0.60	0.90
$K_t = 1$					
Present Analysis (20x20)	2.7722	2.7625	2.7548	2.7470	2.7351
Di Sciuva [15]	2.8432	-	-	-	-
Cheng et al. [14]	2.8077	2.7999	2.7919	2.7839	-
Srinivas and Rao [19]	2.770	-	-	-	-
$K_t = 5$					
Present Analysis (20x20)	4.0461	3.6903	3.8750	3.7889	3.6590
Di Sciuva [15]	4.1362	-	-	-	-
Cheng et al. [14]	4.1183	4.0318	3.9439	3.8554	-
Srinivas and Rao [19]	4.046	-	-	-	-
$K_t = 10$					
Present Analysis (20x20)	4.2013	4.0332	3.8689	3.7075	3.4732
Di Sciuva [15]	4.2022	4.0337	3.8693	3.7079	3.4736
Cheng et al. [14]	4.2833	-	-	-	-
Srinivas and Rao [19]	4.2711	4.1006	3.9321	3.7670	-
$K_t = 15$					
Present Analysis (20x20)	4.0173	3.8197	3.5536	3.2587	2.8784
Di Sciuva [15]	4.0172	3.8201	3.5543	3.2593	2.8789
Cheng et al. [14]	4.1063	-	-	-	-
Srinivas and Rao [19]	4.0977	3.8743	3.6591	3.4535	-

Table 2 Buckling load parameters (χ) of a square composite plate having variable layer thickness under uniaxial compression

3.2 Simply supported square sandwich plate with laminated face sheets

The vibration of the laminated sandwich plate (0/90/../C/../90/0) is studied taking imperfections only at the interfaces between low strength core and high strength laminated face sheets. The stiff face sheets are cross-ply laminates where the number of equal thickness ply in each laminate is taken as 2 and 8, which are stacked symmetrically with respect to the core (0/90/../C/../90/0). The thickness of the core ($E/E_c = 11.945$, $G_{c12}/E_c = G_{c13}/E_c = 1.173/6.279$, $G_{c23}/E_c = 2.415/6.279$, $\nu_{c12} = 0.0025$ and $\rho/\rho_c = 0.6818$) is taken as $0.8h$, while that of each face sheets ($E_{11}/E = 40.0$, $E_{22}/E = 1.0$, $G_{12}/E = G_{13}/E = G_{23}/E = 1.0$, $\nu_{12} = 0.25$, $\rho_f = \rho$) is $0.1h$. In this problem, the imperfection is characterized by $R_{11}^k = R_{22}^k = Rh/E$ where R is varied in a similar manner as done in the previous example. The plate is analyzed with the proposed element using mesh size of 20x20 (full plate) taking thickness ratio (h/a) of 0.01 and 0.10. The frequency parameters $\Omega = 100 \omega a \sqrt{(\rho_c/E_{11})}$ obtained in the present analysis for first six modes are presented in Table 3 with some results obtained Wang et al. [9] for perfect cases. Wang et al. [9] have modeled the deformation of the structure in a conventional manner taking simply two angles of rotation (one for the core and the other for both the face sheets) where certain conditions such as transverse shear stress continuity at the interfaces are not satisfied. This might have given his results on the higher side compared to present results. However, they follow a similar trend.

h/a	R	N[a]	Reference	Mode number					
				1	2	3	4	5	6
0.01	0.00	2	Present	2.2186	5.5928	6.3777	8.3599	10.8467	12.6391
		8	Present	2.2175	5.7869	6.1724	8.3451	11.2865	12.6671
	0.20	2	Present	2.2177	5.5854	6.3643	8.3467	10.8197	12.6089
		8	Present	2.2165	5.7792	6.1702	8.3320	11.2584	12.6295
	0.40	2	Present	2.2167	5.5780	6.3548	8.3334	10.7927	12.5787
		8	Present	2.2155	5.7715	6.1611	8.3188	11.2303	12.5916
	0.60	2	Present	2.2156	5.5705	6.3452	8.3201	10.7657	12.5484
		8	Present	2.2145	5.7637	6.1519	8.3055	11.2022	12.5535
	0.90	2	Present	2.2140	5.5591	6.3305	8.2992	10.7249	12.5019
		8	Present	2.2130	5.7520	6.1379	8.2855	11.1601	12.4960
0.10	0.00	2	Present	10.1805	14.9134	19.6634	20.8018	22.4906	24.3906
			Wang et al. [9]	10.555	16.830	19.648	23.616	-	-
		8	Present	10.1198	15.4679	19.3421	22.4467	22.6176	24.3905
			Wang et al. [9]	10.704	16.823	20.476	24.240	-	-
	0.20	2	Present	10.0809	14.7856	19.4041	20.6373	22.2246	24.3906
		8	Present	10.0237	15.3429	19.0960	22.2876	22.3650	24.3905
	0.40	2	Present	9.9832	14.6600	19.1517	20.4759	21.9654	24.3905
		8	Present	9.9293	15.2201	18.8566	22.1190	22.1314	24.3905
	0.60	2	Present	9.8872	14.5366	18.9059	20.3175	21.7130	24.3905
		8	Present	9.8366	15.0995	18.6235	21.8795	21.9782	24.3905
	0.90	2	Present	9.7464	14.3556	18.5491	20.0849	21.3458	24.3905
		8	Present	9.7006	14.9226	18.2853	21.5315	21.7536	24.3905

[a] Number of ply in each laminated face sheet

Table 3 Frequency parameters (Ω) of a simply supported square sandwich plate (0/90/../C/../90/0) with laminated face sheets

3.3 Skew sandwich plate with laminated face sheets clamped at the four sides

The buckling of the skew sandwich plate (-45/45/45/-45/C/-45/45/45/-45) having equal sides is studied for different values of skew angle (0^0, 15^0, 30^0, 45^0, 60^0 and 75^0) taking thickness ratio (h/a) of 0.05 and 0.10. The material properties and thickness of core and a ply in the laminated face sheets are same as those taken in the previous example. The imperfection is also taken in a similar manner as that of previous example. Taking $R = 0.0$, 0.9, 1.2 and 1.8, the analysis is carried out with the proposed element using a mesh size of 20x20 for all the cases. The buckling load parameters ($\chi = N_x a^2 / E_2 h_c^3$) obtained in the present analysis are plotted against skew angles in Fig. 2.
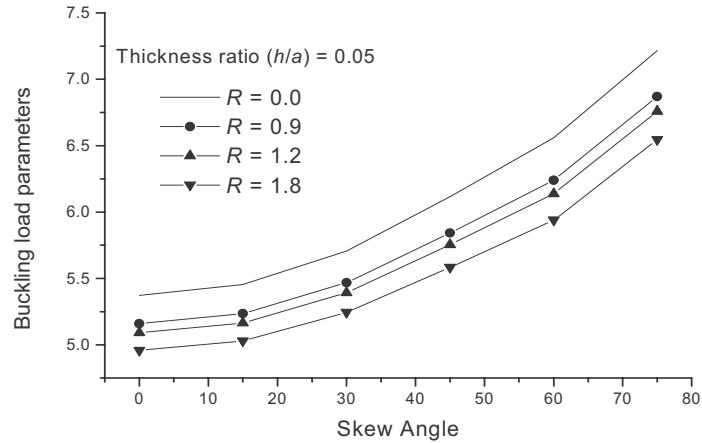
(a)
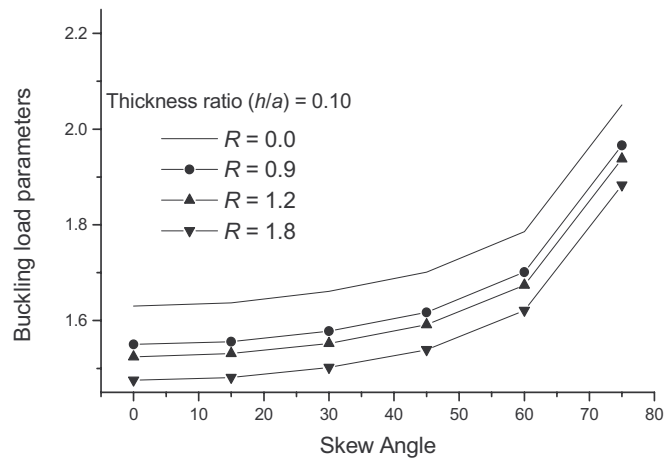
(b)

Figure 2 Effect of skew angle on buckling of a laminated sandwich plate (-45/45/45/-45/C/-45/45/45/-45) having interfacial imperfections

4   CONCLUSIONS

The vibration and buckling of sandwich plates with laminated stiff layers are investigated by an efficient Finite element model based on a refined higher order shear deformation theory taking imperfections at the layer interfaces. A linear spring layer model is used to represent the interfacial imperfections. The most important outcome of this finite element model is that it has all the features for an accurate modeling of the present problem having such complexity. At the same time, it is computationally as elegant as any single layer plate model

since it requires the usual unknowns at the reference plane only. As there is no investigation on the response of laminated sandwich plates with interfacial imperfections for vibration and buckling, a number of problems are solved. It includes different plate geometry, boundary conditions, stacking sequence, thickness ratio and some other aspects with different degrees of imperfection. In this process a number of results are generated, which helps to have some understanding regarding the structural behavior under different situations.

REFERENCES

[1] S. Srinivas, "A refined analysis of composite laminates", *J Sou. Vib.*, 30, 495-507 (1973).

[2] A. Toledano and H. Murakami, "Composite plate theory for arbitrary laminate configurations", *J App. Mech. ASME*, 54, 181-189 (1987).

[3] D.H. Robbins and J.N. Reddy, "Modelling of thick composites using a layer-wise laminate theory", *Int. J Num. Meth. Engg.*, 36, 655-677 (1993).

[4] M. Di Sciuva, "A refined transverse shear deformation theory for multilayered anisotropic plates", *Atti Accademia Scienze Torino*, 118, 279-295 (1984).

[5] K. Bhaskar and T.K. Varadan, "Refinement of higher order laminated plate theories", *AIAA J.*, 27, 1830-1831 (1989).

[6] M. Cho and R.R. Parmerter, "Efficient higher order plate theory for general lamination configurations", *AIAA J.*, 31, 1299-1308 (1993).

[7] Z. Cheng, A.K. Jemah and F.W. Williams, "Theory of multilayered anisotropic plates with weakend interfaces", *J App. Mech. ASME*, 63, 1019-1026 (1996).

[8] M. Di Sciuva, "A geometrically nonlinear theory of multilayered plates with interlayer slip", *AIAA J.*, 35, 1753-1759 (1997).

[9] C.M. Wang, K.K. Ang and L. Yang, "Free vibration of skew sandwich plates with laminated facings", *J Sou. Vib.*, 235, 317-340 (2000).

[10] Z. Cheng, W.P. Howson, and F.W. Williams, "Modelling of weakly bonded laminated composite plates at large deflections", *Int. J Sol. Struc.*, 34, 3583-3599 (1997).

[11] T.P. Khatua and Y.K. Cheung, "Stability analysis of multilayer sandwich structure", *AIAA J.*, 9, 1233-1234 (1973).

[12] Z. Cheng, D.Kennedy and F.W. Williams, "Effect of interfacial imperfection on buckling and bending of composite laminates", *AIAA J.*, 34, 2590-2595 (1996).

[13] M. Di Sciuva, "A general quadrilateral multi-layered anisotropic plate element with continuous interlaminar stresses", *Comp. & Struc.*, 47, 91-105 (1993).

[14] M. Di Sciuva and U. Icardi, "Analysis of thick multi-layered anisotropic plates by a higher order plate element", *AIAA J.*, 33, 2435-2437 (1995).

[15] M. Cho and R.R. Parmerter, "Finite element for composite plate bending based on efficient higher order theory", *AIAA J.*, 32(11), 2241-2245 (1994).

[16] A. Chakrabarti and A.H. Sheikh, "A New Triangular Element to model Inter-Laminar Shear Stress Continuous Plate Theory", *International Journal for Numerical Methods in Engineering*, 60(7), 1237-1257 (2004).

[17] S. Srinivas, and A.K. Rao, "Bending, vibration and buckling of simply supported thick orthotropic rectangular plates and laminates", *Int. J. Sol. Struc.,* 6, 1463-1481 (1970).

DESIGN OF AIRCRAFT FLOOR SANDWICH COMPOSITE PANELS FINITE ELEMENT ANALYSIS AND EXPERIMENTAL VERIFICATION

H. Talebi Mazraehshahi[*], **B. Hamidi Qalehjigh** [†], **A. Vahedi**[†] **and M.A.Vaziri Zanjani** [†]

[*] Aerospace Engineering Department, Sharif University of Technology
Tehran, Iran
e-mail: h_talebi@alum.sharif.edu

† Aerospace Engineering Department, Amirkabir University of Technology
Tehran, Iran
e-mail: b_hamidi_g@yahoo.com
e-mail: av_vahedi@yahoo.com
e-mail: vaziry@hesaco.com

Key words: FEM, Floor composite Sandwich panel, Experimental test.

Summary

As the technological, structural, thermal, acoustical, durability, and other requirements for shell structures increase so does the application of sandwich and composite panels in land, marine, space vehicles, industrial, civil and other structures. Due to their high stiffness and strength to weight ratios, composite sandwich structures have proven their usefulness in a large number of applications in various technical fields, especially in aeronautics, automotive and civil engineering. According to the application of floor panel (with sandwich construction) in civil aircraft and with regards to the fact that they undergo with different loading conditions, it is necessary to have a study on their mechanical behavior that submit stress strength and deflection (stiffness) requirements.

In this paper, analysis of orthotropic and sandwich structure in different boundary conditions are considered. First, the theoretical background for analysis of orthotropic plates is introduced. Next, a finite element model was developed and used as a numerical tool for analysis of these structures under different load and boundary conditions. The detailed design and analysis of sandwich panel required the input of the elastic and strength properties of the sandwich constituents. For this reason at first an improved testing procedure and its results that provided the basic elastic and strength properties are reported in this paper.

The obtained results are then compared with those from theoretical and experimental ones.

In theoretical calculation, the deflection and stress for sandwich plate (isotropic face & orthotropic face), considering various boundary conditions such as clamped (all edge clamped) and simply supported under local and lateral loads are estimated.

Next, finite element method is used to determine the stresses and deflections of panels with various load and boundary conditions. The effect of plate aspect ratio (a / b) on stresses and deflections for simply supported, clamped and bolted conditions are investigated in detail.

Finally, the deflection of a sandwich panel with bolted boundary conditions under lateral load was studied experimentally. The results obtained from FEM, theoretical and experimental investigations are then compared.

1 TESTING OF COMPOSITE SANDWICH PANEL FOR DETERMINETION OF MECHANICAL PERFORMANCE

Following testing procedure was performed for determination of mechanical properties of Fiberlam Grade 1 sandwich panel fabricated by HEXCEL Company, which has, faces with two cross-plied $0°$ and $90°$ of unidirectional glass and nomex honeycomb core [1, 2]:

- Flexural testing (long & short beam) according t0 ASTM C393-98 for face and core strength and stiffness
- Indentation testing according to our procedure for local load strength
- Insert shear testing according to BMS 4-17 for ultimate shear load on insert
- Pull out testing according to BAC 5524 for ultimate tension load on insert

The following mechanical properties were derived from tests. These properties are tabulated in Table 1.

$t_f = 0.38\,mm$	Face thickness
$t_f = 9.525\ mm$	Core thickness
$E_{11} = 58000\,Mpa$	Face elastic modulus in $0°$
$E_{22} = 57000\,Mpa$	Face elastic modulus in $90°$
$G_{xy} = 7000\ Mpa$	Face shear modulus
$\sigma_{11} = 363\ Mpa$	Face ultimate stress (in flexure)
$\sigma_{22} = 290\ Mpa$	Face ultimate stress (in flexure)
$G_L = 115\ Mpa$	Core shear modulus in L direction
$G_W = 69\ Mpa$	Core shear modulus in W direction
$E_c = 600\ Mpa$	Core compression modulus
$\tau_L = 3.5\ Mpa$	Core shear strength (L direction)
$\tau_W = 1.9\ Mpa$	Core shear strength (W direction)
$\sigma_c = 15\ Mpa$	Core compression strength
$\rho = 144\ Kg/m^3$	Density
3738 N	Insert shear load
2450 N	Pull out load
2200 N	Indentation load

Table 1 : Mechanical properties of Fiberlam Grade 1 sandwich panel

2   ANALYTICAL DETERMINATION OF DEFLECTIONS AND STRESSES IN SANDWICH PLATE UNDER UNIFORM LATERAL LOAD

2.1 Simply supported orthotropic face sandwich plate

In this section, Navier method was used for determination of deflection and stress for orthotropic plates [3]. Consider a simply supported rectangular orthotropic plate under uniform load $p(x, y) = p_0$. Note that maximum bending moment and deflection occurs in center of plate, i.e. ($x = a/2$, $y = b/2$).

Deflection of plate can be obtained as follow [3]:

$$w = \frac{16 p_0}{\pi^6} \sum_m^\infty \sum_n^\infty \frac{Sin(m\pi x / a)Sin(n\pi y / b)}{mn[(m^4 / a^4)D_1 + 2D_3(m^2 n^2 / a^2 b^2) + (n^4 / b^4)D_2]} \tag{1}$$

Where a is the smaller dimension of plate ($a \le b$). The moments are then given by:

$$M_x = \frac{16 p_0}{\pi^4} \sum_m^\infty \sum_n^\infty \frac{[D_1(m/a)^2 + D_{12}(n/b)^2]}{mn[(m^4 / a^4)D_1 + 2D_3(m^2 n^2 / a^2 b^2) + (n^4 / b^4)D_2]} Sin(m\pi x / a)Sin(n\pi y / b) \tag{2}$$

$$M_y = \frac{16 p_0}{\pi^4} \sum_m^\infty \sum_n^\infty \frac{[D_2(n/b)^2 + D_{12}(m/a)^2]}{mn[(m^4 / a^4)D_1 + 2D_3(m^2 n^2 / a^2 b^2) + (n^4 / b^4)D_2]} Sin(m\pi x / a)Sin(n\pi y / b)$$

$$M_{xy} = -\frac{32 p_0}{\pi^4} \sum_m^\infty \sum_n^\infty \frac{D_{33}}{ab[(m^4 / a^4)D_1 + 2D_3(m^2 n^2 / a^2 b^2) + (n^4 / b^4)D_2]} Cos(m\pi x / a)Cos(m\pi y / b)$$

2.2 Clamped edges orthotropic face sandwich plate

Let us consider a clamped rectangular orthotropic plate under uniform load $p(x, y) = p_0$. Boundary condition state as follow

$$w = 0 \qquad\qquad \frac{\partial w}{\partial x} = 0 \qquad\qquad (x = \pm \frac{a}{2})$$

$$w = 0 \qquad\qquad \frac{\partial w}{\partial y} = 0 \qquad\qquad (y = \pm \frac{b}{2})$$

Deflection of plate which is calculated from energy method is given [3]

$$w = \frac{49 p_0}{8} \frac{(x^2 - a^2 / 4)^2 (y^2 - b^2 / 4)^2}{7D_1 b^4 + 4D_3 a^2 b^2 + 7D_2 a^4} \tag{3}$$

Maximum deflection occurs at center of plate at $y = 0$, $x = 0$

$$w_{\max} = \frac{0.003418 p_0 a^4}{D_1 + 0.5714 D_3 (a/b)^2 + D_2 (a/b)^2} \tag{4}$$

Also, one can obtain bending moment in plate

$$M_x = -\frac{49p_0}{8}\frac{[D_1(12x^2-a^2)(y^2-b^2/4)^2 + D_{12}(12y^2-b^2)(x^2-a^2/4)^2]}{7D_1b^4 + 4D_3a^2b^2 + 7D_2a^4} \qquad (5)$$

$$M_y = -\frac{49p_0}{8}\frac{[D_2(12y^2-b^2)(x^2-a^2/4)^2 + D_{12}(12x^2-a^2)(y^2-b^2/4)^2]}{7D_1b^4 + 4D_3a^2b^2 + 7D_2a^4}$$

$$M_{xy} = -\frac{(49p_0D_{33})[xy(x^2-a^2)(y^2-b^2)]}{7D_1b^4 + 4D_3a^2b^2 + 7D_2a^4}$$

3 CALCULATION OF DEFLECTION AND STRESSES BY FINITE ELEMENT METHOD

In this section, finite element method is used to determine stress and deflection of panels. Initially the effect of a/b on stresses and deflections for simply supported and clamped condition are investigated. Then, the results were compared with theoretical results which discussed in pervious sections. Since no theoretical results are available for panel with bolted boundary, therefore, finite element method was used to calculate the deflections and stresses in panels. However, the experimental data was used to validate the FE results. Experimental results were obtained by constructing a test rig a shown in figure 1. The panel was installed on a fixture by bolts. The whole rig was set under a chamber and was connected to a vacuum pump. The vacuum pump applied an ultimate pressure equal to $3600\ kg/m^2$ on the panel. The deflection at midpoint of the panel was measured experimentally. The results from the tests are given in Table 4.
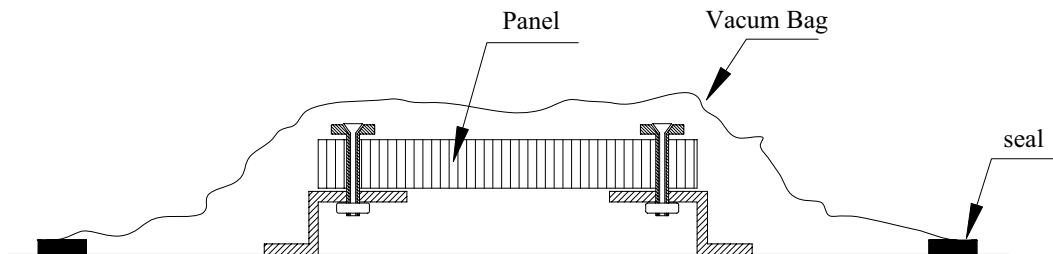
Vaccum Presser $=$ 3600 kg/m2 = 0.35 bar

Figure 1 :schematic of tes procedure for panel

3.1 Calculation of maximum deflection and stress for simply supported plate

Equation (1) used to calculate the deflection of plate. In Calculate of Equation (1) only for terms are used which are ($m=1, n=1,3; m=3, n=1,3$). Considering a lateral load of $p_0 = 3600kgf/m^2$ and $a = 658mm$, the deflection of midpoint of the plate are shown in Table 2. According to Table 2, there is some difference between theoretical and FEM results. This is due to shear effect of core and shear deflection. Because in theoretical formulation shear

modulus of the core was not considered. Actually, the FEM calculation tends to the theoretical calculation if the shear modulus of the core goes to infinity ($G \Rightarrow \infty$).

Calculation of maximum moment and stress calculated from equations (2) and occurs at center of plate ($x = a/2$, $y = b/2$).The last columns of Table 2 shows change in stress relative to aspect ratio (b/a).

b(mm) a=658	b/a	$(\sigma_y)_{max}$ Analytical	$(\sigma_y)_{max}$ FEM (Mpa)	$(\sigma_x)_{max}$ Analytical	$(\sigma_x)_{max}$ FEM (Mpa)	Deflection (FEM)	Deflection (Analytical)
658	1	296.79	283	263	261	36.37	34.59
789.6	1.2	348.647	339	266	267	49.6	47.45
921.2	1.4	411.10	399	252	256	60.3	57.85
1052.8	1.6	455.47	442	232	239	68.4	65.65
1184.4	1.8	485.47	471	210	222	74.2	71.25
1316	2	504.75	490	189	210	78.2	75.11
1447.6	2.2	516.26	503	170	208	81	77.66
1645	2.5	523.72	513.5	147	203	83.4	79.75
1974	3	521.73	512	119	203	84.8	80.48

Table 2 : shows change in deflection and stress relative to aspect ratio(b/a) for simply supported condition

3.2 Calculation of maximum deflection and stress for Clamped edges plate

In this case maximum deflection occurs at center of plate at $y = 0$, $x = 0$

Where $p_0 = 3600 kgf/m^2$, $a = 658mm$ .Results of deflection is as follow:

b(mm) a=658	b/a	$(\sigma_y)_{max}$ Analytical	$(\sigma_y)_{max}$ FEM (Mpa)	$(\sigma_x)_{max}$ FEM (Mpa)	Deflection (FEM)	Deflection (Analytical)
658	1	205	203	194	10.4	9.42
789.6	1.2	271	256	208	13.7	11.35
921.2	1.4	288	292	211	16	12.95
1052.8	1.6	305	314	210	17.4	14.25
1184.4	1.8	318	325	208	18.2	15.31
1316	2	325	330	207	18.5	16.16
1447.6	2.2	328	331	207	18.6	16.86
1645	2.5	331	329	207	18.5	17.68
1974	3	329	326	207	18.3	18.63

Table 3 : shows change in diflection and stress relative to aspect ratio(b/a) for clamped condition

According to Table 3 there is difference between theoretical and FEM results. This due to the shear effect of the core and shear deflection. Because in theoretical formulation shear modulus of the core was not considered. Actually, the FEM calculation tends to the theoretical calculation if the shear modulus of the core goes to infinity ($G \Rightarrow \infty$).

3.3 Bolted plate (panel)

In this case, we use only finite element method for modeling panel with different aspect ratios (b/a). Mechanical properties of core and faces are similar to the mechanical properties which used for simply supported and clamped condition plate. For modeling the bolts, beam elements (Cbar2) are used; bushings (inserts) are modeled with solid element (Chex6) where material properties are similar to material properties of inserts. Also, in order to obtain more accurate results, the adhesive which is used for installation of inserts are also modeled. Adhesive modeled with isotropic material with a modulus of elasticity similar to epoxy resins.

Adhesive is very effective in reducing shear stress around the holes. For this reason, it should be considered in modeling. Figures 2and 3 show the finite element model of the panel.
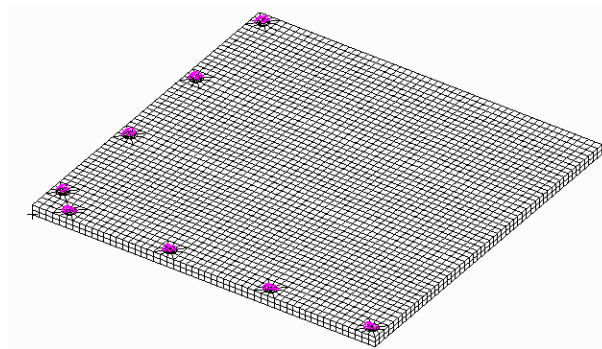
Figure 2 : shows finite element model of panel

Multi point constraints are used for connection between bolt and insert (Rigid element) which is shown in Figure 4. It is noteworthy that only half of the bolt is in contact with the internal area of insert (Figure 4) [4, 5].
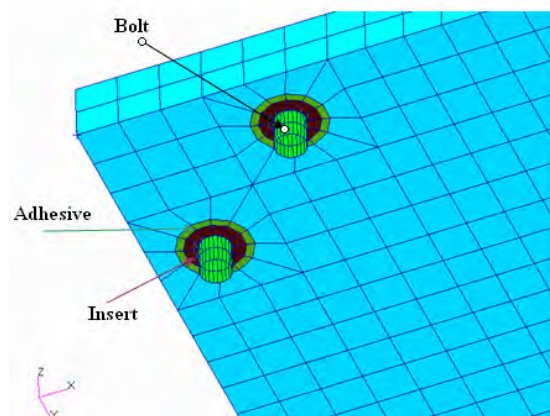
Figure 3 : shows finite element model of panel(bolt ,insert and adhesive).
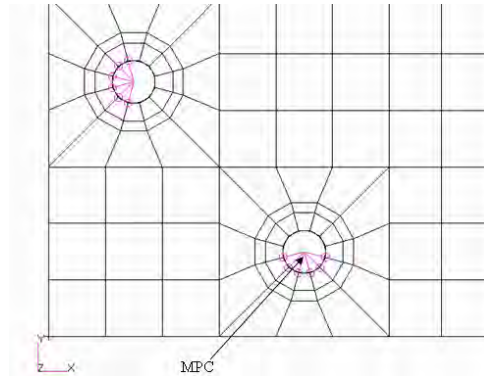
Figure 4: shows Multi point constraint(MPC) for jointing between bolt and insert

Boundary conditions of model are:

- Symmetry condition for x and y direction, (1/4 of panel has been modeled).
- Fix condition in one end of bolts.
- Model Constrain in Z direction along edge of floor beams.

Ultimate Load cases

Case 1 – Lateral load $p_0 = 3600 \, kgf/m^2$ (*Strength reqirement*)

Case 2 – Local Load:
$F = 240 \, kgf$ on $200 * 200 \, mm$ area in center of panel(*Deflection requirement*)

3.3.1 Calculation of maximum deflection and stresses under Load Case 1

The results of this case (bolted panel) with simply supported and clamped conditions are compared first. Table 4 shows change in maximum deflection of panel for different aspect ratios. Good agreement was observed between the deflections calculated by FEM and those obtained by the test.

a (mm) width	b (mm) length	b/a	Stress(FEM) σ_X tension , compression		Stress(FEM) σ_y tension , compression		Deflection mm (FEM)	Deflection mm (Test)
664	674	1.015	134	-166	134	-167	16	-----
664	872	1.313	139	-171	183	-232	23.6	-----
664	1070	1.611	127	-158	210	-270	27.5	30
664	1268	1.909	113	-142	222	-287	29.7	-----
664	1466	2.207	99.8	-128	225	-292	30.6	-----
664	1664	2.506	90.8	-119	224	-292	30.8	-----
664	1862	2.504	85.3	-112	222	-290	30.8	-----
664	2060	3.102	82.3	-109	219	-288	30.8	-----

Table 4 : Moments and stresses for bolted panel with different aspect ratio (b/a)

Figure 5 shows maximum deflection of panel for different boundary conditions. According to this graph, it can be concluded that the bolted condition is a condition which is between clamped and simply supported. However, it seems to be closer to the clamped condition and by increasing the distance between the bolts the condition tends to the simply support condition.

According to Figure 5 and Table 4, by increasing the aspect ratio, b/a the deflection of midpoint of plate increases. The curves became flat approximately for aspect ratios greater than 3. For this reason if we design critical panel according to the deflection requirement (in our company), the remaining panels with lower aspect ratios automatically satisfy the requirement of deflection. The panel used for this investigation has an aspect ratio equal to 1.64 and the allowed deflection under lateral load $p_0 = 3600\,kgf/m^2$ is about 27.8mm.
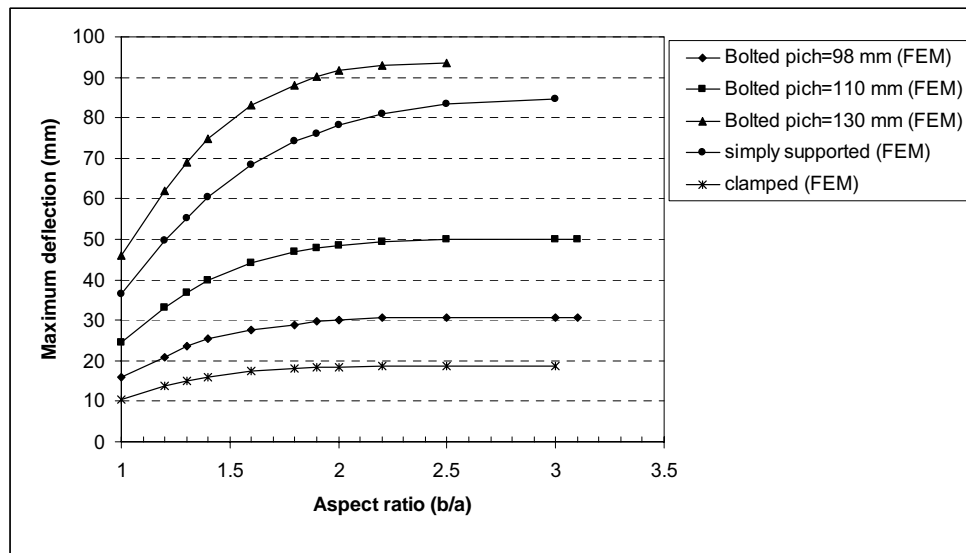
Figure 5: graph of maximum deflection versus aspect ratio (b/a)

Maximum stress in clamped condition occurs in midpoint of long edge, but in simply supported it occurs in center of panel and for bolted condition its can occur in center or edge of the plate depending on pitch distance of bolts. For calculation of strength in bolted condition, the maximum stresses in x and y directions at plate centre were calculated using FEM and were compared with the allowable strength determined from flexural test. Near the hole of bolts, stresses increase due to stress concentration. For this reason, reaction forces ($R_{X,\max}$, $R_{Y,\max}$, $R_{Z,\max}$) on bolts determined from FEM and compared them with forces obtained from insert shear and pull out tests [6]. For pitch bolt equal to 98 mm these forces tabulated in Table 5.

It is notable that by increasing the bolts distance, the reaction forces applied on the bolts increase too. Therefore, one can calculate the critical distance between the bolts by shear or pull-out mode failure.

W/2(mm)	L/W	$R_{X\max}(N)$	$R_{Y\max}(N)$	$R_{Z\max}(N)$
332	1.015	1220	1270	1230
332	1.313	1320	1860	1820
332	1.611	1320	2220	2260
332	1.909	1300	2400	2500
332	2.207	1290	2480	2610
332	2.506	1280	2500	2650
332	2.504	1280	2520	2670
332	3.102	1270	2520	2680
332	3.340	1270	2520	2680

Table 5: Bolt reaction forces for bolted panel (pitch=98 mm) with different aspect ratio (b/a)

3.3.2   Calculation of maximum deflection under Load Case 2

Construct specification of the company for this panel urged the designers that for this load case, maximum deflection of panel should be lower than 0.015W where W is short edge of the panel. The panel under study has a width of 658mm and therefore $\delta_{\max} \leq 0.015*660 = 9.9mm$.

Figure 6 shows fringe plot of deformation (critical panel) under load case 2. According to this plot maximum deflection is 9.65mm wich is lower than the company requirement. The aspect ratio of other panels was less than 1.611 (width of all panels are 658 mm). Regarding to the curves of Figure 5, one can conclude that for panels with lower aspect ratios, the company requirement are automatically satisfied.
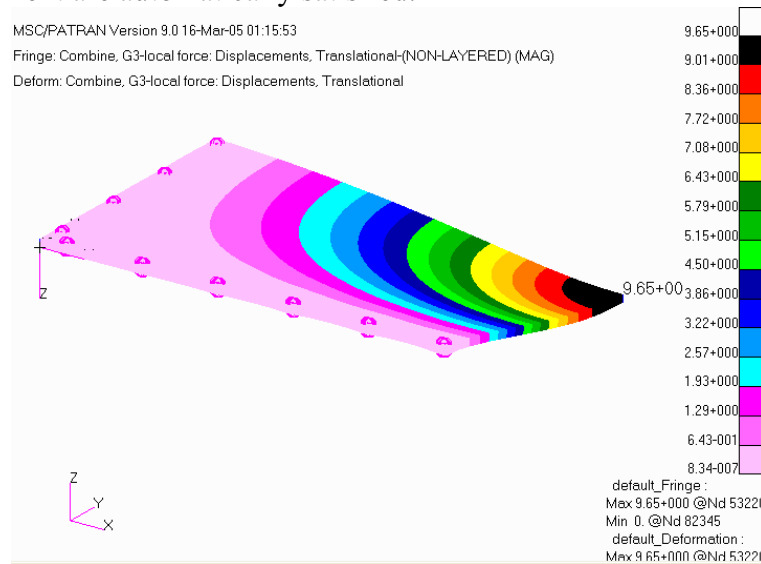
Figure 6: Deformation of panel under load case 2 (local load 240kgf)

4 CONCLUSIONS

A series of mechanical tests were carried out to obtain the mechanical properties of panels. FEM models were built based on the test data for panels with different boundary conditions. For simply and clamped the deflections and stresses from FEM were compared with those calculated using analytical methods.

For bolted panel, the deflection results from FEM model were compared with those obtained from the test. For this purpose, a test rig was constructed and used to measure the deflection at the midpoint of the panel. Good agreement between tests and numerical results show the validity of the FEM model. Having validated the FEM model, it was used to investigate the effect of bolts distance on the panel behavior. It was found that by increasing the bolts distance, the panel condition is getting closer to the simply support condition. However, increasing the bolts distance, increases the reaction forces on the bolts which eventually causes the failure of them due to pull out or shear modes.

REFERENCES

[1] Fiberlam GD-1, *Data Sheet*, Hexcel Composites, F.R.

[2] HRH 10, *Data Sheet*, Hexcel Composites, F.R.

[3] Ansel C.Ugura, *Stresses in Plates and Shells*, Mcgraw-Hill.

[4] R.L. Ramkumar And E.W. Tossavainen, *Bolted Joints in Composite Structure*, Design, Analysis and Verification, Task 1 Test Results-Single Fastener Joints, AFWAL-TR-84-3047, 1984.

[5] G.R. Wichorek, *Experimental Data on Single-Bolt Joints in Quasi-Isotropic Graphite/Polyimide Laminates*, NASA TP-2015, May 1982.

[6] MIL-HDBK-17, Military Handbook, Polymer Matrix Composite, Vol.I. Guidelines, U.S. Dept of Defense, 1994.

ELASTIC-PLASTIC BENDING OF WELDED GRID SHEET

G. Hirt, R. Kopp, M. Franzke and J. van Santen

Institute of Metal Forming (IBF)
RWTH Aachen University
Intzestraße 10, D-52056 Aachen, Germany
e-mail: santen@ibf.rwth-aachen.de (corresponding author), web page: http://www.ibf.rwth-aachen.de

Key words: Grid Sheet, FE-Modeling, Experimental mechanics, Elastic-plastic bending.

Summary. *Welded Grid Sheet is a versatile sandwich material, consisting of two metal face sheets and a core of metal wire mesh. In addition to common properties observed for many other sandwich materials (i.e. high flexural rigidity), this material has an open cellular core, which can be utilized for applications involving heat exchange. The constituents of welded Grid Sheet are assembled to flat panels through a resistance welding process. When curved cooling elements are required, initially flat panels need to be formed. Therefore, the elastic-plastic bending characteristics of this material are investigated in cylindrical die bending experiments. The bending limits of welded Grid Sheet are usually dictated by the strength and ductility of the spot welds, connecting face sheets and wire mesh. Therefore, a better understanding of the failure of these spot welds is essential to increase the insight into the elastic-plastic bending behavior of welded Grid Sheet. For that matter, shear tensile tests were conducted and a Finite Element (FE) model was developed that enabled the consideration of spot weld failure. To validate the FE-model and to determine values for the numerical failure criteria for the spot welds, the shear tensile test was reversely modeled and simulated. Subsequently, the validated FE-model was modified to analyze the elastic-plastic bending behavior of welded Grid Sheet during cylindrical die bending. The results of these FE-simulations were validated by comparing the geometry after spring back and the number of damaged spot welds with experimental results.*

1 INTRODUCTION

The research into the elastic-plastic bending of welded Grid Sheet is part of a multidisciplinary development project, originating from the global awareness that the world is facing a global energy problem. Actively cooled heat shields in steam turbines made form welded Grid Sheet should contribute to an efficiency improvement for (fossil) power plants. This should result in a significant reduction of both CO_2 emissions and fuel consumption for fossil fuel power generation. To apply these actively cooled heat shields onto the inside of steam turbine casings, slightly conical sections – i.e. ring segments – have to be formed from initially flat Grid Sheet panels.

1.1 Global energy problem

Electric power is essential for the functioning and growth of the world's economies. Since power generation relies to a large extent on the combustion of fossil fuels, it is a source for economical and environmental concern as well. In fact, the world is currently facing a global energy problem, which basically consists of three aspects: (i) future energy demand is expected to increase significantly, (ii) fossil fuel reserves are exhaustible energy sources and (iii) power generation based on fossil fuel combustion causes environmental problems. Although the (expected) environmental problems originating from fossil fuel combustion have lately received a lot of media attention (global warming, acid rain, etc), the other aspects are equally important and also need addressing.

There is a strong urge to discover alternative energy sources that solve all three aspects of the global energy problem. Due to the expensiveness of the necessary energy generation technologies and the presence of technical problems, the share of renewable energy for power generation remains relatively small worldwide. Furthermore, renewable energy sources also have an environmental impact that might in some cases be unacceptable, if large quantities of power are to be generated. The development of new renewable energy generation techniques and the improvement of existing technologies will require large amounts of funding and time. In the meantime, non-renewable fossil fuels are needed to fill the gap between the capacity of renewable power generation and electricity demand.

Since fossil fuels will most likely remain an important energy source, efficiency improvements for power generation techniques that rely on these types of fuels are urgently needed. High efficiencies in power generation can be achieved through combined cycle power plants. Combined cycle is a term used when power generation plants employ more than one thermodynamic cycle. Since power plants are only able to use a portion of the energy their fuel generates, the remaining heat from combustion is generally wasted. The combination of two or more cycles results in an improved overall efficiency. In a combined cycle power plant, a gas turbine generator produces electricity and the waste heat from the gas turbine is used to produce steam to generate additional electricity via a steam turbine.

1.2 Welded Grid Sheet in steam turbines

A cumulative efficiency factor of 58% is state-of-the-art in modern (natural gas-fired) combined cycle power plants. To facilitate an increase of the efficiency factor up to 65%, fresh steam temperatures within the steam turbine need to be increased from currently 580-620 °C to approximately 700 °C [1]. The harsh operating conditions within the steam turbine at 700 °C cannot be withstood by materials currently used in the steam turbine construction industry. The innovative idea is therefore to protect the turbine casing by an actively cooled heat shield made from a sandwich material. The open-cellular structure of the core should allow cooling steam to be forced through it to remove heat from the hot surface of the heat shield. Furthermore, the structure should provide sufficient strength to resist the mechanical loads the heat shield will be exposed to. These mechanical loads mainly originate from pressure differences and temperature gradients within and in the surroundings of the heat shield.

Preliminary research has revealed that welded Grid Sheet possesses excellent features to comply with the aforementioned requirements for the heat shield. Grid Sheet consists of two metal face sheets and a core of expanded metal or woven wire mesh that are typically joined by capacitor discharge projection welding, Figure 1 [2]. An effective cooling performance requires a core with excellent multi-axial permeability, which is ensured best by an interlayer made from metal wire mesh. The constituents of welded Grid Sheet are made from a modern high-temperature resistant material – the nickel-base alloy Nicrofer 6025HT [3] – to benefit
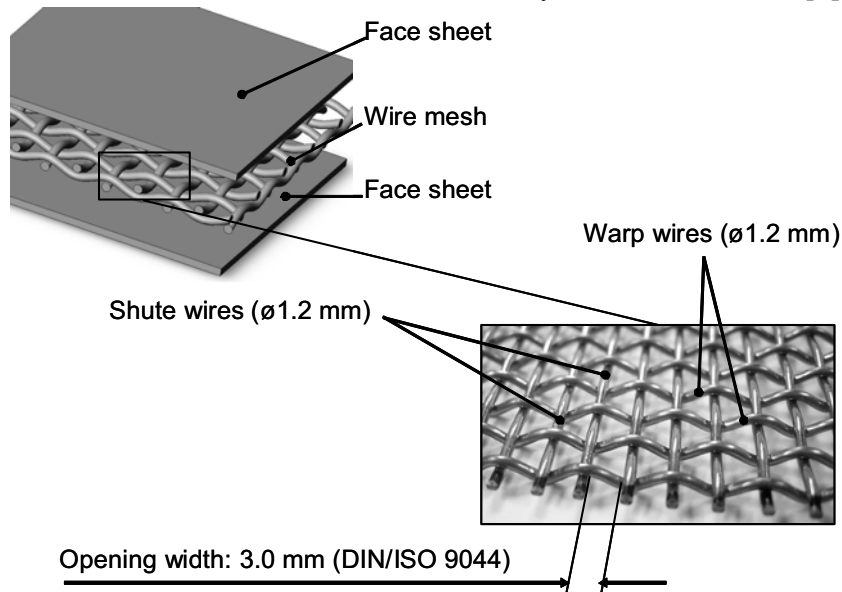
Figure 1: Grid Sheet's composition

from the excellent basic material properties of this material.

To apply the cooled heat shield made from welded Grid Sheet onto the inside of steam turbine casings, conical sections – i.e. ring segments – will need to be produced that accurately fit between the guide blades of the steam turbine that are also mounted onto the turbine casing. Since the constituents of Grid Sheet are assembled by capacitor discharge projection welding of flat sheet metal and metal wire mesh – which results in flat Grid Sheet panels – subsequent forming processes are required to produce conical segments. Similar as well as more complex shapes might also be obtained through the assembly of pre-bent constituents to pre-shaped Grid Sheet panels that only require final calibration to the required shape by a forming process. However, the technology for this type of joining still is in its infancy and it is not yet possible to guarantee a homogenous spot weld strength distribution and accurate shape after joining.

Some sheet metal bending processes are particularly suited to produce tubular shapes – i.e. either cylindrical or conical – from sheet and plate materials. Since bending processes belong to the most common sheet metal forming processes, much is known about the deformation mechanisms. Therefore, bending processes were considered best suited to analyze the elastic-plastic behavior of welded Grid Sheet and to produce curved parts from initially flat panels.

2 RESEARCH OBJECTIVES AND APPROACH

The development of a comprehensive prediction model – accurately describing the bending phenomena observed for welded Grid Sheet – is the ultimate goal for the conducted research activities. The research objectives in this paper have been defined with this goal into mind. Therefore, this paper will make a relatively small but significant contribution to the enhancement of the insight into the bending behavior of welded Grid Sheet. A research procedure has been developed and corresponding experimental and numerical methods have been selected.

2.1 Research objectives

The deformation imposed on the welded Grid Sheet during bending has both elastic and plastic portions. The *plastic* part of the deformation is permanent, and it is not recovered, when the sheet is unloaded. The *elastic* part of the deformation, on the other hand, is recovered upon removal of the load. The term for the latter phenomenon is springback. In order to accurately attain a desired shape, springback is to be accounted for either in tool design and/or through the adjustment of bending parameters; depending on the type of bending process.

Since little is known about the elastic-plastic material behavior of all-metal cellular sandwich structures – having a geometric complexity similar to welded Grid Sheet – more insight into this behavior is required before any conical ring segment can be successfully bent in an efficient way. The research presented in this paper is therefore restricted to the bending of cylindrical instead of conical parts. The knowledge gained through the analysis of bending cylindrical shapes should provide a solid basis for bending conical shapes in the future.

Preliminary bending experiments revealed that a significant number of spot welds might get damaged or even fail, if they are overloaded during forming [3]. The damage to and failure of spot welds does not only diminish the structural strength of welded Grid Sheet, it also affects the final shape of a bent part. Consequently, a reliable non-destructive testing method is required to evaluate the presence and preferably also the quality of individual spot welds. The effect of damaged spot welds on the final geometry of the bent part is also focused on. The influence of damaged spot welds on the remaining structural strength of welded Grid Sheet is investigated by a project partner [4]. Furthermore, the mechanisms leading to spot weld damage or failure are analyzed to gain a comprehensive overview of all aspects relevant to bending welded Grid Sheet.

During the weaving process the warp wires of the metal wire mesh are more severely deformed than the shute wires, which results in a larger amplitude and different mechanical properties for the warp wires. Due to this difference, the contact area between warp wires and face sheets is much larger than the contact area between shute wires and face sheets during capacitor discharge projection welding. As a result, different spot weld strengths are obtained for both types of contact. Therefore, an additional objective is to analyze whether – and if relevant to what extent – the alignment of the metal wire mesh affects the bending behavior.

2.2 Research procedure and methods

Various bending processes can be used to produce tubular shapes from flat panels; e.g. offset folding, roll bending, etc. Hohmeier [5] developed however a flexible cylindrical die bending tool (R=200 mm), which is also used for the experiments discussed in this paper. Two variants of cylindrical die bending can be recognized: free bending and coining (also denoted air bending and bottoming, respectively). For free bending, the work piece is bent without pressing the punch to the bottom of the die. The opposite is the case for coining. The latter variant is characterized by the dimensions of the bent work pieces being almost entirely determined by the geometry of both die and punch. Although the required forces during free bending are smaller, coining is preferred for its higher precision.
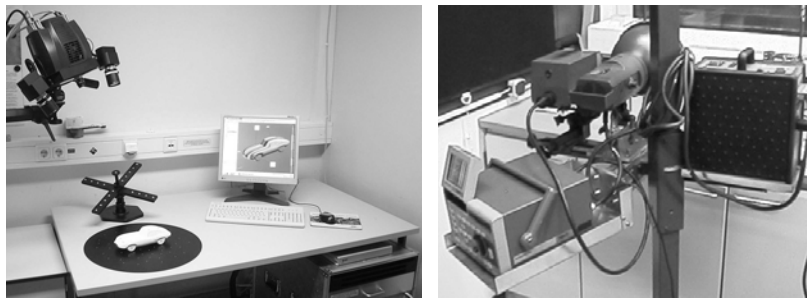
Figure 2: 3D-digitization system (left), Infrared thermography system

Next to a suitable bending process, the enhancement of the insight into the bending behavior of welded Grid Sheet requires a measuring method to evaluate springback after bending. Hohmeier [5] evaluated the springback behavior of welded Grid Sheet (made from other materials) through tracing the geometry of the bent panels on graph paper followed by ruler measurements and calculations. A higher accuracy of the geometry measuring technique is however preferred. Therefore, the digitization system ATOS III [6] has been used to enable a detailed analysis of the geometry of the bent parts. The ATOS III system, Figure 2, is based on the triangulation principle: the sensor unit projects different fringe patterns on the object to be measured and observes them with two cameras. Based on the optical transformation equations, the computer automatically calculates the 3D coordinates for each camera pixel with high precision. Subsequently, the computer can calculate the radius for a defined cross section of the bent part.

Another important evaluation parameter is the presence and quality of the spot welds after bending. Spot welds can be inspected visually with a microscope through the preparation (grinding and polishing) of embedded Grid Sheet specimens. This is however very labor-intensive and relatively inaccurate. Furthermore, this type of inspection actually is a destructive testing method due to the preparation requirement. Therefore, infrared thermography – a non-destructive testing technique – which is commonly used to detect defects in sandwich materials, has been selected for the evaluation of spot weld quality. This technique detects and measures heat emissions and transforms the results into visible images, Figure 2. For welded Grid Sheet one face sheet is heated and viewed from the same side. At

locations where spot welds are (still) present, part of the applied heat is conducted into the wire mesh. This can be observed as a spot on the face sheet having a lower temperature than its direct surroundings. Heat application must be relatively uniform over the area being inspected, which promotes unidirectional heat flow through the material perpendicular to the surface. For welded Grid Sheet this is accomplished best through a flash lamp. After conducting the measurements the images need interpretation, which is currently accomplished through visual non-automated inspections.

Although cylindrical die bending experiments contribute to the enhancement of the insight into the bending behavior, the investigation of the mechanisms determining this behavior are more interesting from a scientific point of view. Since many aspects affect the damage to individual spot welds and the final geometry of the bent part, a precise prediction of springback and spot weld damage by analytic models is rather complicated. Therefore, FE-simulation is used to analyze the mechanisms that affect the bending behavior. Through reverse FE-simulations of the shear tensile test, the 'numerical' strength of the spot welds has been determined. The experimental shear tensile tests have also been used to analyze the shear behavior of welded Grid Sheet. Subsequently, the validated FE-model has been used to simulate the bending behavior of welded Grid Sheet in cylindrical die bending. The FE-simulations of the bending processes have been validated with experimental results. The reference criteria have been: the geometry after spring back and the number of failed or damaged spot welds.

3   RESULTS

The influence of the alignment of the wire mesh, the effect of a heat treatment before bending, and the influence of the specimen length have been investigated in cylindrical die bending experiments. To analyze the mechanisms dictating the bending behavior of welded Grid Sheet, FE-simulations have been conducted.

3.1 Cylindrical die bending experiments

The results of the conducted cylindrical die bending experiments are shown in Figure 3. The ratio between R; radius before spring back and R'; the radius after spring back, is an indication for the amount of spring back that occurred. A ratio of $R/R' = 1$ would correspond to the situation that no spring back has occurred. The radius before spring back remains constant, as it is determined by the radii of either the die or the punch. The error indicators in Figure 3 represent 95% confidence intervals that have been calculated on the basis of the scattering of the springback ratio for specimens bent under identical conditions.

By observing the error indicators in Figure 3, it becomes apparent that a heat treatment significantly reduces the fluctuation in the springback behavior. Furthermore, it becomes clear that a heat treatment generally results in a reduction of springback. The heat treatment is expected to induce an increased ductility near the spot welds, resulting in less spot welds failing or getting damaged during bending. In addition, a heat treatment will most likely homogenize the spot weld strength. In this scenario a heat treatment results in a more constant number of damaged spot welds for specimens bent under identical conditions and hereby an

improved reproducibility of the springback behavior is observed. Since the quiet cracking sound of failing spot welds during bending of welded Grid Sheet specimens that were not subjected to a heat treatment was more pronounced than for heat treated specimens, the aforementioned theory might be a good explanation for this effect. The discrepancy with respect to the acoustic behavior might however also be an indication for differences in fracture behavior; i.e. either ductile or brittle.

Another observation that can be made from Figure 3 is that the spring back for larger specimen lengths is observed to decrease. This is most likely caused by a process-related larger deflection and corresponding higher total strain. The amount of plastic deformation is therewith higher and hereby the self-aligning torque is reduced, which results in a reduction of springback.

Futhermore, the alignment of the wire mesh is observed to have a decisive influence on the springback behavior. If the warp wires are aligned parallel to the specimen length, springback is significantly less than for Grid Sheet specimens, where the warp wires are aligned perpendicular to the specimen length. During capacitor discharge projection welding the contact areas between wires and face sheets are much larger for warp than for shute wires.
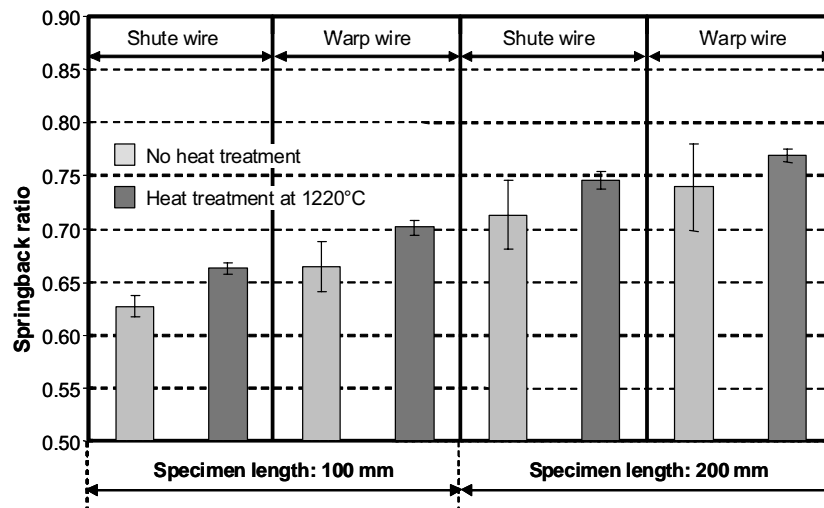
Figure 3:   Results of the cylindrical die bending experiments

Consequently, the spot welds between face sheets and shute wires are very small and can even be considered virtually non-existent. The bonding strength between face sheets and wire mesh (i.e. resistance to delamination) is therefore mainly controlled by the spot welds connecting face sheets and warp wires. Whether the geometry of the spot welds, the shape difference between warp and shute wires, or the difference in mechanical properties for warp and shute wires, are responsible for the aforementioned effect, requires additional research. Since welded Grid Sheet – where the warp wires are aligned parallel to the specimen length – demonstrates superior bending properties, the remainder of this paper is dedicated to this particular type.

Infrared thermography could not reveal any significant differences with respect to

damaged or failed spot welds for the different test conditions. In fact, almost all verified spot welds were still present after bending, Figure 7. Furthermore, the spot welds were not inspected previous to bending, which makes a reliable conclusion with respect to the effect of particular bending parameters on spot weld damage impossible at this moment. The cracking sound of spot welds getting damaged during bending is most likely caused by the failure of the spot welds connecting warp and shute wires in the centre of the interlayer. On the other hand, this sound might also be caused by the failure of the virtually non-existent spot welds between face sheets and shute wires. Both types of spot welds can not or only to a limited extent be evaluated through infrared thermography. The strength of the spot welds connecting face sheets and warp wires apparently is sufficient to withstand the loading originating from a bending radius of 200 mm.

3.2 FE-simulation of cylindrical die bending

Since the bottleneck for the formability of grid sheet is the strength and ductility of the spot welds, a better understanding of the mechanisms leading to spot weld damage and failure is essential. To enable an extensive analysis of both the spot weld damage and the springback behavior, a 3-dimensional model composed of solid elements was constructed with the
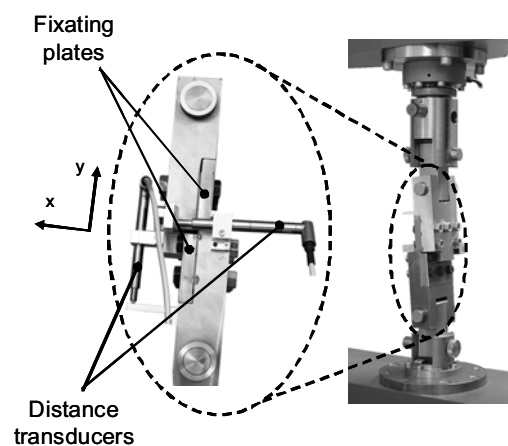
Figure 4: Shear tensile test equipment

software Programmer's Environment for Pre-Postprocessing (PEP) [7]. The standard FE-model was a unity cell, which enables an uncomplicated assembly of multiple unity cells to construct larger FE-models. After the geometrical construction of the FEM-model in PEP, the model was transferred to LS-Dyna. All simulations with conducted with this FE-software utilizing explicit algorithms.

Cylindrical die bending experiments have demonstrated that spot welds might sometimes get damaged or even fail at arbitrary locations during bending. Therefore, one of the requirements for the simulation of cylindrical die bending was to incorporate the possibility of spot weld failure and/or damage into the FE-model. Ideally, a critical shear stress should be defined, which releases the connection between the nodes concerned. Unfortunately, most LS-

Dyna contact cards are only applicable for shell elements. However, the instruction CONSTRAINED_TIED_NODES_FAILURE is compatible with solid elements and allows for the definition of a maximum plastic strain. If this defined maximum is exceeded, the contact between the nodes resembling a spot weld is released. To validate the developed FE-model and to determine the boundary values for the failure criteria for each node pair,
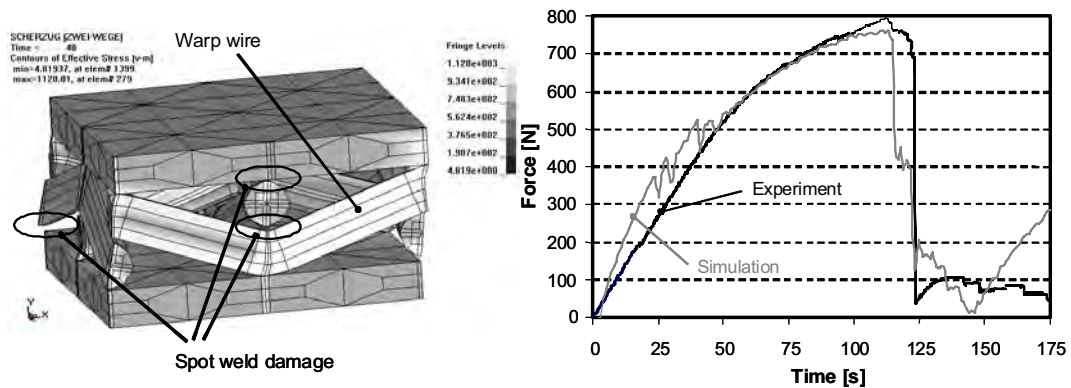
Figure 5: Results of the shear tensile validation simulations

resembling a single spot weld, a shear tensile test fixture was designed and constructed, Figure 4. This special fixture hamstrings bending loads on the face sheet during testing. By
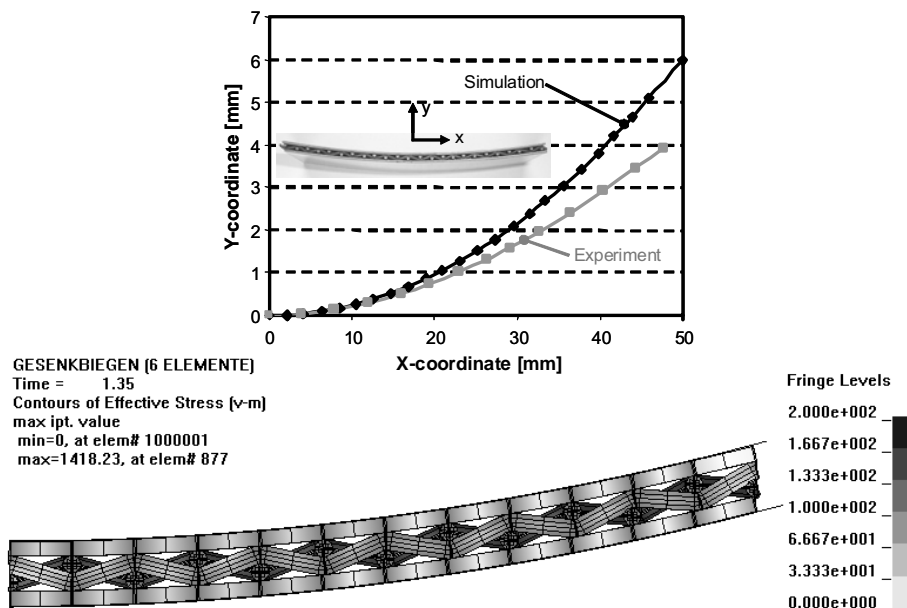
Figure 6: Comparison of calculated and measured springback behavior

reverse modeling of the shear tensile test, in which the failure values for each node pair are adapted until the force and failure time in the FE-simulation correspond to those observed in the experimental shear tensile tests (Figure 5), the starting FE-model for the subsequent

simulation of cylindrical die bending was created.

The forming simulation revealed large stress concentrations at all spot welds locations. After the forming simulation is completed and the grid sheet is completely pressed in the die, the spring back of the bent segment has to be simulated. The spring back calculation of the grid sheet was accomplished using an implicit solver. LS-Dyna provides a tool, designated

Figure 7: Infrared thermography image of welded Grid Sheet

"dynain" in LS-Dyna nomenclature, which uses the output file called "dynain" of the explicit forming simulation. There still is a relatively large discrepancy between the real geometry of Grid Sheet after bending and the calculated geometry after springback, Figure 6. As already explained virtually no spot weld defects could be detected, Figure 7, which makes a comparison of experimental and numerical results with regard to spot weld failure impossible.

4   CONCLUSIONS AND OUTLOOK

Although some interesting (new) properties of welded Grid Sheet have been discovered, additional research is needed to increase the insight into the elastic-plastic bending behavior of welded Grid Sheet and to further develop the research methods and techniques.

4.1 Recapitulation of elastic-plastic bending behavior

Cylindrical die bending experiments revealed that a heat treatment after capacitor discharge projection welding improves the formability of welded Grid Sheet and increases the reproducibility of the geometry after bending (i.e. after springback). Furthermore, it can be concluded that the alignment of the woven wire mesh has a decisive influence on the bending behavior. The reasons for the dependence of the bending behavior on the alignment are currently investigated in more detail.

Although springback can be analyzed through the developed FE-model, the accuracy of the springback calculation should be enhanced in the future. The presented research procedure and developed measuring methods will contribute to the development of a reliable prediction model describing springback and spot weld damage (and failure). Due to the relatively large

bending radius, R=200, only a restricted number of spot welds get damaged during bending. Future research should therefore involve bending of welded Grid Sheet into cylindrical segments with smaller radii.

4.2 Prospective research

Although the research presented in this paper provides important (new) insights into the elastic-plastic bending behavior of welded Grid Sheet, additional research is required to fully understand the mechanisms that determine the elastic-plastic properties of this highly versatile sandwich material. The explained research method – relying on both experimental and simulation techniques – will serve as a guideline for the planning and conduction of future research. To broaden the insight into the forming behavior other welded Grid Sheet variants, having different geometrical and/or material compositions, will be analyzed. The development of a comprehensive and validated prediction model (either of numerical or empirical nature, accurately describing the bending behavior of different types of welded Grid Sheet, will be the ultimate research goal.

The determination of the exact bending limits – i.e. minimum bending radii – for different types of welded Grid Sheet through experimentation will be one of the first challenging objectives. Since the bending limits are typically dictated by the damage and/or failure of spot welds, non-destructive testing methods that enable the evaluation of the presence and/or the quality of spot welds before and after bending will play a decisive role in the realization of this objective. Although infrared thermography has shown promising results, the interpretation of the results is highly operator dependent. Therefore, the used thermography measuring method needs further optimization. Furthermore, the use of additional non-destructive testing techniques has already been considered. Although additional research is needed to develop a reliable evaluation procedure, preliminary experiments have indicated that ultrasonic testing offers an interesting potential. This testing technique should not only enable the evaluation of spot welds connecting face sheet and wire mesh, the quality and/or presence of spot welds connecting warp and shute wires located in the centre of the interlayer of welded Grid Sheet can also be determined through this method. After determining the bending limits, appropriate measures will be developed that enable a minimization of spot weld damage and/or failure to enhance the formability limits of welded Grid Sheet.

The experimental determination of the bending limits of welded Grid Sheet would require many redesigns and reproductions of cylindrical die bending tools every time different radii would need to be bent. Therefore, four-roll bending has been selected as a more cost-efficient alternative to cylindrical die bending to determine the bending limits of welded Grid Sheet. A repositioning of the bending rolls enables a simple adjustment to different bending radii without any physical modifications to the tooling. Furthermore, this bending process is capable of producing cone parts that will ultimately be needed to produce cooling elements made from welded Grid Sheet for steam turbines. The springback behavior is analyzed simultaneously to the evaluation of spot weld quality for different bending radii and the developed simulation and calculation models are modified and (re)validated to enhance the predictability of both spot weld damage and springback. To significantly reduce the

computation time for the FE-simulations, a replacement of solid elements for the wire mesh by beam elements is currently under investigation.

ACKNOWLEDGEMENT

REFERENCES

[1] D. Bohn, "New materials and cooling systems for high temperature, highly loaded components in advanced combined cycle power plants", *Proceedings of the 7th Liège Conference on Materials for Advanced Power Engineering*, 107-120 (2002).

[2] R. Kopp, M. Franzke, P. Hohmeier, J. van Santen, "Bending of Sandwich Structures with Usable Cavities for Active Cooling Applications in Steam Turbines", *Annals of the German Academic Society for Production Engineering*, Vol. XII/1, 71-76 (2005).

[3] Krupp VDM, *Nicrofer 6025 H/HAT-alloy 602/602 CA, Werkstoffblatt-Nr. 4137*, Krupp VDM GmbH (2001).

[3] R. Kopp, M. Nutzmann, J. van Santen, "Formability of Lightweight, Vibration Damping and Medium Perfused Sandwich Sheets, Analysis through Practical Experiments and FE-Simulations, *Proceedings of the 7th International Conference on Sandwich Structures*, 723-732 (2005).

[4] U. Dilthey et al., "Development of Porous Steel Structures for Steam Turbines", *Advanced Engineering Materials*, 111-119 (2001).

[5] P. Hohmeier, *Experimentelle und numerische Untersuchungen zum Umformverhalten von Gitterblechen*, Shaker Verlag (2006).

[6] K. Galanulis, "Optical Measuring Technologies in Sheet Metal Processing", Advanced Materials Research, 19-34 (2005).

[7] M. Franzke, *PEP-Programmer's Environment for Pre-Postprocessing*, User manual 3.30, Institute of Metal Forming (IBF) (2001).

THREE-DIMENSIONAL NONLINEAR ANALYSIS OF SCARF REPAIR IN SANDWICH PANELS

Manabendra Das[*], Erdogan Madenci[*] and Damodar R. Ambur[†]

[*]Department of Aerospace and Mechanical Engineering
The University of Arizona
Tucson, AZ, USA, 85721
e-mail: madenci@email.arizona.edu

[†]Research and Technology Directorate
NASA Langley Research Center
Hampton, VA, USA 23681

Key words: Sandwich structures, Scarf repair, Finite element.

Summary. *The current study presents a special-purpose analysis tool, based on the finite element method, for parametric design studies of sandwich panels with scarf repair. This design tool provides the complete three-dimensional stress and strain fields in scarf-repaired sandwich panels without any requirements for the nature of the lamination and the type of loading. The model takes into account geometric nonlinearity in the adherends and assumes a bi-linear stress-strain relationship for the adhesive. The response of sandwich panels with both full and partial repairs of the top facesheet has been investigated.*

1 INTRODUCTION

Bonded joints have become the most common type of repair, and they exist in a variety of forms, such as lap, scarf, and stepped. The objective of a scarf repair is to restore the static strength and durability of a composite structure that contains damages due to unexpected impact loading on the structure or cracks within the structure after longtime usage, and for environmental reasons. Panels with scarf repair do not experience excessive secondary bending, and the magnitude of transverse shear and peel stress concentration is also not very severe. In fact, in the case of homogeneous adherends, the stress variation inside the adhesive remains fairly uniform. On the other hand, panels made of composite laminates experience non-uniform stress variation within the adhesive [1-4]. Therefore, an accurate prediction of the stress and strain fields is crucial for failure analysis [4].

Analytical and numerical methods have been used in the past to examine scarf and stepped lap joints [5,6]. These methods are two-dimensional in nature, with limitations on the boundary conditions and loading types. These limitations of the analytical methods can be overcome by employing the finite element method [1-4,7,8]. Detailed three-dimensional finite element analysis of scarf joints can be performed using solid elements. Although accurate enough, these models tend to be computationally expensive due to the presence of a thin adhesive layer and the numerous layers of plies in the laminate or the facesheet of a sandwich

panel. Mesh refinement can be significant, especially in the case of nonlinear analysis, where a fine mesh might be required for convergence. Moreover, due to the discretization in the transverse direction, it might not be possible to parameterize the meshing process. Therefore, a new mesh generation is necessary for each panel with a different number of plies, adhesive thickness, or panel dimensions.

An alternative to this approach is to use an element based on a single-layer theory, which utilizes a modest number of degrees of freedom and provides accurate results. The current analysis utilizes one such plate element [9] for the adherents and a separate solid element for the adhesive layer in between the adherents. The tapered scarf is visualized as a stepped joint, with numerous steps in order to replicate the taper as closely as possible. The analysis incorporates geometric and material nonlinearity in the adherent and adhesive elements, respectively. A bi-linear stress-strain relationship is used for the material model, and geo-metric nonlinearity is incorporated based on the total Lagrangian formulation. The analysis accounts for finite boundaries, the presence of a cutout or grind-out in the skin, arbitrary and multiple repair sites, general loading conditions, material anisotropy, different thicknesses of the repair patch and skin, and different repair and parent materials. The material properties are input for each ply without any limitation on refinement in the thickness direction. While it is computationally robust and fast, it leads to accurate stress predictions in each specific ply and the adhesive layer.

2 PROBLEM DEFINITION

The construction of a sandwich panel with the top facesheet under scarf repair is illustrated in Figure 1. The thicknesses of the core, top facesheet, and bottom facesheet are denoted by h_C, h_{TF}, and h_{BF}, respectively. The entire top facesheet, or only a part of it, can be under repair. The panel has a rectangular planar geometry with length L_x and width L_y. The facesheets, as well as the core, can be composed of homogeneous, elastic, and orthotropic material layers. As shown in Figure 1, the panel is subjected to forces and moment and prescribed displacements at the edges. The problem posed herein concerns the determination of the complete three-dimensional stress and strain fields in the base facesheets, repair material, core, and adhesive.

3 PRESENT APPROACH

In the current analysis, both plate and solid elements are utilized to model the panel with a repair. As shown in Figure 2, the base region, consisting of the facesheet and core, is repre-sented through a single plate element, through the thickness. Similarly, plate elements are used to model the repair in the top facesheet. The adhesive layer, on the other hand, is modeled using a solid element. Since all the plate elements are required to have a constant thickness, a fictitious material, with a very low stiffness value, is used in the region where the adherent doesn't occupy any space, as shown in Figure 2.

Manabendra Das, Erdogan Madenci and Damodar R. Ambur.
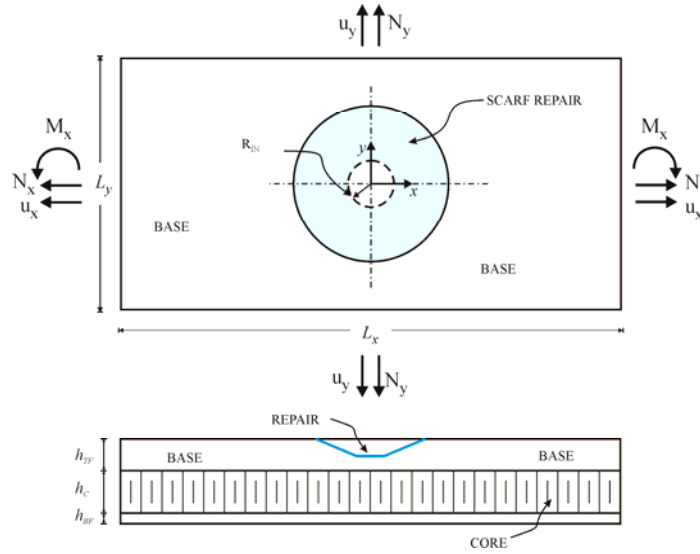
Figure 1: Sandwich panel with scarf repair
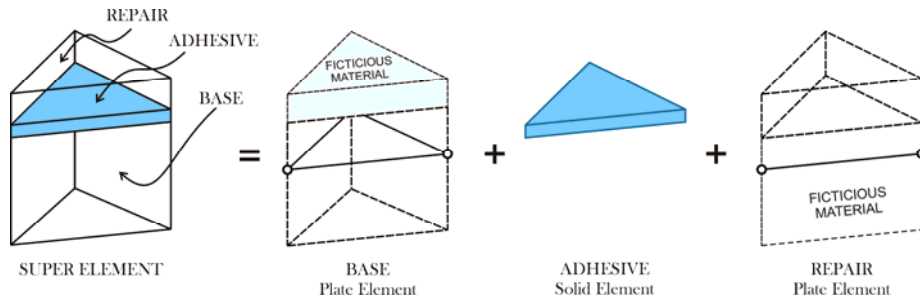
Figure 2: The three layers of the scarf super element

The composite scarf element shown in Figure 2 has the adhesive solid element sandwiched between the adherend plate elements. Since only one layer of adhesive element is used, the nodal displacements of the adhesive element are expressed in terms of the plate element placed above and below the adhesive element. Therefore, the adhesive is comprised of pseudo nodes, without any independent degrees of freedom. The stiffness matrix and the unknown displacement vector of the super element, comprised of the adherend and adhesive layer, have the following form:

$$\mathbf{K}_{\text{Scarf 1}} = \begin{bmatrix} \mathbf{K}_{base}^{HOT32} + \mathbf{K}_{bb}^{adh} & \mathbf{K}_{br}^{adh} \\ \mathbf{K}_{rb}^{adh} & \mathbf{K}_{repair}^{HOT32} + \mathbf{K}_{rr}^{adh} \end{bmatrix}_{78 \times 78} \tag{1}$$

$$\mathbf{v}_{\text{Scarf 1}}^{T} = \left\{ \mathbf{v}_{base} \quad \mathbf{v}_{repair} \right\} \tag{2}$$

where $\mathbf{K}_{base}^{HOT32}$ and $\mathbf{K}_{repair}^{HOT32}$ are the stiffness matrices of the base and repair adherend, respectively, and $\mathbf{K}^{adh}$ is the stiffness matrix of the adhesive layer. Details of the HOT32 plate element with geometric nonlinear capabilities and the adhesive element with material nonlinearity are given in sections 3.1 and 3.2, respectively. The region outside the repair is modeled using the HOT32 plate element.

3.1 Plate Element

The triangular plate element contains 13 degrees of freedom at each node, as shown in Figure 3. These degrees of freedom consist of two in-plane displacements (u,v), two out-of-plane rotations (θ_x,θ_y), and three transverse nodal displacements (w, w_1, w_2) and their derivatives $(w_{,x}, w_{,y}, w_{1,x}, w_{1,y}, w_{2,x}, w_{2,y})$. The weighted-average in-plane displacement components in the x- and y-directions are denoted by u and v, respectively. The weighted-average transverse displacement is denoted by w. The weighted-average bending rotations about the negative x and positive y axes are denoted by θ_x and θ_y, respectively. Their positive sign convention is shown in Figure 3. The transverse displacements (w_1, w_2), not weighted averaged, represent the symmetric and anti-symmetric expansion modes through the thickness of the element. As shown in [9] the displacement components of the sandwich panel are defined in the form

$$u_x(x,y,z) = u(x,y) + h\zeta\theta_y(x,y) + \left(\frac{1}{6} - \frac{\zeta^2}{2}\right)hw_{1,x}(x,y)$$
$$+ h\left(\frac{\zeta}{5} - \frac{\zeta^3}{3}\right)\left[\frac{5}{4}\left(\theta_y(x,y) + w_{,x}(x,y)\right) + w_{2,x}(x,y)\right]$$

(3a)

$$u_y(x,y,z) = v(x,y) + h\zeta\theta_x(x,y) + \left(\frac{1}{6} - \frac{\zeta^2}{2}\right)hw_{1,y}(x,y)$$
$$+ h\left(\frac{\zeta}{5} - \frac{\zeta^3}{3}\right)\left[\frac{5}{4}\left(\theta_x(x,y) + w_{,y}(x,y)\right) + w_{2,y}(x,y)\right]$$

(3b)

$$u_z(x,y,z) = w(x,y) + w_1(x,y)\zeta + w_2(x,y)\left(\zeta^2 - 1/5\right)$$

(3c)

where $\zeta = z/h$ is the normalized thickness and varies in the range $-1 \leq \zeta \leq 1$. In accordance with the {3,2} plate theory, the in-plane displacement components vary cubically and the transverse displacement component varies quadratically across the thickness of the panel. At any point in the panel, the in-plane displacement components in the x- and y-directions are represented by $u_x(x,y,z)$ and $u_y(x,y,z)$, respectively, and the transverse displacement component by $u_z(x,y,z)$.

The governing equations concerning the equilibrium equations and continuity of inter-element displacements along the element edges are derived utilizing the hybrid energy functional. The resulting equations of equilibrium and boundary conditions are derived in [9].
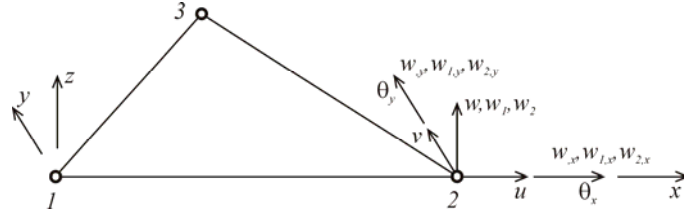
Figure 3: Three-noded triangular element with degrees of freedom at a node

The kinematic continuity conditions are imposed not only on the weighted-average displacements and slopes $(u, v, w, \theta_x, \theta_y)$, but also on the derivatives of the higher-order displacement modes (w_1, w_2) in the transverse direction. Therefore, the finite element implementation of the equilibrium equations requires at least C^1 interelement continuity for the out-of-plane displacement modes of w, w_1, and w_2. Because of this requirement, the finite element implementation of the total potential energy functional in terms of the assumed displacement field becomes rather difficult. The hybrid energy functional formulation overcomes the difficulty of the C^1 interelement continuity requirement because the displacements, as well as the slopes, are independently assumed only along element boundaries, which can be rendered identical along the common boundaries of adjacent elements. However, the kinematic compatibility between the displacements and slopes along the element boundaries is preserved in order to avoid a possible shear-locking phenomenon. Also, as part of the hybrid energy functional formulation, the stress and moment resultants within the element are selected in the form of complex power series so as to satisfy the equilibrium equations.

The hybrid energy functional for an element, Π_H, is defined as

$$\Pi_H = \frac{1}{2} \int_{A_e} \mathbf{S}^T \mathbf{C} \mathbf{S} \, dA - \int_{\Gamma_e} \mathbf{T}_b^T \mathbf{u}_b \, d\Gamma \tag{4}$$

in which the element boundary is denoted by Γ_e and its area by A_e. The vectors $\mathbf{T}_b$ and $\mathbf{u}_b$ include the components of the boundary forces and boundary displacements, respectively. In accordance with the hybrid energy formulation, the resultant stress vector, $\mathbf{S}$, must satisfy the equilibrium equations identically. The derivation of $\mathbf{S}$ satisfying the equilibrium equations is presented in [9]. The boundary displacement vector, $\mathbf{u}_b^{(k)}$, containing the assumed boundary displacement components and the boundary stress vector, $\mathbf{T}_b^{(k)}$, containing the resultant stresses and moments corresponding to the boundary displacement vector $\mathbf{u}_b^{(k)}$ are also given in [9]. Therefore, substituting for the stress vector, the boundary displacement and boundary stress vectors in the hybrid energy functional result in

$$\Pi_H = \frac{1}{2} \mathbf{b}^T \mathbf{H} \mathbf{b} + \boldsymbol{\lambda}^T \mathbf{c} \mathbf{b} + \mathbf{R}_b^T \mathbf{b} - \mathbf{R}_v^T \mathbf{v} - \mathbf{b}^T \mathbf{G} \mathbf{v} + \Pi_0 \tag{5}$$

where

$$\mathbf{H} = \int_{A_e} \mathbf{P}^T \mathbf{C} \mathbf{P} \, dA \tag{6a}$$

$$\mathbf{G} = \sum_{k} \int_{\Gamma_{(k)}} \mathbf{P}^T \, \mathbf{B}_s^{(k)} \mathbf{B}_b^{(k)} \, \mathbf{L}^{(k)} \, d\Gamma \qquad (6b)$$

$$\mathbf{R}_b = \int_{A_e} \mathbf{S}_0^T \, \mathbf{C} \, \mathbf{P} \, dA \qquad (6c)$$

$$\mathbf{R}_v = \sum_{k=1}^{3} \int_{\Gamma_{(k)}} \mathbf{S}_0^T \, \mathbf{B}_s^{(k)} \mathbf{B}_b^{(k)} \, \mathbf{L}^{(k)} \, d\Gamma \qquad (6d)$$

$$\Pi_0 = \frac{1}{2} \int_{A_e} \mathbf{S}_0^T \, \mathbf{C} \, \mathbf{S}_0 \, dA \qquad (6e)$$

in which the explicit definition of each of the matrices and vectors is given in [9]. In matrix form, the hybrid energy functional, Π_H, can be rewritten as

$$\Pi_H = \frac{1}{2} \hat{\mathbf{b}}^T \, \hat{\mathbf{H}} \, \hat{\mathbf{b}} + \hat{\mathbf{R}}_b^T \, \hat{\mathbf{b}} - \mathbf{R}_v^T \, \mathbf{v} + \hat{\mathbf{b}}^T \, \hat{\mathbf{G}} \, \mathbf{v} + \Pi_0 \qquad (7)$$

where

$$\hat{\mathbf{b}}^T = \left\{ \mathbf{b}^T, \boldsymbol{\lambda}^T \right\}, \quad \hat{\mathbf{H}} = \begin{bmatrix} \mathbf{H} & \mathbf{c}^T \\ \mathbf{c} & \mathbf{0} \end{bmatrix}, \quad \hat{\mathbf{R}}_b^T = \left\{ \mathbf{R}_b^T, \mathbf{0}^T \right\}, \quad \hat{\mathbf{G}} = \begin{bmatrix} \mathbf{G} \\ \mathbf{0} \end{bmatrix}$$

In accordance with the concept of energy minimization, the first variation of the hybrid energy functional with respect to the unknown vector $\hat{\mathbf{b}}$ of generalized coordinates yields

$$\delta \hat{\mathbf{b}}^T \left(\hat{\mathbf{H}} \, \hat{\mathbf{b}} + \hat{\mathbf{R}}_b - \hat{\mathbf{G}} \, \mathbf{v} \right) = \mathbf{0} \quad \text{or} \quad \hat{\mathbf{b}} = \hat{\mathbf{H}}^{-1} \left(\hat{\mathbf{G}} \, \mathbf{v} - \hat{\mathbf{R}}_b \right) \qquad (8)$$

With this explicit solution form, the hybrid energy functional becomes

$$\Pi_H = -\frac{1}{2} \mathbf{v}^T \, \mathbf{k}_L \, \mathbf{v} + \mathbf{f}_o^T \mathbf{v} + \Pi_0 \qquad (9)$$

in which the linear stiffness matrix $\mathbf{k}_L$ and the resultant force (load) vector $\mathbf{f}_0$ are defined as

$$\mathbf{k}_L = \hat{\mathbf{G}}^T \, \hat{\mathbf{H}}^{-1} \, \hat{\mathbf{G}} \quad \text{and} \quad \mathbf{f}_0^T = \hat{\mathbf{R}}_b^T \, \hat{\mathbf{H}}^{-1} \, \hat{\mathbf{G}} - \hat{\mathbf{R}}_v^T \qquad (10)$$

Finally, the element equilibrium equation is obtained by requiring the first variation of the hybrid energy functional to vanish:

$$\delta \Pi_H = \delta \mathbf{v}^T \left(\mathbf{k}_L \, \mathbf{v} - \mathbf{f}_0 \right) = 0 \qquad (11)$$

For arbitrary variation of $\delta \mathbf{v}$, the element equilibrium equations become

$$\mathbf{k}_L \mathbf{v} = \mathbf{f}_0 \qquad (12)$$

The nonlinear analysis is based on the total Lagrangian formulation. The principle of virtual work in the total Lagrangian formulation is given by

$$\int_{0V} \sum_k {}^{t+\Delta t}_0 S^{(k)} \delta \, {}_0 E^{(k)} d \, {}^0V = \delta \, {}^{t+\Delta t} \Re \tag{13}$$

In this expression, the left subscript indicates the configuration by which the quantity is measured and the left superscript refers to the configuration of the body at a specific time. The right superscript refers to the kth component of the stress and strain resultant vectors. The right-hand side represents the virtual work done by the conservative external forces on the virtual displacements. The Piola-Kirchoff stress can be decomposed into two components such that

$$^{t+\Delta t}_0 S^{(k)} = {}^{t}_0 S^{(k)} + {}_0 S^{(k)} \tag{14}$$

The incremental Piola-Kirchoff stress vector, ${}_0 S^{(k)}$, represents the incremental loading between $t + \Delta t$ and t and ${}^{t}_0 S^{(k)}$ represents the known component from time t. The Green strain at any state $t + \Delta t$ can be written in terms of linear and nonlinear components as

$$^{t+\Delta t}_0 E^{(k)} = {}^{t+\Delta t}_0 E^{(k)}_L + {}^{t+\Delta t}_0 E^0_{NL} \tag{15}$$

This expression can be written in terms of the unknown displacement as

$$^{t+\Delta t}_0 E^{(k)} = \mathbf{B}_L^{(k)^T} \left({}^t\mathbf{v} + \mathbf{v} \right) + \frac{1}{2} \left({}^t\mathbf{v} + \mathbf{v} \right)^T \mathbf{B}_{NL}^{(k)} \left({}^t\mathbf{v} + \mathbf{v} \right) \tag{16}$$

where $\mathbf{B}_L^{(k)}$ and $\mathbf{B}_{NL}^{(k)}$ are the linear and nonlinear strain-displacement relationship vector and matrix, respectively, corresponding to the kth strain resultant component. Based on the hybrid formulation provided in the previous section, the linear strain-displacement relationship matrix can be expressed as

$$\mathbf{B}_L^T = \mathbf{C}\mathbf{P}\,\hat{\mathbf{H}}^{-1}\hat{\mathbf{G}} \tag{17}$$

The matrix $\mathbf{B}_{NL}^{(k)}$ is obtained based on von Karman assumptions and, therefore, the current analysis is applicable only for small rotations. The incremental strain ${}_0 E^{(k)}$ can be obtained by finding the difference of strain at $t + \Delta t$ and t

$$_0 E^{(k)} = {}^{t+\Delta t}_0 E^{(k)} - {}^{t}_0 E^{(k)} = \mathbf{B}_L^{(k)^T}\mathbf{v} + {}^t\mathbf{v}^T \mathbf{B}_{NL}^{(k)}\mathbf{v} + \frac{1}{2}\mathbf{v}^T \mathbf{B}_{NL}^{(k)}\mathbf{v} \tag{18}$$

The virtual strain increment can be expressed as

$$\delta \, {}_0 E^{(k)} = \mathbf{B}_L^{(k)^T}\delta\mathbf{v} + {}^t\mathbf{v}^T \mathbf{B}_{NL}^{(k)}\delta\mathbf{v} + \mathbf{v}^T \mathbf{B}_{NL}^{(k)}\delta\mathbf{v} \tag{19}$$

The expression for stress can now be written in terms of the unknown displacements as

$$^{t+\Delta t}_0 S^{(k)} = {}^{t}_0 S^{(k)} + \sum_j \widehat{C}_{jk} E^{(j)} = {}^{t}_0 S^{(k)} + \sum_j \widehat{C}_{jk} \left(\mathbf{B}_L^{(j)^T}\mathbf{v} + {}^t\mathbf{v}^T \mathbf{B}_{NL}^{(j)}\mathbf{v} + \frac{1}{2}\mathbf{v}^T \mathbf{B}_{NL}^{(j)}\mathbf{v} \right) \tag{20}$$

where $\widehat{C}_{jk}$ represents the linear relationship between the resultant stresses and strains. Substituting the expressions for virtual incremental strain and total stress from (19) and (20) into the virtual work expression and neglecting the higher-order terms results in

$$\left(\int\limits_{0_V} \left(\sum_k \sum_j \mathbf{B}_L^{(k)} \widehat{C}_{jk} \mathbf{B}_L^{(k)^T} + \sum_k \sum_j \mathbf{B}_L^{(k)} \widehat{C}_{jk}{}^t \mathbf{v}^T \mathbf{B}_{NL}^{(k)} + \sum_k \mathbf{B}_{NL}^{(k)}{}^t \mathbf{v} \widehat{C}_{jk}{}^t \mathbf{B}_L^{(k)^T} \right. \right.$$
$$\left. \left. + \sum_k \mathbf{B}_{NL}^{(k)}{}^t \mathbf{v} \widehat{C}_{jk}{}^t \mathbf{v}^T \mathbf{B}_{NL}^{(k)} + \sum_k {}_0^t S^{(k)} \mathbf{B}_{NL}^{(k)} \right) d\,^0V \right) \mathbf{v} = \mathbf{f}_e - \sum_k {}_0^t S^{(k)} \mathbf{B}_L^{(k)} - \sum_k {}_0^t S^{(k)} \mathbf{B}_{NL}^{(k)}{}^t \mathbf{v} \tag{21}$$

The final nonlinear system of finite element equations can be written as

$$\left(\mathbf{k}_L + \mathbf{k}_v + \mathbf{k}_\sigma \right) \mathbf{v} = \mathbf{f}_e - \mathbf{f}_i \tag{22}$$

where $\mathbf{k}_L$, $\mathbf{k}_v$, and $\mathbf{k}_\sigma$ are the linear, initial displacement, and geometric stiffness matrices and $\mathbf{f}_i$ is the internal force vector. The explicit form of these matrices and vectors is as follows:

$$\mathbf{k}_L = \int\limits_{0_V} \left(\sum_k \sum_j \mathbf{B}_L^{(k)} \widehat{C}_{jk} \mathbf{B}_L^{(k)^T} \right) d\,^0V \tag{23a}$$

$$\mathbf{k}_v = \int\limits_{0_V} \left(\sum_k \sum_j \mathbf{B}_L^{(k)} \widehat{C}_{jk}{}^t \mathbf{v}^T \mathbf{B}_{NL}^{(k)} + \sum_k \mathbf{B}_{NL}^{(k)}{}^t \mathbf{v} \widehat{C}_{jk}{}^t \mathbf{B}_L^{(k)^T} \sum_k \mathbf{B}_{NL}^{(k)}{}^t \mathbf{v} \widehat{C}_{jk}{}^t \mathbf{v}^T \mathbf{B}_{NL}^{(k)} \right) d\,^0V \tag{23b}$$

$$\mathbf{k}_\sigma = \int\limits_{0_V} \left(\sum_k {}_0^t S^{(k)} \mathbf{B}_{NL}^{(k)} \right) d\,^0V \tag{23c}$$

$$\mathbf{f}_i = \int\limits_{0_V} \left(\sum_k {}_0^t S^{(k)} \mathbf{B}_L^{(k)} + \sum_k {}_0^t S^{(k)} \mathbf{B}_{NL}^{(k)}{}^t \mathbf{v} \right) d\,^0V \tag{23d}$$

Note that combining the linear strain-displacement relationship matrix given in (17) with (23a), the linear stiffness matrix obtained from the hybrid formulation, (10), can be reproduced. The complete from of the tangent stiffness matrix that appears in. (1) can be expressed as

$$\mathbf{K}^{HOT32} = \mathbf{k}_L + \mathbf{k}_v + \mathbf{k}_\sigma \tag{24}$$

3.2 Adhesive Element

A six-nodded solid element, shown in Figure 4, is used for the adhesive layer. Unlike the plate element, the adhesive element is based on displacement formulation. Each node has 13 degrees of freedom, as in the case of the plate element. Rather than having independent degrees of freedom, the displacement at these nodes are expressed in terms of the nodal displacements of the adherent plate elements lying above (repair) and below (base) the

adhesive element. Therefore, the adhesive element is composed of pseudo nodes rather than actual nodes, as shown in Figure 4. The adhesive nodal displacements are expressed as

$$\mathbf{v}^{adh} = \begin{Bmatrix} \mathbf{v}^{adh}_{base} \\ \mathbf{v}^{adh}_{repair} \end{Bmatrix} = \begin{bmatrix} \mathbf{T}_{base} & \mathbf{0} \\ \mathbf{0} & \mathbf{T}_{repair} \end{bmatrix} \begin{Bmatrix} \mathbf{v}^{HOT32}_{base} \\ \mathbf{v}^{HOT32}_{repair} \end{Bmatrix} \tag{25}$$

where $\mathbf{v}^{adh}_{base}$ and $\mathbf{v}^{adh}_{repair}$ are displacements at the nodes connected to the base and repair, respectively, and $\mathbf{T}_{base}$ and $\mathbf{T}_{repair}$ are transformation matrices. The displacement field on the bottom and top surfaces of the adhesive element can be expressed in terms of the nodal displacements, $\mathbf{v}^{adh}_{base}$ and $\mathbf{v}^{adh}_{repair}$, as

$$\begin{Bmatrix} \mathbf{u}^{adh}_{bottom} \\ \mathbf{u}^{adh}_{top} \end{Bmatrix} = \begin{bmatrix} \mathbf{N}^{adh}_{xy} & \mathbf{0} \\ \mathbf{0} & \mathbf{N}^{adh}_{xy} \end{bmatrix} \begin{Bmatrix} \mathbf{v}^{adh}_{base} \\ \mathbf{v}^{adh}_{repair} \end{Bmatrix} \tag{26}$$

where the matrix $\mathbf{N}^{adh}_{xy}$ is comprised of the area coordinates for a triangle. The displacement field within the element varies linearly through the thickness, such that

$$\mathbf{u}^{adh} = \begin{Bmatrix} N_{\eta-} & N_{\eta+} \end{Bmatrix} \begin{Bmatrix} \mathbf{u}^{adh}_{bottom} \\ \mathbf{u}^{adh}_{top} \end{Bmatrix} \tag{27}$$

where $N_{\eta-}$ and $N_{\eta+}$ are one-dimensional linear interpolation functions. Therefore, combining (24), (25), and (26), the displacement field inside the element can be expressed as

$$\mathbf{u}^{adh} = \begin{Bmatrix} N_{\eta-} & N_{\eta+} \end{Bmatrix} \begin{bmatrix} \mathbf{N}^{adh}_{xy} & \mathbf{0} \\ \mathbf{0} & \mathbf{N}^{adh}_{xy} \end{bmatrix} \begin{bmatrix} \mathbf{T}_{base} & \mathbf{0} \\ \mathbf{0} & \mathbf{T}_{repair} \end{bmatrix} \begin{Bmatrix} \mathbf{v}^{HOT32}_{base} \\ \mathbf{v}^{HOT32}_{repair} \end{Bmatrix} \tag{28}$$

The strain field inside the element takes the form

$$\boldsymbol{\varepsilon}^{adh} = \mathbf{B}^{adh} \begin{Bmatrix} \mathbf{v}^{HOT32}_{base} \\ \mathbf{v}^{HOT32}_{repair} \end{Bmatrix} \tag{29}$$
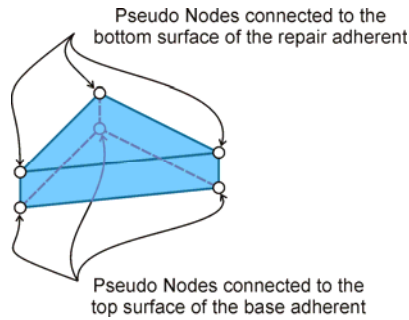

Figure 4: Adhesive element with pseudo nodes

where $\mathbf{B}^{adh}$ is the strain displacement transformation matrix and the strain vector consists of all six components

$$\boldsymbol{\varepsilon}^{adh} = \left\{ \varepsilon_{xx} \quad \varepsilon_{yy} \quad \varepsilon_{zz} \quad \gamma_{yz} \quad \gamma_{xz} \quad \gamma_{xy} \right\}^T \tag{30}$$

The stiffness matrix can be therefore be defined as

$$\mathbf{K}^{adh} = \int_{V^{adh}} \mathbf{B}^{adh^T} \mathbf{D}^{adh} \mathbf{B}^{adh} \, dV = \begin{bmatrix} \mathbf{K}_{bb}^{adh} & \mathbf{K}_{br}^{adh} \\ \mathbf{K}_{br}^{adh} & \mathbf{K}_{rr}^{adh} \end{bmatrix}_{78 \times 78} \tag{31}$$

where $\mathbf{D}^{adh}$ is the stress-strain relationship matrix and the subscripts b and r correspond to the base and repair, respectively. The isotropic adhesive material has a bilinear relation between the effective transverse shear stress, τ_{eff}, and effective transverse shear strain, γ_{eff}. The effective transverse shear stress and strain in the adhesive are defined as

$$\tau_{eff} = \sqrt{\tau_{xz}^2 + \tau_{yz}^2} \tag{32}$$

$$\gamma_{eff} = \sqrt{\gamma_{xz}^2 + \gamma_{yz}^2} \tag{33}$$

As shown in Figure 5 the initial shear modulus of the bilinear adhesive behavior is denoted by G_1, and it reduces to G_2 when the effective transverse shear strain, γ_{eff}, reaches the critical shear strain, γ_c. For a given value of effective strain, γ_{eff}, the effective stress, τ_{eff}, can be obtained from Figure 5. Thereafter, the effective shear modulus can be obtained as

$$G_{eff} = \tau_{eff} / \gamma_{eff} \tag{34}$$

Moreover, the effective Young's modulus can be expressed as

$$E_{eff} = 2G_{eff}\left(1 + v\right) \tag{35}$$

Note that due to the dependence of the effective modulus on the effective strain, the system of equations becomes nonlinear and an iterative method based on the Newton-Raphson method is utilized.

4   RESULTS

In order to demonstrate the capabilities of the current analysis tool, a sandwich panel with a repaired top facesheet is considered. As shown in Figure 6, the facesheet may be subject to full or partial repair. The panel has length and breadth of 40 in and 28 in, respectively, and the scarf ratio is 30. The top facesheet has 40 plies with a stacking sequence of $(45/90/-45)_{5s}$ and the bottom facesheet has 8 plies with a stacking sequence of $(45/90/-45)_2$. Each ply has a thickness of 0.0072 in and the core is 1.0 in thick. The material properties are listed in Table 1. The adhesive has a critical shear strain value of $\gamma_c = 0.06$.
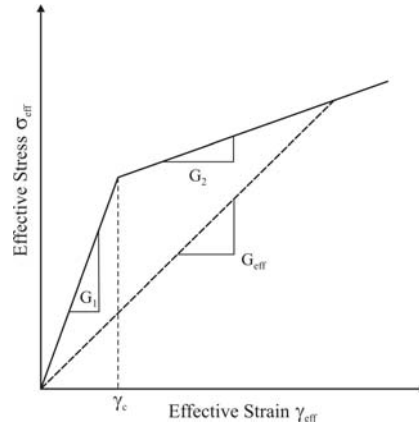
Figure 5: Bilinear relation between effective stress and effective strain
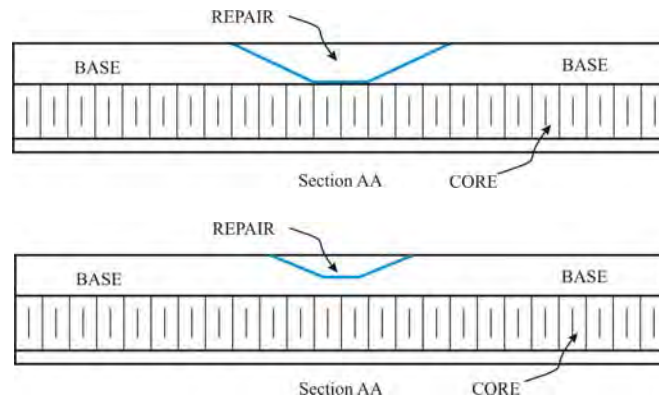
Figure 6: Cross-section of sandwich panel with full (top) and partial (bottom) facesheet repair

	Repair	Facesheet	Core	Adhesive 1	Adhesive 2
E_1(psi)	1.58×10^7	7.50×10^6	1.50×10^2	1.56×10^5	1.75×10^3
E_2(psi)	8.50×10^5	7.50×10^6	7.50×10^1	1.56×10^5	1.75×10^3
E_3(psi)	8.50×10^5	1.15×10^6	2.00×10^5	1.56×10^5	1.75×10^3
G_{12}(psi)	4.40×10^5	6.30×10^5	1.00×10^3	6.00×10^4	6.00×10^2
G_{13}(psi)	4.40×10^5	6.30×10^5	1.00×10^3	6.00×10^4	6.00×10^2
G_{23}(psi)	2.80×10^5	6.00×10^5	4.00×10^4	6.00×10^4	6.00×10^2
ν_{12}	0.34	0.06	1.20	0.30	0.46
ν_{13}	0.34	0.34	1.00×10^{-5}	0.30	0.46
ν_{23}	0.53	0.34	1.00×10^{-5}	0.30	0.46

Table 1: Material properties of different components of the sandwich panel.

In the first case, the panel top facesheet is subject to full repair. Also, the panel is subjected to a resultant moment of $M_x = 500.0$ lbs-in/in. The variation of transverse shear strain, γ_{rz}, and stress, σ_{rz}, inside the adhesive along the x-axis is shown in Figures 7 and 8, respectively. Although, an external moment is applied to the panel, the top facesheet remains under tension and the effect of stress stiffening is not very significant. Therefore, no significant difference is observed between the linear and nonlinear solutions.

In the second case, the panel top facesheet is subject to partial repair. The top 20 plies of the top facesheet are under scarf repair and the rest are undamaged. In this case, the panel is subjected to a displacement of $u_x = u_y = 0.18$ in. Under the influence of the prescribed displacement, the effective strain inside the adhesive exceeds the critical strain, thereby triggering a nonlinear material response. The transverse shear strain, γ_{rz}, and stress, σ_{rz}, inside the adhesive along the line that makes a 45° with the x-axis is shown in Figures 9 and 10, respectively. Since the effective strain in certain regions exceeds the critical value of $\gamma_c = 0.06$, the elastic modulus in those regions gets degraded. This results in higher strain values in comparison to the linear response and the stresses in these regions are reduced and more load is carried by the facesheet in the undamaged region.

5 CONCLUSION

An analysis tool for scarf repair analysis of sandwich panels has been developed and verified against predictions based on the commercially available finite element program ANSYS. It has been demonstrated that sandwich panels with complete or partial repair of the top facesheet can be analyzed without any difficulty. The analysis takes into account both geometric and material nonlinearity. The loading, material properties and panel geometry can be arbitrary. While offering computational efficiency, this analysis tool provides accurate stress and strain fields.
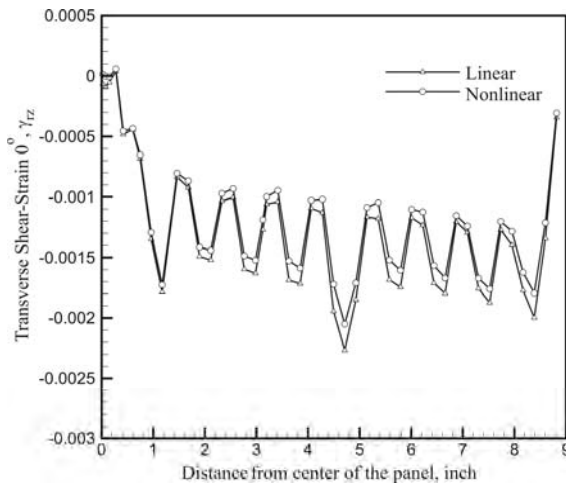
Figure 7: Transverse shear strain, γ_{rz} Figure 8: Transverse shear stress, σ_{rz}
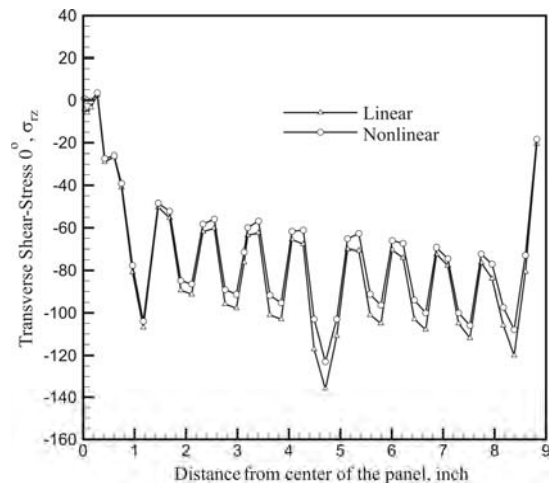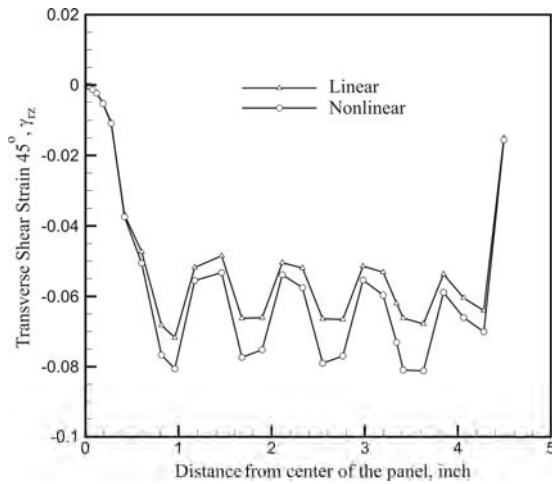
Figure 9: Transverse shear strain, γ_{rz}
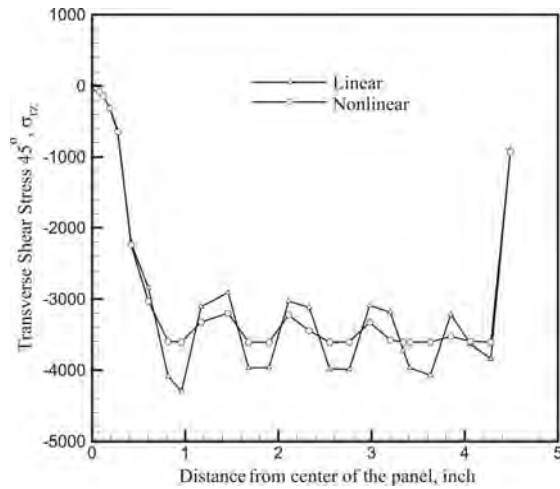
Figure 10: Transverse shear stress, σ_{rz}

REFERENCES

[1]   C.H. Wang and A.J. Gunnion, "On the design methodology of scarf repairs to composite laminates," 68, 35-46 (2008).

[2]   A.A. Baker, R.J. Chester, G.R. Hugo and T.C. Radtke, "Scarf repairs to highly strained graphite/epoxy structure," *Int. J. Adhesion and Adhesives*,19, 161-71 (1999).

[3]   A.B. Harman and C.H. Wang, "Improved design methods for scarf repairs to highly strained composite aircraft structure" *Compos. Struct.* 75, 132–44 (2006).

[4]   L. Johnson, "Effect of ply stacking sequence on stress in a scarf joint," *AIAA J.*, 27, 79-86 (1989).

[5]   L.J. Hart-Smith, "Adhesive-bonded scarf and stepped-lap joints," *NASA CR-112237* (1973).

[6]   M.M. Ratwani and H.P. Kan, "Analysis of composite-to-metal joints with bondline flaws," *Compos. Sci. Technol.* 23, 53-72 (1985).

[7]   C . Soutis and F.Z. Hu, "Strength analysis of adhesively bonded repairs," *Recent Advances in Structural Joints and Repairs for Composite Materials* (L. Tong and C. Soutis, eds.), Kluwer Academic Publishers (2003).

[8]   J. Gunnion and I. Herszberg, "Parametric study of scarf joints in composite structures," *Compos. Struct.* 75, 364–376 (2006).

[9]   M. Das, A. Barut, E. Madenci and D.R. Ambur, "Complete stress field in sandwich panels with a new triangular finite element of single-layer theory," *Comput. Methods Appl. Mech. Eng.*194, 2969-3005 (2005).

ANALYSIS OF LAMINATED SANDWICH PLATES BASED ON AN IMPROVED HIGHER ORDER ZIGZAG THEORY

Mihir K. Pandit[*], Abdul H. Sheikh[†] and Bhrigu N. Singh[¶]

[*] Department of Ocean Engineering and Naval Architecture, Indian Institute of Technology, Kharagpur-721302, India
e-mail: m_pandit@naval.iitkgp.ernet.in, Tel: +91 3222 281601; Fax: +91 3222 255303

[†] Department of Ocean Engineering and Naval Architecture, Indian Institute of Technology, Kharagpur-721302, India
e-mail: hamid@naval.iitkgp.ernet.in, Tel: +91 3222 283790; Fax: +91 3222 255303

[¶] Department of Aerospace Engineering, Indian Institute of Technology, Kharagpur-721302, India
e-mail: bnsingh@aero.iitkgp.ernet.in, Tel: +91 3222 283026; fax: +91 3222 255303

Key words: Sandwich plates, Plate theory, Finite element analysis, Natural frequency.

Summary. *In the present study, an improved higher order zigzag theory is proposed and it is applied to study the bending and free vibration response of laminated sandwich plates. The theory satisfies the condition of continuity in transverse shear stresses at all the layer interfaces and transverse shear stress free condition at the top and bottom of the plate. In addition to that it accounts for the transverse flexibility effect of the core. The variation of in-plane displacements through thickness is assumed to be cubic, while transverse displacement varies quadratically only within the core. The core is modelled as a 3-D elastic continuum. An efficient C^0 finite element is proposed for the implementation of the proposed plate theory. The accuracy and range of applicability of the present formulation are established by comparing the present results with 3-D elasticity solutions and other results available in the literature.*

1 INTRODUCTION

Sandwich and composite constructions are quite popular for design and development of aerospace, underwater and automotive structures because of their lightweight and directional properties. Some of the attractive properties of these structures are high heat resistance, high strength-to-weight ratio, good energy and sound absorption, and often also low production cost. The accurate prediction of the structural behaviour of laminated sandwich plates is quite complicated because of the complex variation of their through-thickness properties. Due to the low shear modulus compared to that of extensional rigidity, the effect of shear deformation plays a significant role in the analysis of composite structures. In case of sandwich, large difference of values of elastic moduli of the face sheets and cores makes this effect more pronounced and severe. In order to model the effect of shear deformation in a realistic manner

several laminated plate theories proposed by many researchers. As an initial effort in this direction, the first order shear deformation theory [1] may be stated where uniform transverse shear strain is taken over the entire laminate thickness. The performance of the first order shear deformation theory is strongly dependant on shear correction factors. For a better representation of the transverse shear deformations, higher order plate theories are proposed by Lo et al. [2], Reddy [3], Khedir and Reddy [4] and few others where the use of the shear correction factor could be eliminated. It gives continuous variation of transverse shear strain across the entire thickness, which leads to discontinuity in the variation of the transverse shear stresses at the layer interfaces. Unfortunately the actual situation is entirely opposite and the degree of discontinuity in the transverse shear strain is severe in the sandwich plates at the core face sheet interfaces due to a wide variation of their material properties. In order to overcome this problem, layer-wise plate theories are proposed by Srinivas [5], Toledano and Murakami [6], Li and Liu [7], Robins and Reddy [8] where unknowns are taken at each layer interface. The major disadvantage of these theories is their computational involvement since the number of unknowns increases with the number of layers. With the idea of layer-wise theory the unknowns for the in-plane displacements at the different layer interfaces are expressed in terms of those at the reference plane and it is termed as refined theories [9- 11]. In these plate theories the in plane displacements have a piecewise linear variation across the plate thickness, which gives a zigzag pattern. A further improvement in this direction is due to Di Sciuva [12], Bhaskar and Varadan [13], Cho and Parmerter [14, 15] and some other investigators who considered the variation of inplane displacements to be superposition of linearly varying piecewise field on an overall higher order variation.

The refined plate theories discussed above do not take into account the compressibility effect of the core. When the cores are made of transversely soft/flexible materials, the effect of core transverse normal strain becomes quite important. So, the conventional modeling techniques [16-20] are not adequate to accurately predict the behaviour of soft core sandwich plates which neglect transverse flexibility of the core. In this situation the 3-D elasticity solutions of Pagano [21] for static response and some similar studies due to Srinivas and Rao [22] and Noor [23] for vibration problem can give an exact picture but being analytical in nature their applications are limited to a specific class of problem only.

A finite element investigation of the problem is carried out by Lee and Fan [24] considering transverse normal deformation of the core where the laminated face sheets are simply modeled as Mindlin's plates while the displacements of the core are linearly interpolated from the displacements of the face sheets. Oskooei and Hansen [25] have similarly modeled the face sheets as Reissner-Mindlin plates but a higher order through thickness variation is adopted for the core displacements taking additional unknowns within the core layer. A similar attempt based on spline finite strip method is made by Yuan and Dawe [26] where the variation of in-plane displacements over the core thickness is taken as quadratic utilizing additional unknowns at the core mid-plane. Kant and Swaminathan [27] presented an analytical solution for vibration of simply supported composite and sandwich plate considering the effect of transverse normal strain/stress but the analysis is based on higher order theory, which fails to predict the transverse shear strain discontinuity at the layer interfaces as discussed earlier. A layer-wise model is proposed by Rao and Desai [28] who

have taken three displacements and three transverse stresses at the interfaces, which are used to have a cubic through thickness variation for the three displacement components in any layer. As it involves a large number of unknowns, the model applicable for a layer is applied to the whole laminate to have a simplified model defined as equivalent single layer theory where they have also used layer-wise theory based on mixed formulation. Frostig and Thomsen [29] have presented an efficient analytical model based on higher order sandwich panel theory to study the vibration of sandwich panels with flexible core.

Considering all these aspects in view, in this study an attempt has been made to develop an improved plate model to predict the behaviour of laminated sandwich plate considering the effect of the transverse normal deformation of the core. The in-plane displacement fields are assumed as a combination of a linear zigzag model with different slopes in each layer and a cubically varying function over the entire thickness. The out of plane displacement is assumed to be quadratic within the core and constant throughout the faces. The plate model is implemented with a computationally efficient C^0 finite element developed for this purpose and applied to solve a number of the sandwich plate problems.

2 MATHEMATICAL FORMULATION

The through thickness variation of in-plane displacements as shown in Fig. 1 may be expressed as follows

$$U = u + z\theta_x + \sum_{i=1}^{n_u-1}(z-z_i^u)H(z-z_i^u)\alpha_{xu}^i + \sum_{j=1}^{n_l-1}(z-z_j^l)H(-z+z_j^l)\alpha_{xl}^j + \beta_x z^2 + \eta_x z^3 \qquad (1)$$

$$V = v + z\theta_y + \sum_{i=1}^{n_u-1}(z-z_i^u)H(z-z_i^u)\alpha_{yu}^i + \sum_{j=1}^{n_l-1}(z-z_j^l)H(-z+z_j^l)\alpha_{yl}^j + \beta_y z^2 + \eta_y z^3 \qquad (2)$$

where, u, v denote the inplane displacement of any point in the reference plane (plate midplane), θ_x and θ_y are the rotations of the normal to the midplane about y-axis and x-axis respectively, n_u and n_l are number of upper and lower layers respectively, β_x, β_y, η_x, η_y are the higher order unknowns, α_{xu}^i, α_{xl}^i, α_{yu}^i and α_{yl}^i are the change of slopes at the upper/lower i-th interface between i-th and (i+1)th layer and $H(z-z_i^u)$ and $H(-z+z_j^l)$ are the unit step functions.

The transverse displacement as shown in Fig. 2 may be expressed as

$$W = l_1 w_u + l_2 w + l_3 w_l, \text{ for core}$$
$$= w_u, \text{for upper faces} \qquad (3)$$
$$= w_l, \text{for lower faces}$$

where, w_u, w and w_l are the values of the transverse displacement at the top, middle and the bottom layer of the core, respectively and l_1, l_2 and l_3 are Lagrangian interpolation functions in the thickness co-ordinate.

The stress-strain relationship of an orthotropic layer/lamina (say k-th layer) having any fibre orientation with respect to structural axes system (x-y-z) may be expressed as

$$\{\bar{\sigma}\} = \left[\bar{Q}^k\right]\{\bar{\varepsilon}\} \tag{4}$$

where, $\{\bar{\sigma}\}$, $\{\bar{\varepsilon}\}$ and $\left[\bar{Q}^k\right]$ are the stress vector, the strain vector and the transformed rigidity matrix of k-th lamina, respectively [30].
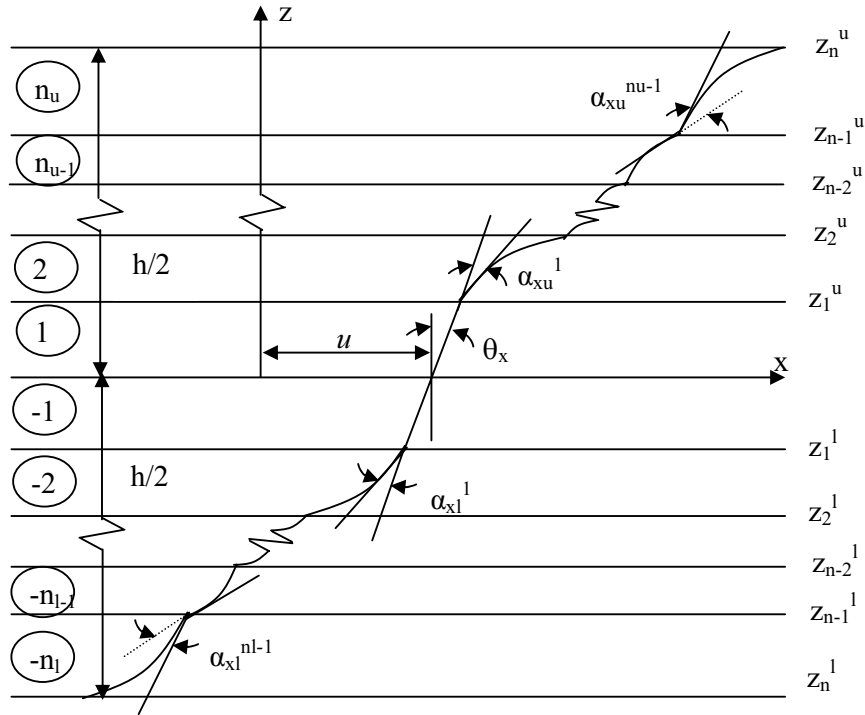
Fig. 1. General lamination scheme and displacement configuration
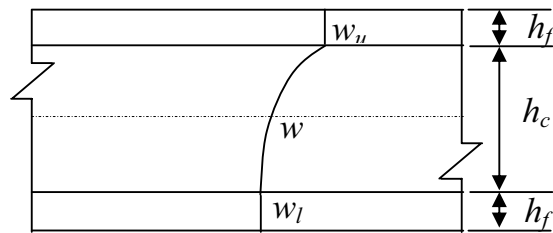
Fig. 2. Variation of transverse displacement (W) through the thickness of sandwich plate

Utilizing the condition of zero transverse shear stress at the top and bottom surfaces of the plate and imposing the condition of the transverse shear stress continuity at the interfaces between the layers, β_x, β_y, η_x, η_y, α^i_{xu}, α^i_{xl}, α^i_{yu} and α^i_{yl} may be expressed as

$$\{\beta\} = [A]\{\alpha\} \tag{5}$$

where, $\{\beta\}^T = \left\{\beta_x \; \eta_x \; \beta_y \; \eta_y \; \alpha_{xu}^1 \; \alpha_{xu}^2 \; ... \; \alpha_{xu}^{n_u-1} \; \alpha_{xl}^1 \; \alpha_{xl}^2 \; ... \; \alpha_{xl}^{n_l-1} \; \alpha_{yu}^1 \; \alpha_{yu}^2 \; ... \; \alpha_{yu}^{n_u-1} \; \alpha_{yl}^1 \; \alpha_{yl}^2 \; ... \; \alpha_{yl}^{n_l-1}\right\}^T$

$\{\alpha\}^T = \left\{u \; v \; w \; \theta_x \; \theta_y \; w_{u,x} \; w_{u,y} \; w_{l,x} \; w_{l,y}\right\}^T$ and the elements of $[A]$ are dependent on the material properties.

With the help of the above equation the displacement field is modified which now contains first order derivatives of w_u and w_l, which usually requires C^1 continuous shape functions for finite element approximation. In order to avoid the usual difficulties associated with satisfaction of C^1 continuity, $w_{u,x}$, $w_{u,y}$, $w_{l,x}$ and $w_{l,y}$ are replaced with θ_{ux}, θ_{uy}, θ_{lx} and θ_{ly}, respectively where θ_{ux}, θ_{uy}, θ_{lx} and θ_{ly} are considered as independent field variables. It has imposed the following constrains, which are enforced variationally through penalty approach.

$$w_{u,x} - \theta_{ux} = 0, w_{u,y} - \theta_{uy} = 0, w_{l,x} - \theta_{lx} = 0, w_{l,y} - \theta_{ly} = 0 \tag{6}$$

Using linear strain-displacement relation and Eqs. (1)- (3), the strain vector $\{\bar{\varepsilon}\}$ may be expressed in terms of unknowns as

$$\{\bar{\varepsilon}\}^T = \left[\frac{\partial U}{\partial x} \; \frac{\partial V}{\partial y} \; \frac{\partial W}{\partial z} \; \frac{\partial U}{\partial y} + \frac{\partial V}{\partial x} \; \frac{\partial U}{\partial z} + \frac{\partial W}{\partial x} \; \frac{\partial V}{\partial z} + \frac{\partial W}{\partial y}\right]^T or, \{\bar{\varepsilon}\} = [H]\{\varepsilon\} \tag{7}$$

where, $\{\varepsilon\}$ is strain vector and the elements of $[H]$ are functions of z and unit step functions. The displacement components at any point within the plate may also be expressed as

$$\{\bar{f}\} = \left\{\begin{matrix} U \\ V \\ W \end{matrix}\right\} = [S]\{f\} \tag{8}$$

where, $\{f\}^T = \left[u \; v \; w \; \theta_x \; \theta_y \; \theta_{ux} \; \theta_{uy} \; \theta_{lx} \; \theta_{ly} \; w_u \; w_l\right]^T$ and the elements of $[S]$ are functions of z and unit step functions.

With the quantities found in the above equations, the Lagrangian of the system may be expressed as

$$L = T - U_s + W_{ext.} - P_\lambda \tag{9}$$

where U_s, T are the strain energy and kinetic energy, respectively, $W_{ext.}$ is the work done by the external transverse loads, and P_λ is the penalty term for the satisfaction of the constraints expressed in Eq. (6).

Using Eqs. (4) and (7), the strain energy is expressed as

$$U_s = \frac{1}{2}\sum_{k=1}^{n}\iiint\{\bar{\varepsilon}\}^T\left[\bar{Q}^k\right]\{\bar{\varepsilon}\}\,dxdydz = \frac{1}{2}\iint\{\varepsilon\}^T\left[D\right]\{\varepsilon\}\,dxdy \tag{10}$$

where,

$$[D] = \sum_{k=1}^{n}\int[H]^T\left[\bar{Q}^k\right][H]\,dz \tag{11}$$

Using Eq. (8), the kinetic energy is expressed as

$$T = \frac{1}{2}\sum_{k=1}^{n}\iiint\{\dot{\bar{f}}\}^T\rho_k\{\dot{\bar{f}}\}\,dxdydz = \frac{1}{2}\iint\{\dot{f}\}^T[R]\{\dot{f}\}\,dxdy \tag{12}$$

where, $[R] = \sum_{k=1}^{n}\int[S]^T\rho_k[S]\,dz$, ρ_k is the mass density of the k-th layer and the dot indicates derivative with respect to time 't'.

The work done by a distributed transverse load of intensity $q(x, y, t)$ is

$$W_{ext.} = \iint W\,q\,dxdy \tag{13}$$

Using Eq. (6), the penalty term is expressed as

$$P_\lambda = \frac{\gamma}{2}\iint\left(\begin{array}{l}\{w_{u,x}-\theta_{ux}\}^T\{w_{u,x}-\theta_{ux}\}+\{w_{u,y}-\theta_{uy}\}^T\{w_{u,y}-\theta_{uy}\}\\ +\{w_{l,x}-\theta_{lx}\}^T\{w_{l,x}-\theta_{lx}\}+\{w_{l,y}-\theta_{ly}\}^T\{w_{l,y}-\theta_{ly}\}\end{array}\right)dxdy \tag{14}$$

where γ is the penalty parameter.

2.1 Finite element formulation

A nine-noded quadrilateral C^0 isoparametric element is used in the present study. The generalized displacement vector δ at any point may be expressed as

$$\delta = \sum_{i=1}^{n}N_i\delta_i \tag{15}$$

where, δ_i is the displacement vector corresponding to node i, N_i is the shape function associated with the node i and n is the number of nodes per element, which is nine in the present study.

With the help of above Eq. (15), the strain vector $\{\varepsilon\}$ as appeared in Eq. (7) and the displacement vector $\{f\}$ may be expressed in terms of $\{\delta\}$ as

$$\{\varepsilon\} = [B]\{\delta\},\ \{f\} = [C]\{\delta\} \tag{16}$$

where, $[B]$ is the strain-displacement matrix in the Cartesian co-ordinate system and $[C]$ is a matrix, similar to that of $[B]$.

The Lagrangian as given in Eq. (9) may be rewritten with the help of Eqs. (10)- (16) as

$$L = \frac{1}{2}\{\dot{\delta}\}^T [M_e]\{\dot{\delta}\} - \frac{1}{2}\{\delta\}^T [K_e]\{\delta\} + \{\delta\}^T \{F_e\} - \frac{1}{2}\{\delta\}^T [K_p]\{\delta\} \qquad (17)$$

where, $[M_e]$, $[K_e]$ and $[K_p]$ are the element stiffness matrix, the mass matrix and the penalty matrix, respectively and $[F_e]$ is the elemental load vector.

The equation of motion of the plate system can be obtained by applying Hamilton's principle $\delta \int_{t_1}^{t_2} L dt = 0$, which finally yields the generalized eigenvalue problem as

$$[M]\{\ddot{\delta}\} + [K]\{\delta\} = \{P\} \qquad (18)$$

where, $[K]$, $[M]$ are the global stiffness matrix and mass matrix, respectively, and $\{P\}$ is the global load vector.

Now governing equations for different types of analysis can easily be written as follows:

Static analysis: $[K]\{\delta\} = \{P\}$ \qquad (19)

Free vibration analysis: $[K]\{\phi\} = \omega^2 [M]\{\phi\}$ \qquad (20)

where, ω is the natural frequency, and $\{\phi\}$ are the vectors defining the mode shapes.

After incorporating the boundary conditions, the governing equations for different cases are solved to get displacements and stresses in case of static analysis and natural frequency (ω) for the requisite number of modes required in case of free vibration problem.

3 NUMERICAL RESULTS AND DISCUSSIONS

In order to show the performance of the present formulation, several numerical examples of the laminated sandwich plates are analyzed and the results obtained are compared with the published results.

The following non-dimensional quantities used in the present analysis are defined as

$$\left(\overline{\sigma}_x, \overline{\sigma}_y, \overline{\sigma}_z, \overline{\sigma}_{xy}\right) = \frac{h^2}{q_0 a^2}\left(\sigma_x, \sigma_y, \sigma_z, \sigma_{xy}\right), \left(\overline{\sigma}_{xz}, \overline{\sigma}_{yz}\right) = \frac{h}{q_0 a}\left(\sigma_{xz}, \sigma_{yz}\right), \overline{w} = \frac{100 w E_2 h^3}{q_0 a^4}.$$

3.1 Simply supported rectangular sandwich plate with different aspect ratios

A simply supported sandwich plate (0/90/C/90/0) with aspect ratios b/a=1.0 and 2.0 is considered. The material properties used for the core are taken as E_1=E_2=0.04E, E_3=0.5E, G_{12}=0.016E, G_{23}=G_{13}=0.06E, v_{12}=0.25, t_c=0.8h, while those of each face sheet are E_1=25E, E_2=E, G_{23}=0.2E, G_{12}=G_{13}=0.5E, v_{12}=0.25, t_f=0.05h, with h being the total thickness of the plate. It is subjected to a distributed load of intensity $q = q_0 \sin(\pi x / a)\sin(\pi y / b)$. The non-dimensional deflections ($\bar{w}$) at the plate mid-plane and stresses at the important points are calculated for different mesh divisions and presented with those of the 3-D elasticity solution [21] in Table 1. The present results are in very good agreement with the 3-D solution [21]. The table also shows that the convergence of the results with mesh refinement is excellent.

b/a	h/a	References	$\bar{w}$ $\left(\frac{a}{2},\frac{b}{2},0\right)$	$\bar{\sigma}_x$ $\left(\frac{a}{2},\frac{b}{2},\frac{h}{2}\right)$	$\bar{\sigma}_y$ $\left(\frac{a}{2},\frac{b}{2},\frac{h}{2}\right)$	$\bar{\sigma}_{xz}$ $\left(0,\frac{b}{2},0\right)$	$\bar{\sigma}_{yz}$ $\left(\frac{a}{2},0,0\right)$	$\bar{\sigma}_{xy}$ $\left(0,0,\frac{h}{2}\right)$
1.0	0.01	Present (4×4)[a]	0.8864	1.06428	0.0527	0.1930	0.1763	0.04207
		Present (6×6)	0.8861	1.0827	0.05364	0.19626	0.17933	0.04280
		Present (8×8)	0.8860	1.0889	0.05395	0.1974	0.18034	0.04304
		Present (10×10)	0.8860	1.0917	0.05409	0.1979	0.1808	0.04315
		Present (12×12)	0.8860	1.0932	0.05416	0.1981	0.1810	0.0432
		3-D Elasticity [21]	0.8867	1.0974	0.05048	0.1850	0.1687	0.0434
	0.1	Present (4×4)[a]	1.7226	1.1080	0.05898	0.1917	0.1770	0.0458
		Present (6×6)	1.7212	1.1271	0.06000	0.1950	0.1800	0.04660
		Present (8×8)	1.7210	1.1335	0.060336	0.19606	0.1810	0.04686
		Present (10×10)	1.7209	1.1364	0.06049	0.1966	0.1814	0.04699
		Present (12×12)	1.7209	1.1380	0.06057	0.1968	0.1817	0.04705
		3-D Elasticity [21]	1.7240	1.1417	0.06321	0.1839	0.1694	0.04712
2.0	0.01	Present (4×4)[a]	1.6126	1.9228	0.03847	0.3284	0.0518	0.03837
		Present (6×6)	1.6120	1.95626	0.03914	0.3340	0.0527	0.03904
		Present (8×8)	1.6119	1.9674	0.03936	0.3359	0.0530	0.03927
		Present (10×10)	1.6118	1.9725	0.0395	0.3367	0.0531	0.0394
		Present (12×12)	1.6118	1.9752	0.0395	0.3371	0.0531	0.0394
		3-D Elasticity [21]	1.6127	1.9823	0.0397	0.3146	0.0497	0.0396
	0.1	Present (4×4)[a]	2.9681	1.9473	0.04816	0.3199	0.069709	0.04802
		Present (6×6)	2.9657	1.9810	0.04898	0.3253	0.070900	0.04885
		Present (8×8)	2.9653	1.9923	0.049254	0.32714	0.07129	0.04913
		Present (10×10)	2.9652	1.9974	0.04938	0.32798	0.07148	0.04925
		Present (12×12)	2.9652	2.0001	0.04945	0.3284	0.07157	0.04932
		3-D Elasticity [21]	2.9712	2.0073	0.05206	0.3064	0.0671	0.04940

Table 1: Non-dimensional deflection ($\bar{w}$) and stresses ($\bar{\sigma}_x, \bar{\sigma}_y, \bar{\sigma}_{xz}, \bar{\sigma}_{yz}, \bar{\sigma}_{xy}$) at the important points of a simply supported sandwich plate
[a] : Quantities within the parenthesis indicates mesh size

3.2 Square sandwich plate under all edges clamped condition

A square sandwich (0/C/0) plate, clamped in all four edges and subjected to distributed load of intensity $q = q_0 \sin(\pi x / a) \sin(\pi y / b)$ is studied by taking thickness ratios, h/a=0.01, 0.02, 0.05, 0.10 and 0.25. The thickness of each face is $0.1h$ and that of core is $0.8h$. The material properties are same as given in the previous example. The deflection, the stresses at some important points obtained from the present formulation are presented in Table 2. It may be noted from the results that the percentage increase in the transverse displacement for higher thickness ratios i.e. from 0.10 to 0.25 is much higher than those for lower thickness ratios i.e. from 0.01 to 0.02. Same kind of observations may also be noted for the stress values except the transverse shear stress ($\overline{\sigma}_{xz}$) which decreases as the thickness ratio increases.

h/a	References	$\overline{w}$ $\left(\dfrac{a}{2},\dfrac{b}{2},0\right)$	$\overline{\sigma}_x$ $\left(\dfrac{a}{2},\dfrac{b}{2},\dfrac{h}{2}\right)$	$\overline{\sigma}_y$ $\left(\dfrac{a}{2},\dfrac{b}{2},\dfrac{h}{2}\right)$	$\overline{\sigma}_{xz}$ $\left(0,\dfrac{b}{2},0\right)$	$\overline{\sigma}_{yz}$ $\left(\dfrac{a}{2},0,0\right)$	$\overline{\sigma}_{xy}$ $\left(0,0,\dfrac{h}{2}\right)$
0.01	Present	0.2256	0.4382	0.0175	0.3445	0.0501	0.0006
0.02	Present	0.2723	0.4412	0.0207	0.3236	0.0529	0.0010
0.05	Present	0.5728	0.4550	0.0410	0.2660	0.0686	0.0028
0.10	Present	1.4363	0.5081	0.0858	0.1975	0.0978	0.0063
0.25	Present	5.6674	0.9977	0.1647	0.1273	0.1276	0.0141

Table 2: Non-dimensional deflection ($\overline{w}$) and stresses ($\overline{\sigma}_x, \overline{\sigma}_y, \overline{\sigma}_{xz}, \overline{\sigma}_{yz}, \overline{\sigma}_{xy}$) at the important points of a clamped square sandwich plate under sinusoidal load

3.3 Simply supported cross-ply laminated plate

A symmetric cross-ply square laminate with different E_1/E_2 ratios is considered in the present problem. The non-dimensional fundamental frequency parameters ($\lambda = \left(\omega b^2 / h\right)\sqrt{\rho/E_2}$) of the laminate (3, 5 and 9 layers) with the thickness ratio, $h/a = 0.2$, are presented in Table 3 for $E_1/E_2 = 3, 10$ and 20. The orthotropic material properties of the individual layers in the laminate are $E_2 = E_3$, $G_{12} = G_{13} = 0.6E_2, G_{23} = 0.5E_2$ and $\nu_{12} = \nu_{13} = \nu_{23} = 0.25$. The three dimensional elasticity solution of Noor [23] is also presented in the table for necessary comparison. The table clearly shows that the performance of the present formulation is very good in terms of solution accuracy and the rate of convergence with mesh refinement.

E_1/E_2	References	No. of Layers		
		3	5	9
3	Present (6×6)	6.5527	6.5789	6.5907
	Present (8×8)	6.5519	6.5781	6.5899

	Present (10×10)	6.5517	6.5779	6.5897
	Present (12×12)	6.5516	6.5778	6.5896
	Present (14×14)	6.5516	6.5778	6.5896
	Noor [23]	6.6185	6.6468	6.66
	% Error	1.02	1.04	1.06
10	Present (6×6)	8.1532	8.4005	8.5101
	Present (8×8)	8.1522	8.3996	8.5091
	Present (10×10)	8.1520	8.3993	8.5089
	Present (12×12)	8.1519	8.3992	8.5087
	Present (14×14)	8.1519	8.3992	8.5087
	Noor [23]	8.2103	8.5223	8.608
	% Error	0.71	1.46	1.16
20	Present (6×6)	9.2404	9.7726	10.0142
	Present (8×8)	9.2395	9.7718	10.0132
	Present (10×10)	9.2393	9.7715	10.0129
	Present (12×12)	9.2392	9.7714	10.0128
	Present (14×14)	9.2392	9.7714	10.0128
	Noor [23]	9.5603	9.948	10.1368
	% Error	3.47	1.80	1.23

Table 3: The non-dimensional fundamental frequency parameters ($\lambda = (\omega b^2/h)\sqrt{\rho/E_2}$) of a simply supported cross-ply square laminated plate

3.4 Simply supported rectangular sandwich plate with different aspect ratios

A simply supported rectangular sandwich plate (0/90/C/90/0) is considered. The material properties used are same as given in sub-section 3.1. The analysis is performed for three different aspect ratios (b/a=1.0, 2.0 and 3.0) and two different thickness ratios (h/a=0.1 and 0.2) with mesh division of 12×12. The non-dimensional frequency parameters ($\lambda = (\omega b^2/h)(\rho/E_2)_f^{1/2}$) for first six modes are presented in the Table 4. It may be noted from the results that frequency parameters increases with the increase in aspect ratios whereas it decreases with the increase in thickness ratio.

b/a	h/a	References	Mode numbers					
			1	2	3	4	5	6
1.0	0.1	Present (12×12)	8.881	16.661	17.725	22.6609	24.6137	24.615
	0.2	Present (12×12)	5.664	9.396	9.904	12.2588	12.2613	12.421
2.0	0.1	Present (12×12)	24.641	27.076	35.524	49.9979	66.7487	66.904
	0.2	Present (12×12)	12.318	17.723	22.659	29.6987	36.8789	37.023
3.0	0.1	Present (12×12)	36.963	58.711	65.146	73.9247	79.9526	100.894
	0.2	Present (12×12)	18.479	36.947	38.106	42.7467	50.9948	55.3739

Table 4: Non-dimensional frequency parameters ($\lambda = (\omega b^2/h)(\rho/E_2)_f^{1/2}$) of a simply supported sandwich plate

4   CONCLUSIONS

In this paper an improved higher order zigzag plate theory for bending and vibration analysis of soft core sandwich plate is proposed. It satisfies shear free conditions at the top and bottom surfaces of the plate and inter-laminar shear stress continuity at the layer interfaces. The through thickness variation for the in-plane displacements is cubic with discontinuity in the transverse shear strain at the layer interfaces. A quadratic variation of the transverse displacement is taken for the core layer. The most attractive feature of such an involved plate theory is that it requires sufficiently less number of unknowns. An efficient C^0 finite element formulation is developed to implement the improved sandwich plate model. The results obtained for the deflection, stresses and natural frequencies of the sandwich plate structure show excellent performance of the present formulation. The convergence of the results with mesh refinement is found to be very good indicating reasonably less number of elements can attain the desired accuracy. Some new results for different thickness ratios and aspect ratios are also reported for future references.

REFERENCES

[1] P.C. Yang, C.H. Norris, Y. Stavsky, "Elastic wave Propagation in heterogeneous plates", *Int. J. Solids Struct,* 2, 665-684 (1966).

[2] K.H. Lo, R.M. Christensen, E.M. Wu, "A higher order theory of plate deformation, Part 2: Laminated plates", *Trans. ASME, J. Appl. Mech,* 44, 669-676 (1977).

[3] J.N. Reddy, "A simple higher-order theory for laminated composite plates", *ASME J. Appl. Mech,* 51, 745-752 (1984).

[4] A.A. Khedir, J.N. Reddy, "Free vibration of laminated composite plates using second order shear deformation theory", *Comput. Struct,* 71, 617-626 (1999).

[5] S. Srinivas, "A refined analysis of composite laminates", *J. Sound Vibr,* 30, 495-507 (1973).

[6] A. Toledano, H. Murakami, "A composite plate theory for arbitrary laminate configuration", *J. Appl. Mech,* 54, 181-189 (1987).

[7] X. Li, D. Liu, "Zigzag theory for composite laminates", *AIAA J,* 33(6), 1163-1165 (1995).

[8] D.H. Robbins, J.N. Reddy, "Modelling of thick composites using a layerwise laminate theory", *Int. J. Numer. Meth. Engng,* 36, 665-677 (1993).

[9] M. Di Scuiva, "A refined transverse shear deformation theory for multilayered anisotropic plates", *Atti Academia Scienze Torino,* 118, 279-295 (1984).

[10] H. Murakami, "Laminated composite plate theory with improved in-plane responses", *J. Appl. Mech.* 53, 661-666 (1986).

[11] D. Liu, X. Li, "An overall view of laminate theories based on displacement hypothesis, *J. Compos. Mater,* 30, 1539-1560 (1996).

[12] M. Di Scuiva, "Multilayered anisotropic plate models with continuous interlaminar stress", *Comput. Struct,* 22(3), 149-167 (1992).

[13] K. Bhaskar, T.K. Varadan, "Refinement of higher order laminated plate theories", *AIAA J,* 27, 1830-1831 (1989).

[14] M. Cho, R.R. Parmerter, "An efficient higher order plate theory for laminated composites", *Compos. Struct,* 20, 113-123 (1992).

[15] M. Cho, R.R. Parmerter, "Efficient higher order composite plate theory for general lamination configurations", *AIAA J,* 31(7), 1299-1306 (1993).

[16] F.J. Plantema, *Sandwich construction,* John Wiley & Sons, New York, 1966.

[17] H.G. Allen, *Analysis and Design of Structural Sandwich Panels*, Pergamon, Oxford, 1969.

[18] T.P. Khatua, Y.K. Cheung, "Bending and vibration of multilayer sandwich beams and plates", *Int. J. Numer. Meth Engng,* 6, 11-24 (1973).

[19] A. Chakraborti, A.H. Sheikh, "Vibration of laminate-faced sandwich plate by a new refined element", *J. Aero. Engng,* 17(3), 123-134 (2004).

[20] C.M. Wang, K.K. Ang, L. Yang, E. Watanabe, "Free vibration of skew sandwich plates with laminated facings", *J. Sound Vibr,* 235(2), 317-340 (2000).

[21] N.J. Pagano, "Exact solution of rectangular bi-directional composites and sandwich plates", *J. Compos. Mater,* 4, 20-34 (1970).

[22] S. Srinivas, A.K. Rao, "Bending, vibration and buckling of simply supported thick orthotropic rectangular plates and laminates", *Int. J. Solids Struct,* 6, 1463-1481 (1970).

[23] A.K. Noor, "Free vibration of multilayered composite plates", *AIAA J,* 11(7), 1038-1039 (1973).

[24] L.J. Lee, Y.J. Fan, "Bending and vibration analysis of composite sandwich plates", *Comput. Struct,* 60(1), 103-112 (1996).

[25] S. Oskooei, J.S. Hansen, "Higher order finite element for sandwich plates", *AIAA J,* 38(3), 525-33 (2000).

[26] W.X. Yuan, D.J. Dawe, "Free vibration of sandwich plates with laminated faces", *Int. J. Numer. Meth. Engng,* 54, 195–217 (2002).

[27] T. Kant, K. Swaminathan, "Analytical solutions for free vibration of laminated composite and sandwich plates based on a higher refined theory", *Compos. Struct,* 53, 73-85 (2001).

[28] M.K. Rao, Y.M. Desai, "Analytical solutions for vibrations of laminated and sandwich plates using mixed theory", *Compos. Struct,* 63, 361-373 (2004).

[29] Y. Frostig, O.T. Thomsen, "High-order free vibration of sandwich panels with a flexible core", *Int. J. Solids Struct,* 41, 1697-1724 (2004).

[30] R.M. Jones, *Mechanics of Composite Materials,* McGraw-Hill, New York, 1975.

A LAYERWISE FINITE ELEMENT WITH THROUGH-THICKNESS DEFORMATION

R.A.S. Moreira[*] and J. Dias Rodrigues[†]

[*] Departamento de Engenharia Mecânica
Universidade de Aveiro
Campo universitário de Santiago, 3810-193 Aveiro, Portugal
e-mail: rmoreira@ua.pt, web page: http://www.mec.ua.pt

[†] Faculdade de Engenharia da Universidade do Porto (FEUP)
Universidade do Porto
Rua Dr. Roberto Frias, 4200-465 Porto, Portugal
e-mail: jdr@fe.up.pt, web page: http://www.fe.up.pt

Key words: Sandwich structures modeling, layerwise model, transversal deformation, soft cores

Abstract

Sandwich plates represent an efficient structural element providing a high stiffness-weight ratio characteristic. Moreover, when using this structural element, different design configurations and materials in the core can be adopted in order to obtain desired properties. From high dissipation elastomers to light and stiff honeycombs, several core materials can be applied, looking for high damping ratios or simply to obtain an high flexural stiffness/weight ratio.

Despite the huge interest on the sandwich structures, its numerical modeling requires special attention in the representation of the skin/core relation phenomena. This aspect assumes an important role when dealing with soft cores. In fact, despite the difficulties arising from the high skin/core modulus ratio, which requires a representative displacement field descriptor, the numerical model should take into consideration the permissible transversal deformation to which the core may be submitted to. Currently, the modeling of such behavior requires the application of layerwise models accomplishing for a complete 3D spatial field description, which lead usually to a high computational cost during the simulation of sandwich panels.

In this paper, to trim down the computational cost, it is proposed a simpler and cost-effective layerwise model based on a two-dimensional displacement field descriptor. This finite element is formulated by using a plate finite element to represent the in-plane and out-plane deformation field of each layer, and a bar finite element to represent the nodal transversal displacement degree-of-freedom. The proposed finite element formulation and numerical implementation are assessed by comparison with results obtained from other modeling methodologies. Furthermore, the finite element model is also validated through the correlation analysis between the numerical results and the experimental data obtained from a dynamic analysis of representative specimens.

1 Introduction

Sandwich plates are nowadays an interesting structural element, presenting a good stiffness-weight relation. Such elements are becoming interesting solutions in the structural engineering, being gradually introduced in light-weight structures, like automobile bodies and aircraft fuselages and internal panels.

Despite the interest on these structural solutions, the numerical simulation of sandwich panels, especially those with soft cores, is difficult due to the specificity of the required spatial model. Currently, the embedding of thin damping layers within a sandwich panel configuration, following a single core or multiple core configurations [1], is gaining attention as potential solutions to improve the structure dynamic response, safety and durability, while maintaining an high stiffness/weight ratio.

These sandwich plates, as well as those with a soft foam core, are usually modeled by commercial finite element packages using the well-known classical laminate plate theory (CLPT) or an equivalent single layer theory (ESL). However, both approaches are unable to take into account for the high shear deformation pattern developed inside the damping layers or the soft material core. To overcome such difficulties, a layered scheme of plate and solid brick finite elements [2-4] is usually applied, providing a correct description of the in-plane displacement field along the layers. Though this modeling approach is able to describe accurately the displacement field and the shear deformation pattern of laminates and sandwich structures with high material ratios, it leads to a high computational cost and time consuming spatial modeling task and restricts significantly the model modification capability, an important issue during optimization design simulations.

Seeking for accurate and generalized finite elements, able to be easily manipulated in order to modify the laminate configuration and the material allocation without the need for re-meshing tasks, layerwise plate and facet-shell finite elements [5-12] have been recently proposed, demonstrating its ability to represent the high shear patterns developed inside the soft cores of sandwich panels. However, since these finite elements are usually based on the application of facet-shell formulations to each individual layer, forcing the displacement continuity condition directly in the laminate displacement field, the out-of-plane displacement is usually neglected, being unable to describe the real behavior of thick soft cores which may undergo through-thickness deformation.

In this work a facet-shell layerwise finite element is enhanced by introducing a through the thickness stiffness matrix to account for the out-of-plane displacement of each layer. The generalized formulation is described in section 2, the finite element implementation is presented in section 3 and section 4 presents numerical tests, results and discussion of the finite element accuracy and capability.

2 Plate layerwise formulation

Considering that the multi-layer laminate or sandwich structure can be divided into several homogeneous and isotropic or orthotropic layers, each layer can be individually treated as a thick plate

following the Reissner-Mindlin assumptions, ensuring the interface displacement continuity directly at the respective displacement field description.

Each layer is modeled according to the following assumptions:

- extensional and shear deformations of all the layers are accounted;

- deformation through the thickness is neglected;

- translational and rotary inertias of all the layers are accounted;

- linear theories of elasticity and viscoelasticity are used;

- materials are isotropic or orthotropic, and homogeneous in each layer.

2.1 Displacement field

Considering a generic layer k of the sandwich plate with thickness h_k, its displacement field $\{\mathbf{u}\}_k$ can be defined as:

$$\{\mathbf{u}\}_k = \begin{Bmatrix} u_k \\ v_k \\ \overline{w}_k \end{Bmatrix} = \begin{Bmatrix} u_0 + \dfrac{h_1}{2}\beta_1^x + \sum_{j=2}^{k-1} h_j \beta_j^x + \dfrac{h_k}{2}\beta_k^x + z_k \beta_k^x \\ v_0 + \dfrac{h_1}{2}\beta_1^y + \sum_{j=2}^{k-1} h_j \beta_j^y + \dfrac{h_k}{2}\beta_k^y + z_k \beta_k^y \\ \dfrac{w_{k-1}}{2} + \dfrac{w_k}{2} \end{Bmatrix} \qquad (1)$$

where u_0 and v_0 are the translations of the reference layer ($k=1$) and β_k^x, β_k^y are the rotations of the normal about the y and x axes, respectively. The continuity of the displacement field between the layers is guaranteed through a set of coupling terms in the displacement field definition.

To take into account for the through the thickness deformation, the layer's assumption of null out-plane deformation is alleviated at the laminate level, considering that an out-of-plane displacement can be prescribed at each interface level. Nevertheless, the displacement continuity of the out-plane component is directly imposed and the plane stress state condition at the layer level is ensured by using a constant through the thickness displacement parameter in the displacement field description of each individual layer. Therefore, the transversal translation $\overline{w}_k$ of the generic k-th layer is defined by the mean value of the top and bottom transversal translations, respectively w_{k-1} and w_k.

The displacement field, $\{\mathbf{u}\}_k$, can be represented through a set of generalized variables as:

$$\{\mathbf{u}\}_k = [\mathcal{N}]_k \{d\} \qquad (2)$$

where:

$$\{d\} = \{u_0, v_0, w_0, \beta_1^x, \beta_1^y, w_1, \cdots, \beta_k^x, \beta_k^y, w_k, \cdots, \beta_n^x, \beta_n^y, w_n\}^T \tag{3}$$

represents the generalized displacement field and $[\mathcal{N}]_k$ an allocation matrix.

2.2 Strain and stress fields

The strain field for a generic k-th layer, $\{\varepsilon\}_k$, is obtained from the displacement field through the application of a differential operator matrix $[\mathcal{L}]$ as:

$$\{\varepsilon\}_k = [\mathcal{L}]\{\mathbf{u}\}_k \tag{4}$$

which can be defined in terms of the generalized displacement field through the application of the deformation matrix $[\mathcal{B}]_k$ as:

$$\{\varepsilon\}_k = [\mathcal{B}]_k \{d\} \tag{5}$$

where $[\mathcal{B}]_k = [\mathcal{L}][\mathcal{N}]_k$.

Consecutively, the stress field of this generic layer is defined from the strain field by application of the constitutive law of the material, represented by the constitutive matrix $[\mathsf{D}]_k$, which is layer's material dependent:

$$\{\sigma\}_k = [\mathsf{D}]_k \{\varepsilon\}_k \tag{6}$$

The local constitutive matrices are directly defined at the layer level by the isotropic material properties or determined from the lamina constitutive matrix $[C]$ for an orthotropic material, applying a coordinate system transformation.

When frequency dependent materials are applied in the core, which occur for integrated damping treatments with viscoelastic materials or sandwich panels using viscoelastic foams of cork compounds, the constitutive matrices become frequency dependent and require a special solution method, like the direct frequency analysis to obtain a frequency domain solution, or the application of rheological parametric models, such as the GHM method [13], the ADF approach [14] or the fractional derivative models [15]. Regardless the specificity of the solution method and constitutive model approach, the finite element spatial model formulation is completely independent of the viscoelastic constitutive relation.

2.3 Velocity field and inertia matrix

The velocity field can be obtained as the time derivative of the displacement field, as:

$$\{\dot{\mathbf{u}}\}_k = \frac{\partial}{\partial t}\left(\{\mathbf{u}\}_k\right) = [\mathcal{N}]_k \{\dot{d}\} \tag{7}$$

The inertia matrix $[J]_k$ for the k-th generic layer is defined by:

$$[J]_k = [\mathcal{N}]_k^T [\mathsf{J}]_k [\mathcal{N}]_k \tag{8}$$

where

$$[\mathsf{J}]_k = \rho_k [I]_{3x3} \tag{9}$$

being ρ_k the mass density of layer k.

2.4 Strain and kinetic energies

Once defined the stress, strain, displacement and velocity fields at the layer level, the elastic storage energy and the kinetic energy for the entire layered spatial domain can be calculated through the adding up of the energy contribution of each individual layer, as:

$$\Pi^P = \sum_{k=1}^{n} \left[\frac{1}{2} \int_{\Omega_k} \{\varepsilon\}_k^T \{\sigma\}_k d\Omega_k \right] = \sum_{k=1}^{n} \left[\frac{1}{2} \int_A \int_{z_k} \{d\}^T [\mathcal{B}]_k^T [\mathsf{D}]_k [\mathcal{B}]_k \{d\} dz_k dA \right] \tag{10}$$

$$\Pi^K = \sum_{k=1}^{n} \left[\frac{1}{2} \int_{\Omega_k} \{\dot{\mathbf{u}}\}_k^T [\mathsf{J}]_k \{\dot{\mathbf{u}}\}_k \Omega_k \right] = \sum_{k=1}^{n} \left[\frac{1}{2} \int_A \int_{z_k} \{\dot{d}\}^T [J]_k \{\dot{d}\} dz_k dA \right] \tag{11}$$

where n stands for the number of layers of the plate and A represents the in-plane domain.

2.5 Virtual work of the surface loads

The virtual work δW produced by a transverse distributed load $\{q\}$ acting on the face layers of the layered plate is defined by:

$$\delta W = \int_S \{\delta d\}^T \{q\} dS \tag{12}$$

where S is the surface area of the distributed load and $\{\delta d\}$ is the virtual displacement vector.

2.6 Variational formulation

To derive the variational statement equivalent to the governing differential equations, as well as the natural boundary conditions, it is herein applied the Hamilton's principle, which can be formally stated as:

$$\delta \int_{t_1}^{t_2} (\Pi^K - \Pi^P) dt + \int_{t_1}^{t_2} \delta W dt = 0 \tag{13}$$

where Π^K and Π^P are, respectively, the kinetic and strain energies of the system and δW is the virtual work done by the external forces.

Introducing Equations (10), (11) and (12) into (13), and performing the variation and an integration by parts, the above stated Hamilton's principle yields:

$$\int_{t_1}^{t_2} (-\sum_{k=1}^{n}\int_A \{\delta d\}^T [J]_k \{\ddot{d}\}dA - \sum_{k=1}^{n}\int_A \{\delta d\}^T [\mathcal{B}]_k^T [\mathrm{D}]_k [\mathcal{B}]_k \{d\}dA + \int_S \{\delta d\}^T \{q\}dS)dt = 0 \quad (14)$$

which, since it must be satisfied for an arbitrary variation $\{\delta d\}$ within the time interval $[t_1, t_2]$, the variational statement or the weak form can be defined as:

$$\begin{aligned}
&\sum_{k=1}^{n}\int_A \{\delta d\}^T [J]_k \{\ddot{d}\}dA + \sum_{k=1}^{n}\int_A \{\delta d\}^T [\mathcal{B}]_k^T [\mathrm{D}]_k [\mathcal{B}]_k \{d\}dA \\
&- \int_S \{\delta d\}^T \{q\}dS = 0; \quad \forall\{\delta d\}
\end{aligned} \quad (15)$$

3 Finite element formulation

3.1 Coordinate systems and interpolation basis

The proposed finite element, which is based on the 4-node isoparametric quadrilateral element and herein denoted as **layw4x**, is reproduced from a similar layerwise finite element (layw4m) [11], which will be recalled herein as a reference for performance and results comparison.

The three-dimensional domain under analysis is represented onto a global cartesian coordinate system (X, Y, Z) whereas the stiffness and mass matrices of each element are computed in a local cartesian coordinate system (x, y, z) coplanar with the element face. These element matrices are transformed back to the global coordinate system, where global assembly is then possible to be performed.

The local geometry of the finite element is mapped into a natural coordinate system (ξ, η, ζ), where the ζ direction is coincident with the z direction, in which the standard set of bilinear interpolation functions are used to interpolate the geometry and the variables within the finite element domain. The elemental generalized displacement field $\{d^e\}$ is approximated by using this set of interpolation functions, represented by the shape functions matrix $[N]$, and the elemental vector of nodal degrees of freedom $\{d_i^e\}$ as:

$$\{d^e\} = [N]\{d_i^e\} \quad (16)$$

3.2 Weak form finite element discretization

The global weak form stated in (15) can be expressed as the sum of the elemental integral forms, allowing the definition of the matrices and vectors at the element level. Therefore, the global weak form can be expressed from the contributions of the entire set of n_E finite elements, as:

$$
\begin{aligned}
\sum_{e=1}^{n_E}(\{\delta d_i^e\}^T &\sum_{k=1}^{n}\int_{A^e}\int_{z_k}{}^e[N]^T[J]_k[N]dA^e dz_k{}^e\{\ddot{d}_i^e\} \\
&+\{\delta d_i^e\}^T\sum_{k=1}^{n}\int_{A^e}\int_{z_k}{}^e[N]^T[\mathcal{B}]_k^T[\mathsf{D}]_k[\mathcal{B}]_k[N]dA^e dz_k{}^e\{d_i^e\} \\
&-\{\delta d_i^e\}^T\int_{A^e}[N]^T\{q\}dA^e)=0
\end{aligned}
\tag{17}
$$

which allows the definition of the element mass $[M^e]$ and stiffness $[K^e]$ matrices, as well as the element load vector $\{f_i^e\}$, as:

$$
[M^e]=\sum_{k=1}^{n}[M^e]_k=\sum_{k=1}^{n}\int_{A^e}\int_{z_k}{}^e[N]^T[J]_k[N]dA^e dz_k{}^e
\tag{18}
$$

$$
\sum_{k=1}^{n}[K^e]_k=\sum_{k=1}^{n}\int_{A^e}\int_{z_k}{}^e[B]_k^T[\mathsf{D}]_k[B]_k dA^e dz_k{}^e
\tag{19}
$$

$$
\{f_i^e\}=\int_{A^e}[N]^T\{q\}dA^e
\tag{20}
$$

where $[B]_k=[\mathcal{B}]_k[N]$ is the deformation matrix for a generic layer k of the finite element.

The assembly of the element contributions requires the relation between the degrees of freedom of each individual element $\{d_i^e\}$ and the global degrees of freedom vector $\{d_i\}$, which is commonly established through the connectivity matrices $[R^e]$, as:

$$
\{d_i^e\}=[R^e]\{d_i\}
\tag{21}
$$

3.3 Equations of motion

The global semi-discrete equations of motion for the entire layered structure can be expressed as:

$$
[M]\{\ddot{d}_i\}+[K]\{d_i\}=\{f_i\}
\tag{22}
$$

where the assembled global mass $[M]$ and stiffness $[K]$ matrices and the assembled global force vector $\{f_i\}$ are described as a result of the application of the connectivity matrices onto the element matrices.

3.4 Finite element improvement

Since the intended main application of the finite element formulation is the modeling of thin sandwich or layered composite plates with soft and viscoelastic cores, some attention must be paid onto the finite element formulation in order to avoid common locking problems. In this finite element formulation some known and well founded numerical strategies are applied, following the same approach applied in the layw4m formulation [11]. Thus, a non-conforming interpolation scheme is applied to the membrane formulation, following the work of Wilson *et al.* [16] and Taylor *et al.*[17], to avoid the in-plane shear or trapezoidal locking of the bilinear quadrilateral element. Additionally, the shear locking problem, to which the finite element formulation hereby proposed is vulnerable, is alleviated through the application of a generalization of the MITC [18] approach to the layerwise model. Details on these numerical strategies and its implementation into the layerwise formulation can be found at [11,12].

3.5 Out-plane stiffness

As initially proposed, the out-of-plane displacement on each individual layer is considered to be constant, but not necessarily identical to the remaining layers of the laminate. To ensure the out-of-plane continuity at the layer interfaces, the generalized displacement vector contains $n+1$ out-of-plane degrees-of-freedom, and the layer formulation considers a constant out-of-plane displacement value, identical to the mean of transversal displacements at top and bottom interfaces of the layer.

The transversal stiffness of each layer can be modeled as four transversal and independent linear springs, whose degrees-of-freedom are these top and bottom layer transversal displacements w_{k-1} and w_k.

Therefore, the stiffness matrix of a generic layer k is defined as the superposition of this transversal spring stiffness onto the original plate stiffness, as depicted in Figure 1.
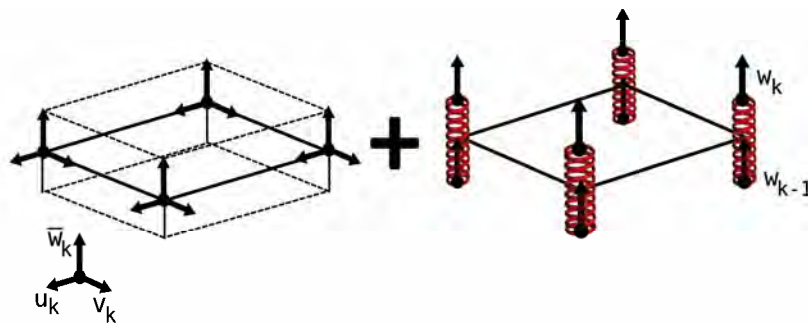
Figure 1 – Transversal spring stiffness concept

To derive the equivalent stiffness of each transversal spring it is considered to be materialized as a laterally restrained bar finite element with a cross section A_k^z identical to one quarter of the element layer area and length equal to the layer thickness. Considering all these assumptions, the individual stiffness matrix for each nodal spring of layer k, for an isotropic material, is defined as:

$$\left[K^Z\right]_k = A_k^z \frac{E_k}{h_k} \frac{(1-\nu_k)}{(1+\nu_k)(1-2\nu_k)} \begin{bmatrix} 1 & -1 \\ -1 & 1 \end{bmatrix} \tag{23}$$

These individual matrices are assembled onto a global transversal matrix which is added to the finite element stiffness matrix at the layer level. No mass contribution of these fictitious add-on spring elements is considered.

4 Finite element testing: numerical results

The finite element formulation was implemented in Matlab$^{®}$ environment using the SDT$^{®}$ toolbox [19] for the finite element model manipulation, the matrix assembly and solving tasks.

A generic test, based on the determination of the modal parameters for a rectangular sandwich plate with a high modulus ratio and different core Poisson's ratios, is applied to demonstrate the contribution of the transversal stiffness. The results obtained with a similar layerwise finite element, with a formulation that overlooks the through the thickness deformation, and the results achieved by the application of a layered model formed by hexahedral solid finite elements (see [3] for details) are used as a reference for validation of the hereby proposed formulation.

Additionally, the present model is also applied in the calculation of the natural frequencies for a simply supported square sandwich plate with orthotropic composite skins and an isotropic foam core. For this example, layer level and global level finite element results are available, which provided a reference basis for validation.

Finally, the finite element is applied to simulate a long span sandwich beam with a soft core to which numerical and experimental data is available.

4.1 Example 1: natural modes of a sandwich plate with soft core

This example exploits the soft core effect in a rectangular sandwich plate. The plate, described in Table 1, has thin aluminum skins and a soft core with a high modulus ratio. Both thin and thick sandwich conditions are applied and two different Poisson's ratios for the core material are also introduced in this example, demonstrating the effect of the compressibility grade of the core in the symmetric mode shapes frequencies.

Table1 - Geometry parameters and material properties of Example 1

Geometry		
Length	a	$300\ mm$
Width	b	$200\ mm$
	h_1	$1\ mm$
Thickness	h_2	$40\ mm\ /\ 2\ mm$
	h_3	$1\ mm$
Material properties		
• Skins - *Aluminum*		
Young modulus	$E_{1,3}$	$72\times10^9\ Pa$
Poisson ratio	$\nu_{1,3}$	0.32
Density	$\rho_{1,3}$	$2710\ Kg/m^3$
• Core - hypothetic soft foam		
Young modulus	E_2	$2\times10^3\ Pa$
Poisson ratio	ν_2	0.25/0.49
Density	ρ_2	$1140\ Kg/m^3$
Boundary conditions		C-F-F-F

C: clamped / F: free

The results obtained with the present finite element model (layw4x) are compared with those obtained using a layered model approach with solid brick finite element (Model 3H). More details on these layered approaches can be found in [3]. Additionally, an analogous layerwise model (layw4m) which shares the same plate formulation but does not consider the through the thickness deformation, is applied for comparison of the anti-symmetric natural modes results.

The sandwich plate is considered to be clamped in one of its smallest sides and totally free at the remaining ones. It was modeled by a 18x12 finite elements mesh and, when using model 3H, 3 layers of hexa8 finite elements were applied through the thickness, one for each material layer. Similarly, 3 layers are used for the layerwise models. This through-thickness coarse spatial modeling, which does not introduce an important error in the interesting natural modes, intends to avoid the large set of deformation mode shapes of the core that is obtained when it is represented by an higher number of solid layers in the model 3H or numerical layers in the layerwise models.

The computed natural frequencies are listed on tables 2-3 and Figure 2 represents the corresponding mode shapes, obtained with the layw4x finite element (graphical post-processing is applied to depict the three-dimensional deformed geometry of the mode shapes).

Table 2 - Natural frequencies of sandwich plate with soft core – Thick core (40mm) [Hz]
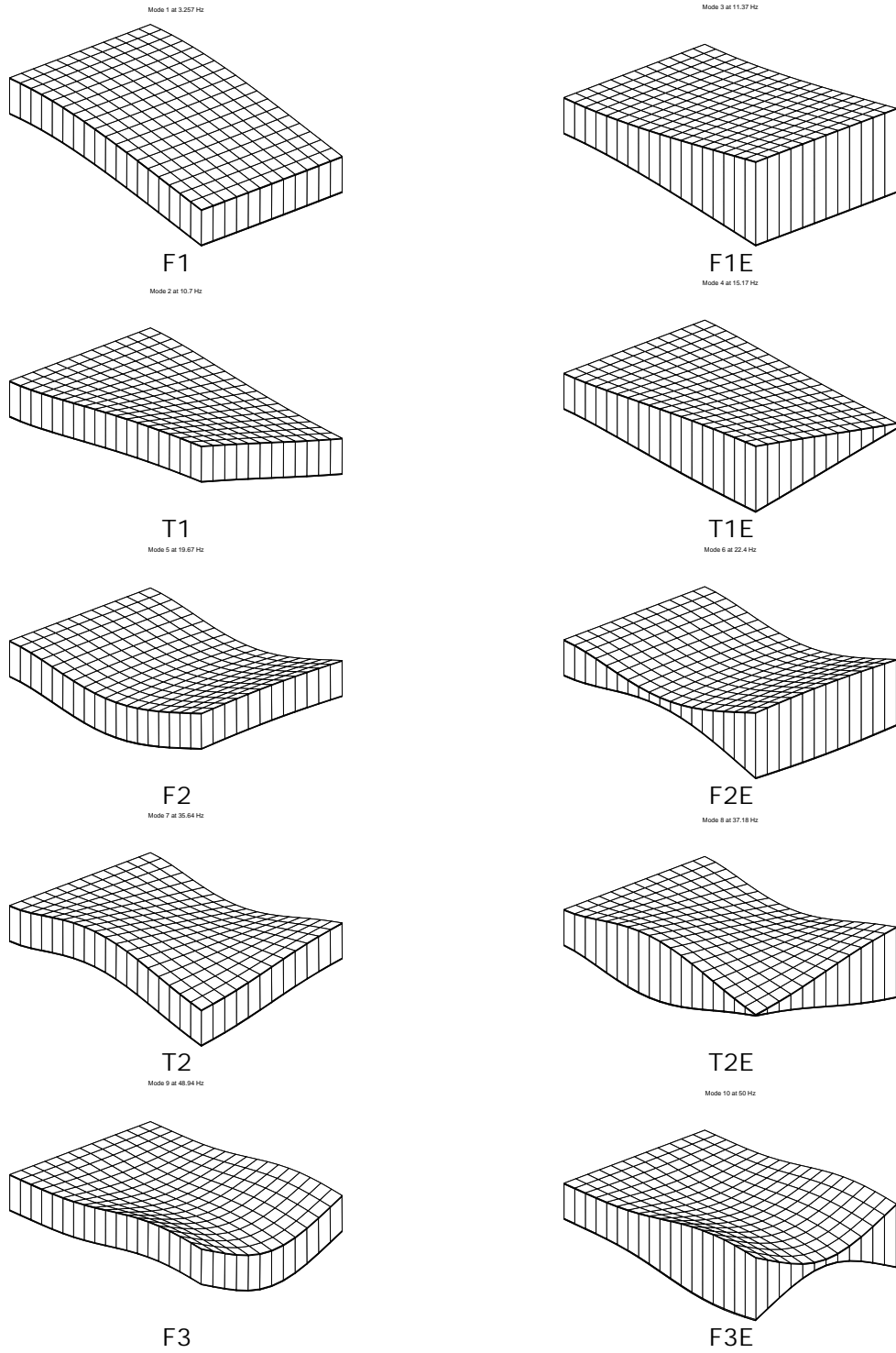
Mode	compressible core $v_2 = 0.25$			incompressible core $v_2 = 0.49$		
	Model 3H	layw4x	layw4m	Model 3H	layw4x	layw4m
F1	3.25	3.26	3.26	3.23	3.24	3.24
T1	10.62	10.70	10.70	10.58	10.66	10.66
F2	19.50	19.67	19.67	19.47	19.64	19.64
T2	35.13	35.64	35.64	35.10	35.61	35.61
F3	47.57	48.94	48.94	47.54	48.90	48.90
F1E	11.34	11. 37	---	41.27	41.40	---
T1E	14.99	15.17	---	42.06	42.84	---
F2E	22.16	22.40	---	45.03	45.93	---
T2E	36.60	37.18	---	53.39	54.84	---
F3E	48.53	50.00	---	61.62	64.59	---

Table 3 - Natural frequencies of sandwich plate with soft core – Thin core (2mm) [Hz]

Mode	compressible core $v_2 = 0.25$			incompressible core $v_2 = 0.49$		
	Model 3H	layw4x	layw4m	Model 3H	layw4x	layw4m
F1	8.07	8.08	8.08	8.06	8.07	8.07
T1	26.77	26.96	26.96	26.74	26.95	26.95
F2	49.88	50.07	50.07	49.87	50.06	50.06
T2	90.20	91.12	91.12	90.19	91.12	91.12
F3	122.11	124.80	124.80	122.10	124.80	124.80
F1E	125.91	126.10	---	467.90	475.40	---
T1E	127.63	129.00	---	Na	477.20	---
F2E	134.26	135.80	---	Na	479.20	---
T2E	153.30	155.82	---	Na	486.10	---
F3E	172.64	178.11	---	Na	495.90	---

Na: unavailable data

The results for the layered model (model 3H) were obtained using Nastran hexa8 finite elements. As it is well known, this solid finite element (hexa8), from the MSC.Nastran finite element library, has shear locking and volume locking protection mechanisms, which additionally provides a validation analysis for the finite element remedies introduced in the proposed finite element.

Mode 1 at 3.257 Hz

Mode 3 at 11.37 Hz

F1

F1E

Mode 2 at 10.7 Hz

Mode 4 at 15.17 Hz

T1

T1E

Mode 5 at 19.67 Hz

Mode 6 at 22.4 Hz

F2

F2E

Mode 7 at 35.64 Hz

Mode 8 at 37.18 Hz

T2

T2E

Mode 9 at 48.94 Hz

Mode 10 at 50 Hz

F3

F3E

Figure 2 – Mode shapes for sandwich plate with soft core (thick core)

4.2 Example 2: simply supported sandwich plate with orthotropic skins

In this example a square sandwich plate with orthotropic cross-ply laminate skins (0º|90º|core|0º|90º) is analyzed [20]. Both thin and thick sandwich plates are considered.

Geometry parameters, material properties and boundary conditions are summarized in Table 4.

Table 4 - Geometry parameters and material properties for Example 2

Geometry

Square sandwich plate $a \times b$	
Thickness/width ratio	$h/b = 1:10 \mid 1:100$
Skin/core thickness ratio	$h_{core}/h_{skin} = 10:1$

Material properties

- Skins –*cross-ply orthotropic laminate*

$$E_1 = 131\,GPa\,; E_2 = E_3 = 10.34\,GPa$$
$$G_{12} = G_{13} = 6,895\,GPa\,; G_{13} = 6.205\,GPa$$
$$\nu_{12} = \nu_{13} = 0.22\,; \nu_{23} = 0.49$$
$$\rho = 1627\,Kg/m^3$$

- Core – *isotropic material*

$$E = 6.89\,MPa$$
$$G = 3.45\,MPa$$
$$\nu = 0.0$$
$$\rho = 97\,Kg/m^3$$

Boundary conditions	S-S-S-S
	S: simply supported

The results obtained for this example, the natural frequencies, are normalized as:

$$\overline{\omega} = \omega \frac{b^2}{h} \sqrt{\left(\frac{\rho}{E_2}\right)_{skin}} \tag{24}$$

These natural frequencies normalized values for the thick and thin sandwich plate are listed in tables 5 and 6, respectively. The results obtained by a semi-analytical approach using a mixed layerwise model [21], which is reported to produce accurate results [22], are also listed, providing the analysis

reference. Numerical results obtained from local higher-order models [22] are also presented in the tables for finite element assessment.

Table 5 – Normalized natural frequencies of sandwich square plate: a/h=10

Solution	Natural Modes					
	1,1	1,2	2,2	1,3	2,3	3,3
layw4x (antisymmetric)	1.8522	3.2426	4.3280	5.3155	6.1941	7.8266
Rao and Desai (LW) [21]	1.8480	3.2196	4.2894	5.2236	6.0942	7.6762
Zhen et al [22] 7th ord	1.8740	3.2620	4.3427	5.3065	6.1573	7.7703
Zhen et al [22] 5th ord	1.8889	3.2831	4.3683	5.3320	6.1868	7.8055
Zhen et al [22] 3rd ord	1.9742	3.3944	4.5413	5.5484	6.4678	8.2285
Rao and Desai (ESL) [21]	4.9624	8.1934	11.987	10.517	13.749	16.451
Kant and Swaminathan [20]	4.8594	8.0187	10.297	11.738	13.471	16.132
Kant and Swaminathan [23]	4.8519	7.9965	10.255	11.681	13.389	16.004
Reddy [24]	7.0473	11.909	15.290	17.321	19.812	23.507
Senthilnathan et al [25]	7.0473	11.962	15.290	17.370	19.833	23.507
Whitney-Pagano [26]	13.869	30.643	41.558	50.939	58.364	71.372
layw4x (symmetric)	12.219	12.378	12.594	12.868	13.150	13.823

Table 6 – Normalized natural frequencies of sandwich square plate: a/h=100

Solution	Natural Modes					
	1,1	1,2	2,2	1,3	2,3	3,3
layw4x (antisymmetric)	11.962	23.524	31.117	36.538	41.849	50.322
Rao and Desai (LW) [21]	11.940	23.402	30.943	36.143	41.447	49.762
Zhen et al [22] 7th ord	12.040	23.738	31.860	36.733	43.154	49.989
Zhen et al [22] 5th ord	12.090	23.890	32.080	37.005	43.474	50.245
Zhen et al [22] 3rd ord	12.248	24.359	32.761	37.861	44.485	51.563
Rao and Desai (ESL) [21]	15.548	39.265	55.151	73.495	84.292	106.590
Kant and Swaminathan [20]	15.509	39.029	54.762	72.757	83.441	105.378
Kant and Swaminathan [23]	15.465	38.923	54.633	72.593	83.269	105.181
Reddy [24]	15.952	42.227	60.127	83.998	96.313	124.205
Senthilnathan et al [25]	15.952	42.371	60.127	84.425	96.716	124.205
Whitney-Pagano [26]	16.218	44.707	64.504	94.910	108.905	143.797

Only for comparison, the published results using ESL [21] and global higher-order models [20,23] are also listed in tables 5 and 6, which clearly over estimate the natural frequency values for soft core

sandwich plates, as also reported by Zhen et al [22]. Additionally, for the thick sandwich plate, Table 5 also reports the normalized frequency values for the symmetric mode shapes, demonstrating the ability of the present finite element to represent the through the thickness deformation.

From the results listed in Tables 5 and 6, and considering the mixed layerwise model as a reference for this example, it is possible to conclude that the present model is able to produce valuable results, even for a coarse mesh as the one applied in this analysis (20x20 finite elements). It is also important to mention that the finite element model applied in this analysis only considered 5 numerical layers, one for each material lamina. A finer subdivision of the material layers into several numerical layers, which is easily achieved when using a generic layerwise model as the layw4x, would produce more accurate results with some computational cost increase.

4.3 Example 3: sandwich beam with a soft polymer foam core

This example is not a classic benchmark test but became interesting since experimental data is available [27]. It consists in a wide beam with thin steel skins and a thick soft polymer foam core. Model details can be found in Table 7, which replicate the original data from the work of Sokolinsky and co-workers [27].

Table 7 - Geometry parameters and material properties for Example 3

Geometry		
Length	L	260 mm
Width	b	59.9 mm
	h_1	1.9 mm
Thickness	h_2	34.8 mm
	h_3	1.9 mm
Material properties		
• Skins - *Steel*		
Young modulus	$E_{1,3}$	$210 \times 10^9 \ Pa$
Poisson ratio	$v_{1,3}$	0.30
Density	$\rho_{1,3}$	7900 Kg/m^3
• Core – *Divinycell H60*		
Young modulus	E_2	$56 \times 10^6 \ Pa$
Poisson ratio	v_2	0.27
Density	ρ_2	60 Kg/m^3
Boundary conditions		C-F-F-F
		C: clamped / F: free

The beam is considered to be clamped at one end where rotations and translations are restrained.

The results presented in Table 8 were obtained with the present finite element (layw4x) using three numerical layers in the core (5 layers in total) and only one numerical layer to represent the core (3 layers in total). The remaining presented results were published in the original study [27] and were obtained using a higher order theory and a two dimensional finite element analysis using a refined mesh. The experimental results presented in the same publication are also listed in Table 8, but do not provide a reference for the analysis since the experimental boundary conditions aren't exactly replicated by the numerical work. Moreover, the applied frequency resolution in the frequency band corresponding to the analyzed symmetric mode shapes, forbid the proper identification of these frequencies.

Table 8 - Natural frequencies of cantilever sandwich beam [Hz]

	Mode	layw4x (5layers)	layw4x (3layers)	Higher order theory [27]	2D Finite Element [27]	Experimental Horizontal [27]	Experimental Vertical [27]
Flexion anti-symmetric	F1	164.9	165.2	165	165	194	--
	F2	514.1	517.1	511	512	553	544
	F3	925.2	936.4	910	913	949	950
	F4	1416	1441	1373	1379	1404	1391
Torsion anti-symmetric	T1	1134	1145				
	T2	1417	1428		unavailable data		
	T3	1970	2014				
	T4	2445	2494				
Flexion symmetric	F1E	2571	2521	2393	2476		
	F2E	2589	2538	2398	2509	--	2350-2400
	F3E	2649	2592	2430	2558		
	F4E	2800	2725	2534	2567		
Torsion symmetric	T1E	3138	3092				
	T2E	3220	3160		unavailable data		
	T3E	3393	3309				
	T4E	3687	3566				

From Table 8 it is possible to conclude that the present model is able to provide results similar to those reported in the literature and are consistent with those obtained experimentally. Since the applied boundary conditions does not entirely agree with the experimental ones, as it was impossible to represent the core discontinuity at the cantilever root (the experimental specimen presents a small gap in the core at the fixed root), it is easily recognized the effect of this incoherency for the high frequency modes.

5 Conclusion

The layerwise model hereby presented provides a valuable tool for the analysis of isotropic or orthotropic laminates or sandwich plates with high modulus ratios. The improvement presented in this finite element, providing the ability to consider the through-thickness deformation, permits to maintain the interesting capabilities of the layerwise theory, while providing the core compression stiffness description, which is very important for the analysis of soft core sandwich plates. In fact, the application of a layerwise finite element to model a laminated structure provides flexibility and customization freedom, which is not easily achieved by other modeling approaches.

The results obtained in the finite element test permitted to verify the formulation robustness and accuracy of the developed layerwise finite element with through-thickness deformation.

Acknowledgement

References

[1] Moreira RAS, Dias Rodrigues J (2005) Sandwich damping treatments with multi-layer and multi-material viscoelastic cores, Proceedings of the II ECCOMAS Thematic Conference on Smart Structures and Materials, Paper No. E090MOD, C.A. Mota Soares, J.Holnicki-Szulc, A. Suleman and C.M. Mota Soares (editors), ECCOMAS, Lisbon, Portugal, 18-21 July.

[2] Plouin A, Balmès E (1999) A test validated model of plates with constrained viscoelastic materials. Proceedings of IMAC XVII, Kissimmee, FL, USA:194-200

[3] Moreira R, Rodrigues JD (2004) Constrained damping layer treatments: the finite element modelling. Journal of Vibration Control **10**(4): 575-595

[4] Johnson CD, Kienholz DA (1982) Finite element prediction of damping in structures with constrained viscoelastic layers. AIAA Journal **20**(9): 1284-1290

[5] Reddy JN (1997) Mechanics of laminated composite plates: theory and analysis. CRC Press. Boca Raton

[6] Carrera E (2003) Theories and finite elements for multilayered plates and shells: a unified compact formulation with numerical assessment and benchmarking. Archives of Computational Methods in Engineering **10**(3): 215--296.

[7] Bhimaraddi A (1995) Sandwich beam theory and the analysis of constrained layer damping. Journal of Sound and Vibration **179**(4): 591--602

[8] Saravanos DA, Pereira JM (1995) Dynamic characteristics of specialty composite structures with embedded damping layers. Journal of Vibration and Acoustics **117**: 62-69

[9] Cupial P, Niziol J (1995) Vibration and damping analysis of a three-layered composite plate with a viscoelastic mid-layer. Journal of Sound and Vibration **183**(1): 99-114

[10] Suzuki K, Kageyama K, Kimpara I, Hotta S, Ozawa T, Kabashima S, Ozaki T (2003) Vibration and damping prediction of laminates with constrained viscoelasic layers - numerical analysis by a multilayer higher-order-deformable finite element and experimental observations. Mechanics of Advanced Materials and Structures, **10**: 43-75

[11] Moreira RAS, Dias Rodrigues, J, Ferreira, AJM (2005) A generalized layerwise finite element for multi-layer damping treatments, Computational Mechanics, 37 (5): 426-444.

[12] Moreira RAS, Dias Rodrigues, J (2006) A layerwise model for thin soft core sandwich plates. Computers and Structures, 84 (19-20): 1256-1263.

[13] McTavish DJ, and Hughes PC (1993) Modeling of linear viscoelastic space structures. Journal of Vibration and Acoustics **115**: 103-110.

[14] Lesieutre GA, and Bianchini, E (1995) Time domain modeling of linear viscoelasticity using anelastic displacement fields. Journal of Vibration and Acoustics **117**: 424-430

[15] Bagley RL, and Torvik PJ (1983) Fractional calculus - A different approach to the analysis of viscoelastically damped structures. AIAA Journal **21**(5): 741-748.

[16] Wilson EL, Taylor RL, Doherty WP, and Ghaboussi J (1973) Incompatible displacement models. Numerical and Computer Meth. in Struc. Mech., S.T. Fenves, et. al (eds), Academic Press, pp. 43-57.

[17] Taylor RL, Beresford PJ, and Wilson EL (1976) A nonconforming element for stress analysis. International Journal for Numerical Methods in Engineering **10**: 1211-1219.

[18] Dvorkin EN, and Bathe K-J (1984) A continuum mechanics based four-node shell element for general non-linear analysis. Engineering Computations **1**: 77-88.

[19] Balmès E (2001) Structural Dynamics Toolbox, V5.0, SDTools, France.

[20] Kant T, Swaminathan K (2001) Free vibration of isotropic, orthotropic, and multilayer plates based on higher order refined theories, Journal of Sound and Vibration, 24182): 319-327.

[21] Rao MK, Desai YM (2004) Analytical solutions for vibrations of laminated and sandwich plates using mixed theory, Composite Structures 63:361-373.

[22] Zhen W, Cheung YK, Lo SH and Wanji C (2008) Effects of higher-order global-local shear deformations on bending, vibration and buckling of multilayered plates, Composite Structures 81:277-289, 2008.

[23] Kant T, Swaminathan K (2000) Analytical solutions using higher order refined theory for the stability analysis of laminated composite and sandwich plates, Struct Eng Mech 10(4):337-357.

[24] Reddy JN (1989) On refined computational models of composite laminates, Int J Numerical Methods Engineering 27:361-382.

[25] Whitney JM, Pagano NJ (1970) Shear deformation in heterogeneous anisotropic plates, J Applied Mechanics, 37: 1031-1036.

[26] Senthilnathan NR, Lim KH, Lee KH, Chow ST (1987) Buckling of shear deformation plates, AIAA J, 25:1268-1271.

[27] Sokolinsky VS, Von Bremen HF, Lavoie JA and Nutt SR (2004) Analytical and experimental study of free vibration response of soft-core sandwich beams, J. Sandwich Structures and Materials, 6:239-261.

NEW 3-D FAILURE CRITERION
FOR SANDWICH FOAM CORES BASED ON PMI

Matthias Alexander Roth[*], Arnim Kraatz[†]

[*] Evonik Röhm GmbH, Kirschenallee, D-64293 Darmstadt, Germany
e-mail: alexander.roth@evonik.com, web page: http://www.rohacell.com

† German Institute for Polymers (DKI), Schloßgartenstraße 6, D-64289 Darmstadt, Germany
e-mail: akraatz@dki.tu-darmstadt.de, web page: http://www.dki-online.de

Key words: Sandwich Structures, PMI Foam, ROHACELL[®], Failure Criterion, FEM

Summary. *This article deals with new 3-D failure criterion to calculate the material effort of foam cores based on polymethacrylimide (ROHACELL[®]) for sandwich constructions under multiaxial conditions. In collaboration with the German Institute for Polymers (DKI) this 3-D failure criterion for ROHACELL[®] was developed. This model is suitable to describe the compressible material behaviour and the strength differential effect of PMI-foams. New tubular test specimen made of ROHACELL[®] 51 WF, 110 WF and 200 WF and a new test facility were developed to determine the mechanical properties under different loading conditions. To measure the strain distribution parallel and perpendicular to the loading direction the non-contact measurement system ARAMIS was used. For each stage of load, the 3-D coordinates of the object surface are calculated from the 2-D digital images. The developed 3-D failure criterion need only three free parameters to describe the surface of the breakage in the 3-D stress space. These parameters can be determined by using the results of pure tension, compression and shear stress states. Combined tension/shear and compression/shear stress states were carried out to validate the 3-D failure criterion. The new 3-D failure criterion is more suitable to describe the material behaviour of ROHACELL[®] than other potential bodies (e. g. von Mises). This 3-D failure model is easy to implement in commercial FE programs. Due to the present results the use of the 3-D failure criterion to determine the material effort of ROHACELL[®] is recommendable.*

1 INTRODUCTION

Sandwich structures are generally made up of one upper and one lower thin and stiff face sheet, which are supported by a thick low density core material [1]. These three components are bonded with two adhesive layers. The stiff and strong face sheets are used to carry the in-plane stresses while the core is used to carry the shear stresses produced by transverse loads. Sandwich structures have a high bending stiffness and strength to weight ratio in comparison to monolithic structures. This sandwich principle is primarily used for light weight transport applications (e. g. aircrafts, trains, trucks, cars, boats) and is well known as a natural design concept, e. g. bones and botanical stems [2].

ROHACELL® is a closed-cell polymethacrylimide (PMI) foam that is ideally suited for strong, lightweight sandwich construction. ROHACELL®'s natural color is white to slightly yellow. Production of ROHACELL® starts when three precisely determined quantities of colorless liquids (two monomers and the blowing agent) are mixed (Figure 1). During the first stage of the process, the mixture is converted by free radical polymerization to a slightly yellow, transparent plastic sheet, which still contains the unchanged blowing agent. During the second stage, the plastic sheet is heated to temperatures around 390 °F (200 °C) yielding rigid, white, closed cell foam. Simultaneously, the chemical structure of the original unfoamed polymer is changed by various cyclization reactions, which are chemical reactions where both the blowing agent and the plastic take part in. Substances, which are gaseous at this temperature, are liberated, forming small gas bubbles in the plastic [3].

ROHACELL® sandwich foam cores offer a high level of stiffness and strength to weight ratio, good fatigue properties, high temperature resistance (up to 180 °C/ 356 °F), excellent resistance to compressive creep (< 2 %) due to the pressure during processing (up to 0.7 MPa/ 100 PSI), good consolidation of prepreg skins on top and bottom as well as underneath of profiles (e. g. A-stiffener), ease of machining and thermoforming, provide stiffener profile geometry, reduction in lay-up and manufacturing costs, reduction in manufacturing cost due to co-curing, reduction in tooling costs, comprehensive QM system as well as a proven logistic concepts.
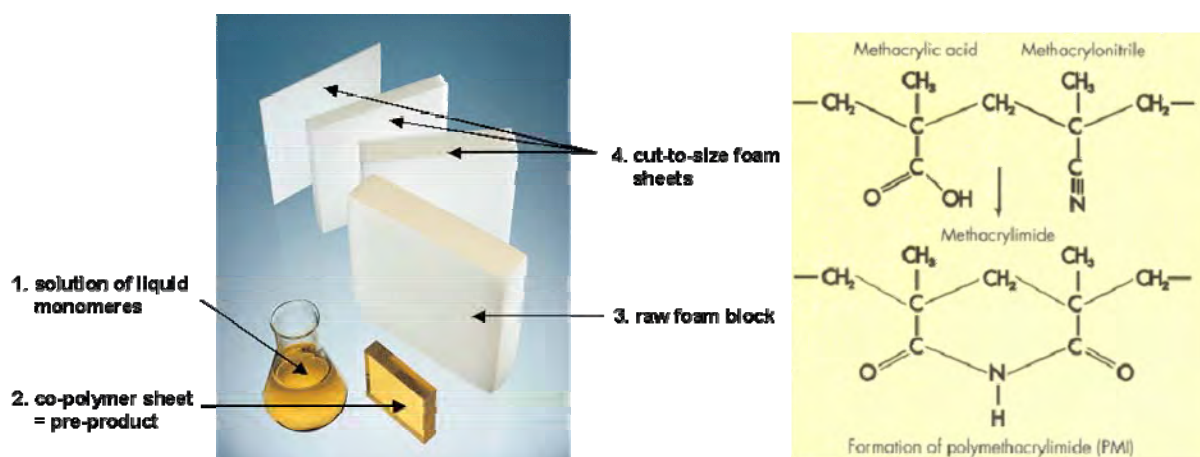
Figure 1: Manufacturing and chemistry of ROHACELL® closed-cell PMI foam [3]

Structural ROHACELL® sandwich foam cores are successfully used in a number of such kinds of aircraft applications. One of the most prominent applications is the air inlet duct panels for the centre engine of the Boeing MD 11 aircraft (Figure 2). The precisely CNC-machined and thermoformed-to-shape foam profiles contribute to significant cost savings during lay-up. High-performance PMI foam cores offer excellent resistance to compressive creep during the cure, resulting in a thorough laminate consolidation without surface dimpling effects. In contrast to honeycomb cores, the isotropic cellular structure of PMI foams provides dimensional stability also against lateral pressure during the autoclave cure, eliminating the necessity of core profile stabilizers, typically used for honeycomb cures. Also the foam core

evenly transfers the autoclave pressure to the surface layers of the shell underneath, resulting in a good consolidation without any marks or other surface imperfections.
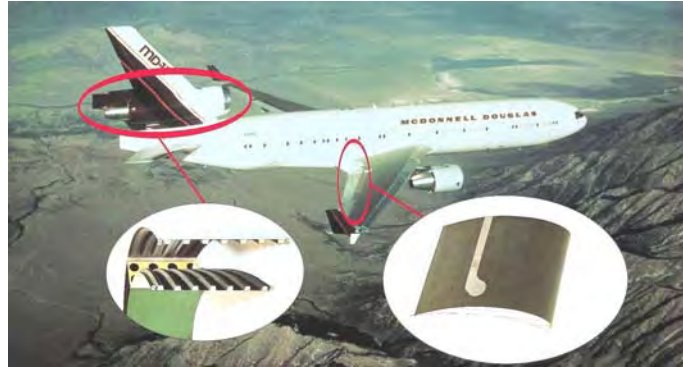

Figure 2: Boeing MD11

In [4], [5] and [6] the potential of a bi-functional usage of PMI foam cores for realizing cost and weight optimized A-Stringer profiles is outlined. It will be discussed that the foam core can serve as a mandrel during lay-up and cure and as a structural member of the stringer component. It can also be concluded that a PMI foam-filled A-Stringer can contribute to increasing the stability and buckling resistance of a thin-walled CFRP-structure significantly. Furthermore foam-filled A-Stringers can improve the strength and the fatigue life of the stiffener and the skin/stiffener interface in comparison to hollow A-Stringers [3], [4]. If ROHACELL$^®$ is also used as a structural member, the wall-thickness of the covering CFRP face sheets can be reduced by approximately one to two plies, offering a "weight-neutral" solution compared to a monolithic A-former [6]. Thus it is necessary to take the core material of sandwich structures into account to use the bi-functional usage of ROHACELL$^®$ PMI foams, serving as a mandrel and as a structural member of the sandwich design. To use ROHACELL$^®$ as a structural core it is necessary to analyse the stress distribution of the sandwich structure under loading condition. Afterwards the effort of the core material can be determined using the three dimensional stresses and a suitable 3-D failure criterion. This would exploit the full inherent cost and weight saving potential of the ROHACELL$^®$ foam-filled sandwich design.

2   THEORY OF 3-D FAILURE CRITERION FOR RIGID FOAMS BASED ON PMI

In [7] a new 3-D failure criterion for rigid foams based on PMI (ROHACELL$^®$) is developed using invariant theory. In the invariant notation the present state of stress in an object is described independent of the selected coordinate system [7].

A stress tensor comprises a hydrostatic component (axiator) and a deviator. The axiator describes a state of omnidirectional tension or compression, whereas the deviator contains a resultant tensile, compressive, or shear stress respectively. No statement about the direction of the stress is implied [8].

The potential chosen in [7] is an ellipsoid potential with its general mathematical formulation being

$$\Phi_2 = \frac{3 \cdot I_2' + a_1 \cdot \sigma_V \cdot I_1 + a_2 \cdot I_1^2}{1 + a_1 + a_2} = \sigma_V^2 \tag{1}$$

with the first invariant

$$I_1 = \sigma_{kk} \tag{2}$$

and the second deviatory invariant

$$I_2' = \frac{\sigma_{ij}' \cdot \sigma_{ji}'}{2} \tag{3}$$

Principally there are the following constraints for the material dependent characteristic values a_1 and a_2 [7]:

$$a_2 \geq 0 \tag{4}$$

and

$$a_1 \in \left]-(1 + a_2), -\frac{2 \cdot a_2 \cdot (1 + a_2)}{a_2 - 1}\right] \tag{5}$$

The equivalent stress σ_V can be determined according to the following equation [9]:

$$\sigma_V = \frac{\sqrt{(12 a_2 + 12 a_1 + 12) I_2' + (4 a_2^2 + (4 a_1 + 4) a_2 + a_1^2) I_1^2} + a_1 I_1}{2 a_2 + 2 a_1 + 2} \tag{6}$$

The factor of material effort f_E equals the ratio of actual equivalent stress σ_V to the action plane resistance to tensile failure R^+ [9]:

$$f_E = \frac{\sigma_V}{R^+} \tag{7}$$

The invariants I_1 and I_2' are calculated from the components of the spatial stress matrix [9]:

$$I_1 = \sigma_{11} + \sigma_{22} + \sigma_{33} = \sigma_{kk} \tag{8}$$

and

$$I_2' = \frac{1}{3}\left[\sigma_{11}^2 + \sigma_{22}^2 + \sigma_{33}^2 - \sigma_{11} \sigma_{22} - \sigma_{11} \sigma_{33} - \sigma_{22} \sigma_{33} + 3(\sigma_{12}^2 + \sigma_{13}^2 + \sigma_{23}^2)\right]. \tag{9}$$

Implying the first invariant I_1 regards the influence of hydrostatic stress states on compressible solids. In contrast to solid steel, for example, cellular solids are prone to failure under hydrostatic compression. Potentiating I_1 to the power of an uneven exponent allows to describe the different behaviour of the foam when exposed to tensile versus compressive stress. Including I_1 with an even exponent enables a closed shape of the potential´s field [7].

Parameters a_1 and a_2 are derived from the material specific characteristic values k_V and d_V, which provide information about the ratio of shear to tensile strength (k_V) and compressive to tensile strength (d_V). Consequently their determination requires results from pure axial tensile test (R^+ = action plane resistance of the foam to tensile failure = tensile strength) and compressive tests (R^- = action plane resistance of the foam to compressive failure = compressive strength) and pure shear tests (R_s = action plane resistance of the foam to shear failure = shear strength). Those parameters can be computed using the following equations [7]:

$$a_1 = \frac{k_V^2 \cdot (d_V - 1)}{d_V} \tag{10}$$

and

$$a_2 = \frac{k_V^2}{d_V} - 1 \tag{11}$$

with

$$k_V = \sqrt{3} \cdot \frac{R_S}{R^+} \tag{12}$$

$$d_V = \frac{R^-}{R^+} \tag{13}$$

The above mentioned criterion assumes isotropic and homogeneous material behaviour and is suitable to describe the typical compressible material behaviour and the strength differential effect (i. e. tensile strength ≠ compressive strength ≠ shear strength) of PMI foams [10].

The new developed 3-D failure criterion according to DKI/ Röhm need only three free parameters to describe the surface of the breakage in the 3-D stress space. These parameters can be determined by using the results of pure tension, compression and shear loadings (Chapter 3). Combined tension/shear and compression/shear loadings were carried out to validate the 3-D failure criteria (Chapter 4).

2 MATERIAL

The ROHACELL[®] 51 WF, 110WF and 200 WF grades were tested. The averaged density ρ of tested specimens are presented in Table 1. In general, a low standard deviation of the density was observed between specimens of the same ROHACELL[®] type.

	ROHACELL[®]		
	51 WF	110 WF	200 WF
Foam Density ρ [kg/m^3]	50.4 ± 0.6	102.8 ± 0.7	194.8 ± 1.7
Cell Diameter d_{cell} [μm]	405	434	476

Table 1: Density and cell diameter of ROHACELL[®] foams

The average cell diameter d_{cell} of ROHACELL[®] WF with different densities are analysed with micro computed tomography (μ-CT) and scanning electron microscopy (SEM) [7] and are listed in Table 1. The homogeneous and 100 % closed-cell foam structure of ROHACELL[®] 110 WF is shown in Figure 3.
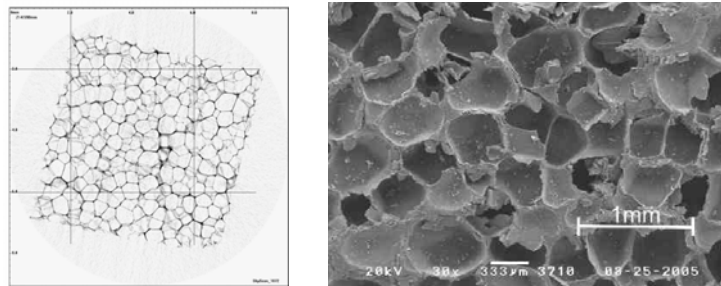
Figure 3: µ-CT and SEM of ROHACELL® 110 WF

3 EXPERIMENTAL PROCEDURE

The needed parameters of the 3-D failure criterion to describe the surface of the breakage in the 3-D stress space are determined by using the results of quasi-static pure tension, compression and shear load experiments. A new tubular specimen was developed and used to realize the experiments with one and the same geometry (Figure 4). The tubular test specimens are made of ROHACELL® 51 WF, 110 WF and 200 WF using shape-cutting operation. Afterwards the tubular test specimens are glued on flanges using coaxial centering device for the assembling.
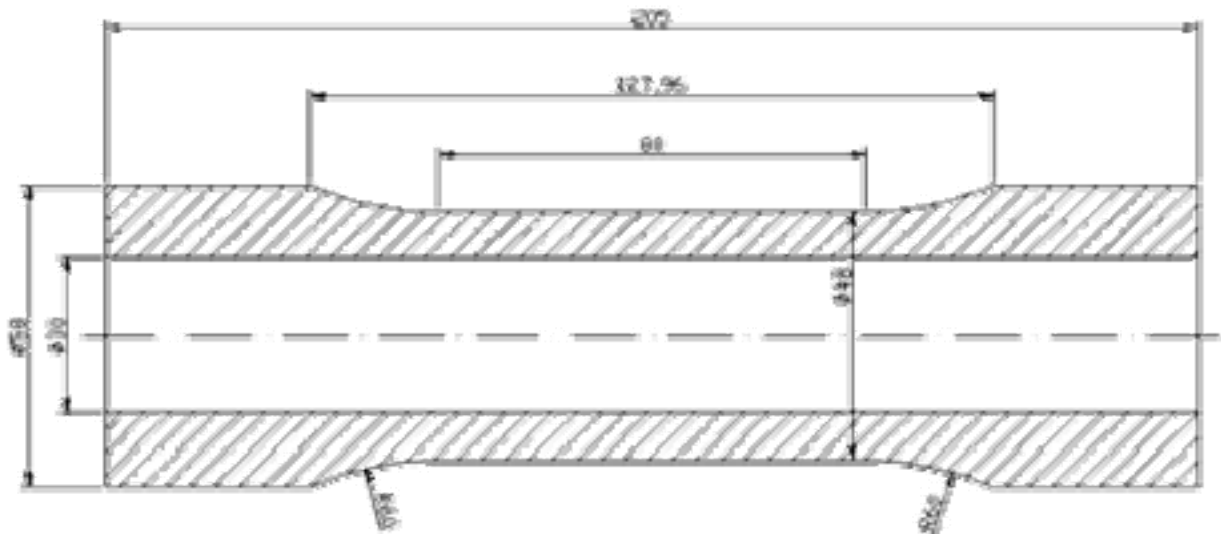
Figure 4: Geometry of tubular test specimen

A tension-/ compression-/torsion testing machine including an optical deformation measurement system was used to perform quasi-static uniaxial and combined tests (Figure 5). The strain distribution parallel and perpendicular to the loading direction was measured using the non-contact measurement system ARAMIS. For each stage of load, the 3-D coordinates of the object surface are calculated from the 2-D digital images (Figure 5).
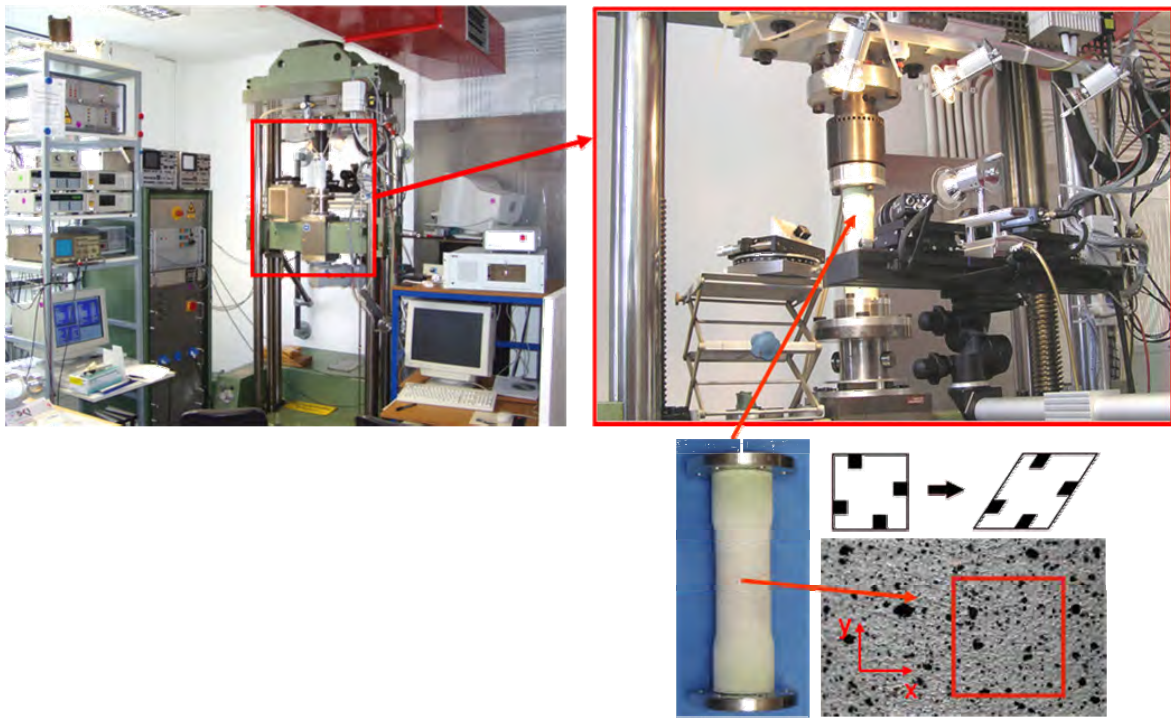
Figure 5: Tension-/ compression-/torsion testing machine including the optical deformation measurement system ARAMIS

During the quasi-static compression test the actual stress at the first collapse of the cell structure is used for the compressive strength R^-. Otherwise the stresses at breakage point are used for tensile strength R^+ and shear strength R_S during the quasi-static tension and torsion testing. The determined mechanical properties of ROHACELL® 51 WF, 110 WF and 200 WF are shown in Table 2.

	ROHACELL®		
	51 WF	**110 WF**	**200 WF**
Tensile Young's Modulus E_{Zug} [MPa]	83.3 ± 3.0	188.5 ± 1.1	388.2 ± 1.3
Poison Ratio ν_{Zug} [1]	0.32 ± 0.02	0.38 ± 0.00	0.38 ± 0.03
Tensile Strength R^+ [MPa]	1.25 ± 0.03	3.66 ± 0.06	5.27 ± 0.11
Compressive Young's Modulus E_{Druck} [MPa]	73.1 ± 2.9	179.7 ± 2.3	375.8 ± 1.7
Poison Ratio ν_{Druck} [1]	0.28 ± 0.02	0.39 ± 0.01	0.37 ± 0.02
Compressive Strength R^- [MPa]	0.86 ± 0.02	3.89 ± 0.12	6.84 ± 0.13
Shear Modulus G [MPa]	29.6 ± 2.0	84.9 ± 6.2	175.2 ± 0.7
Shear Strength R_S [MPa]	0.60 ± 0.01	2.19 ± 0.05	4.28 ± 0.09

Table 2: Mechanical properties of ROHACELL® 51 WF, 110 WF and 200 WF

The needed parameters for the 3-D failure criterion a_1, a_2, k_V and d_V can be determined using the results of Table 2 including equations 10 to 13 and are listed in Table 3.

	ROHACELL[®]		
	51 WF	**110 WF**	**200 WF**
k_V [1]	0.86	1.13	1.43
d_V [1]	0.66	1.16	1.23
a_1 [1]	-0.31	0.07	0.45
a_2 [1]	0.00077	0.02	0.53

Table 3: Parameters for the 3-D failure criterion a_1, a_2, k_V and d_V of
ROHACELL[®] 51 WF, 110 WF and 200 WF

In Figure 6 the parameters k_V and d_V related to density of PMI foams are shown. It can be concluded, that the needed parameters for the 3-D failure criterion k_V, d_V, a_1 and a_2 depend on the density of the foam and are not constant. Therefore it is necessary to determine the characteristic values d_V and k_V for any density.

In general PMI foam shows no von Mises behaviour, cause k_V and d_V are unequal one.
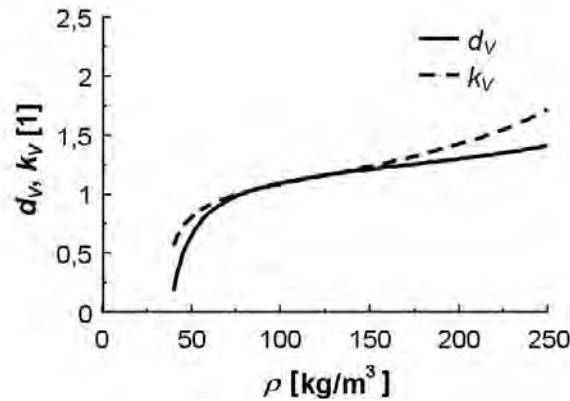
Figure 6: d_V/ρ- and k_V/ρ-diagram

In Figure 7 the 3-D failure criterion of ROHACELL[®] 51 WF, 110 WF and 200 WF in σ_{11}/τ_{12}-plane are presented. It is shown, that the surface of the breakage in the 3-D stress space increase with the density of the foam. The DKI/ Röhm criterion includes compressibility and strength differential effect of PMI-foams.
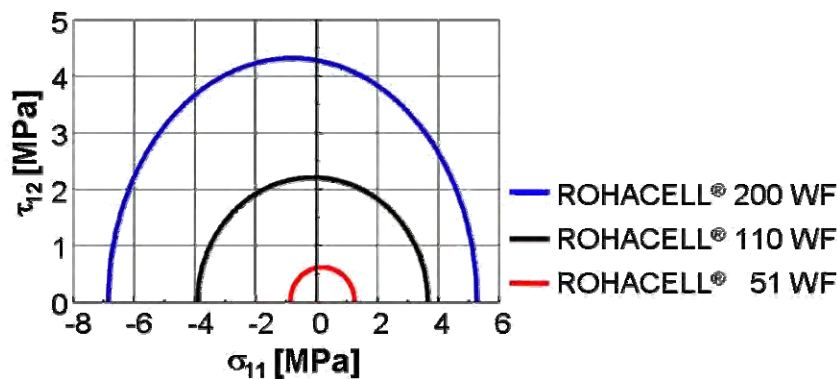
Figure 7: 3-D failure criteria of ROHACELL[®] 51 WF, 110 WF and 200 WF in σ_{11}/τ_{12}-plane

4 VALIDATION OF 3-D FAILURE CRITERION

Combined tension/shear and compression/shear loadings were used to validate the 3-D failure criterion of the considered PMI foams using the same test specimen geometry and test facility, which was described in Chapter 3. The criteria in σ_{11}/τ_{12}-plane of ROHACELL® 51 WF, 110 WF and 200 WF are presented in Figure 8 to 10.If the potential body according to von Mises is calibrated using the tensile strength, the obtained compressive stresses are too high for ROHACELL® 51 WF (Figure 8). Otherwise if the potential body according to von Mises is calibrated using the compressive strength, the obtained tensile stresses are too low.
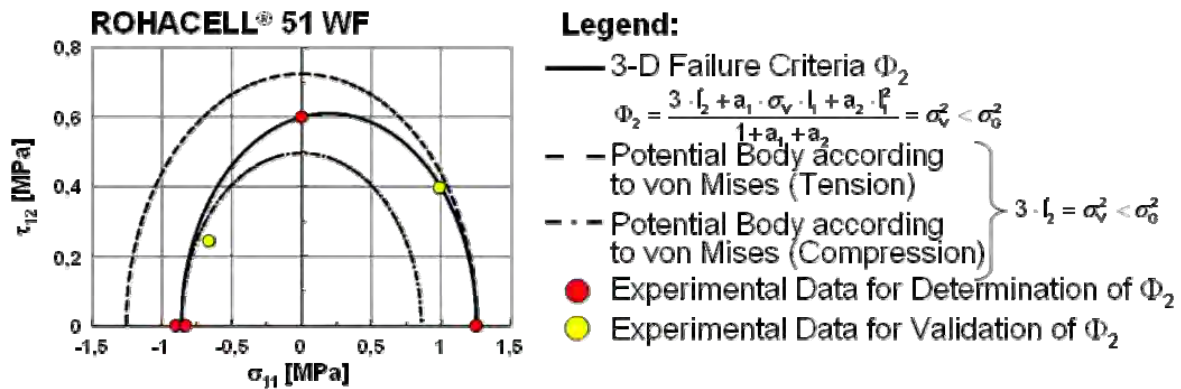
Figure 8: 3-D failure criterion of ROHACELL® 51 WF and
potential body according to von Mises in σ_{11}/τ_{12}-plane

For ROHACELL® 110 WF the potential body according to von Mises is suitable (Figure 9), cause the parameters d_V and k_V are nearby equal to one.
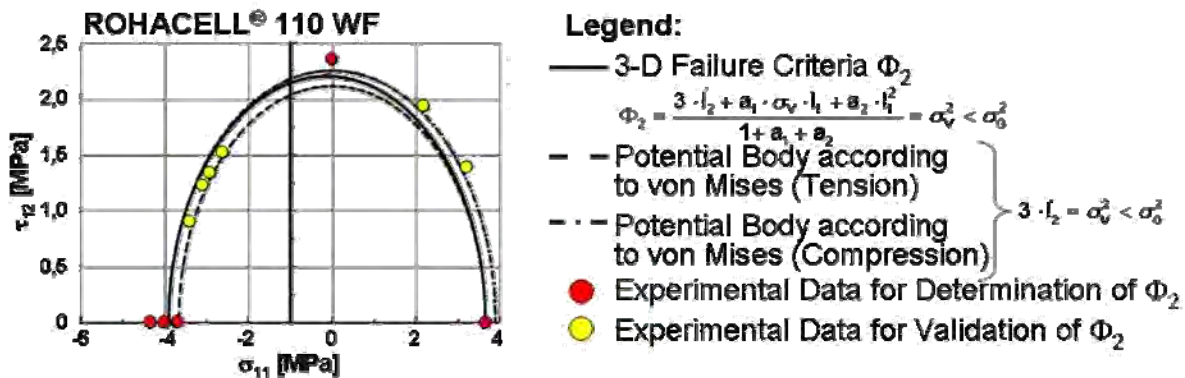
Figure 9: 3-D failure criterion of ROHACELL® 110 WF and
potential body according to von Mises in σ_{11}/τ_{12}-plane

If the potential body according to von Mises is calibrated using the tensile strength, the compressive stresses obtained are too low for ROHACELL® 200 WF. Otherwise if von Mises is calibrated using the compressive strength, the tensile stresses obtained are too high.

It can be concluded, that all experimental results fit very well with the σ_{11}/τ_{12}-curve of 3-D failure criterion according to DKI/ Röhm. Therefore the 3-D failure criteria of ROHACELL[®] 51 WF, 110 WF and 200 WF in σ_{11}/τ_{12}-plane are validated.
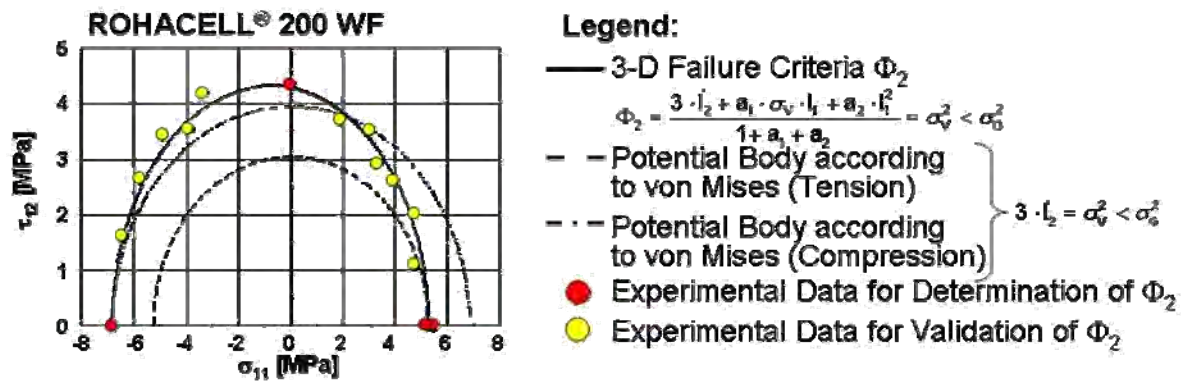

Figure 10: 3-D failure criterion of ROHACELL[®] 200 WF and
potential body according to von Mises in σ_{11}/τ_{12}-plane

Furthermore the 3-D failure criterion was independently validated by Composite Technology Center GmbH (CTC) and Fraunhofer Institut für Werkstoffmechanik (IWMH) [11]. Hereby 3-D failure criterion according to DKI/ Röhm as well as other criteria (e. g. von Mises, Beltrami, Sandel and Tresca) were implemented in a numerical program. A 4-point-bending loaded sandwich beam with PMI foam as core material and face sheet made of CFRP were simulated and analysed (Figure 11). Experimental results using 4-point-bending test were used to validate the numerical results. The sandwich beam failed due to a shear crack in the core material. The calculated material effort f_E of ROHACELL[®] using the DKI/ Röhm criterion agree very well with experimental results. The new 3-D failure criterion according to DKI/ Röhm is more suitable to describe the material behaviour of ROHACELL[®] than the other potential bodies [11]. This 3-D failure model is easy to implement in commercial FE programs. Due to the present results the use of the 3-D failure criterion to determine the material effort of ROHACELL[®] is recommendable.
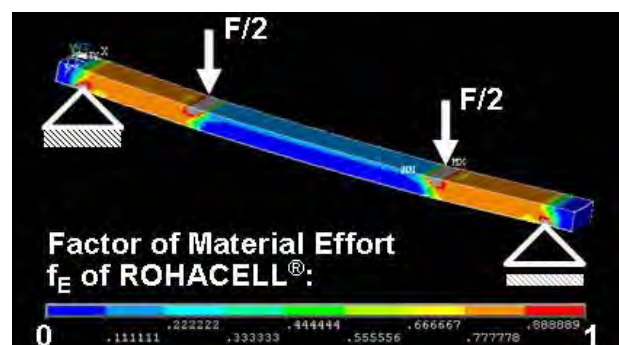

Figure 11: Numerical results of the material effort f_E of the PMI foam core (ROHACELL[®])
of a 4-point-bending loaded sandwich beam

5   SUMMARY

ROHACELL$^{®}$ sandwich foam cores are successfully used in a number of applications. ROHACELL$^{®}$ can be used as manufacturing aid during the manufacturing process due to its excellent resistance to creep compression during the cure, resulting in a thorough laminate consolidation without surface dimpling effects. In addition to a manufacturing aid ROHACELL$^{®}$ can be used as a structural core due to its high specific mechanical properties. The core material carries especially the shear and compressive stresses produced by transverse loads while the stiff and strong face sheets are used to carry the in-plane stresses. Furthermore ROHACELL$^{®}$ can contribute to increasing the stability and buckling resistance of a thin-walled CFRP-structure (e. g. A-stringer) significantly. If ROHACELL$^{®}$ is also used as a structural member, the wall-thickness of the covering CFRP face sheets can be reduced. To use ROHACELL$^{®}$ as a structural core it is necessary to analyse the stress distribution of the sandwich structure under loading condition. Afterwards the effort of the core material can be determined using the three dimensional stresses and a suitable 3-D failure criterion.

In cooperation with the German Institute for Polymers (DKI) a 3-D failure criterion for PMI foams ROHACELL$^{®}$ was developed. This model is suitable to describe the compressible material behaviour and the strength differential effect (i. e. tensile strength $\neq$ compressive strength $\neq$ shear strength) of PMI foams. New tubular test specimen made of ROHACELL$^{®}$ 51 WF, 110 WF and 200 WF and a new test facility were developed to determine the mechanical properties under different loading conditions (pure tension, compression, shear as well as combined tension/shear as well as compression/shear). A tension-/ compression-/torsion test machine including the optical deformation measurement system ARAMIS was used. The new developed 3-D failure criterion need only three free parameters to describe the surface of the breakage in the 3-D stress space. These parameters can be determined by using the results of pure tension, compression and shear loadings. Combined tension/shear and compression/shear loadings were carried out to validate the 3-D failure criterion. The new 3-D failure criterion is more suitable to describe the material behaviour of ROHACELL$^{®}$ than other well-known potential bodies, e. g. von Mises. The implementation of this 3-D failure criterion in numerical finite element programs is easy and it is already implemented in commercial finite element programs like ABAQUS, ANSYS$^{®}$ and ESAComp. Due to the present results the use of the 3-D failure criterion to determine the material effort of ROHACELL$^{®}$ is recommendable.

6 ACKNOWLEDGEMENTS

REFERENCES

[1] Zenkert, D.: The Handbook of Sandwich Construction. London, United Kingdom: Engineering Materials Advisory Services Ltd., 1997.

[2] Nachtigall, W.: Bau-Bionik Natur – Analogien – Technik. Berlin, Heidelberg, New York: Springer-Verlag, 2003.

[3] DEGUSSA, Röhm GmbH: Data CD 'ROHACELL® - The Core for Sandwich Solutions', March 2007.

[4] Ames, H., Rother, M.: Untersuchung über eine kostengünstige CFK-Bau-weise für längs- und radialversteifte Schalen. Endbericht, Dornier GmbH, 1983.

[5] Alsup, P.J.: A comparison of composite hat stiffeners using Teflon and remain-im-place foam mandrels subjected to static and fatigue loads. Air Force Wright Aeronautical Laborarories, 1985.

[6] Krämer, R.; Roth, M. A.: Experimental and numerical analysis of hollow and foam-filled A-Stringer/ A-Former under axial compression load and bending moment. Sandwich Structures 7: Advancing with Sandwich Structures and Materials. 7. Proceedings of the 7th International Conference on Sandwich Structures, Aalborg University, Aalborg, Denmark, 29th - 31st August 2005. Dordrecht, Netherlands: Springer Verlag, 2005, S. 1017 – 1026.

[7] Kraatz, A.: Anwendung der Invariantentheorie zur Berechnung des dreidimensionalen Versagens- und Kriechverhaltens von geschlossenzelligen Schaumstoffen unter Einbeziehung der Mikrostruktur. Dissertation an der Martin-Luther-Universität Halle-Wittenberg, 2007.

[8] Altenbach, H.; Altenbach, J.; Zolochevsky, A.: Erweiterte Deformationsmodelle und Versagenskriterien der Werkstoffmechanik. Leipzig, Stuttgart: Dt. Verl. für Grundstoffindustrie, 1995

[9] Roth, M. A.: ROHACELL® in Sandwich-Strukturen mit Deckschichten aus Faser-Kunststoff-Verbunden. Vorlesungsunterlagen, Hochschule Darmstadt, 04. Juni 2007.

[10] Roth, M. A.; Kraatz, A.; Moneke, M.; Kolupaev, V.: Advanced Material Models for the Creep Behaviour of Polymer Hard Foams. Latest Advancements of Applied Composite Technology. Proceedings 2006 of the SAMPE Europe, 27th International Conference, Paris EXPO, Porte de Versailles, Paris, France, 27th – 29th March 2006. ISBN 3-9522677-2-4. pp. 253 - 258.

[11] Rinker, M; Zahlen, P.; Schäuble, R.: Herstellung von CFK-Sandwichplatten – Untersuchung des Verformungs- und Versagensverhaltens. Springer Verlag, Konstruktion, Ingenieur-Werkstoffe – Verbundwerkstoffe, Juli/ August 7/8 2007. Seite IW 6 bis IW 9.

DEVELOPMENT OF A DESIGN TOOL FOR INITIAL ANALYSIS OF INSERTS IN SANDWICH STRUCTURES

Peter H. Bull⋆ and Ole T. Thomsen⋆

⋆Department of Mechanical Engineering
Aalborg University
Pontoppidanstrde 101, DK9000 Aalborg East, Denmark
e-mail: peb@ime.aau.dk, web page: http://www.ime.aau.dk

Key words: Sandwich structures, Modeling, Experimental mechanics, Manufacturing.

Summary. *A design tool for initial dimensioning of inserts in sandwich panels is being developed. The design tool is based on a high order sandwich beam theory, and can predict the strength of an insert in a sandwich panel subjected to four different load cases, pull out normal to the face of the sandwich plate, shear parallel to the face of the sandwich plate, torsion around the axis of the insert, and bending moment around an axis parallel to the plane of the sandwich plate. For brevity only the pull out load case is considered in the present investigation. Strength predictions from the design tool are being compared to predictions using finite element (FE) analysis and destructive material tests.*

1 Introduction

It is generally accepted that sandwich structures have a superior weight to stiffness and weight to strength ratio compared to monolithic structures. The layered nature of the sandwich does however, with the soft core in its center, pose some limits to its capability to carry localized loads. In order to increase this, local reinforcements called inserts can be embedded in the core [1]. Analyzing the strength of inserts in sandwich plates is not trivial, and there are few tools available to do so. The aim of the present work is to develop a tool for initial strength analysis of inserts in sandwich plates which will be implemented in the composite analysis code ESAComp.

In the *Insert design handbook* [2] three main groups of inserts are identified. They are called type A, B and C and they are defined according to the list below. Although the developed method can be used to analyze through thickness (B,iii), fully potted (B,ii), and partially potted inserts (B,i), only fully potted inserts are presented in this investigation for brevity.

A Inserts of this type are placed into the core material prior to the assembly of the sandwich component. Thus they are fully bonded to both skins and core material.

B These inserts are the main focus of this study; they are placed into the sandwich component post manufacturing. They exist in three sub categories:

  i Partially potted, which only goes through one face sheet and do not extend through the full thickness of the core material, see figure 2.
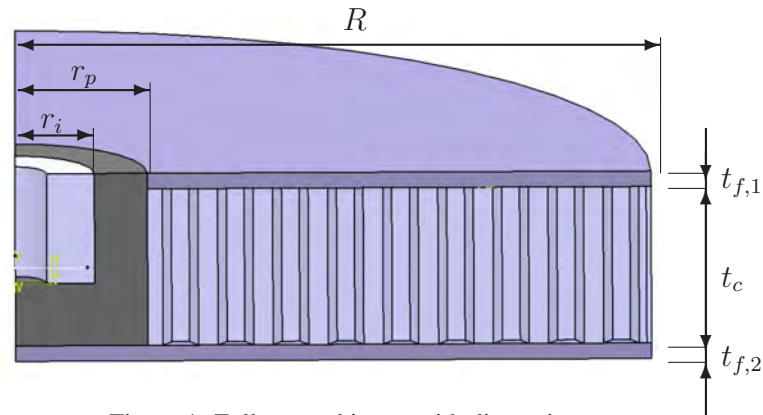
Figure 1: Fully potted insert with dimensions

    ii Fully potted, which extends through the full thickness of the core material and one of the face sheets, see figure 1

   iii Through the thickness, which extends through the full thickness of the core material and both face sheets, see figure 3

  C This group contains mechanically fastened inserts which consist of two threaded parts. The parts are entered into drilled holes through the sandwich component from each side and screwed into each other.
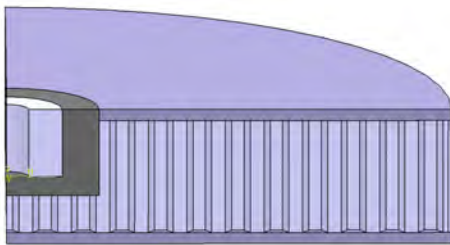

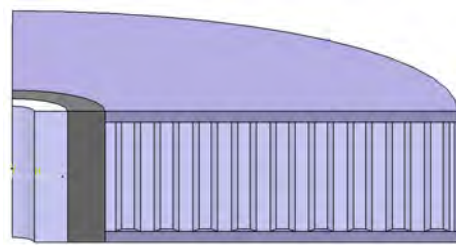Figure 2: Circular sandwich plate with partially potted insert

Figure 3: Circular sandwich plate with through thickness insert

Models available in the literature can be divided into two main categories; analytical and finite element models. The analytical models, of which two have been found in the literature, Thomsen [3, 4, 5, 6] and Kristensen [7], have to be solved using a numerical method. Thus they cannot be directly used for hand calculation. Since they are inherently made in a parametric form, once they have been implemented into a code they can be used to solve problems with different geometries. However, there are some limitations to the accuracy of the result in some load cases due to the restrictive assumptions in the models. E.g. the method presented by Kristensen [7] is based on fracture mechanics modeling of the core material alone and does not take the face sheets into account. Using a fracture mechanics approach might not yield

reasonable results for sandwich with aluminum honeycomb core since the most common failure is shear buckling of the honeycomb walls. The method presented by Thomsen [3, 4, 5, 6] assumes that in plane stiffness in the core is zero. Expanding the model to take in plane stiffness into account is possible, but the complexity of the model is increased dramatically and the accuracy of predictions does not increase notably.

A finite element model has to be generated specifically for each problem to be solved, thus it is tailor made for that single problem and cannot necessarily be used for another. The level of detail in a finite element model can vary from a very detailed 3D model such as in the work of Bunyawanichakul [8] to an, in comparison, coarse 2D model as the one utilized by Bozhevol-naya and Lyckegaard [9], [10], or Tsouvalis and Kollarini [11]. Therefore, the complexity of the FE model depends on the level of detail required to analyze the problem at hand. Thus finite element analysis can be used to analyze most combinations of materials and load cases for inserts in sandwich panels.

2 Governing equations

The problem of a circular sandwich plate with a through-thickness or fully potted insert sub-jected to external loads is formulated and solved numerically in terms of a high-order sandwich plate theory in which the 2 face sheets and the core and potting materials are modeled sepa-rately, Thomsen [3]. In this model, the problem is governed by 24 fundamental field variables as shown in eqn. (2), they are defined in [3]. They are defined with respect to the coordinate system shown in figure 4. The 20 variables, marked with index 1 and 2, describe the behavior of the upper and lower face sheets respectively. The behavior of the core material is described by 2 shear stress variables, τ_{rz} and $\tau_{\theta z}$, and their derivatives with respect to r; $\partial \tau_{rz}/\partial r = q_r$ and $\partial \tau_{\theta z}/\partial r = q_\theta$.

$$
\begin{aligned}
\{y(r,\theta)\} \quad = \quad & \{u_{r0}^1, u_{\theta 0}^1, w^1, \beta_r^1, \beta_\theta^1, N_r^1, N_{r\theta}^1, M_r^1, M_{r\theta}^1, Q^1, \\
& \tau_{rz}, q_r, \tau_{\theta z}, q_\theta, \\
& u_{r0}^2, u_{\theta 0}^2, w^2, \beta_r^2, \beta_\theta^2, N_r^2, N_{r\theta}^2, M_r^2, M_{r\theta}^2, Q^2\}
\end{aligned}
\tag{1}
$$

From these governing field variables a system of 24 first order partial differential equation can be derived, see [3]. The equation system is solved by piecewise direct numerical integration along the r direction. The method is called "multiple point shooting method" or the "multi segment method of integration". In order for the system to be solvable a total of 24 boundary condition have to be defined.

3 Boundary conditions

The boundary conditions were chosen to, as closely as possible, simulate the boundary con-ditions of the actual test setup used to measure the pull-out strength of inserts in sandwich plates as described in the *E*SA Insert Design Handbook [2]. However, the model can handle completely arbitrary boundary conditions. Since the model assumes circular symmetry, the
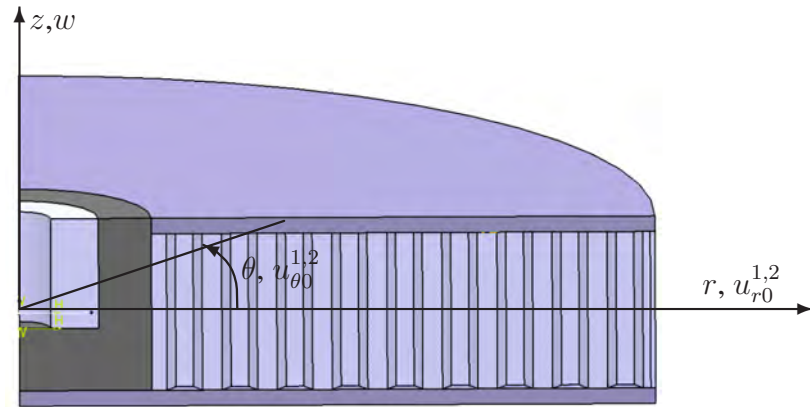
Figure 4: Sandwich plate with fully potted insert and coordinate system

plate is not allowed to move in the r or θ directions at the center. Neither is it allowed to rotate around the r or z axis, see fig. 5.

Figure 5 shows a schematic of simply supported boundary conditions in the $\theta = 0$ plane. The edge of the plate is not allowed to move in the z direction, but it is allowed to move in the r direction, and it is allowed to rotate around the θ axis
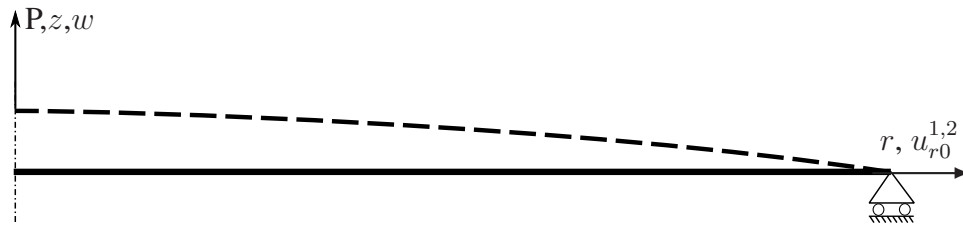

Figure 5: Schematic of simply supported boundary conditions in the $\theta = 0$ plane

In the analysis the imposed, simple support conditions are treated in a way similar to what is shown in the schematic in figure 6. At the edge, the face sheet which would be in contact with the support in a test condition is not allowed to move in the z direction. As a result, normal forces, and bending moments are set equal to zero at the plate edge. Under the general assumption of small deflections it is reasonable to assume that the membrane stresses that arise from movement in the r direction from deflection in the z direction are negligible.

Ideally shear stresses should also be set equal to zero at the plate edge. Because the system of governing equations is solved by piecewise integration, and the very low local bending stiffness of the face sheet, setting the shear stresses equal to zero results in very large deflections close to the plate edge, to reduce this effect the total vertical resultant of the shear stresses working on the area of the plate edge are set to be equal to the point load at the middle of the plate.
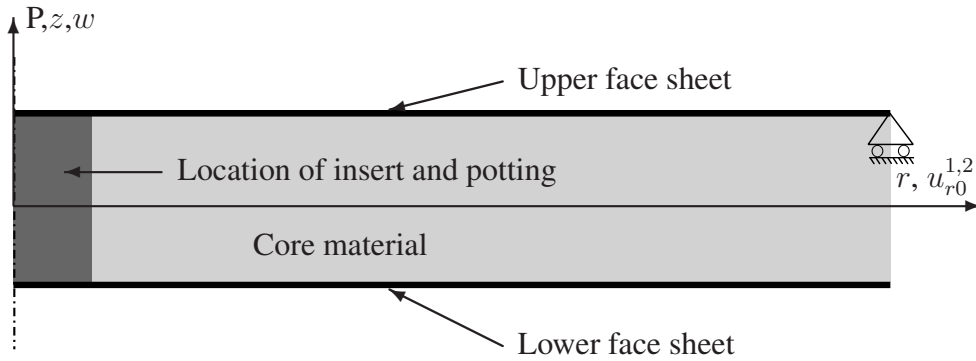
Figure 6: Interpretation of simply supported boundary conditions in the $\theta = 0$ plane

4 Benchmarking

The developed analysis model has been benchmarked against three different alternative models. The load case considered in the present work was pull out of the insert normal to the plane of the sandwich plate. One model was an analytical expression for the deflection of a circular sandwich plate with a point load at its center. Two models were made using the finite element code Ansys [12]. A 2 dimensional axisymmetric plane finite element model, and a 3 dimensional shell finite element model constructed of a quarter model of a circular plate. The face sheets were modeled as aluminum, and the core material as aluminum honeycomb with smeared out material properties. One reason for this was that it was impossible to model orthotropic face sheets, with reasonable accuracy, in a two dimensional axisymmetric FE model. That would have required a three dimensional quarter model of a circular plate with every constituent modeled with solid elements. Which in its turn would have resulted in a model which was too large to analyze with the FE code licenses available. It was also found reasonable to question the accuracy of such a model since the core material was modeled as solid with smeared out material properties. The elements would have been significantly smaller than the cell size of the honeycomb core. Therefore it was decided to limit the benchmarking to face sheets of aluminum. Definition of the dimensions of the sandwich plate and insert together with the material properties of the constituent materials can be found in table 1 and figure 1.

The geometry considered was a circular axisymmetric plate with a fully potted insert as shown in figure 1. The pull-out load, $P = 1kN$, was placed in the plate center, and the boundary conditions considered were simply supported.

4.1 Analytical expression

The analytical model is based on classical sandwich theory, as described by Zenkert [13]. According to this, the deflection of a sandwich plate consists of two independent modes, one governed by bending deformation, and one governed by shear deformation. Assuming that both face sheets have the same material properties and the same thickness, the bending stiffness D and the shear stiffness S are defined as follows in eqns. (2) and (3) respectively.